Gene Editing and Hereditary Optic Neuropathies: CRISPR/Cas-Based Rescue of Missplicing Induced by *OPA1* Mutation

Dissertation

der Mathematisch-Naturwissenschaftlichen Fakultät
der Eberhard Karls Universität Tübingen
zur Erlangung des Grades eines
Doktors der Naturwissenschaften
(Dr. rer. nat.)

vorgelegt von
Sinja Kieninger
aus Leonberg

Tübingen
2023

Gedruckt mit Genehmigung der Mathematisch-Naturwissenschaftlichen Fakultät der Eberhard Karls Universität Tübingen.

Tag der mündlichen Qualifikation:	09.10.2023
Dekan:	Prof. Dr. Thilo Stehle
1. Berichterstatter/-in:	Prof. Dr. Bernd Wissinger
2. Berichterstatter/-in:	Prof. Dr. Stefan Liebau

Erklärung:

Ich erkläre hiermit, dass ich die zur Promotion eingereichte Arbeit mit dem Titel:

„Gene Editing and Hereditary Optic Neuropathies: CRISPR/Cas-Based Rescue of Missplicing Induced by *OPA1* mutation"

selbständig verfasst, nur die angegebenen Quellen und Hilfsmittel benutzt und wörtlich oder inhaltlich übernommene Stellen (alternativ: Zitate) als solche gekennzeichnet habe. Ich erkläre, dass die Richtlinien zur Sicherung guter wissenschaftlicher Praxis der Universität Tübingen (Beschluss des Senats vom 25.5.2000) beachtet wurden. Ich versichere an Eides statt, dass diese Angaben wahr sind und dass ich nichts verschwiegen habe. Mir ist bekannt, dass die falsche Abgabe einer Versicherung an Eides statt mit Freiheitsstrafe bis zu drei Jahren oder mit Geldstrafe bestraft wird.

26.03.23 Sinja Kieninger

Für Mama und Papa

Table of contents

1 Introduction

1.1 Hereditary optic neuropathies

Optic neuropathies comprise disorders associated with damage of the optic nerve. The optic nerve is formed from the axons of the retinal ganglion cells and transmits electrical signals generated by the retina to the visual cortex where the signals are processed into an image (Camara et al., 2022) (Figure 1).

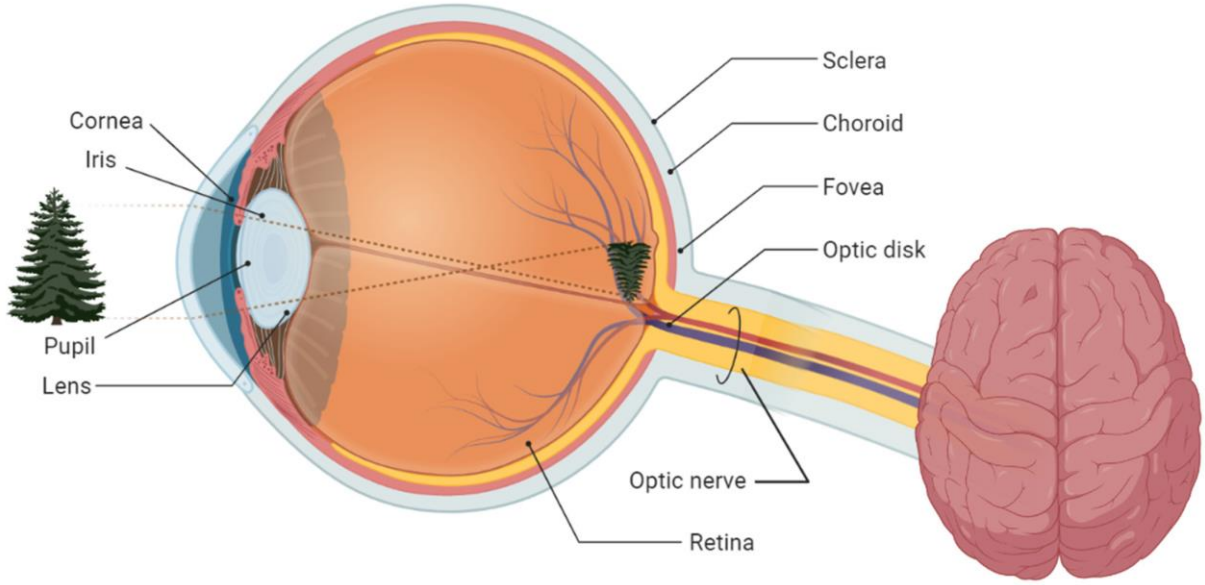

Figure 1: Transmission of visual impressions from the eye to the brain. Light is transformed into electrical signals by retinal cells. The electrical signals are transmitted to the visual cortex through the optic nerve. Reproduced from Camara et al., 2022.

Vision loss occurs when the retinal ganglion cells are damaged or degenerated, which can be caused by various factors such as insufficient blood supply or inflammation of the optic nerve, tumor invasion, or direct damage to the optic nerve from injury, but nutritional deficiencies and ingestion of toxic substances also play a significant role (Bennett, 2019; Currie et al., 1988; Margolin & Shemesh, 2022; Patel & Margo, 2017; Steinsapir & Goldberg, 1994). In addition to the already mentioned factors, there are also inherited optic neuropathies caused by genetic alterations. Hereditary optic neuropathies are characterized by painless, progressive, and bilateral loss of central vision and are caused by mutations in nuclear or mitochondrial encoded genes that cause mitochondrial dysfunction (V. Carelli et al., 2004). Mitochondria are eukaryotic cell organelles that produce adenosine triphosphate (ATP) as part of the respiratory chain, providing energy for various cellular processes. The cell organelles consist of an outer and inner membrane. The latter forms invaginations known as cristae into the inner space (matrix) of the

mitochondria (Figure 2). The matrix also contains the mitochondrial DNA which is inherited exclusively from the mother (Nunnari & Suomalainen, 2012). Mitochondria not only exist as single organelles, but also form dynamic networks by undergoing cycles of fusion and fission (Adebayo et al., 2021). Mutations in genes associated with mitochondrial function can lead to disruption of cristae structure, dysfunctional fission and fusion, and also decreased energy production (Del Dotto et al., 2018). Mitochondrial dysfunction is a particular burden for retinal ganglion cells, which have a high demand for ATP (Yu et al., 2013). Therefore, ATP deficiency leads to increased cell death of retinal ganglion cells and consequent loss of vision. The most common inherited optic neuropathies are Leber´s hereditary optic neuropathy and dominant optic atrophy (La Morgia et al., 2014).

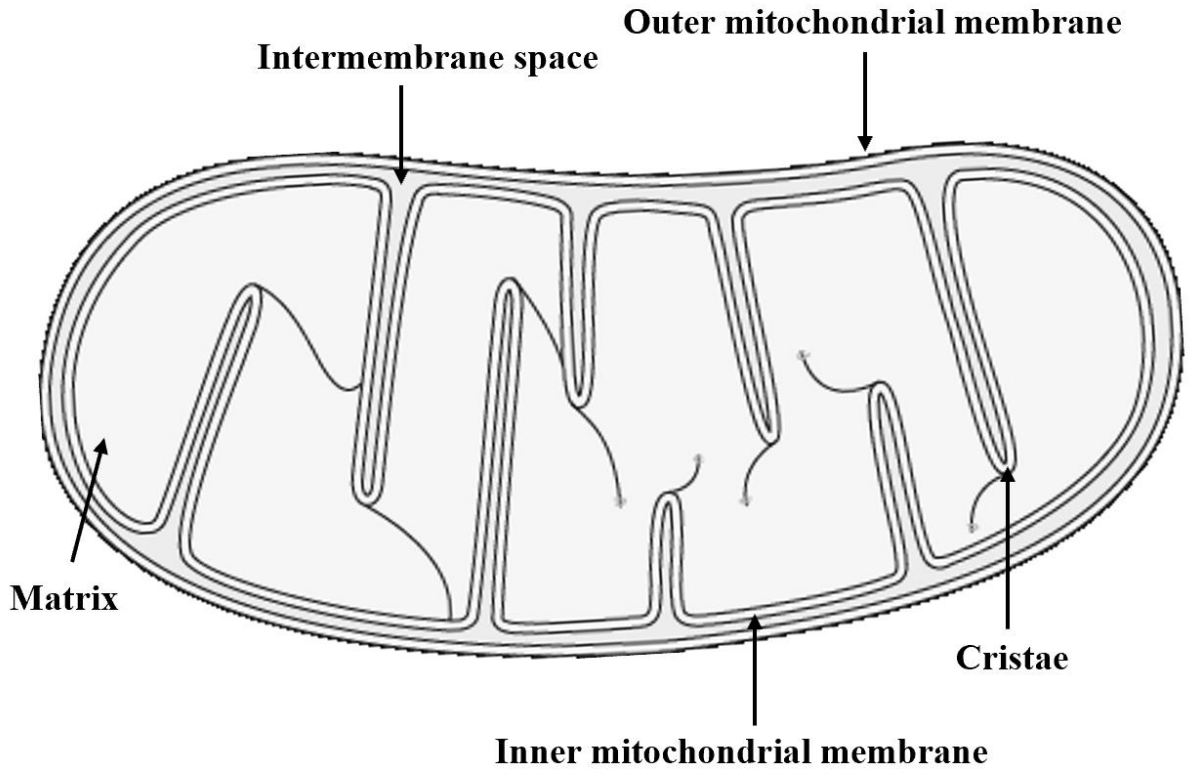

Figure 2: Schematic representation of a mitochondrion. Modified illustration from Servier Medical Art by Servier, licensed under a Creative Commons Attribution 3.0 unported license (https://smart.servier.com/).

1.1.1 Leber´s hereditary optic neuropathy

Leber´s hereditary optic neuropathy (LHON) was named after ophthalmologist Theodor Leber, who first described the disease in 1871 (Leber, 1871). LHON occurs in the second or third decade of life, affects predominantly men and was reported to have a prevalence of 1:54 000 in the Danish population (Rosenberg et al., 2016). LHON patients initially present with painless,

progressive acute or subacute unilateral vision loss, which manifests in the second eye after weeks to months (Huoponen, 2001). The visual acuity in LHON patients can decrease to <0.1, which is considered as legally blind in the United States of America. Spontaneous recovery of the visual acuity to ≥0.2 could be observed in patients even months after onset of the disease (Mashima et al., 2017). LHON is mainly associated with three point mutations in the mitochondrial DNA and is therefore inherited from the maternal side: m.11778G>A in *MT-ND4*, m.3460G>A in *MT-NDI* and m.14484T>C in *MT-ND6* (Yu-Wai-Man et al., 2011). Mitochondrial DNA mutations are known to cause deficient ATP synthesis, resulting in an increased production of reactive oxygen species (ROS) and apoptosis of retinal ganglion cells (V Carelli et al., 2004). Improvement in visual acuity can be achieved by treatment with idebenone (Zhao et al., 2020). Idebenone is an antioxidant that can reduce apoptosis of retinal ganglion cells caused by ROS production (Zuccarelli et al., 2020). In addition to drug administration, gene therapies represent another potential therapeutic strategy to improve disease progression. Gene replacement therapy showed improved visual acuity in patients harboring the mutation m.11778G>A in *MT-ND4* (Vignal et al., 2018). In this study, subjects with LHON received a single intravitreal injection of adeno-associated viruses expressing the ND4 protein .

In addition to mitochondrial inheritance, biallelic variants in the nuclear-encoded gene *DNAJC30* were described in 2021 to cause autosomal recessive LHON (arLHON). Both the phenotype and sex bias resemble that of mitochondrial inherited LHON (Stenton et al., 2021).

1.1.2 Dominant optic atrophy

In 1957, ophthalmologist Poul Kjer reported 19 families with optic atrophy that showed a dominant mode of inheritance (Kjer, 1957). Dominant optic atrophy (DOA) is characterized by progressive bilateral vision loss due to retinal ganglion cell degeneration and currently has a prevalence between 1:10 000 in the Danish population to 1:40 000 worldwide (Almind et al., 2012; Xu et al., 2021). DOA usually occurs in the first or second decade of life and varies both inter- and intrafamilially, exhibiting incomplete penetrance, meaning that not all individuals carrying a DOA genotype also exhibit a clinical phenotype (Cohn et al., 2007). The majority of DOA patients have isolated optic atrophy, but approximately 20% have a syndromal form of DOA with additional extraocular symptoms, which mainly include neurological impairments such as peripheral neuropathy, ataxia, chronic progressive external ophthalmoplegia, spasticity, mental retardation, and hearing loss (Felicio et al., 2008; Huang et al., 2009; Lenaers et al., 2012; Pretegiani et al., 2011; Yu-Wai-Man et al., 2010). These conditions are also referred to as dominant optic atrophy plus or Behr syndrome. To date, there are no approved therapies for DOA,

but various gene therapy approaches are in pre-clinical development (Jüschke et al., 2021; Sarzi et al., 2018). Unlike LHON, DOA is associated with mutations in nuclear-encoded genes that encode proteins related to mitochondrial function. The majority of DOA cases (at least 75%) are caused by mutations in the *OPA1* gene (Lenaers et al., 2012). Other DOA-causing genes are rarely associated with isolated DOA but more often with syndromic neurological disorder such as *OPA3* correlating with DOA and cataract, *AFG3L2* with spinocerebellar ataxia type 28, *SPG7* with hereditary spastic paraplegia type 7, *DNM1L* with infantile encephalopathy, *MFN2* with Charcot-Marie-Tooth neuropathy type 2A or hereditary motor and sensory neuropathy type VI, *NR2F1* with Bosch-Boonstra-Schaaf optic atrophy syndrome, *WFS1* with DOA and hearing loss and *SSBP1* with DOA, retinopathy, nephropathy and deafness (Al-Harbi et al., 2019; Bosch et al., 2014; Del Dotto et al., 2020; Eiberg et al., 2006; Hamedani et al., 2021; Klebe et al., 2012; Lenaers et al., 2021; Reynier et al., 2004; Smets et al., 2014; Waterham et al., 2007).

1.1.2.1 *OPA1* gene mutations

OPA1 is located on chromosome 3q28-q29 and comprises 31 exons, including a noncoding exon (Eiberg et al., 1994; Jonasdottir et al., 1997; Lunkes et al., 1995; Votruba et al., 1997). Exons 4, 4b and 5b are alternatively spliced exons that generate eight different isoforms, the proportion of which varies in different tissues (Delettre et al., 2001). The OPA1 protein is a dynamin-related GTPase that is localized in the inner mitochondrial membrane and is specifically involved in mitochondrial fusion, cristae structure formation, apoptosis, oxidative phosphorylation and mtDNA maintenance (Amati-Bonneau et al., 2008; Frezza et al., 2006; Hudson et al., 2008; Lee et al., 2004; Olichon et al., 2002; Zanna et al., 2008). OPA1 consists of several protein domains including the GTPase domain, which is highly conserved and catalyzes the hydrolysis of GTP to GDP (Li et al., 2019) (Figure 4). The middle domain is known to play a role in oligomerization, the pleckstrin homology (PH) domain can specifically bind to phosphoinositides of the lipid membrane (Praefcke & McMahon, 2004) and the GTPase effector domain (GED) contributes to the activity of the GTPase. The mitochondrial targeting sequence (MTS) enables the transport of the protein into the mitochondria. After import of OPA1 into the mitochondria, the MTS is cleaved off by the mitochondrial processing peptidase (MPP) exposing the transmembrane domain, which is used to anchor OPA1 into the mitochondrial membrane (Olichon et al., 2002). The anchored version of OPA1 corresponds to the long isoform of OPA1 (L-OPA1). L-OPA1 stabilizes cristae structure (Pernas & Scorrano, 2016) and interacts with mitofusin 1 (MFN1) to regulate inner- and outer mitochondrial membrane fusion

(Cipolat et al., 2004) (Figure 3). To remove damaged mitochondria or upon stress in general, the metalloendopeptidase OMA1 cleaves L-OPA1 into the shorter and soluble isoform S-OPA1 missing the transmembrane domain (Ehses et al., 2009; Head et al., 2009). Cleavage of L-OPA1 promotes fission and results in the fragmentation of mitochondria, followed by release of cytochrome C and the final apoptosis of damaged mitochondria (Lenaers et al., 2012). The appropriate ratio of L-OPA1 and S-OPA1 was shown to be crucial for efficient mitochondrial network dynamics and the maintenance of healthy mitochondria (Ge et al., 2020).

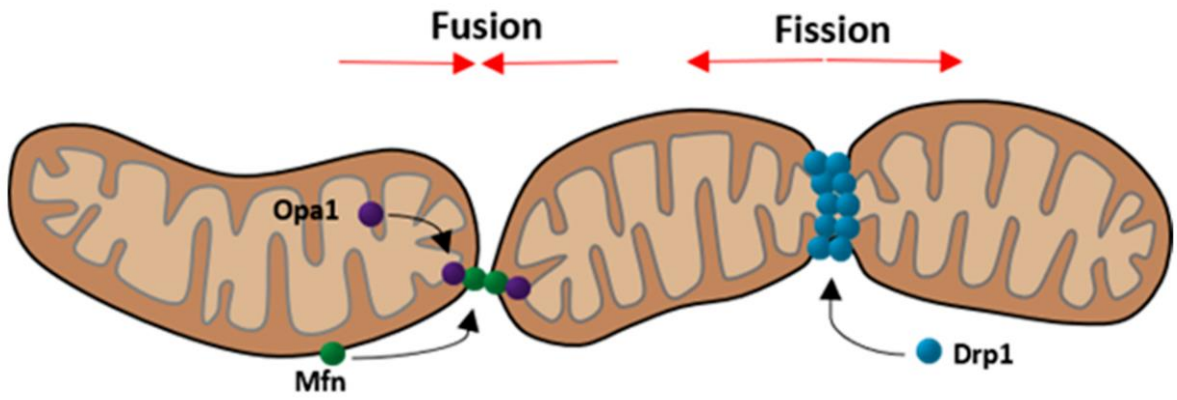

Figure 3: Proteins involved in mitochondrial fusion and fission. Mitofusin (Mfn) regulates fusion of the outer mitochondrial membrane and Opa1 is responsible for inner mitochondrial membrane fusion. Drp1 regulates mitochondrial fission. Reproduced from Mendelsohn et al., 2022.

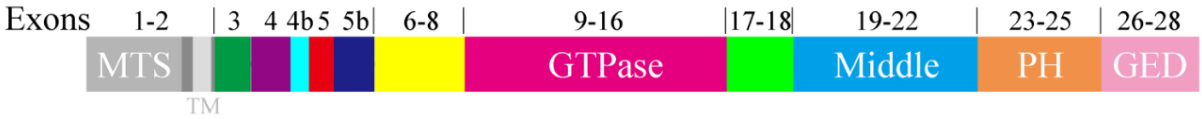

Figure 4: Scheme of the OPA1 protein domains. The OPA1 protein is composed of a mitochondrial targeting sequence (MTS) (encoded by exons 1 and 2) followed by a transmembrane (TM), a GTPase domain (encoded by exons 9-16), a middle domain (encoded by exons 19-22), a pleckstrin homology (PH) domain (encoded by exons 23-25) and a GTPase effector domain (GED) (encoded by exons 26-28). Reproduced from Li et al. 2019.

To date, 667 unique *OPA1* variants have been published (https://dabases. Lovd .nl /shared/genes/OPA1). The mutation spectrum includes missense variants, nonsense variants, frameshift variants, and variants associated with aberrant splicing (Weisschuh et al., 2021). In addition, structural variants are being identified with increasing frequency, but are often overlooked in routine genetic diagnostics. The majority of variants are loss-of-function variants that generate a premature termination codon (PTC) (Lenaers et al., 2021). Most aberrant transcripts that harbor a PTC are recognized and degraded by a control mechanism found in eukaryotic

cells, called nonsense-mediated mRNA decay (NMD) (Frischmeyer & Dietz, 1999). The pathophysiology of *OPA1*-related DOA is thought to be mainly due to haploinsufficiency of OPA1 (Pesch et al., 2001). Haploinsufficiency describes a condition in which the amount of protein produced by the wild-type allele is insufficient for physiological processes, resulting in the manifestation of disease symptoms. Missense variants and in-frame deletions found in the GTPase domain of OPA1 are mainly identified in syndromic forms of DOA and are associated with a dominant-negative effect (Amati-Bonneau et al., 2008). Biallelic mutations are rarely found in patients with isolated DOA but are more common in patients with Behr syndrome. In 2014, Bonifert et al. reported several families with Behr syndrome who were compound heterozygous for a deep intronic and a missense variant in *OPA1* (Bonifert et al., 2014). Heterozygous and homozygous carriers of the missense variant p.I437M are asymptomatic. Symptoms manifest only when an additional null allele is present, which is why the variant p.I437M is referred to as hypomorphic allele or modifier. Biallelic *OPA1* loss-of-function mutations are not known, as they are most likely embryonically lethal (Davies et al., 2007).

1.2 The process of pre-mRNA splicing

The pathway of protein biosynthesis was first published in 1958 by Francis Crick and declares that proteins are generated from RNA and RNA is generated from DNA (Crick, 1958). The synthesis of RNA from DNA is referred to as transcription and the subsequent synthesis of proteins from RNA is called translation. In eukaryotic cells, DNA is transcribed into messenger RNA (mRNA) by RNA polymerase II in the cell nucleus (Figure 5). The mature mRNA is then transported into the cytoplasm where the information of the mRNA is translated by ribosomes into amino acids, the components of proteins. During transcription, the pre-mRNA is processed into the mature mRNA. This process includes splicing, 5´-capping and 3´-polyadenylation (Bentley, 2014). Capping of the 5´end and polyadenylation of the 3´end protects the mRNA from degradation by enzymes and facilitates the transport from the cell nucleus to the cytoplasm.

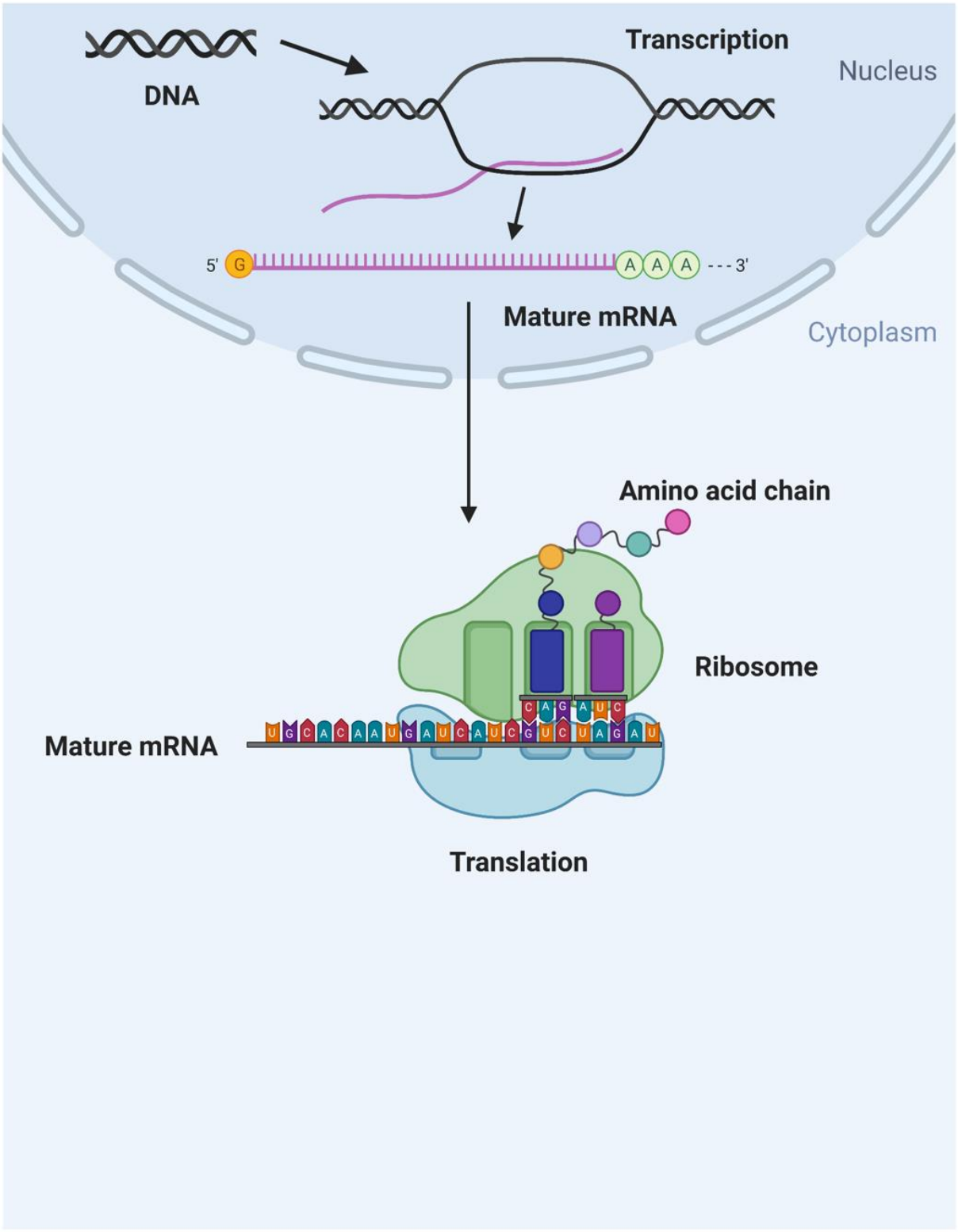

Figure 5: Protein biosynthesis in eukaryotic cells. During Transcription, pre-mRNA is synthesized from DNA and further processed into mature mRNA in the cell nucleus. During Translation, the mRNA sequence is translated into amino acids forming proteins. Adapted from "intracellular pathway comparison", by BioRender.com (2022). Retrieved from https://app.biorender.com/biorender-templates.

The pre-mRNA still consists of exons and introns. During splicing, the non-coding introns are removed to obtain a mature mRNA which exclusively contains exons. The splicing process is catalyzed by a complex of RNA and proteins, called spliceosome (Will & Lührmann, 2011). There are two different types of spliceosomes in human cells, the major and minor spliceosome (Patel & Steitz, 2003). The major spliceosome consists of five different RNAs and more than 100 different proteins forming the five small nuclear ribonucleoproteins (snRNPs) U1, U2, U4, U5 and U6. The letter "U" correlates with the uridine-rich RNAs of the snRNPs. The minor spliceosome consists of the snRNPs U11, U12, U5, U4atac, U6atac. The major spliceosome removes the most abundant canonical introns, whereas the minor spliceosome removes rare introns with non-canonical consensus sequences. The splicing process is accomplished by two transesterifications which are catalyzed by the snRNP complexes. The major spliceosome recognizes and cuts specific sequence regions on the pre-mRNA including the canonical GU dinucleotide also known as 5´splice site or donor splice site, the canonical AG dinucleotide also known as 3´splice site or acceptor splice site, and the branch site adenosine, which is located 20-40 nucleotides upstream of the 3´splice site and is followed by polypyrimidine residues (Kreivi & Lamond, 1996) (Figure 6). Introns with non-canonical splice sites lack this so called polypyrimidine tract. Splicing at acceptor and donor sites is additionally regulated by splicing factors such as heterogeneous nuclear ribonucleoproteins (hnRNPs) or SR proteins which include a high number of serine and arginine (SR) residues (Krecic & Swanson, 1999; Zahler et al., 1992). Binding motifs for these proteins are located on the pre-mRNA and are called splicing regulatory elements (SREs). SREs include exonic and intronic splicing enhancers (ESE, ISE), which promote splicing of an exon or intron, as well as exonic and intronic splicing silencer (ESS, ISS), which inhibit splicing of an exon or intron (Lee & Rio, 2015). SREs are playing an important role not only in constitutive splicing but also in the process of alternative splicing (Montes et al., 2019).

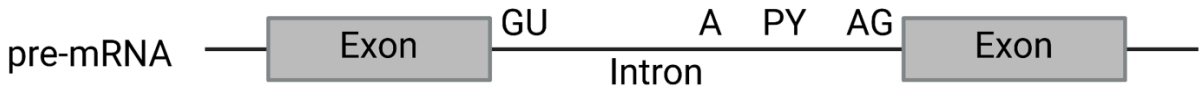

Figure 6: Canonical splice sites on the pre-mRNA. Conserved elements that are recognized by the major spliceosome include the 5´splice site sequence GU, the 3´splice site sequence AG and the branch point adenosine (A) followed by the polypyrimidine tract (PY). Created with BioRender.com.

Alternative splicing comes in different forms such as skipping of exons, retention of introns, use of cryptic splice sites or mutually exclusive splicing of adjacent exons (Ule & Blencowe,

2019) (Figure 7). More than 95% of the human genes are known to be alternatively spliced, including the *OPA1* gene (see 1.1.2.1 *OPA1* gene mutations), allowing the formation of different transcripts and thus also different proteins from a single DNA sequence (Pan et al., 2008). However, incorrect alternative splicing can also cause various diseases including cancer, muscular dystrophies, neurodegenerative diseases but also inherited retinal diseases (Tazi et al., 2009).

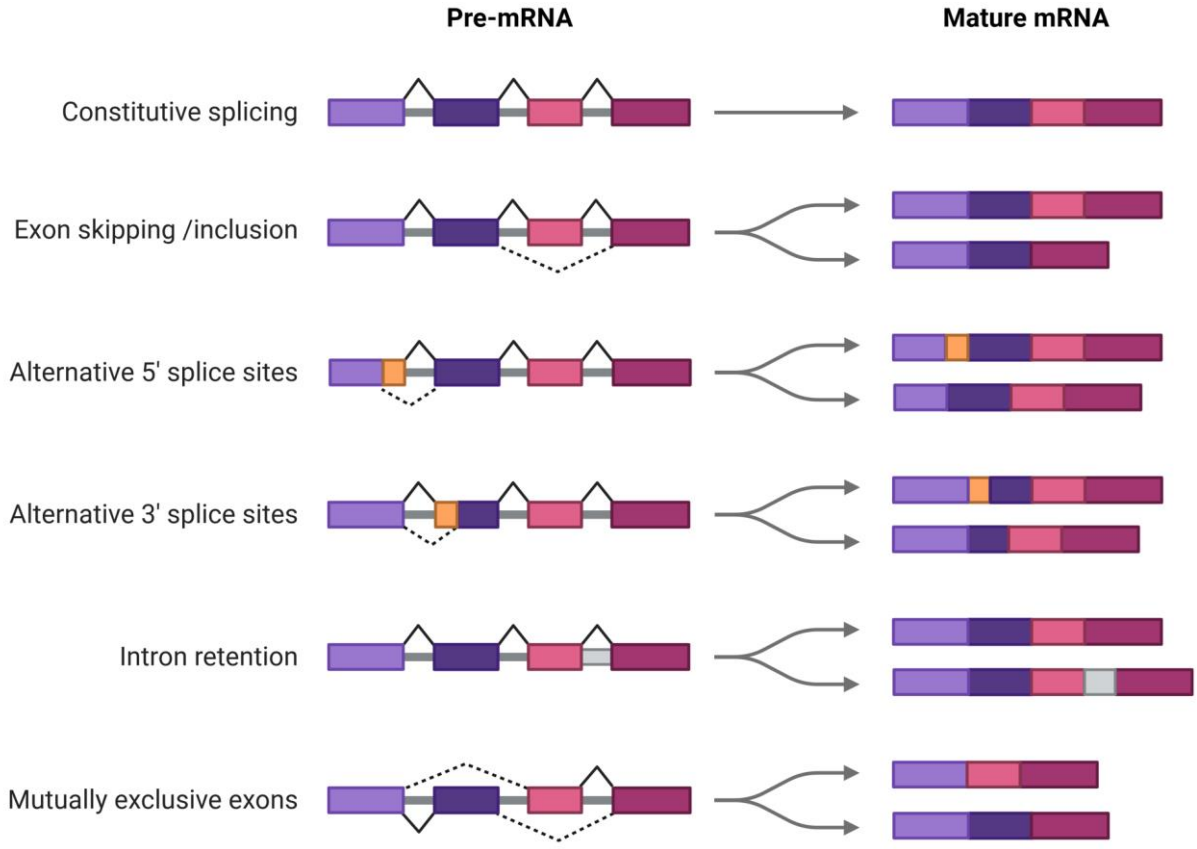

Figure 7: Constitutive and alternative splicing. Reprinted from "mRNA splicing types", by BioRender.com (2022). Retrieved from https://app.biorender.com/biorender-templates.

1.2.1 Missplicing induced by deep intronic mutations in *OPA1*

Defects in the splicing machinery, splicing factors or mutations in regulatory sequences can cause aberrant splicing. In 2021, Weisschuh et al. published an overview of likely pathogenic variants in the *OPA1* gene in a cohort of 755 index patients diagnosed with dominant optic atrophy. A total of 156 unique likely pathogenic variants were identified, of which 48 accounted for variants affecting splicing. Fourty-four of these were found in intronic sequences including 37 single nucleotide substitutions and 7 deletions, insertions or duplications affecting splice sites. The single nucleotide substitutions comprised 23 variants affecting canonical splice sites, 12 variants in the vicinity of canonical splice sites and two deep intronic variants. The described

variants are all predicted to cause aberrant splicing but with different underlying mechanisms. Some variants were shown to activate cryptic splice sites which are usually suppressed, others were shown to result in skipping of an exon or inclusion of a pseudoexon. The latter was associated with the two deep intronic variants.

Until now, most pathogenic variants have been found in coding regions or exon-flanking intronic regions, as genetic diagnostics focused mainly on these regions. Usually disease-causing variants are mainly located in coding exons or flanking sequence regions. By now, it is known that variants located deep within intronic regions can also be linked to a variety of diseases, demonstrating the importance of prospective whole genome sequencing in genetic diagnostics (Vaz-Drago et al., 2017). The majority of deep intronic mutations are associated with the activation of a cryptic splice site and the following inclusion of a pseudoexon in the mature mRNA resulting in a premature termination codon and aberrant transcript formation. In 2014, Bonifert et al. first reported a deep intronic mutation in the *OPA1* gene found in patients from a family with Behr syndrome-like symptoms including near-blind vision, cerebellar ataxia, external ophthalmoplegia, peripheral neuropathy, muscle atrophy, ptosis and spasticity. Interestingly, the mother as well as the father and three of six children did not show disease symptoms whereas the other three siblings showed a severe form of multisystemic neurodegeneration. Exon sequencing of candidate genes followed by intron sequencing of *OPA1* revealed the presence of the missense variant c.1311A>G;p.(Ile437Met) and the deep intronic mutation c.610+364G>A. Both variants were found in compound heterozygous state in the three siblings with Behr syndrome (Figure 8). The father was homozygous for the missense variant while the mother was carrying the deep intronic mutation in heterozygous state. The three unaffected siblings inherited only the missense mutation from the father.

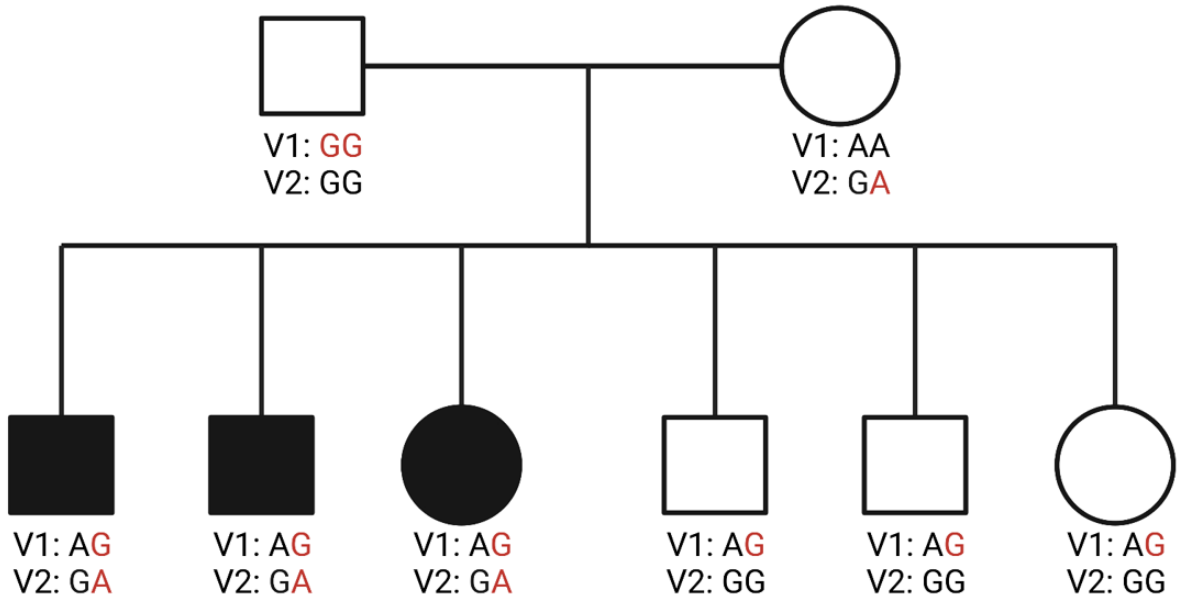

Figure 8: Pedigree of family OAK 587. The unaffected father was shown to be homozygous for the missense variant c.1311A>G;p.(Ile437Met) (V1) in *OPA1*. The unaffected mother harbors the deep intronic mutation c.610+364G>A (V2) in *OPA1* in heterozygous state. Three of their children are affected by Behr syndrome and inherited the missense variant from the father and the deep intronic mutation from the mother. The three unaffected children inherited only the missense variant from the father. Adapted from Bonifert et al., 2014. Created with BioRender.com.

Since neither the father nor the three children were showing disease symptoms, the missense mutation did not appear to be pathogenic even in homozygous state. To explain the severe phenotype, Bonifert et al. hypothesized that the missense variant acts as an intralocus modifier that, in combination with the deep intronic mutation, causes a severe form of dominant optic atrophy plus, or in the present case, Behr syndrome. The underlying disease mechanism of the deep intronic mutation is based, as in most cases, on the activation of a cryptic acceptor splice site, which is usually not recognized by the splicing machinery. The activated splice site results in the expression of aberrant transcripts including a pseudoexon, leading to a frameshift and a premature termination codon (Figure 9). The aberrant transcripts most likely undergoe nonsense-mediated mRNA decay leading to reduced protein levels of OPA1 and an impaired mitochondrial network (Bonifert et al., 2014). The disease phenotype is eventually caused by haploinsufficiency.

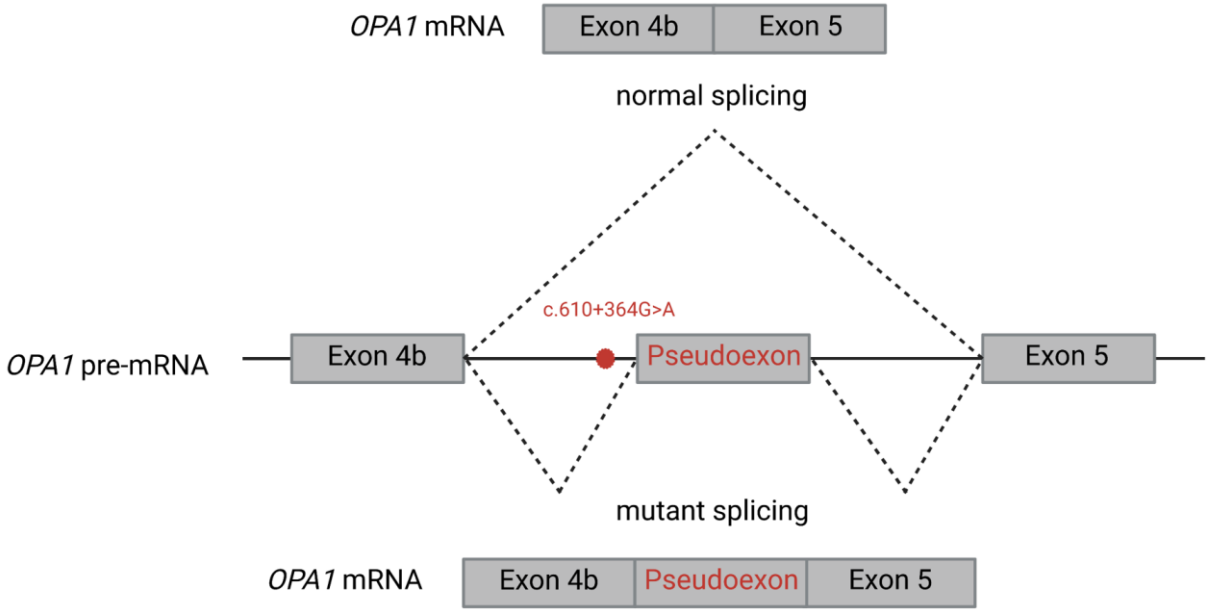

Figure 9: Scheme of the aberrant transcript formation due to the deep intronic mutation c.610+364A>G in *OPA1*. The deep intronic mutation is located between exon 4b and exon 5 of the *OPA1* gene and activates a cryptic acceptor splice site resulting in aberrant splicing of the pre-mRNA. This leads to the inclusion of a pseudoexon in the mature mRNA harboring a premature termination codon. In case of normal splicing the pseudoexon is not included in the mature mRNA. Exons and introns are not drawn to scale. Adapted from Bonifert et al., 2014. Created with BioRender.com.

1.3 The CRISPR/Cas9 machinery

CRISPR is the abbreviation for "clustered regularly interspaced short palindromic repeats" and describes a method which is based on the adaptive immune response of bacteria against viruses (bacteriophages) (Barrangou et al., 2007; Jansen et al., 2002; Makarova et al., 2006; Mojica et al., 2005) (Figure 10). Bacteriophages inject their DNA into bacteria to replicate themselves. As a result of the adaptive immune response, part of the virus DNA is inserted into genetic loci of the bacteria. This genetic loci is defined by a series of repeats which are separated by spacers including the viral DNA sequence (Ishino et al., 1987). This genetic loci is transcribed into a RNA sequence, known as crRNA (Brouns et al., 2008). Upon re-infection with bacteriophages, the viral DNA is recognized since the spacer sequence of the crRNA is complementary to the viral DNA. The Cas9 nuclease binds the repeat sequence of the crRNA and cuts the viral DNA thereby preventing the replication of the bacteriophages (Gasiunas et al., 2012). The function of the Cas9 nuclease is also dependent on the presence of the protospacer adjacent motif (PAM) in the target DNA (Gasiunas et al., 2012; Mojica et al., 2009). The PAM of Cas9 can be any nucleotide followed by two guanines (NGG). Cas9 nuclease cuts approximately three nucleotides upstream of the PAM sequence (Garneau et al., 2010). Besides the Cas9 protein family,

there are over 40 other Cas families which are divided into two classes (Haft et al., 2005). Class I nucleases are formed from a complex of effector proteins, whereas class II nucleases consist of a single effector protein (Nishimasu & Nureki, 2017). Cas9 belongs to the class II proteins and is the most commonly used Cas nuclease in research. In addition to the crRNA and the Cas9 nuclease, a functional CRISPR complex also contains a trans-acting crRNA, short tracrRNA (Deltcheva et al., 2011). Part of the tracrRNA is complementary to the crRNA. Through binding of the tracrRNA to the crRNA, a stabilized, active CRISPR complex is formed.

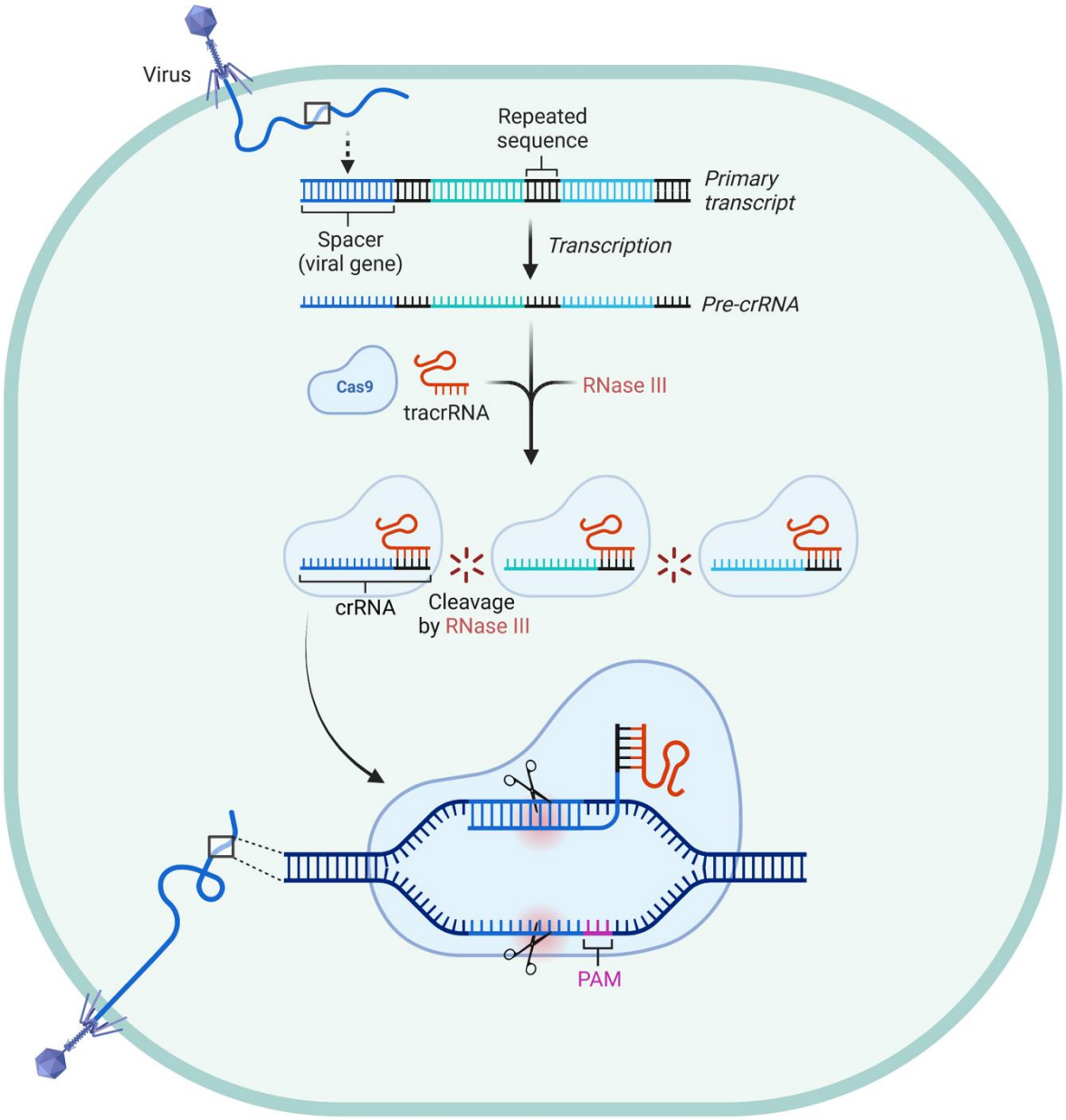

Figure 10: Adaptive immune response of bacteria against bacteriophages using CRISPR/Cas. Upon infection, viral DNA is inserted as spacer into the CRISPR locus. After transcription of the CRISPR locus, the resulting crRNA is forming a complex with tracrRNA and Cas9 enzyme. The RNA duplex is further processed by RNase III. Viral DNA is recognized and cleaved by the CRISPR complex after re-infection with bacteriophages. Adapted from

"Streptococcus´adaptive immune system against viruses: CRISPR-Cas9", by BioRender.com (2022). Acknowledgement: Brady Cress PhD, Lucie Bardet et al., Doudna Lab. Retrieved from https://app.biorender.com/biorender-templates.

In 2012, Emmanuelle Charpentier, Jennifer Doudna and colleagues demonstrated that the CRISPR principle can be used to specifically cut and change a target DNA sequence in the genome of bacteria. For this purpose, a single RNA combining crRNA and tracrRNA, called guide RNA (gRNA) can be used (Jinek et al., 2012). This gRNA is complementary to the target sequence and can easily be exchanged, thus enabling cutting of any desired DNA sequence. In 2013, Cong and colleagues demonstrated that the CRISPR system is also applicable in eukaryotic cells (Cong et al., 2013). To edit the genome using the CRISPR/Cas9 system, a gRNA is custom-designed *in silico* depending on the target sequence. The gRNA and the Cas9 nuclease can be delivered to target cells either directly as ribonucleoproteins or indirectly via plasmid expression. The Cas9-generated cut creates a double-strand break in the DNA. The double-strand break activates repair mechanisms of the cell, primarily through non-homologous end joining (NHEJ), or homology-directed repair (HDR) (Cong et al., 2013) (Figure 11). NHEJ rejoins the separated DNA strands whereby errors often occur. Due to those errors, the resulting DNA sequence harbors variable deletions, insertions or a combination of both (indels) (Chang et al., 2017). HDR uses a template sequence to repair DNA and is therefore more accurate compared to NHEJ. By applying CRISPR/Cas9, a targeted region of the DNA can be removed and repaired by NHEJ or altered and replaced by HDR through the addition of a DNA template (Hryhorowicz et al., 2017).

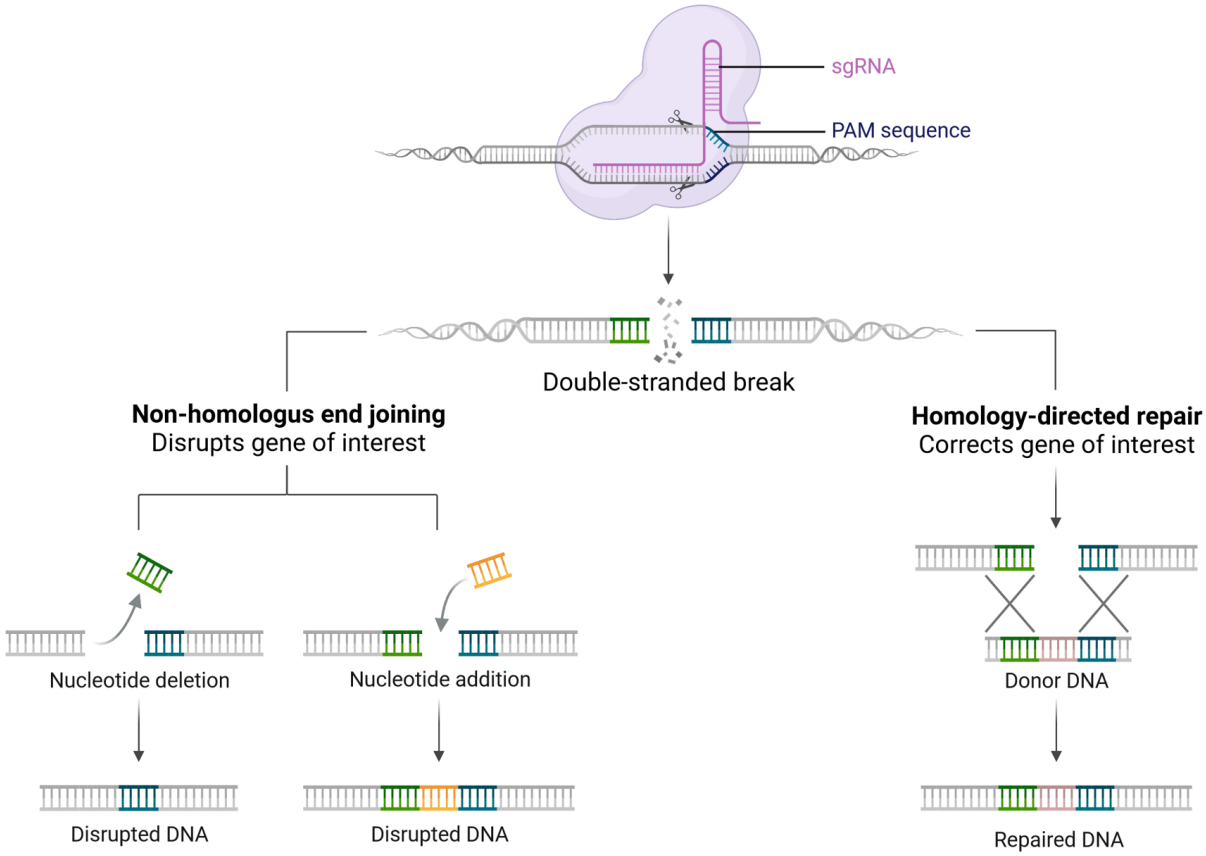

Figure 11: CRISPR-induced DNA repair mechanisms. CRISPR-induced double-strand breaks are repaired by non-homologous end joining (NHEJ) resulting in the formation of deletions, insertions or indels. If a homologous DNA template is available, the disrupted DNA is repaired by homology-directed repair (HDR) with integration of the template. Adapted from "CRISPR/Cas9 gene editing", by BioRender.com (2022). Acknowledgement: Esmeé Dragt. Retrieved from https://app.biorender.com/biorender-templates.

Nowadays, CRISPR genome editing is applied in a wide variety of research fields, including food production, parasite eradication, generation of disease models, tissue engineering or cell-based therapies (Chen et al., 2019; Janssen et al., 2018; Li et al., 2015; Liu et al., 2017). The first clinical trial using CRISPR/Cas9 started in 2019 and targets the deep intronic mutation c.2991+1655A>G in the *CEP290* gene, which is the most common gene mutation found in patients with Leber congenital amaurosis, a congenital retinal dystrophy (Sheck et al., 2018). The deep intronic mutation creates a cryptic donor splice site resulting in the inclusion of a pseudoexon, harboring a premature termination codon, in the mRNA (den Hollander et al., 2006). To target the deep intronic mutation in patients, an adeno-associated virus (AAV) expressing the Cas9 enzyme and *CEP290*-specific gRNAs is injected subretinally ("First CRISPR therapy dosed," 2020). The approach was previously tested in mice and non-human primates with successful editing of the *CEP290* gene (Maeder et al., 2019).

However, the CRISPR/Cas9 method is also prone to errors and is often associated with so-called off-target effects, meaning that the system frequently also cuts at non-specific sites in the genome evoking unwanted mutations (Yee, 2016). For this reason, further improvement of the CRISPR method is necessary to be widely applied in human gene therapy approaches.

1.3.1 CRISPR genome editing using Cas9 nickase

To date, Cas9 is the most commonly used Cas protein in the field of genome engineering. One reason for this is that Cas9 only requires a short and simple PAM sequence (NGG). The nuclease can be isolated from a variety of bacteria, but the most widely used Cas9 originates from the bacterium *Streptococcus pyogenes* (SpCas9). Also commonly used and well studied is the Cas9 protein from *Staphylococcus aureus* (SaCas9). However, SaCas9 only cuts the target DNA sequence in the presence of the more complex PAM sequence NNGRRT (Ran et al., 2015). A significant advantage of SaCas9 over SpCas9 is its small size. At 3159 bp and 1053 aa, SaCas9 is nearly 1 kb smaller than SpCas9 (4104 bp, 1368 aa), allowing for easy *in vitro* and *in vivo* delivery by viral vectors such as AAV, whose packaging capacity is limited to approximately 4.7 kb (Grieger & Samulski, 2005; Kim et al., 2017). In a recent study, SaCas9 was used to improve hearing loss in a mouse model harboring a mutation in the myosin VI gene Myo6$^{WT/C442Y}$ mice exhibit hearing loss consistent with the phenotype of human patients. The injection of AAV vectors expressing SaCas9 and a respective gRNA in Myo6$^{WT/C442Y}$ mice resulted in rescued auditory function up to 5 months post injection (Xue et al., 2022).

In addition to naturally occurring Cas9 variants, there are also a number of genetically engineered Cas9 alternatives that have been developed to improve certain properties of the wild-type Cas9 protein for genome editing. A drawback of the relative simple NGG PAM sequence of SpCas9 is the increased risk of off-target effects (Zhang et al., 2015). In order to increase the specificity of SpCas9, a Cas9 nickase variant was developed (Cong et al., 2013; Ran et al., 2013). The Cas9 variant was generated by introducing mutations in its endonuclease domain: the D10A mutation inactivates the RuvC domain and H840A inactivates the HNH domain of Cas9 (Figure 12). HNH usually catalyses cleavage of the crRNA complementary target DNA strand, whereas RuvC cuts the non-targeted DNA strand. Inactivation of one domain results in the formation of single strand nicks instead of double-strand breaks. To create double-strand breaks, two gRNAs are required to target the respective DNA strands.

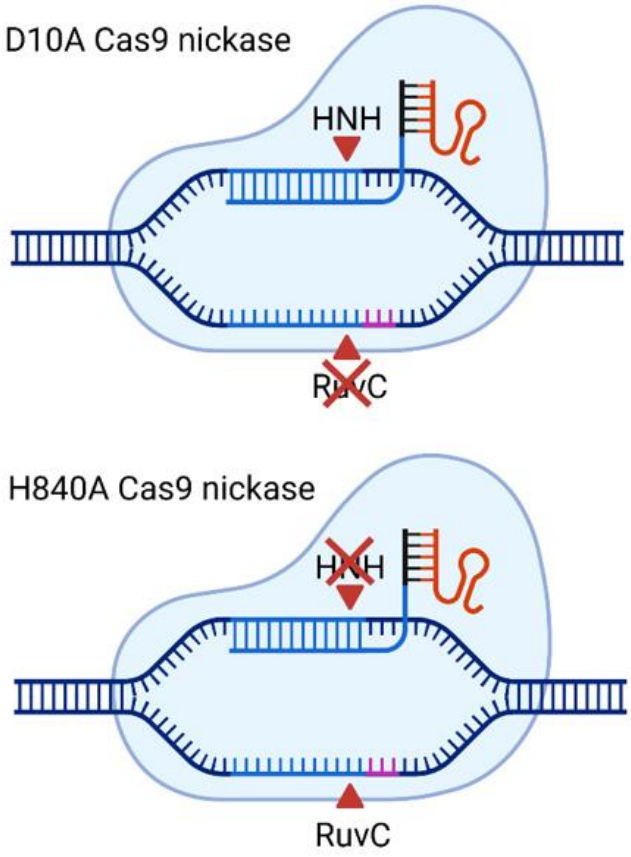

Figure 12: Cas9 nickase variants. The D10A mutation inactivates the RuvC domain of Cas9, whereas H840A inactivates the HNH domain. Adapted from "Streptococcus´adaptive immune system against viruses: CRISPR-Cas9", by BioRender.com (2022). Acknowledgement: Brady Cress PhD, Lucie Bardet et al., Doudna Lab. Retrieved from https://app.biorender.com/biorender-templates.

Since the function of Cas9 nickase is dependent on the use of a gRNA pair, the number of off-targets is reduced, making the Cas9 variant a powerful tool for genome engineering, particularly in the context of clinical CRISPR applications. To increase the efficacy of the CRISPR/Cas9 nickase strategy, the gRNA pairs should be designed so that their protospacer motifs are far apart (PAM-out) rather than in close proximity to each other (PAM-in). In addition, a distance of 40-68 nt for Cas9 nickase D10A and 51-68 nt for Cas9 nickase H840A was shown to increase the editing efficacy to over 50% (Schubert et al., 2021). In 2018, Gopalappa et al. investigated the cleavage efficacy of D10A Cas9 nickases in comparison to H840A Cas9 nickases in mammalian cells. The D10A variant was associated with a significantly higher indel frequency than the H840A variant, indicating a higher cleavage activity of the HNH domain compared with the RuvC domain (Gopalappa et al., 2018). Schubert et al. also demonstrated a higher efficiency in D10A-mediated HDR than in H840A-mediated HDR (Schubert et al., 2021). Recently, the successful application of CRISPR/Cas9 D10A nickase was reported in an *in vitro* model of

mucopolysaccharidosis IVA (MPS IVA), an inherited lysosomal disease associated with mutations in a gene encoding the GALNS enzyme (Leal & Alméciga-Díaz, 2022). In their work, they describe the knock-in of an expression cassette with GALNS cDNA in patient-derived fibroblasts using HDR. The CRISPR approach resulted in a long-term increase of the GALNS activity.

1.3.2 CRISPR genome editing using Cpf1

Besides Cas9, there are other naturally occurring Cas nucleases such as Cpf1, nowadays also known as Cas12a. In contrast to Cas9, Cpf1 uses a T-rich PAM sequence and is therefore particularly suitable for AT-rich target regions. Cpf1 was originally identified in the genus of *Prevotella* and *Francisella* bacteria (Schunder et al., 2013). In 2015, Zetsche et al. identified two Cpf1 enzymes from the bacteria *Acidaminococcus* (AsCpf1) and *Lachnospiraceae* (LbCpf1), which proved to be efficient for genome editing in human cells. Besides the PAM, Cpf1 also differs from Cas9 in terms of its structure and cleavage site (Figure 13). Cpf1 only requires a crRNA and functions without the involvement of a tracrRNA (Zetsche et al., 2015). In addition, Cpf1 cuts approximately 20 nucleotides downstream of the recognition site and generates sticky ends instead of blunt ends as in Cas9.

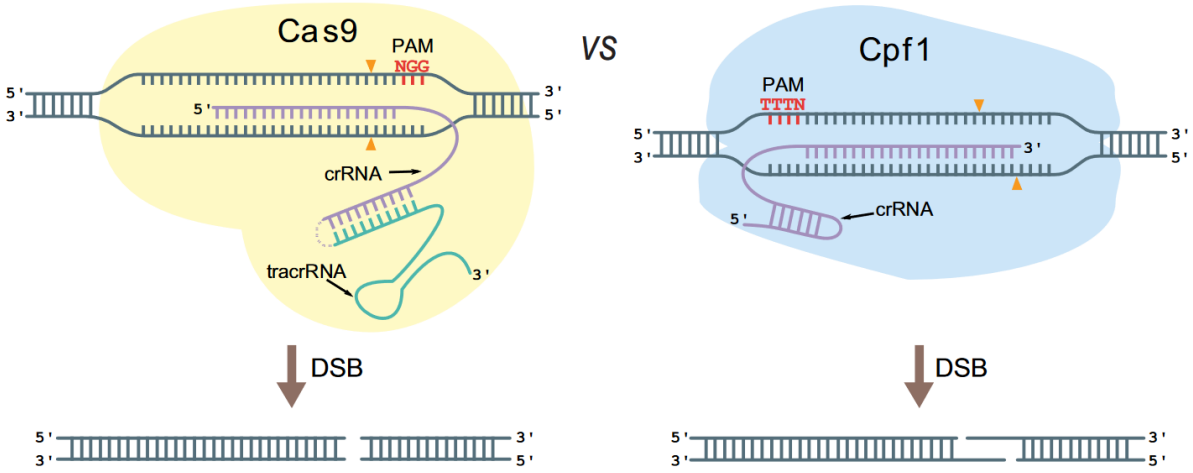

Figure 13: Comparison of Cas9 and Cpf1 nuclease. DSB, double strand break. Reproduced from Vanegas et al., 2019.

With a size of 1228 aa for LbCpf1 and 1307 aa for AsCpf1, the nuclease is slightly smaller than SpCas9 (1368 aa) (Alok et al., 2020). Since Cpf1 uses a single RNA molecule, the size of the gRNA is also reduced compared to Cas9. The aforementioned properties facilitate the delivery of Cpf1 into target cells or organisms. The activity of Cpf1 also has a lower number of off-targets compared to Cas9, providing a higher level of safety for clinical applications (Kim et

al., 2016; Kleinstiver et al., 2016). CRISPR/Cpf1 is widely used in plant genome editing, but is also increasingly being used in therapeutic research (Alok et al., 2020; Ding et al., 2022). Zhang and colleagues first reported on a Cpf1-based correction of mutations in patient-derived induced pluripotent stem cells (iPSCs) and an animal disease model of Duchenne muscular dystrophy (DMD) (Zhang et al., 2017). DMD is an inherited disease associated with mutations in the dystrophin gene and can result in lethal cardiomyopathy. Zhang et al. differentiated the Cpf1-corrected iPSCs into cardiomyocytes and obtained a restored dystrophin expression and improved cardiomyocyte function.

1.4 Induced pluripotent stem cells in basic and therapeutic research

Induced pluripotent stem cells (iPSCs) can be generated from various somatic cell types by reprogramming. The term pluripotency describes the ability of stem cells to further differentiate into almost all cell types of the three germ layers. The properties of iPSCs make them a valuable tool for basic and therapeutic research.

In 2006, Takahashi and Yamanaka demonstrated that mouse embryonic or adult fibroblasts can be reprogrammed into induced pluripotent stem cells by the addition of certain transcription factors to the cell culture, including Oct3/4, Sox2, c-Myc, Klf4 (Takahashi & Yamanaka, 2006). In 2007, the first direct reprogramming of human cells was reported (Takahashi et al., 2007; Yu et al., 2007), followed by the first generation of disease-specific iPSCs in 2008 (Dimos et al., 2008; Park et al., 2008). The first clinical study using iPSCs was conducted in 2014 in Japan. In this study, autologous iPS cells were differentiated into retinal epithelium cells (RPEs) and transplanted into patients with age-related macular degeneration (AMD), resulting in improved vision (Kim et al., 2022; Takahashi, 2013).

One of the most common cell types used for reprogramming are fibroblasts which can be easily obtained from skin biopsies (González et al., 2011). In addition, keratinocytes from hair follicles, or blood cells are frequently used as donor cells. The reprogramming factors are nowadays mainly delivered using non-integrating methods such as episomal vectors, Sendai virus or mRNA. Episomal vectors are non-integrating vectors based on the sequence of BK virus, bovine papilloma virus 1 and Epstein-Barr virus and are characterized by stable extrachromosomal replication (Van Craenenbroeck et al., 2000). The Sendai virus is a respiratory virus usually infecting rats and mice. The RNA virus does not integrate into the host genome, can be used for reprogramming of a range of cell types and has a high transduction efficiency (Malik &

Rao, 2013). Another delivery method is the transfection of transcripts using modified RNA. Comparison of the non-integrating methods revealed that mRNA delivery is characterized by a higher transfection efficacy, lower aneuploidy rate, quicker reprogramming and lower number of required input cells compared to the other methods (Schlaeger et al., 2015). However, the reliability was significantly higher for the Sendai virus and episomal vector method, and the work load was also less compared with mRNA transfection.

Nowadays, iPSCs are used as models in developmental biology, as disease models, in drug screening, in cell therapies or in the development of personalized medicine (Diecke et al., 2014) (Figure 14). The combination of the iPSC and CRISPR/Cas technology opens up a new therapeutic strategy (Hockemeyer & Jaenisch, 2016). Patient-derived somatic cells can be reprogrammed into iPSCs that are genetically modified *in vitro* with CRISPR/Cas9 to correct a gene mutation, for example. The CRISPR-edited iPSCs can be further differentiated in any cell type of interest and transplanted into the patient or used for further investigations. One of the first gene therapeutic studies that combined CRISPR/Cas and iPSCs was conducted in 2015 (Li et al., 2015). In this study, iPSCs were derived from patients suffering from DMD. The underlying mutation in the dystrophin gene was corrected by CRISPR-induced editing of the patient-derived iPS cells. The edited iPSCs were further differentiated into skeletal muscle cells which showed restored levels of the dystrophin protein. A subsequent study in which iPSCs were differentiated into cardiomyocytes was performed by Zhang et al. as described in chapter 1.3.2.

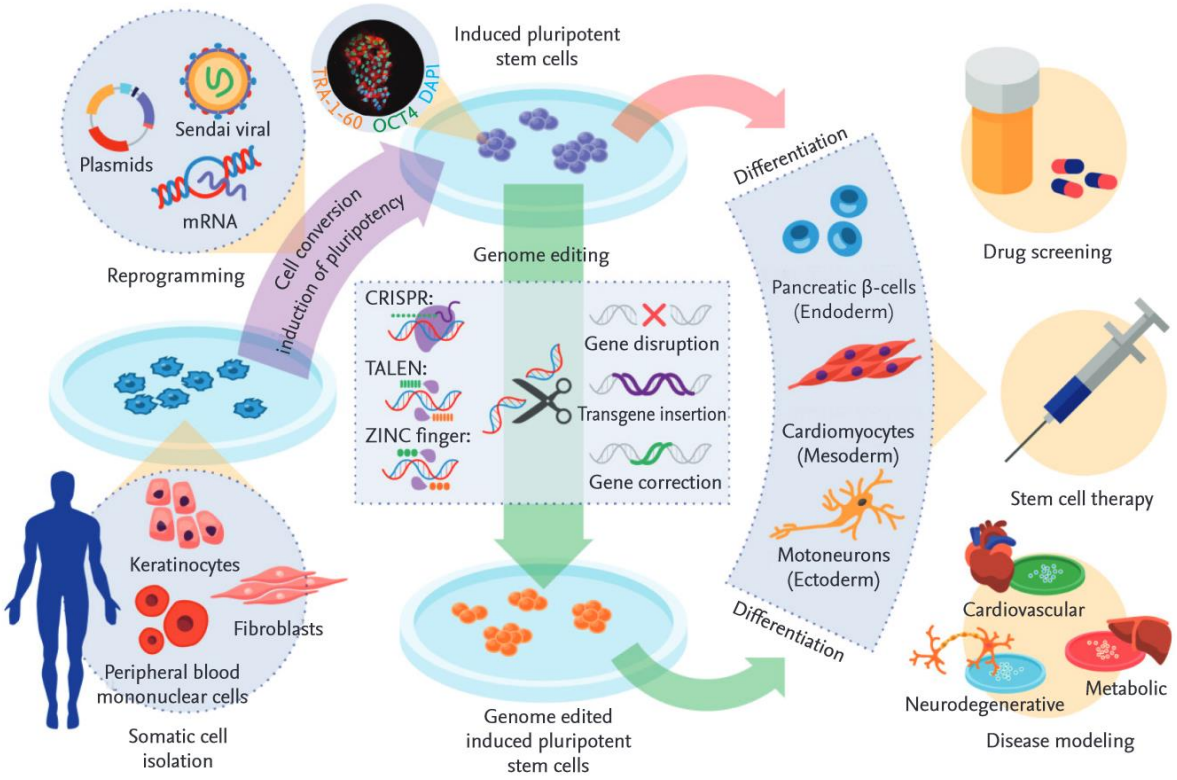

Figure 14: Induced pluripotent stem cells in disease modelling and therapeutic research. Induced pluripotent stem cells (iPSCs) are generated by reprogramming of somatic cells from patients using defined factors which are delivered with plasmids, viral vectors or mRNA. The generated patient-derived iPSCs can be directly differentiated into various cell types of interest and used as disease models, for drug screening or therapeutic approaches. Prior to differentiation, gene mutations can be corrected using genome editing approaches in patient-derived iPSCs. Reproduced from Diecke et al. 2014.

1.5 Aim of the project

1.5.1 Main project of this thesis: CRISPR genome editing of patient-derived iPSCs to rescue missplicing induced by *OPA1* deep intronic mutation c.610+364G>A.

The main aim of this thesis was to establish and validate CRISPR-based genome editing in patient-derived iPSCs to rescue a splicing defect caused by the deep intronic variant c.610+364G>A in *OPA1*. This variant in combination with a modifier allele causes a severe Behr syndrome phenotype due to the inclusion of a pseudoexon in the transcript (see 1.2.1 Missplicing induced by deep intronic mutation in *OPA1*). In 2016, Bonifert and colleagues aimed to restore splicing in patient-derived fibroblasts harboring the c.610+364G>A variant (Bonifert et al., 2016). They achieved a splice correction of 55% by transfecting antisense oligonucleotides (AONs) that were designed to bind the pre-mRNA at either the site of the cryptic splice acceptor or the putative cryptic branch point. In my thesis, I aimed to explore further

strategies to rescue missplicing induced by the deep intronic mutation c.610+364G>A in *OPA1*, focusing on CRISPR/Cas genome editing in patient-derived induced pluripotent stem cells, followed by *OPA1* transcript analysis, relative quantification of OPA1 protein and morphological analysis of mitochondria. To generate iPSCs, fibroblasts were isolated from a skin biopsy from a patient harboring the DIM c.610+364G>A and the missense variant c.1311A>G; p.(Ile437Met) in *OPA1* compound heterozygously (Hauser et al., 2016). The patient-derived fibroblasts were reprogrammed using episomal vectors expressing *hOCT4*, *hSOX2*, *hKLF4*, *hL-MYC* and *hLIN28*. Patient-derived iPSCs were generated by Stefan Hauser and colleagues at the German Center for Neurodegenerative Diseases (DZNE), Tuebingen, and kindly provided to us for the execution of this project.

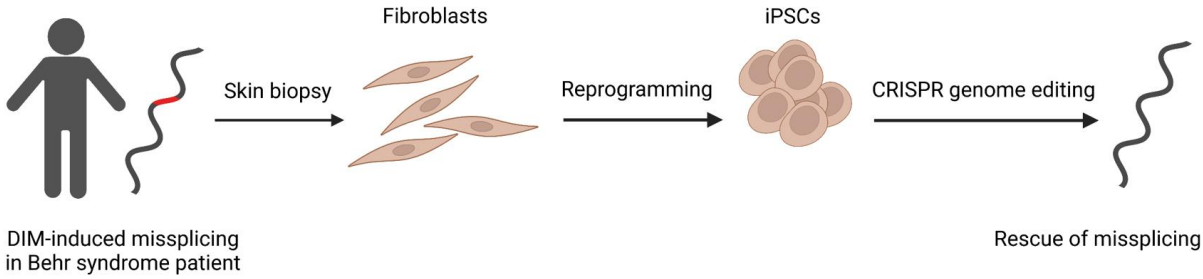

Figure 15: Rescue of DIM-induced missplicing in patient-derived iPSC using CRISPR genome editing. Fibroblasts were obtained from a skin biopsy from a Behr syndrome patient carrying the deep intronic mutation c.610+364G>A and the missense variant c.1311A>G;p.(Ile437Met) in *OPA1*. The fibroblasts were reprogrammed to generate patient-derived iPSCs which were subject to CRISPR genome editing. Created with BioRender.com.

1.5.2 Side project of this thesis: *DNAJC30* screening of patients with suspected Leber´s hereditary optic neuropathy and optic atrophy.

For a long time, Leber´s hereditary optic neuropathy was exclusively associated with mutations in genes encoded by the mitochondrial genome (see 1.1.1 Leber´s hereditary optic neuropathy). In 2021, Stenton et al. identified three missense variants (c.152A>G;p.(Tyr51Cys), c.232C>T;p.(Pro78Ser), c.302T>A;p.(Leu101Gln)) in the nuclear-encoded gene *DNAJC30* causing an autosomal recessive form of LHON (arLHON). To investigate the genetic cause of our previously unexplained Central European cohort of 800 patients with suspected LHON, we screened the entire *DNAJC30* gene for putative pathogenic variants. In addition, we included genetically unexplained cases of 402 patients diagnosed with optic atrophy (OA), since optic atrophy and LHON are both inherited optic neuropathies with a similar disease phenotype. Retrospective *DNAJC30* screening of 1202 patients with LHON or OA was performed in

collaboration with Ting Xiao, Institute for Ophthalmic Research, University Hospital Tuebingen, with equal division of labor.

2 Material

2.1 Instruments

Analytical balance Entris	Sartorius AG, Göttingen, Germany
AxioCam MRm	Carl Zeiss AG, Oberkochen, Germany
Axio Imager Z1	Carl Zeiss AG, Oberkochen, Germany
CCD camera (Model B-139-3U7N)	Herolab GmbH Laborgeräte, Wiesloch, Germany
Centrifuge 5702	Eppendorf, Hamburg, Germany
Centrifuge Sigma 4-16k	Sartorius AG, Göttingen, Germany
CO2 incubator Heracell VIOS 160i	Thermo Fisher Scientific, Waltham, MA, USA
CO2 incubator CB210	Binder GmbH, Tuttlingen, Germany
Cryogenic freezer MVE TEC 3000	Chart Industries Inc., Ball Ground, GA, USA
Electronic Multistep & Multichannel pipettes	INTEGRA Biosciences GmbH, Biebertal, Germany
Electrophoresis chamber/combs	BioRad Laboratories GmbH, München, Germany
Electrophoresis power supply Consort E802	MERCK KGaA, Darmstadt, Germany
Electrophoresis power supply PowerPac Universal/3000	BioRad Laboratories GmbH, München, Germany
Fusion FX	Vilber Lourmat Deutschland GmbH, Eberhardzell, Germany
Genetic Analyzer ABIPRISM 3130xl	Applied Biosystems, Waltham, MA, USA
Heating block	Bachofer GmbH & Co. KG, Weilheim an der Teck, Germany
Imaging System EVOS XL Core	Invitrogen AG, Carlsbad, CA, USA
Incubation shaker Infors HAT Minitron	INFORS HT Germany, Einsbach, Germany
Incubator Heraeus B6060	Thermo Fisher Scientific, Waltham, MA, USA
Inverted Fluorescence Microscope Axio Vert.A1	Carl Zeiss AG, Oberkochen, Germany

Inverter microwave	Sharp Electronics GmbH, Hamburg, Germany
Magnetic stirrer IKAMAG RCT/RCT basic/RH basic	IKA Werke, Staufen im Breisgau, Germany
Medical Printer P95	Mitsubishi Electric Corporation, Tokyo, Japan
Micro centrifuge Heraeus Fresco 21	Thermo Fisher Scientific, Waltham, MA, USA
Mini centrifuge Color Sprout Plus	Biozym Scientific GmbH, Hessisch Oldendorf, Germany
Mini-PROTEAN 3 Cell	BioRad Laboratories GmbH, München, Germany
Mini Trans-Blot Cell	BioRad Laboratories GmbH, München, Germany
Mixer 5432	Eppendorf, Hamburg, Germany
Multichannel pipette Biohit Proline	Sartorius AG, Göttingen, Germany
Multifuge Heraeus 1L-R	Thermo Fisher Scientific, Waltham, MA, USA
Multimode plate reader Tecan SPARK 10M	Tecan Deutschland GmbH, Crailsheim, Germany
Multistep pipette Multipette M4	Eppendorf, Hamburg, Germany
Neon Transfection System	Thermo Fisher Scientific, Waltham, MA, USA
pH Meter SevenMulti	Mettler-Toledo, Giessen, Germany
Pipette controller PIPETBOY Pro	INTEGRA Biosciences GmbH, Biebertal, Germany
Pipettes PIPETMAN	Gilson Germany, Limburg-Offheim, Germany
Precision balance BL 610	Sartorius AG, Göttingen, Germany
PyroMark Q96 ID	Qiagen N.V., Hilden, Germany
PyroMark Q96 Vacuum Workstation	Qiagen N.V., Hilden, Germany
Roll mixer RS-TR 05	Phoenix Instrument GmbH, Garbsen, Germany
Safety cabinet	BDK Luft-und Reinraumtechnik GmbH, Sonnenbühl, Germany

Safety cabinet MSC-Advantage	Thermo Fisher Scientific, Waltham, MA, USA
Spectrophotometer Nanodrop ND-1000	PEQLAB Biotechnologie GmbH, Erlangen, Germany
Spectrophotometer TRINEAN Xpose	Unchained Labs Germany GmbH, Berlin, Germany
Thermal cycler Veriti 96-well	Applied Biosystems, Waltham, MA, USA
Thermomixer Comfort	Eppendorf, Hamburg, Germany
UV transilluminator	Bachofer GmbH & Co. KG, Weilheim an der Teck, Germany
VACUSAFE	INTEGRA Biosciences GmbH, Biebertal, Germany
Vortex-Genie 2	Scientific Industries Inc., Bohemia, NY, USA
Waterbath HAAKE Fisons D1-G	Thermo Fisher Scientific, Waltham, MA, USA
Waterbath IKA TS2	IKA Werke, Staufen im Breisgau, Germany
Waterbath Julabo F30-HC	JULABO GmbH, Seelbach, Germany

2.2 Chemicals

2-β-Mercaptoethanol	Carl Roth GmbH & Co.KG, Karlsruhe, Germany
4’,6-Diamino-2-phenylindole (DAPI)	Invitrogen AG, Carlsbad, CA, USA
Agar *bacteriological grade*	MP Biochemicals Germany GmbH, Eschwege, Germany
Amphotericin B (100x)	MERCK, Darmstadt, Germany
Ampicillin sodium salt	Fluka, Sigma Aldrich Chemie GmbH, Stein-heim, Germany
Bacto-Tryptone	AppliChem, Darmstadt, Germany
Betaine	Sigma Aldrich Chemie GmbH, Steinheim, Germany
Blotting-Grade Blocker	BioRad Laboratories GmbH, München, Germany

Boric acid	Carl Roth GmbH & Co.KG, Karlsruhe, Germany
Bromophenol blue sodium salt	Carl Roth GmbH & Co.KG, Karlsruhe, Germany
Carbenicillin di-sodium salt	Applichem GmbH, Darmstadt, Germany
Dithiothreitol (DTT)	Carl Roth GmbH & Co.KG, Karlsruhe, Germany
DMSO (Dimethylsulphoxide)	Sigma Aldrich Chemie GmbH, Steinheim, Germany
EDTA, Di-sodium salt dihydrate	Carl Roth GmbH & Co.KG, Karlsruhe, Germany
Ethanol absolute for analysis	AppliChem, Darmstadt, Germany
Ethidium bromide	Carl Roth GmbH & Co.KG, Karlsruhe, Germany
Ficoll	Amersham Pharmacia Biotech, Freiburg, Germany
Gelatine	MERCK, Darmstadt, Germany
Glycerol	Carl Roth GmbH & Co.KG, Karlsruhe, Germany
Glycine	Carl Roth GmbH & Co.KG, Karlsruhe, Germany
Kanamycin	Carl Roth GmbH & Co.KG, Karlsruhe, Germany
LE-Agarose SeaKem	Biozym Scientific GmbH, Oldendorf, Germany
Magnesium chloride hexahydrate	MERCK, Darmstadt, Germany
Methanol (100%)	Honeywell, Morristown, NJ, USA
MOPS	Carl Roth GmbH & Co.KG, Karlsruhe, Germany
Nonidet®-P 40	Fluka, Sigma Aldrich Chemie GmbH, Steinheim, Germany
Nuclease-free water	Thermo Fisher Scientific, Waltham, MA, USA
Paraformaldehyde solution, 4% in PBS	Santa Cruz Biotechnology, Inc., Heidelberg, Germany
Ponceau-S	Sigma Aldrich Chemie GmbH, Steinheim, Germany

Potassium chloride	Sigma Aldrich Chemie GmbH, Steinheim, Germany
Sodium chloride	VWR International GmbH, Darmstadt, Germany
Sodium deoxycholate	Fluka, Sigma Aldrich Chemie GmbH, Steinheim, Germany
Sodium dodecyl sulfate (SDS)	Sigma Aldrich Chemie GmbH, Steinheim, Germany
TritonX-100	AppliChem, Darmstadt, Germany
Trizma-Base	Sigma Aldrich Chemie GmbH, Steinheim, Germany
Trizma-HCl	Sigma Aldrich Chemie GmbH, Steinheim, Germany
Tween 20	Sigma Aldrich Chemie GmbH, Steinheim, Germany
Xylene cyanol	BioRad Laboratories GmbH, München, Germany
Yeast extract	AppliChem, Darmstadt, Germany

2.3 Commercial reagents and media

10-beta/Stable Outgrowth Medium	New England Biolabs GmbH, Frankfurt a.M., Germany
Adenosine 5´-Triphosphate (ATP)	New England Biolabs GmbH, Frankfurt a.M., Germany
Bovine Serum Albumin (BSA)	New England Biolabs GmbH, Frankfurt a.M., Germany
Cell Dissociation Buffer, Enzyme-free, PBS-based	Thermo Fisher Scientific, Waltham, MA, USA
CloneR Supplement	STEMCELL Technologies Germany GmbH, Köln, Germany
Cycloheximide solution (100 mg/mL in DMSO)	Sigma Aldrich Chemie GmbH, Steinheim, Germany
DAKO Fluorescent Mounting Medium	Agilent Technologies Deutschland GmbH, Waldbronn, Germany

dNTP-Mix (5mM dATP, dTTP, dCTP, dGTP)	peqLAB Biotechnologie GmbH, Erlangen, Germany
Dulbeccos`s Modified Eagle Medium (DMEM), high glucose, pyruvate, no glutamine	Thermo Fisher Scientific, Waltham, MA, USA
Dulbeccos`s Phosphate Buffered Saline (DPBS)	Thermo Fisher Scientific, Waltham, MA, USA
Dulbeccos`s Phosphate Buffered Saline (DPBS), calcium, magnesium	Thermo Fisher Scientific, Waltham, MA, USA
Essential 8 Flex Medium	Thermo Fisher Scientific, Waltham, MA, USA
Fetal Bovine Serum (FBS)	Thermo Fisher Scientific, Waltham, MA, USA
HI-DI Formamide	Applied Biosystems, Waltham, MA, USA
KnockOut Serum Replacement	Thermo Fisher Scientific, Waltham, MA, USA
Lipofectamine 3000/RNAiMAX/CRISPRMAX/Stem	Thermo Fisher Scientific, Waltham, MA, USA
Opti-MEM I	Thermo Fisher Scientific, Waltham, MA, USA
Penicillin/Streptomycin (100x)	Sigma Aldrich Chemie GmbH, Steinheim, Germany
Pierce ECL Western Blotting Substrate	Thermo Fisher Scientific, Waltham, MA, USA
Primocin	Invivogen, San Diego, CA, USA
Protease Inhibitor Cocktail Set III	Calbiochem, MERCK KGaA, Darmstadt, Germany
Protein Assay Dye Reagent Concentrate	BioRad Laboratories GmbH, München, Germany
QuickExtract DNA Extraction Solution, Lucigen	Biozym Scientific GmbH, Oldendorf, Germany
Q-PAGE Bis-Tris Precast Gel, SMOBIO	7BioScience, Neuenburg am Rhein, Germany

ReLeSR	STEMCELL Technologies Germany GmbH, Köln, Germany
RevitaCell Supplement	Thermo Fisher Scientific, Waltham, MA, USA
SOC Outgrowth Medium	New England Biolabs GmbH, Frankfurt a.M., Germany
StemPro Accutase	Thermo Fisher Scientific, Waltham, MA, USA
Streptavidin Sepharose High Performance beads	GE Healthcare GmbH, Solingen, Germany
Trypsin-EDTA (0.05%)	Thermo Fisher Scientific, Waltham, MA, USA
Vitronectin (VTN-N) Recombinant Human Protein, Truncated	Thermo Fisher Scientific, Waltham, MA, USA

2.4 Kits

Big Dye® Terminator v.3.1 Cycle Sequencing Kit	Applied Biosystems, Waltham, MA, USA
CloneJet PCR Cloning Kit	Thermo Fisher Scientific, Waltham, MA, USA
DNase I Kit	Sigma Aldrich Chemie GmbH, Steinheim, Germany
EndoFree Plasmid Maxi Kit	Qiagen N.V., Hilden, Germany
Maxima H Minus First Strand cDNA Synthesis Kit	Thermo Fisher Scientific, Waltham, MA, USA
QiaQuick PCR Purification Kit	Qiagen N.V., Hilden, Germany
MinElute Reaction Cleanup Kit	Qiagen N.V., Hilden, Germany
Monarch Plasmid Miniprep Kit	New England Biolabs GmbH, Frankfurt a.M., Germany
NucleoSpin Gel and PCR Clean up Kit	Macherey-Nagel, Düren, Germany

PCR Cloning Kit	New England Biolabs GmbH, Frankfurt a.M., Germany
peqGOLD Blood & Tissue DNA Mini Kit	VWR International GmbH, Darmstadt, Germany
peqGOLD Total RNA Kit	VWR International GmbH, Darmstadt, Germany
PyroMark Gold Q96 Reagents	Qiagen N.V., Hilden, Germany
SupreDye v.3.1 Cycle Sequencing Kit	BioCat GmbH, Heidelberg, Germany
TA Cloning Kit	Invitrogen AG, Carlsbad, CA, USA

2.5 Enzymes

DNA polymerases

LongAMP® Taq DNA Polymerase	New England Biolabs GmbH, Frankfurt a.M., Germany
PfuUltra HF DNA Polymerase	Agilent Technologies Deutschland GmbH, Waldbronn, Germany
Phusion® HF DNA Polymerase	Thermo Fisher Scientific, Waltham, MA, USA
Taq DNA Polymerase (5 U/µl)	ATG Biosynthetics, Merzhausen, Germany
Taq DNA Polymerase E	Genaxxon bioscience GmbH, Ulm Germany

Restriction enzymes

*Bbs*I, *Bsa*I-HF, *Bsm*BI_v2, *Dpn*I, *Eco*RV, *Spe*I, *Sap*I	New England Biolabs GmbH, Frankfurt a.M., Germany
*Bam*HI, *Not*I	Thermo Fisher Scientific, Waltham, MA, USA

Ligases

T4 DNA Ligase (40 U/µl)	New England Biolabs GmbH, Frankfurt a.M., Germany
T7 DNA Ligase (3000 U/µl)	McLab Headquarters, South San Francisco, CA, USA

Nucleases

ExoSAP-IT	Applied Biosystems, Waltham, MA, USA
Plasmid Safe ATP-Dependent DNase	Epicentre, Madison, WI, USA

Other enzymes

Alt-R®S.p. Cas9 D10A Nickase V3	Integrated DNA Technologies, Leuven, Belgium
Proteinase K	VWR International GmbH, Darmstadt, Germany
T4 Polynucleotide Kinase	Thermo Fisher Scientific, Waltham, MA, USA

2.6 Size standards

DNA size standard

λ/*Hin*d III	Fermentas GmbH, St. Leon-Rot, Germany
GeneRuler 1 kb DNA Ladder	Thermo Fisher Scientific, Waltham, MA, USA
GeneRuler 1 kb Plus DNA Ladder	Thermo Fisher Scientific, Waltham, MA, USA
GeneScan 500 ROX dye Size Standard	Applied Biosystems, Waltham, MA, USA
Low Molecular Weight DNA Ladder	New England Biolabs GmbH, Frankfurt a.M., Germany
pcDNA3.1 Zeo/Taq I = KEB (in house manufactured)	Established by Katja Köppen, Molecular Genetics Laboratory, Institute for Ophthalmic Research, Tuebingen, Germany

Protein size standard

Novex Sharp Pre-Stained Protein Standard	Invitrogen AG, Carlsbad, CA, USA
Yes Blot Western Marker I, SMOBIO	7BioScience, Neuenburg am Rhein, Germany

2.7 Plasmids

Table 1: Used plasmids

Vector	Description	Resistance	Source
Mito-meGFP	Fluorescence reporter vector	Kanamycin, Neomycin	Addgene (#172481), Depositing Lab: Thomas Schwarz
pCR2.1	Cloning vector	Ampicillin, Kanamycin	Thermo Fisher Scientific, Waltham, MA, USA

pJET1.2	Cloning vector	Ampicillin	Thermo Fisher Scientific, Waltham, MA, USA
pMiniT2.0	Cloning vector	Ampicillin	New England Biolabs GmbH, Frankfurt a.M., Germany
pSPL3	Splicing vector	Ampicillin	Invitrogen AG, Carlsbad, CA, USA (discontinued)
pX461	SpCas9n (D10A nickase mutant) vector	Ampicillin	Addgene (#48140), Depositing Lab: Feng Zhang
pY094	huAsCpf1 vector	Ampicillin, Kanamycin, Neomycin	Addgene (#84743), Depositing Lab: Feng Zhang

2.8 Antibodies

Table 2: Used first and second antibodies

Antibody	Source	Manufacturer
Anti-Actin	Mouse	MERCK KGaA, Darmstadt, Germany
Anti-OPA1	Mouse	BD Bioscience, Heidelberg, Germany
HRP-linked anti-mouse	Goat	Calbiochem, MERCK KGaA, Darmstadt, Germany

2.9 Cell lines

All human cell lines used in this work are listed in the following table.

Table 3: Used cell lines

Cell line	Mutation	Source	Comment
HEK293T	-	ATCC, Manassas, VA, USA	-
iPSCs-OPA1-BEHR	*OPA1*: c.610+364G>A; c.1311A>G	Stefan Hauser, DZNE, Tuebingen, Germany	Reprogrammed from human skin fibroblasts isolated from Behr syndrome patient
iPSCs-CO-53	-	Stefan Hauser, DZNE, Tuebingen, Germany	Reprogrammed from human skin fibroblasts isolated from healthy proband

2.10 Bacteria strains

NEB® 5-alpha Competent *E. coli* (high efficiency): DH5α^{TM} derivative, (Genotype: huA2a(argF-lacZ)U169 phoA glnV44 a80a(lacZ)M15 gyrA96 recA1 relA1 endA1 thi-1 hsdR17) by New England Biolabs GmbH, Frankfurt a.M., Germany.

NEB® 10-beta Competent *E. coli* (high efficiency): DH10β^{TM} derivative, (Genotype: araD139 Δ(ara-leu)7697 fhuA lacX74 galK (Φ80 Δ(lacZ)M15) mcrA galU recA1 endA1 nupG rpsL (Str^{R}) D(mrr-hsdRMS-mcrBC) by New England Biolabs GmbH, Frankfurt a.M., Germany.

2.11 Oligonucleotides

Oligonucleotides (Primers, gRNAs, crRNAs) were ordered as standard-desalting purified at Integrated DNA Technologies (IDT), Leuven, Belgium or at Sigma-Aldrich Chemie GmbH, Steinheim, Germany. Fluorescence-labelled (5´-FAM) and biotinylated (BTN) primers were ordered at Eurofins Genomics, Ebersberg, Germany or Sigma-Aldrich Chemie GmbH, Steinheim, Germany (HPLC or standard-desalting purified). The lyophilized primers and gRNAs were resuspended in 1/4 TE buffer to a final concentration of 100 pmol/µl. Primers were further aliquoted to a concentration of 10 pmol/µl to proceed with in respective experiments. Primers used for sequencing were aliquoted to 2-5 pmol/µl. crRNAs were resuspended in nuclease-free duplex buffer provided by IDT to 100 pmol/µl.

Table 4: Standard primers to amplify and sequence vectors

Name	Sequence 5´-3´	Vector
Cloning Analysis_F Cloning Analysis_R	ACCTGCCAACCAAAGCGAGAA AGTCCCAATAACAGAGTACTCGC	pMiniT2.0
ET_SA2 ET_SD6	ATCTCAGTGGTATTTGTGAGC TCTGAGTCACCTGGACAACC	pSPL3
mU6_F	CAGCACAAAAGGAAACTCACC	CRISPR vectors
hU6_F	GAGGGCCTATTTCCCATGATT	CRISPR vectors
pBR322ori_F	GGGAAACGCCTGGTATCTTT	CRISPR vectors

Table 5: Primers to amplify and sequence the *OPA1* gene

Name	Sequence 5´-3´	Position
JH_CRISPR_Intr4b_F2 JH_CRISPR_Intr4_large_R1	GGCAAACTCATTATCCTTTAGGTGG TCAGCCACATACCACTGGCATTA	Intron 4b-5
OPA1_Ex3_F OPA1_Ex3_R	AATTTTTCTTTACATGTTTATTTGGC TTTCTCTTTCCTCGAGATGACC	Exon 3
OPA1_Ex4_F OPA1_Ex4_R	TTTTGTAGGGTTGTCATGAGG AAAAATGTCCTGTTTTTCATTGG	Exon 4
OPA1_Ex4b_F OPA1_Ex4b_R	GTGGTTGGACCAATTTGGTGGT CCTAAAGGATAATGAGTTTGCC	Exon 4b
OPA1_Ex5_F OPA1_Ex5_R	TGGAGAATGTAAAGGGCTGC TCTTTCAAGACTACCTACATGAACAA	Exon 5

Table 6: Primers to amplify and sequence the *DNAJC30* gene

Name	Sequence 5´-3´	Position
DNAJC30_Ex1_F	GGCACCCGGTTTTTATGTC	Exon 1
DNAJC30_Ex1_R	GCAGGGGGAGTACAGTTCCT	

Table 7: Primers used for Pyrosequencing experiments. Modification with biotin is highlighted

Name	Sequence 5´-3´	Comment
Hs_OPA1_N158S_F	TGGATTGTGCCTGACATTGT	Amplification
Hs_OPA1_N158S_Rbi	**(BTN)**CCGTTTCTTCCGGAGAACCTAA	
Hs_OPA1_N158S_seq	TTAGAAAAGCCCTTCCT	Sequencing

Table 8: Primers used for inverse PCR/*in vitro* mutagenesis

Name	Sequence 5´-3´	Comment
Clone 7_F Clone 7_R	GTTTT- CCGGCCAGGCGCGGTGGCT- CATGCCTG AAACAAATTTAAATGTCAAC- CATGACAGGG	Amplification of *OPA1* minigene construct with integration of Nickase editing events
Clone 28_F Clone 28_R	TTTAAATTTGTTTT- CCGGCCGGGCGCGGTGGCT- CATGCCTG CGCCCGGCCG- GAAAACAAATTTAAATGTCA- ACCATGACAGGGCAG	Amplification of *OPA1* minigene construct with integration of Nickase editing events
Clone 31_F Clone 31_R	GGCGCGGTGGCTCATGCCT TGACAGGGCAGAT- GAGACAAAC	Amplification of *OPA1* minigene construct with integration of Nickase editing events
Clone 2512_R	TAAATTAAATGTCAACCAT- GACAGGGCAG	Amplification of *OPA1* minigene construct with integration of Nickase editing events
Clone 2515_F Clone 2515_R	GCGGTGGCTCATGCC AACCATGACAGGGCAGATG	Amplification of *OPA1* minigene construct with integration of Nickase editing events
Clone 2516_R	GCAGAT- GAGACAAACTAAAATTACTT- TTC	Amplification of *OPA1* minigene construct with integration of Nickase editing events
Clone 2518_R	AAATGTCAACCAT- GACAGGGCAG	Amplification of *OPA1* minigene construct with integration of Nickase editing events

Clone 2520_F Clone 2520_R	CGCGGTGGCTCATGC AACAAATTTAAATGTCAAC-CATGACA	Amplification of *OPA1* minigene construct with integration of Nickase editing events
Clone 2521_F Clone 2521_R	TGTAATAATAAAGGTGGCATA AAGGTGGCTCATGCCTGTAA GGCATGAGCCACAAATT-TAAATGTCAAC	Amplification of *OPA1* minigene construct with integration of Nickase editing events
Clone 2522_R	AACCATGACAGGGCAGAT-GAGAC	Amplification of *OPA1* minigene construct with integration of Nickase editing events
Inverse PCR_clone 6_F Inverse PCR_clone 6_R	CATTTAAATTTGTTTTCCGGC TGACAGGGCAGAT-GAGACAAAC	Amplification of *OPA1* minigene construct with integration of Cpf1 editing events
Inverse PCR_clone 8_F Inverse PCR_clone 8_R	GACATTTAAATTTGTTTT-CCGGC GACAGGGCAGAT-GAGACAAACTAAA	Amplification of *OPA1* minigene construct with integration of Cpf1 editing events
Inverse PCR_clone 10_F Inverse PCR_clone 10_R	GACATTTAAATTTGTTTT-CCGGC CTGACAGGGCAGAT-GAGACAAA	Amplification of *OPA1* minigene construct with integration of Cpf1 editing events
OPA1_In4b_IVM_F OPA1_In4b_IVM_R	TTTGTCTCA-TCTGCCCTGTCGGGACATT-TAAATTTGTTTTCC GGAAAACAAATTTAAAT-GTCCCGACAGGGCAGAT-GAGACAAA	IVM primer to mutate second acceptor splice site (A>G) in *OPA1* intron 4b generated by Cpf-editing (iPSC-clone 10 editing)

Table 9: Primers used for RT-PCR and generation of midigene construct. *Not*I and *Bam*HI restriction sites used for cloning are highlighted

Name	**Sequence 5´-3´**	**Comment**
NotI_F BamHI_R	TATATATA**GCGGCCGC**TGCTT-GTTTGCTGAGACCAC TATATATA**GGATCC**TTT-CCAGAACTGCCACGTAA	Amplification of *OPA1* Exon 3-5 + *Not*I/*Bam*HI restriction site
pSPL3seqcDNA_F pSPL3seqcDNA_R	TGGACAACCTCAAAGGCACC AGTGAATTGGTCGAATGGATC	Amplification of pSPL3 inserts
HsOPA1-Ex4bint_F	TCACAAATTGGTTAGTGAAGT-CAT	Analysis of *OPA1* DIM c.610+364G>A
OPA1_cDNA_Ex3-6_F OPA1_cDNA_Ex3-6_R	GTGGTTGGACCAATTTGGTGGT CCTAAAGGATAATGAGTTTGCC	Amplification of Exon 3, 4, 4b, 5 and 6 of *OPA1* from cDNA

Table 10: Primers used for analysis of CRISPR genome editing

Name	Sequence 5´-3´	Comment
gRNApair1_F gRNApair1_R	GCTGATTTTTCACAGGT-CACA TGACAGGGCAGAT-GAGACAA	Nickase editing
OPA1intr4b_g4-6_F OPA1intr4b_g4-6_R	AGGCAGGCGGATCAT-GAGGTCA AACCTCCGCCTCCTGGGTT-CAA	Nickase editing
ABCA4_In36_CRISPR.Check3_F ABCA4_In36_CRISPR.Check2_R	CCGGACCTATACACCT-GAACAG CTGCCTGGTCTCTCA-CTCTTTC	Nickase editing
CLEC16A-Ex2_F CLEC16A-Ex2_R	ACCCTTCAAAGCATT-GTCTGC AACTTCCCCATTTTTGGCTTG	Cpf1 editing

Table 11: Fluorescence-labelled primers. 5´FAM modification is highlighted

Name	Sequence 5´-3´	Comment
pSPL3seqcDNA_F_FAM	**(6FAM)**TGGACAAC-CTCAAAGGCACC	Splicing assay
OPA1_cDNA_Ex3-6_F_FAM	**(6FAM)**GGATTGTGCCT-GACATTGTG	Splicing Assay
gRNApair1_Rev_FAM	**(6FAM)**TGACAGGGCA-GATGAGACAA	Nickase editing
JH_Fwd2_FAM	**(6FAM)**GGCAAACTCAT-TATCCTTTAGGTGG	CRISPR editing
OPA1intr4b_g4-6_FAM	**(6FAM)**AGGCAGGCG-GATCATGAGGTCA	Nickase editing
ABCA4_In36_Nickase-Ana_F_FAM	**(6FAM)**ACGCTGGCTT-CTCTCACTCCCA	Nickase editing
CLEC16A-Ex2_F_FAM	**(6FAM)**ACCCTTCA-AAGCATTGTCTGC	Cpf1 editing

Table 12: gRNA oligonucleotides used for CRISPR genome editing. Recognition site for cloning into CRISPR vector is highlighted

Name	Sequence 5´-3´	Comment
OPA1-gRNA1-BbsI_F OPA1-gRNA1-BbsI_R	**CACCG**CAAACTCATTATCCTTTAGG **AAAC**CCTAAAGGATAATGAGTTTG**C**	Nickase editing
OPA1-gRNA2-SapI_F OPA1-gRNA2-SapI_R	**TTTG**TTTGCCTAATATAGTTCTG **AAC**CAGAACTATATTAGGCAAA**C**	Nickase editing
OPA1-gRNA3-BbsI_F OPA1-gRNA3-BbsI_R	**CACCG**TGTTTTCCGGCCGGGCGCGG **AAAC**CCGCGCCCGGCCGGAAAACA**C**	Nickase editing
OPA1_gRNA3_DIM_F OPA1_gRNA3_DIM_R	**CACCG**TGTTTTCCGGCCAGGCGCGG **AAAC**CCGCGCCTGGCCGGAAAACA**C**	Nickase editing

OPA1-gRNA4-SapI_F OPA1-gRNA4-SapI_R	**TTTG**TTTAAATGTCAACCATGACA **AAC**TGTCATGGTTGACATTTAAA**C**	Nickase editing
OPA1-gRNA5-BbsI_F OPA1-gRNA5-BbsI_R	**CACCG**TGTAGTCCTAGCTACTCGGG **AAAC**CCCGAGTAGCTAGGACTACA**C**	Nickase editing
OPA1-gRNA6-SapI_F OPA1-gRNA6-SapI_R	**TTTG**TTGTATTTTTAGTAGAGATG **AAC**CATCTCTACTAAAAATACAA**C**	Nickase editing
OPA1-gRNA7-BbsI_F OPA1-gRNA7-BbsI_R	**CACCG**AAAAAATTTGCCGGGCGTGG **AAAC**CCACGCCCGGCAAATTTTTT**C**	Nickase editing
OPA1-gRNA8-BbsI_F OPA1-gRNA8-BbsI_R	**CACCG**AAAAATACAAAAAATTTGCC **AAAC**GGCAAATTTTTTGTATTTTT**C**	Nickase editing
OPA1-gRNA9-BbsI_F OPA1-gRNA9-BbsI_R	**CACCG**ATTTAAATTTGTTTTCCGGC **AAAC**GCCGGAAAACAAATTTAAAT**C**	Nickase editing
OPA1-Cpf1-gRNA1_F OPA1-Cpf1-gRNA1_R	**AGAT**TCTCATCTGCCCTGTCATGGTTG **AAAA**CAACCATGACAGGGCAGATGAGA	Cpf1 editing
OPA1-Cpf1-gRNA2_F OPA1-Cpf1-gRNA2_R	**AGAT**AATGTCAACCATGACAGGGCAGA **AAAA**TCTGCCCTGTCATGGTTGACATT	Cpf1 editing
OPA1-Cpf1-gRNA3_F OPA1-Cpf1-gRNA3_R	**AGAT**CCGGCCGGGCGCGGTGGCTCATG **AAAA**CATGAGCCACCGCGCCCGGCCGG	Cpf1 editing
OPA1-Cpf1-gRNA3-DIM_F OPA1-Cpf1-gRNA3-DIM_R	**AGAT**CCGGCCAGGCGCGGTGGCTCATG **AAAA**CATGAGCCACCGCGCCTGGCCGG	Cpf1 editing
OPA1-Cpf1-gRNA4_F OPA1-Cpf1-gRNA4_R	**AGAT**GTAGAGATGGGGTTTCACCGTGT **AAAA**ACACGGTGAAACCCCATCTCTAC	Cpf1 editing
CLEC16A-Cpf1-cr1_F CLEC16A-Cpf1-cr1_R	**AGAT**ACCAAAAACACCACAGTCA-CAGAA **AAAA**TTCTGTGACTGTGGTGTTTTTGGT	Cpf1 editing

Table 13: crRNA oligonucleotides used for Nickase genome editing with RNPs. Alt-R modification is highlighted

Name	RNA sequence 5´-3´	DNA sequence 5´-3´
OPA1_crRNA3_WT	**/AltR1/**rUrGrU rUrUrU rCrCrG rGrCrC rGrGrG rCrGrC rGrGrG rUrUrU rUrArG rArGrC rUrArU rGrCrU **/AltR2/**	tgttttccggccgggcgcgg
OPA1_crRNA3_DIM	**/AltR1/**rUrGrU rUrUrU rCrCrG rGrCrC rArGrG rCrGrC rGrGrG rUrUrU rUrArG rArGrC rUrArU rGrCrU **/AltR2/**	tgttttccggccaggcgcgg
OPA1_crRNA4	**/AltR1/**rUrUrU rArArA rUrGrU rCrArA rCrCrA rUrGrA rCrArG rUrUrU rUrArG rArGrC rUrArU rGrCrU **/AltR2/**	tttaaatgtcaaccatgaca

2.12 Buffers and solutions

DNA buffers

Tris-EDTA buffer (1xTE)
10 mM Tris-HCl, pH 7.5

¼ TE
2.5 mM Tris-HCl, pH 8.0

1mM EDTA

0.25 mM EDTA

PCR

dNTP-Mix
5 mM dATP
5 mM dCTP
5 mM dGTP
5 mM dTTP
5 mM Tris, pH 7.0

10x Ampli I-buffer (AT I)
100 mM Tris, pH 8.3
500 mM KCl
15 mM $MgCl_2$
0.01% (w/v) Gelatine

10x Ampli II-buffer (AT II)
100 mM Tris, pH 8.6
500 mM KCl
15 mM $MgCl_2$
0.01% Gelatine

10x Ampli III-buffer (AT III)
100 mM Tris, pH 8.9
500 mM KCl
15 mM $MgCl_2$
0.01% Gelatine

10x Buffer 17 (BOM 17)
100 mM Tris-HCl, pH 8.9
500 mM KCl
20 mM $MgCl_2$

10x Buffer 18 (BOM 18)
100 mM Tris-HCl, pH 8.9
500 mM KCl
30 mM $MgCl_2$

Agarose gel electrophoresis

Tris-Borate-EDTA-Buffer (TBE)
89 mM Tris base, pH 8.0
89 mM Boric acid
2.5 mM EDTA

10x Loading buffer
20% Ficoll 400
100 mM EDTA
0.2% Bromphenol Blue
0.2% Xylene Cyanol

Loading buffer
3 ml 10x Loading buffer
29 ml 50% Glycerol

Ethidium bromide solution
100 µg/ml in TE

Pyrosequencing buffers

Annealing buffer
20 mM Tris acetate
2 mM Mg acetate

Denaturation buffer
0.2 M NaOH

Binding buffer
10 mM Tris-HCl, pH 7.6
2 M NaCl
1 mM EDTA
0.1% Tween 20

Washing buffer
10 mM Tris acetate, pH 7.6

Bacteria culture

LB medium
1% (w/v) Bacto-Tryptone
0.5% (w/v) Yeast-Extract
170 mM NaCl
pH 7.5

LB-Agar
1.5% Agar in LB medium

Medium additives
0.15 mg/ml Ampicillin
0.05 mg/ml Carbenicillin
0.05 mg/ml Kanamycin

Cell culture

Culture medium HEK293T (DMEM +)
10% (v/v) FBS
1% (v/v) Penicillin/Streptomycin
1% (v/v) Amphotericin B
in DMEM

Culture medium HEK293T (DMEM-)
10% (v/v) FBS
in DMEM

Culture medium iPSCs (E8 Flex +)
2% Essential 8 Flex Supplement (50x)
0.2% Primocin (50 mg/ml)
in Essential 8 Flex Basal Medium (1x)

Culture medium iPSCs (E8 Flex -)
2% Essential 8 Flex Supplement (50x)
in Essential 8 Flex Basal Medium (1x)

Western Blot

RIPA buffer
50 mM Tris base
150 mM NaCl
1mM EDTA
1% (v/v) Nonidet P-40
0.25% (w/v) Sodium deoxycholate
1 mM DTT
1% (v/v) Protease Inhibitor Cocktail Set III
pH 7.4

Laemmli buffer
60 mM Tris-HCl, pH 6.8
2% SDS
10% Glycerol
5% β-Mercaptoethanol
0.01% Bromphenol blue

SDS-PAGE Running buffer (1x MOPS)
6.06 g Tris base
10.46 g MOPS
1 g SDS
0.3 g EDTA
in 1 l MilliQ water

Towbin buffer
25 mM Tris base
192 mM Glycin
0.05% (w/v) SDS
20% (v/v) MeOH

Ponceau-S solution
0.2% Ponceau-S powder
in 3% Trichloracetic acid

1x TBS
10 mM Tris-HCl, pH 8.0
150 mM NaCl

1x TBST
10 mM Tris-HCl, pH 8.0
150 mM NaCl
0.1% (v/v) Tween 20

5% milk-TBST
5% (w/v) Blotting-Grade Blocker in 1x TBST

	1% milk-TBST 1% (w/v) Blotting-Grade Blocker in 1x TBST

2.13 Consumables

Commercially available laboratory consumables such as plastic goods, pipette tips, reaction vessels, etc. were purchased from various laboratory suppliers.

2.14 Software

Benchling (https://www.benchling.com/)	Benchling Inc., San Francisco, CA, USA
CellProfiler cell image analysis software	Developed by: Anne E. Carpenter and others, Broad Institute, Cambridge, MA, USA
DNASTAR® Lasergene Package 5.08 *(EditSeq* and *Seqman)*	DNASTAR Inc., Madison WI, USA
E.A.S.Y Win32 A+B N5	Herolab GmbH Laborgeräte, Wiesloch, Germany
GeneMapper Software 5	Applied Biosystems, Waltham, MA, USA
Graphpad Prism7	Graphpad Software, San Diego, CA, Diego
HEXplorer Score (https://www2.hhu.de/rna/html/hexplorer_score.php)	Developed by: Heiner Schaal, Institute for Virology, Düsseldorf, Germany
ImageJ-win64	Developed by: Wayne Rasband, National Institutes of Health (NIH), Bethesda, MD, USA
MaxEntScan (http://hollywood.mit.edu/burgelab/maxent/Xmaxentscan_scoreseq_acc.html)	Developed by: Gene Yeo and Cristopher Burge, Massachusetts Institute of Technology, Cambridge, MA, USA
MutationTaster (https://www.mutationtaster.org/)	Jana M. Schwarz, Dominik Seelow, Charité Berlin, Germany
NNSPLICE 0.9 version (https://www.fruitfly.org/seq_tools/splice.html)	Coded by: Martin G. Reese, Lawrence Berkeley National Laboratory, Berkeley, CA, USA
PolyPhen-2 (http://genetics.bwh.harvard.edu/pph2/)	Ivan A. Adzhubei., Harvard Medical School, Boston, MA, USA
PyroMark Q96 ID Software	Qiagen N.V., Hilden, Germany

Sequencing Analysis 5.2	Applied Biosystems, Waltham, MA, USA
ZEN 2.3 Imaging Software (blue edition)	Carl Zeiss AG, Oberkochen, Germany
ZEN 2.3 lite (blue edition)	Carl Zeiss AG, Oberkochen, Germany

3 Methods

3.1 Molecular biology techniques

3.1.1 Amplification of DNA fragments using Polymerase chain reaction (PCR)

The polymerase chain reaction (PCR) is a method to amplify DNA *in vitro* (Mullis & Faloona, 1987; Saiki et al., 1985) (Figure 16). The thermostable *Taq* DNA polymerase, which is derived from the hot spring bacterium *Thermus aquaticus*, is used for PCR. Other components of the PCR include buffer solutions, template DNA, deoxyribonucleoside triphosphates (dNTPs), and a primer pair. The reaction takes place in a thermocycler.

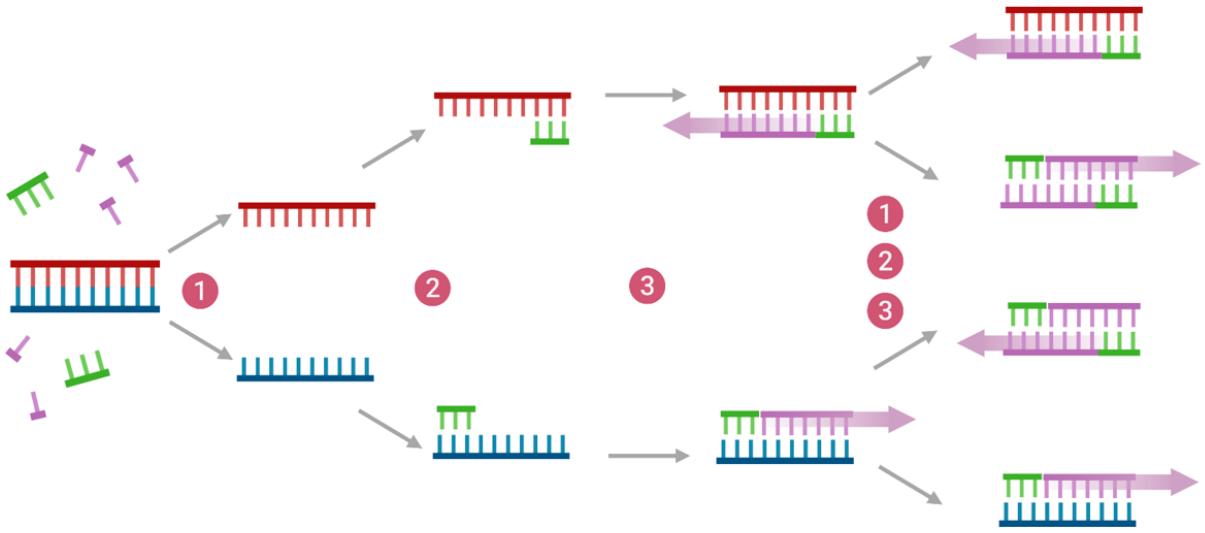

Figure 16: Scheme of the polymerase chain reaction (PCR). (1) Double-stranded DNA is denatured at 94-98 °C. (2) Annealing of primer pair. The annealing temperature depends on the length and sequence of the primer pair and usually ranges between 55 °C and 65 °C. (3) Elongation using DNA polymerase and dNTPs. The elongation temperature is set between 68 °C and 72 °C depending on the working optimum of the polymerase. Adapted from "Polymerase chain reaction (PCR)", by BioRender.com (2022). Retrieved from https://app.biorender.com/biorender-templates.

The following protocol was used to perform a standard PCR:

Table 14: Components of a standard PCR with volumes for a 25 µl approach. Standard PCR was conducted with 50-200 ng of genomic or plasmid DNA and 2 µl of cDNA. Buffer ATI, ATII, ATIII, BOM17 or BOM18 were used.

Component	Volume/25 µl
Buffer (10x)	2.5 µl
Template DNA	x µl
dNTP mix (5 mM per dNTP)	1 µl

Forward primer (10 pmol/µl)	1 µl
Reverse primer (10 pmol/µl)	1 µl
Taq DNA polymerase (5 U/µl)	0.2 µl
ddH_2O	add to 25 µl

Table 15: Thermocycler PCR program for standard PCR.

	Temperature	**Time**	**Cycles**
Initialization	95 °C	3 min	1
Denaturation	95 °C	15 sec	40
Annealing	60 °C	15 sec	
Elongation	72 °C	1 min/kb	
Final Elongation	72 °C	7 min	1
Final Hold	8 °C	∞	

Because of its high-fidelity feature, the Phusion HF DNA polymerase (Thermo Fisher Scientific, Waltham, MA, USA) was used for cloning experiments such as allelic cloning and the generation of an extended minigene construct.

Table 16: Components of a Phusion HF DNA polymerase PCR with volumes for a 50 µl approach. PCR was conducted with 50-200 ng of genomic DNA.

Component	**Volume/50 µl**
Phusion HF buffer (5x)	10 µl
Template DNA	x µl
dNTP mix (5 mM per dNTP)	2 µl
Forward primer (10 pmol/µl)	2.5 µl
Reverse primer (10 pmol/µl)	2.5 µl
Phusion HF DNA polymerase (2 U/µl)	0.5 µl
ddH_2O	add to 50 µl

Table 17: Thermocycler PCR program for PCR with Phusion HF DNA polymerase.

	Temperature	**Time**	**Cycles**
Initialization	98 °C	30 sec	1
Denaturation	98 °C	10 sec	30-35
Annealing	60 °C	30 sec	
Elongation	72 °C	30 sec/kb	
Final Elongation	72 °C	10 min	1
Final Hold	8 °C	∞	

The *PfuUltra* HF DNA polymerase (Agilent Technologies Deutschland GmbH, Waldbronn, Germany) was used for *in vitro* mutagenesis experiments, where high accuracy and a robust amplification of a long target is needed.

Table 18: Components of a *PfuUltra* HF DNA polymerase PCR with volumes for a 50 µl approach. PCR was conducted with 50-200 ng of plasmid DNA.

Component	Volume/50 µl
PfuUltra HF reaction buffer (10x)	5 µl
Template DNA	x µl
dNTP mix (5 mM per dNTP)	2 µl
Forward primer (10 pmol/µl)	1.5 µl
Reverse primer (10 pmol/µl)	1.5 µl
PfuUltra HF DNA polymerase (2.5 U/µl)	1 µl
ddH_2O	add to 50 µl

Table 19: Thermocycler PCR program for PCR with *PfuUltra* HF DNA polymerase.

	Temperature	Time	Cycles
Initialization	95 °C	1 min	1
Denaturation	95 °C	30 sec	15-20
Annealing	56-58 °C	1 min	
Elongation	68 °C	1 min/kb	
Final Elongation	68 °C	10 min	1
Final Hold	8 °C	∞	

The LongAmp *Taq* DNA Polymerase (New England Biolabs GmbH, Frankfurt a.M., Germany) was used for amplification of long DNA fragments.

Table 20: Components of a LongAmp *Taq* DNA polymerase PCR with volumes for a 25 µl approach. PCR was conducted with 50-200 ng of genomic DNA.

Component	Volume/25 µl
LongAmp *Taq* reaction buffer (5x)	5 µl
Template DNA	x µl
dNTP mix (5 mM per dNTP)	1.5 µl
Forward primer (10 pmol/µl)	1 µl
Reverse primer (10 pmol/µl)	1 µl
LongAmp *Taq* DNA Polymerase (2.5 U/µl)	1 µl
ddH_2O	add to 25 µl

Table 21: Thermocycler PCR program for PCR with LongAmp *Taq* DNA polymerase.

	Temperature	Time	Cycles
Initialization	94 °C	30 sec	1
Denaturation	94 °C	30 sec	30
Annealing	60 °C	30 sec	
Elongation	65 °C	1 min/kb	
Final Elongation	65 °C	10 min	1
Final Hold	8 °C	∞	

3.1.2 Colony PCR

In order to identify positive bacteria clones (i.e., clones that have taken up the plasmid with the desired insert after transformation), a colony PCR was performed. The day after transformation, individual bacteria clones were picked for screening from the agar plate. Fourty microliter of ddH_2O and a fresh agar plate were inoculated with the picked bacteria clone. The inoculated agar plate was incubated overnight at 37 °C and served as a back-up plate. Certain criteria were considered in the selection of PCR primers: i) a product size around 500 bp, ii) location of the binding site in the backbone, flanking the insert or iii) one primer binding the insert and one the backbone, or iv) both primers binding the insert. A master mix of the following reagents was prepared and added to the inoculated ddH_2O:

Table 22: Components of a colony PCR with volumes for a 50 µl approach.

Component	Volume/50 µl
Inoculated ddH_2O	40 µl
BOM17 buffer (10x)	5 µl
dNTP mix (5 mM per dNTP)	2 µl
Forward primer (10 pmol/µl)	1.3 µl
Reverse primer (10 pmol/µl)	1.3 µl
Taq DNA polymerase (5 U/µl)	0.4 µl

Table 23: Thermocycler PCR program for colony PCR.

	Temperature	Time	Cycles
Lysis of cells	60 °C	20 min	1
Initialization	96 °C	4 min	1
Denaturation	96 °C	20 sec	25
Annealing	58 °C	30 sec	
Elongation	72 °C	1 min/kb	
Final Elongation	72 °C	5 min	1
Final Hold	8 °C	∞	

3.1.3 Agarose gel electrophoresis

Agarose gel electrophoresis was used to separate PCR fragments after amplification. Thereby the PCR product can be identified based on its size. Prior to electrophoresis, 5-10 µl of the PCR samples (in case of a restriction digest, the entire PCR product was used) was mixed with 2 µl of 10 x loading buffer. To prepare an agarose gel, agarose powder was dissolved in 1 x TBE buffer by boiling in a microwave. The density of the gel matrix varies depending on the agarose concentration which was typically 1-3%. After adding ethidium bromide (100 µg/ml), the melted agarose was poured in a tray and a gel comb was inserted. Ethidium bromide is a DNA-

binding fluorescent agent that makes DNA visible under UV light. Thereby, the resulting pattern of bands is identifiable. Once the gel has set, the gel comb was removed and the gel on the tray was placed in a gel chamber. The chamber was filled with running buffer (1 x TBE buffer). The PCR samples were pipetted into the sample pockets. In addition, a size marker was loaded. Electrophoresis took place at 70-90 volts for 1-2 hours. In the electric field, the negatively charged DNA moves towards the anode, separating the nucleic acids according to their size in the gel. The gel image was obtained using the Herolab documentation system and E.A.S.Y Win32 software (Herolab GmbH Laborgeräte, Wiesloch, Germany).

3.1.4 Restriction digestion

Restriction digestion can be used for various purposes: to cut a larger DNA fragment into smaller fragments, for cloning a DNA fragment into a target plasmid construct or also for performing a diagnostic digest to analyse DNA fragments or plasmid constructs. The restriction digest is done by means of restriction enzymes cutting at an individual recognition site. The digest reaction mixture contains one or more restriction enzymes, buffer, PCR product or plasmid DNA and ddH_2O to fill up the reaction volume to 20-50 µl. The used restriction enzymes are listed in (see 2.5 Enzymes). One microliter of enzyme was used for each digest. For buffer, 10 x NEBuffer3.1, 10 x CutSmart buffer (New England Biolabs GmbH, Frankfurt a.M., Germany) or 10 x BamHI buffer (Thermo Fisher Scientific, Waltham, MA, USA) was used depending on the enzyme and the manufacturer´s recommendation. For digestion, 400 ng of plasmid DNA and 5 µl or the total reaction of PCR product were used. The incubation took place at 37 °C (42 °C when using BsmBI_v2) for 2 hours.

3.1.5 Phosphorylation of PCR products

Ligation of a blunt PCR product into a plasmid construct requires phosphorylation. The phosphorylation reaction is performed by means of a T4 polynucleotide kinase enzyme (PNK). The PNK catalyzes the transfer of a phosphate from ATP to the 5´end of the PCR product.

The components of the phosphorylation reaction are shown in the following table:

Table 24: Components of a phosphorylation reaction with volumes for a 40 µl approach. The total amount of purified PCR product was used.

Component	Volume/40 µl
T4 DNA ligase buffer (10 x)	4 µl
PCR product	x µl
ATP (10 mM)	4 µl
T4 PNK (10 U/µl)	1 µl

ddH_2O	add to 40 µl

The phosphorylation reaction takes place at 37 °C for 30 minutes. Prior to ligation, the reaction is heat inactivated at 65 °C for 20 minutes.

3.1.6 Cloning of PCR products

3.1.6.1 Ligation after restriction enzyme digestion

For cloning of the extended *OPA1* minigene construct, the PCR primers were designed with addition of a *Not*I and *Bam*HI recognition site at the 5´end. After purification of the PCR reaction, the PCR product and the minigene construct were digested with *Not*I and *Bam*HI and the reaction was purified once again before ligation with the T4 ligase. T4 ligase catalyzes the binding between two DNA fragments by generating a phosphodiester bond using ATP. The NEBioCalculator (New England Biolabs GmbH, Frankfurt a.M., Germany) was used to calculate the required insert mass for a 3:1 molar insert:vector ratio. The ligation reaction took place at 16 °C over night. The components and volumes for a 20 µl approach of the T4 ligation are shown as follows:

Table 25: Components of a ligation reaction with T4 ligase.

Component	Volume/20 µl
T4 DNA ligase buffer (10 x)	2 µl
Plasmid construct	x µl
Insert	x µl
T4 Ligase (40 U/µl)	1 µl
ddH_2O	add to 20 µl

The T4 ligase was also used in *in vitro* mutagenesis experiments. In this case, the PCR products were digested with *Dpn*I which only cuts when its recognition site is methylated, thereby cutting only the plasmid template. After clean-up of the *Dpn*I-digestion, the PCR products were phosphorylated as described in (3.1.5 Phosphorylation of PCR products). The phosphorylated PCR product was ligated to form a circular plasmid construct by adding 1 µl T4 ligase to the heat-inactivated phosphorylation reaction. The ligation reaction was incubated overnight at 16 °C.

3.1.6.2 PCR cloning kits

For subcloning of PCR products different PCR cloning kits were used. The TA cloning kit (Invitrogen AG, Carlsbad, CA, USA) uses the pCR2.1 vector which is provided linearized with

thymine overhangs at its 5´end. The *Taq* DNA polymerase adds an adenosine at the 3´end of the PCR product and thereby the fragment can be cloned by the sticky ends into the pCR2.1 vector. The NEB PCR cloning kit (New England Biolabs GmbH, Frankfurt a.M., Germany) uses the linearized pMiniT2.0 vector and allows cloning of phosphorylated or unphosphorylated DNA fragments with sticky or blunt ends. The same holds true for the CloneJET PCR cloning kit (Thermo Fisher Scientific, Waltham, MA, USA) using the pJET1.2 vector. Cloning of the PCR products was performed according to the manufacturer´s instructions.

3.1.7 Generation of CRISPR constructs

3.1.7.1 *In silico* design of guide RNAs (gRNAs)

The cloud-based software tool Benchling (Benchling Inc., San Francisco, CA, USA) was used to design the gRNAs. For the Cas9-nickase editing the following parameter were selected: Paired guides, 20 nucleotides guide length and a NGG-PAM (where "N" can be any nucleotide base). Nine gRNAs were chosen based on the location and the on-target score. The on-target score of Benchling is optimized for 20 bp gRNAs with NGG PAMs and based on Doench, Fusi et al., 2016. The score is ranging from 0 to 100, the higher the better. Four guides upstream of the *OPA1* pseudoexon were selected, with one of them covering also the deep intronic mutation c.610+364G>A as well as the pseudoexon. In addition, six guides downstream of the pseudoexon were selected for the nickase experiments. The design of the guides for the Cpf1 editing included the following parameters: Single guides, 23 nucleotides guide length, TTTN-PAM (where "N" can be any nucleotide base). Four gRNAs were selected that are located in the region of interest with a small T-stretch (not more than 3 T´s). Two guides are located upstream of the pseudoexon, one is covering the deep intronic mutation and the pseudoexon and one is situated downstream of the pseudoexon, partly covering it. The on-target score was not considered when designing gRNAs for Cpf1, since there are only on-target scores available for Cas9 PAM sequences. For cloning of the gRNAs into the respective CRISPR construct, the gRNA oligonucleotides were designed including overhangs for Golden-Gate assembly. Cas9-nickase guide pairs were cloned using the restriction enzymes *Bbs*I (first guide is expressed under hU6 promoter) and *Sap*I (second guide is expressed under mU6 promoter). Two oligos for each guide were synthesized according to the following scheme:

Cloning with *Bbs*I: 5´- CACCGNNNNNNNNNNNNNNNNNNN - 3´
3´- CNNNNNNNNNNNNNNNNNNNCAAA - 5´

Cloning with *Sap*I: 5´- TTTGNNNNNNNNNNNNNNNNNN - 3´
3´- CNNNNNNNNNNNNNNNNNNNCAA - 5´

For Cpf1 guides, two oligos of the following form were designed to be cloned with *Bsm*BI:

5´- AGATNNNNNNNNNNNNNNNNNN - 3´
3´- NNNNNNNNNNNNNNNNNNNNAAAA - 5´

3.1.7.2 Cloning of gRNAs

The guides were cloned into the respective CRISPR plasmid construct by means of Golden Gate Assembly (Engler et al., 2008). Golden Gate cloning uses type IIS restriction enzymes which cut beyond their recognition site creating non-palindromic overhangs for the ligation with the gRNAs which are also designed with the corresponding overhang sequences. The advantage of this strategy is the opportunity to assemble multiple DNA fragments in one run and perform restriction digestion and ligation in the same reaction, since the final construct is not containing the restriction site anymore.

Before Golden Gate cloning, the synthesized oligo pairs for each gRNA were annealed in the following reaction:

Table 26: Components for annealing of oligo pairs with volumes for a 50 µl approach.

Component	Volume/50 µl
Oligo 1 (100 µM)	1 µl
Oligo 2 (100 µM)	1 µl
T4 ligation buffer (10 x)	5 µl
ATP (10 mM)	5 µl
T4 polynucleotide kinase (10 U/µl)	1 µl
ddH_2O	add to 50 µl

Table 27: Thermocycler program for annealing of oligo pairs.

Temperature	Time	Cycles
37 °C	30 min	1
95 °C	5 min	1
95 °C 25 °C ↓ Ramp down to 25°C in 1°C steps	12 sec 12 sec	71
8 °C	∞	

For cloning of the single guides into the backbone of the Cpf1 plasmid construct, 100 ng of plasmid and restriction enzyme *Bsm*BI with NEBuffer 3.1 (New England Biolabs GmbH, Frankfurt a.M., Germany) were used. Cloning of guide pairs into the Cas9-nickase construct required 200 ng of plasmid and restriction enzymes *Bbs*I and *Sap*I with CutSmart buffer (New England Biolabs GmbH, Frankfurt a.M., Germany). A higher cloning efficiency was observed when performing a first run of the reaction with only *Bbs*I and the respective oligo duplex, followed by a second run with *Sap*I and the respective oligo duplex being added to the reaction. The Golden Gate reaction was assembled as follows:

Table 28: Components for Golden Gate Assembly with volumes for a 20 µl approach.

Component	Volume/20 µl
Backbone plasmid	x µl
Oligo duplex 1 (1:40 diluted)	2 µl
Oligo duplex 2 (1:40 diluted)	2 µl
Buffer (10 x)	2 µl
ATP (10 mM)	1 µl
DTT (10 mM)	1 µl
Restriction enzyme (10 U/µl)	1 µl
T7 ligase (3000 U/µl)	0.5 µl
ddH_2O	add to 20 µl

Table 29: Thermocycler program for Golden Gate Assembly.

Temperature	Time	Cycles
37 °C (42 °C for *Bsm*BI)	5 min	6
21 °C	5 min	
8 °C	∞	

To prevent formation of unwanted recombination products the reaction was treated with an exonuclease using the following protocol:

Table 30: Components for exonuclease treatment with volumes for a 15 µl approach.

Component	Volume/50 µl
Golden Gate reaction	11 µl
Plasmid-Safe reaction buffer (10 x)	1.5 µl
ATP (10 mM)	1.5 µl
Plasmid-Safe ATP-dependent DNase (10 U/µl)	1 µl

Table 31: Thermocycler program for exonuclease treatment.

Temperature	Time	Cycles
37 °C	30 min	1

70 °C	30 min	1
8 °C	∞	

Afterwards, competent *E. coli* cells were transformed with the reaction.

3.1.8 cDNA synthesis using reverse transcription

Reverse transcription is the process of transcribing RNA into complementary DNA (cDNA), using the enzyme reverse transcriptase. In contrast to genomic DNA, cDNA does not contain introns. Prior to the cDNA synthesis, the isolated RNA was digested with DNase to prevent amplification from genomic DNA. For this purpose, the following reagents were mixed and incubated for 20 minutes at room temperature:

Table 32: Components for DNase digestion with volumes for a 10 µl approach.

Component	Volume/10 µl
RNase-free H_2O	add to 10 µl
RNA isolate (1.3 µg)	x µl
DNase buffer (10 x)	1 µl
DNase1 (1 U/µl)	1 µl

Afterwards, 1 µl of Stop buffer was added to the reaction, followed by an incubation step for 10 minutes at 70 °C. The cDNA synthesis was performed using the Maxima H Minus First Strand cDNA Synthesis Kit (Thermo Fisher Scientific, Waltham, MA, USA) according to the manufacturer´s instructions. The total amount from the DNase digestion was mixed with gene-specific reverse primers: ET_SA2 for *OPA1* minigene assays, OPA1_cDNA_Ex3-6_R for Pyrosequencing experiments and RT-PCR with isolated RNA from CRISPR-edited iPSC clones.

3.1.9 Sanger sequencing of DNA fragments and plasmids

Sanger sequencing can be used to determine the nucleotide sequence in a DNA molecule. By inserting a fluorescently labelled dideoxynucleotide (ddNTP) during PCR elongation, a chain termination is generated resulting in fragments of different length. These are separated in a capillary electrophoresis and detected by fluorescence.

Prior to the sequencing reaction, PCR products were purified by an enzyme mixture of an exonuclease and an alkaline phosphatase (ExoSAP-IT™ by Applied Biosystems, Waltham, MA, USA). The exonuclease degrades the single-stranded primers and the alkaline phosphatase hydrolyzes the non-incorporated dNTPs. Depending on the strength of the band in the agarose gel

electrophoresis, between 1 µl and 6 µl of PCR sample were mixed with 5 µl of 1:20 diluted ExoSAP-IT™. The mixture was incubated at 37 °C for 15 minutes, followed by 15 minutes at 80 °C in a thermal cycler.

The sequencing reaction for PCR products and plasmids was prepared with the Big Dye® Terminator v.3.1 Cycle Sequencing or SupreDye v.3.1 Cycle Sequencing Kit (Applied Biosystems, Waltham, MA, USA). The following components were added:

Table 33: Components of a sequencing reaction with PCR products with volumes for a 10 µl approach. Forward or reverse primer was added per reaction.

Component	Volume/10 µl
Purified PCR product	1 µl
Primer (2-5 pmol/µl)	1 µl
Big Dye Terminator v.3.1	1 µl
Big Dye Terminator v.3.1 buffer (5 x)	2 µl
ddH_2O	5 µl

Table 34: Components of a sequencing reaction with plasmids with volumes for a 20 µl approach. Forward or reverse primer was added per reaction. Between 200 and 500 ng of plasmid DNA were used for sequencing.

Component	Volume/20 µl
Plasmid DNA	x µl
Primer (2-5 pmol/µl)	1 µl
Big Dye Terminator v.3.1	2 µl
Big Dye Terminator v.3.1 buffer (5 x)	4 µl
ddH_2O	add to 20 µl

Table 35: Thermocycler program of a sequencing reaction.

	Temperature	Time	Cycles
Initialization	96 °C	2 min	1
Denaturation	96 °C	10 sec	25
Annealing	53 °C	15 sec	
Elongation	60 °C	4 min	
Final Hold	8 °C	∞	

To remove salts from the sequencing reaction, a precipitation with alcohol was performed. For this purpose, 5 µl of EDTA (125 mM), and 75 µl of ethanol (100%) were pipetted to the reaction mixture, which was made up to 20 µl with ddH_2O if necessary. Centrifugation was performed at 2580 x g for 30 minutes and followed by dry spinning at 440 x g for 30 seconds. The pellet was washed with 60 µl ethanol (80%) and centrifuged again at 1650 x g for 15 minutes, followed by dry spinning.

After precipitation, pellets were resuspended in 50 µl of HiDi formamide. Capillary sequencing was performed using the ABIPRISM® 3130*xl* Genetic Analyzer (Applied Biosystems, Waltham, MA, USA) and evaluated with the Sequencing Analysis 5.2 (Applied Biosystems, Waltham, MA, USA) and SeqMan (DNASTAR Inc., Madison WI, USA) software.

3.1.10 Analysis of PCR fragments using capillary sequencer

PCR fragments were analysed regarding their size and quantity using the ABIPRISM 3130 *xl* genetic analyzer (Applied Biosystems, Waltham, MA, USA). A primer tagged with 6-carboxyfluorescein (6-FAM) was used for the PCR reaction to generate fluorescently-labelled PCR fragments. The fluorescently-labelled PCR fragments were analysed on the capillary sequencer using the GeneScan mode and further evaluated with the GeneMapper software 5 (Applied Biosystems, Waltham, MA, USA).

For the analysis of the DNA fragments, the fluorescently labelled PCR products were diluted 1:1, 1:10, 1:30 or 1:50 with ddH_20 depending on the intensity of the gel bands. One microliter of the diluted PCR products was mixed with 8.5 µl Hi-Di Formamide (Applied Biosystems, Waltham, MA, USA) and 0.5 µl GeneScan 500 ROX dye size standard (Applied Biosystems, Waltham, MA, USA). The samples were run on the capillary sequencer under the following parameters: Fragment Analysis 2 (Results Group) and FragmentAnalysis_36_POP7_D (Instrument Protocol). The fragments were separated according to their length and quantified by means of the fluorescence intensity. The software GeneMapper displays each fragment as a peak. The fluorescence intensity (y-axis) of the peak is relative to the amount of the fragment, the x-axis indicates the size (in bp) of the fragment.

For CRISPR editing experiments, the cleavage efficacy of gRNAs was determined by calculating the ratio of edited fragments to the total amount of fragments based on the area under the curve provided by GeneMapper. Genomic DNA from untransfected cells or mock-electroporated cells (electroporation without plasmid DNA) served as a negative control in editing experiments with plasmid transfection. For RNP transfection, the cells were solely transfected with the Cas9 nickase enzyme without the gRNA duplex. A gRNA pair targeting the *ABCA4* gene was used as a positive control in Cas9 nickase experiments and provided by Pietro De Angeli, Institute for Ophthalmic Research, University Hospital Tuebingen. The Cpf1 experiments were performed with a positive control construct targeting the *CLEC16A* gene based on Ma et al., 2018.

3.1.11 Pyrosequencing

Pyrosequencing is based on the "sequencing by synthesis" method. The integration of a nucleotide during DNA synthesis results in the release of a pyrophosphate. The ATP sulfurylase catalyzes the generation of ATP out of the released pyrophosphate and adenosine 5´phosphosulfate (APS). A luciferase converts luciferin to oxyluciferin under ATP consumption resulting in the emission of light which is recorded by the pyrosequencer. Nucleotides that were not integrated are degraded by the apyrase enzyme (Figure 17).

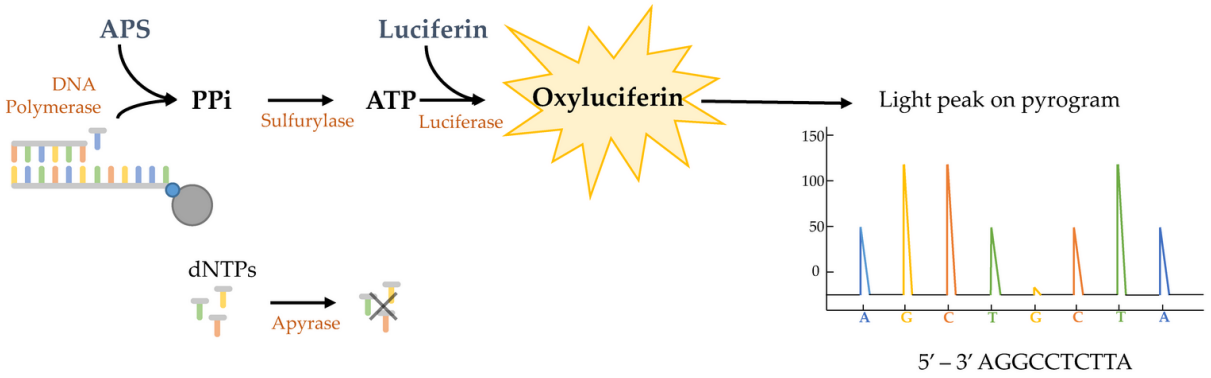

Figure 17: Scheme of pyrosequencing. The integration of a nucleotide during DNA synthesis releases a pyrophosphate which is transformed into ATP with adenosine 5´phosphosulfate (APS) and ATP sulfurylase. Luciferase catalyzes the formation of oxyluciferin from ATP and luciferin generating a light peak on the pyrogram. Apyrase degrades excess nucleotides. Adopted from van der Torre et al., 2020.

The pyrosequencing method was used to detect correctly spliced transcripts in CRISPR-edited iPSCs. The PCR primer pair was designed to exclusively amplify transcripts without inclusion of a pseudoexon. The sequencing primer was specific for a single nucleotide polymorphism (SNP) discriminating the wild-type and mutant allele. During pyrosequencing the ratio of the SNP was calculated and the relative abundance of the alleles was quantified. Thereby, correctly spliced transcripts from the mutant allele could be detected and quantified.

For each sample, three PCR reactions were prepared and analysed (= three technical replicates per sample). The PCR amplification was prepared as follows:

Table 36: Components of the PCR amplification for Pyrosequencing with volumes for a 50 µl approach. The forward primer Hs_OPA1_N158S_F and the biotinylated reverse primer Hs_OPA1_N158S_Rbi were used.

Component	Volume/50 µl
Buffer ATII (10x)	5 µl
cDNA	5 µl
dNTP mix (5 mM per dNTP)	2 µl

Forward primer (10 pmol/µl)	2 µl
Reverse primer (10 pmol/µl)	2 µl
Taq DNA polymerase (5 U/µl)	0.4 µl
ddH_2O	33.6 µl

Table 37: Thermocycler program for 3-step PCR.

	Temperature	Time	Cycles
Initialization	94 °C	4 min	1
Denaturation	94 °C	30 sec	5
Annealing	60 °C	30 sec	
Elongation	72 °C	30 sec	
Denaturation	94 °C	30 sec	5
Annealing	56 °C	30 sec	
Elongation	72 °C	30 sec	
Denaturation	94 °C	30 sec	30
Annealing	54 °C	30 sec	
Elongation	72 °C	30 sec	
Final Elongation	72 °C	5 min	1
Final Hold	8 °C	∞	

After the amplification, 40 µl of PCR product were mixed with 3 µl streptavidin-sepharose beads and 37 µl binding buffer in a 96-well plate. The plate was covered with adhesive tape and mixed for 10 minutes at room temperature on an orbital shaker, thereby the beads were bound to the biotinylated PCR product. In the next step, the samples were purified using a vacuum manifold. The sepharose beads were picked from the PCR plate and washed with 70% ethanol for 5 seconds. Next, the samples were treated with the denaturation solution for 5 seconds and washed with washing buffer for 10 seconds. After draining of excess fluid the beads were released into the sequencing 96-well plate containing 1.2 µl Pyrosequencing primer (Hs_OPA1_N158S_seq; 10 pmol/µl) and 38.8 µl annealing buffer per well. To bind the primer to the cDNA fragment, the reaction was denatured at 82 °C for 2 minutes. The enzyme-mix and substrate-mix for the pyrosequencing run were prepared at room temperature by adding the indicated amount of ddH_2O to the respective reagent bottles and the calculated amount of enzyme-mix, substrate-mix and the four nucleotides were pipetted to the cartridge in the indicated wells. The sequencing plate containing the samples and the cartridge were placed into the pyrosequencer and the run with the assay name OPA1_N158S_Pyrosequencing_#61 was started. The pyrosequencing process was monitored by the PyroMark Q96 ID software (Qiagen N.V., Hilden, Germany) and the software tool Allele Quantification (AQ) was used to obtain the pyrogram of each analysed SNP per sample.

3.2 Microbiological techniques

3.2.1 Transformation of competent *E.coli* cells

Chemically competent *E.coli* cells (NEB 10-beta or NEB 5-alpha by New England Biolabs GmbH, Frankfurt a.M., Germany) were transformed with the ligation reaction. Usually 1-2 µl of the ligation reaction were mixed with 20-50 µl *E.coli* cells and incubated on ice for 30 minutes, followed by a heat shock at 42 °C for 30 seconds. After placing the transformation reaction on ice for 5 minutes, 300-950 µl of pre-warmed NEB SOC or NEB 10-beta/Stable Outgrowth Medium (New England Biolabs GmbH, Frankfurt a.M., Germany) were added to the mixture and incubated for 1 hour in an incubation shaker at 37 °C. Between 25 and 100 µl of the cell suspension were spread onto pre-warmed LB-agar plates containing antibiotics and incubated overnight at 37 °C.

3.2.2 Preparation of glycerol stocks

For long-term storage of plasmids, 500 µl of an overnight culture of transformed bacteria was mixed with 500 µl glycerol (50%) and frozen at -80 °C.

3.3 Isolation of nucleic acid samples

3.3.1 Plasmid isolation from *E. coli* cells

E. coli cells were transformed with plasmids in order to propagate them. The transformed bacteria were spread onto LB-agar plates containing antibiotics. After incubation overnight at 37 °C, single bacteria colonies were picked and 3 ml of LB medium containing antibiotics was inoculated. The cell solution was again incubated overnight in a shaker at 37 °C and used for plasmid extraction the next day. Plasmid isolation was performed according to the manufacturer´s instructions using the Monarch Plasmid Miniprep Kit (New England Biolabs GmbH, Frankfurt a.M., Germany). For electroporation of iPSCs, plasmids needed to be prepared endotoxin-free. For this purpose, 250 ml LB medium containing antibiotics were inoculated with the transformed bacteria and the extraction was conducted using the EndoFree Plasmid Maxi Kit (Qiagen N.V., Hilden, Germany).

3.3.2 DNA isolation from cell cultures

After harvesting pellets of cell cultures, the genomic DNA was isolated according to the manufacturer´s protocol using the peqGOLD Blood & Tissue DNA Mini Kit (VWR International GmbH, Darmstadt, Germany). For rapid extraction of DNA from CRISPR-edited iPSC clones,

the Lucigen QuickExtract DNA extraction solution (Biozym Scientific GmbH, Oldendorf, Germany) was used. The cells were pelleted at 300 x g for 5 minutes and 100 µl of the solution was added before vortexing for 15 seconds. Afterwards, the cell solution was heated up to 65 °C for 6 minutes and vortexed again for 15 minutes, followed by an incubation at 98 °C for 2 minutes. The extracted DNA was stored at -20 °C for short-term and for long-term storage at –80 °C.

3.3.3 RNA isolation from cell cultures

Genomic RNA from cell cultures was extracted using the manufacturer´s instructions of the peqGOLD Total RNA Kit (VWR International GmbH, Darmstadt, Germany).

3.3.4 Purification of DNA from enzymatic reactions

After performing a PCR, restriction digest or other enzymatic reactions, the product was purified by means of cleanup kits to remove non-incorporated dNTPs, short oligonucleotides, enzymes and salts prior to following experiments. The purification was performed by using the QiaQuick PCR Purification Kit (Qiagen N.V., Hilden, Germany) for DNA between 100 bp and 10 kb, the MinElute Reaction Cleanup Kit (Qiagen N.V., Hilden, Germany) for DNA between 70 bp and 4 kb, or the NucleoSpin Gel and PCR Clean up Kit (Macherey-Nagel, Düren, Germany) for DNA between 50 bp and 20 kb. The purification was carried out according to the manufacturers´ manuals.

3.3.5 Determination of nucleic acid concentrations

Determination of the nucleic acid concentration of plasmid DNA, genomic DNA or genomic RNA was conducted using the spectrophotometer Nanodrop ND-1000 (PEQLAB Biotechnologie GmbH, Erlangen, Germany) or TRINEAN Xpose (Unchained Labs Germany GmbH, Berlin, Germany). As a blank control the respective elution buffer of the nucleic acid sample was used and the measurement was carried out at a wavelength of 260 nm.

3.4 Western Blot

3.4.1 Protein isolation from cell cultures

To evaluate the effect of the CRISPR-Cpf1 genome editing on the OPA1 protein level, Western blots were performed with protein lysates from the edited iPSC cultures, the unedited iPSC culture as well as from a control iPSC line. Cell pellets were harvested by centrifugation at 300 x g for 5 minutes and resuspended in 1 ml DPBS. After transfer into a 2 ml tube, the cells were again centrifuged at 300 x g for 5 minutes and resuspended in 20-50 µl RIPA buffer. To break

up the cells and isolate the proteins, the cell lysates were thawed and frozen four times using liquid nitrogen. To remove the cell debris, the lysate was centrifuged at 2200 rpm for 20 minutes at 4 °C and the supernatant was transferred to a new tube. The cell lysates were stored at – 80 °C.

3.4.2 Determination of the protein concentration using Bradford assay

The Bradford assay is based on the binding of proteins to the coomassie blue dye, resulting in a color reaction which is dependent on the protein abundance in the sample. By creating a standard curve, the protein concentration of an unknown sample can be determined. The standard curve is generated using bovine serum albumin (BSA). A serial BSA dilution with seven different concentrations was prepared as follows:

Table 38: Serial BSA dilution scheme.

Desired concentration in µg/ml	Volume of BSA in µl	Volume of ddH_2O in µl
1000	10 µl of 20 mg/ml stock	190
750	75 µl of 1000 µg/ml dilution	25
500	50 µl of 1000 µg/ml dilution	50
250	50 µl of 500 µg/ml dilution	50
100	10 µl of 1000 µg/ml dilution	90
50	10 µl of 500 µg/ml dilution	90
20	20 µl of 100 µg/ml dilution	80

The protein lysates were diluted 1:10 with ddH_20 before measurement. In addition, 30 µl ddH_2O was included as a blank control. RIPA buffer, diluted 1:10 with ddH_2O was used to substract the background value from the calculation of the protein concentration. The Bradford reagent (5 x) was diluted 1:5 with ddH_2O and 200 µl of the dilution were used for each sample. The protein lysates, standards, blank and RIPA buffer were measured in duplicates. For this, 10 µl of the samples were mixed with the Bradford reagent (1 x) in the 96-well plate. The samples were incubated in the dark for 5 minutes, followed by measurement of the absorbance using the Tecan plate reader (Tecan Deutschland GmbH, Crailsheim, Germany) at 595 nm. Protein concentrations were determined using the established standard curve.

3.4.3 SDS-PAGE

Proteins were separated electrophoretically using a SDS-PAGE. For sample preparation, 15 µg of the isolated protein were filled up with ddH_2O to 20 µl and mixed with 5 µl Laemmli buffer (5 x) to a final volume of 25 µl. The samples were denatured at 99 °C for 5 minutes in a thermal

block and afterwards placed on ice. For the SDS-PAGE, precast gels were used. The SDS-PAGE was inserted into an electrophoresis chamber filled with 1 x MOPS running buffer (Mini-PROTEAN 3 Cell by BioRad Laboratories GmbH, München, Germany). The gel pockets were filled with the entire amount of sample and two protein standards (2 µl of SMIO YesBlot by 7BioScience, Neuenburg am Rhein, Germany and 10 µl of Novex Sharp protein standard by Invitrogen AG, Carlsbad, CA, USA) were loaded to the right and left of the protein samples. Five microliter of Laemmli buffer (5 x) were pipetted into empty pockets. Electrophoresis was performed with 25 mA for each gel for approximately 2 hours. The migration of protein bands was monitored using the pre-stained protein standards.

3.4.4 Blotting

The transfer of proteins to a nitrocellulose membrane was done in a Mini Trans-Blot Cell (BioRad Laboratories GmbH, München, Germany). The blotting sandwich was prepared in the following order in a dish filled with Towbin buffer: blotting cassette with the black side facing downwards, a sponge, filter paper and the SDS-PAGE gel placed onto the filter paper, the nitrocellulose membrane, filter paper and sponge. To remove any trapped air bubbles, a 50 ml falcon tube was used to roll over the sandwich. The blotting cassette was closed and placed into the blotting chamber filled with Towbin buffer and an ice pack. The blotting was performed at 200 mA for 1 hour.

3.4.5 Blocking and Immunolabelling

After blotting, the nitrocellulose membrane was placed in Ponceau-S solution for 30 seconds and washed with distilled water to visualize the protein bands. Before blocking, the membrane was cut into two parts at approximately the level of the 50 kDa band. The upper part was used for immunodetection of OPA1 (80 and 100 kDa), the lower part for detection of actin (42 kDa). To prevent non-specific binding of antibodies the membranes were blocked in 5% skimmed milk-TBST solution for 1 hour on a rotating mixer at room temperature. After blocking, the membranes were incubated in 4 ml primary antibody solution on a rotating mixer at 4 °C overnight. The OPA1 primary antibody was diluted 1:500 in 1 x TBST with 5% milk and the primary antibody against actin was diluted 1:4000 in 1 x TBST with 1% milk. After incubation with the first antibody the membranes were washed in 1 x TBS three times for 10 minutes. The secondary antibody is conjugated to a horseradish peroxidase (HRP) and was diluted 1:10000 in 1 x TBST with 1% milk. The membranes were incubated in 4 ml of the diluted secondary

antibody for 1 hour at room temperature on a rotating mixer. Before immunodetection, the membranes were washed again with 1 x TBS three times for 10 minutes.

3.4.6 Immunodetection

The Pierce ECL Western Blotting Substrate (Thermo Fisher Scientific, Waltham, MA, USA) was used to detect the HRP on the immunoblots. The kit consists of two reagents that were mixed 1:1 and the membranes were incubated in 4 ml of the mixture for 2 minutes prior to detection. The luminescence detection was performed using the Fusion FX imaging system (Vilber Lourmat Deutschland GmbH, Eberhardzell, Germany).

3.5 Cell biological techniques

3.5.1 Cultivation and transfection of HEK293T cells

3.5.1.1 Thawing of HEK293T cells

After long-term storage in liquid nitrogen tanks, the cells were thawed in a 37 °C water bath and transferred in 10 ml DMEM+ medium. The cells were centrifuged at 300 x g for 5 minutes and the pellet was resuspended in 1 ml DMEM+. One milliliter of the cell suspension was transferred in a T75 culture flask filled with 25 ml DMEM+. Cultivation of the cells proceeded at 37 °C in a CO_2 incubator. Cells were passaged when they reached 90% confluence.

3.5.1.2 Passaging of HEK293T cells

After removal of medium, the cell layer was rinsed with 10 ml 1 x DPBS. After removal of PBS, 2 ml Trypsin were added to cover the entire cell layer. The flask was incubated at 37 °C for 3 minutes to enhance Trypsin digestion. After incubation, the Trypsin digestion was stopped by adding 13 ml DMEM+. The cell suspension was transferred to a 50 ml tube and centrifuged at 300 x g for 5 minutes. The cell pellet was resuspended in 4 ml DMEM+ (prior to transfection, cells are resuspended in 4 ml DMEM-) and transferred to a T75 culture flask with 25 ml DMEM+. For a cultivation period of 4 days, 100 µl of the cell suspension and for a cultivation period of 3 days, 250 µl of the cell suspension were seeded into the culture flask.

3.5.1.3 Cryopreservation of HEK293T cells

Cell cultures with approximately 90% confluence were used for cryopreservation. The cell pellet was harvested as described in the passaging protocol and the cells were resuspended in 4.5 ml 37% FCS in DMEM+. Six cryotubes were prepared adding 750 µl of cell suspension

and 750 µl of 20% DMSO in DMEM+ in each tube. The cryotubes were stored at -80 °C in a freezing container and transferred to liquid nitrogen storage the next day.

3.5.1.4 Transfection of HEK293T cells

HEK293T cells were transfected with Lipofectamine 3000 reagent (Thermo Fisher Scientific, Waltham, MA, USA). The cells were seeded one day before transfection in a 24-well plate. For this, 2.5 x 10^5 cells were mixed with 500 µl DMEM- per well and incubated at 37 °C overnight. For transfection, 1.5 µl Lipofectamine 3000 were mixed with 48.5 µl Opti-MEM and 0.5 µg of plasmid DNA were diluted with 1 µl P3000 reagent and Opti-MEM to a final volume of 50 µl. The Lipofectamine and plasmid mixture was combined and incubated for 15 minutes at room temperature. The complete transfection solution was carefully added to the seeded cells. The cells were incubated overnight at 37 °C before harvesting the cell pellet for DNA or RNA isolation.

3.5.1.5 Lipofection of HEK293T with ribonucleoproteins (RNPs)

For CRISPR genome editing, RNP complexes were used, compiled of a S.p.Cas9 D10A nickase enzyme (Integrated DNA Technologies, Leuven, Belgium), crRNA and tracrRNA. The crRNA guides the Cas9-nickase to the target region, since its sequence is composed of a complementary region to the target DNA and the tracrRNA. The tracrRNA is a universal RNA sequence that is necessary to generate a functional RNP complex. A fluorescently labelled tracrRNA-ATTO 550 was used to monitor the transfection efficacy with the RNPs.

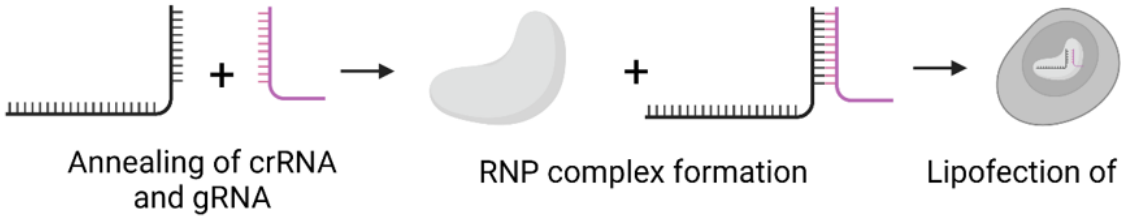

Figure 18: Workflow of RNP complex formation and transfection. Modified from IDT, Integrated DNA technologies, Genome editing with CRISPR-Cas9 (https://eu.idtdna.com/pages/products/crispr-genome-editing/alt-r-crispr-cas9-system). Created with BioRender.com.

Prior to transfection, the crRNA and tracrRNA were annealed to form a gRNA complex. The lyophilized RNAs were resuspended in nuclease-free duplex buffer provided by IDT (Integrated DNA Technologies, Leuven, Belgium) to a 100 µM stock concentration and mixed in equimolar concentrations to a final concentration of 1 µM. The RNA-duplex was formed by

heating at 95 °C for 5 minutes. The nickase enzyme was diluted to a working concentration of 1 µM in Opti-MEM. Formation of the RNP complex was performed for transfection in a 24-well plate using the following protocol:

Table 39: Components and volumes for RNP complex formation based on transfection with different lipofection reagents.

Component	**3000** (µl per well)	**RNAiMAX** (µl per well)	**CRISPRMAX** (µl per well)
gRNA duplex (1 µM)	1.5	1.5	1.5
Nickase enzyme (1 µM)	1.5	1.5	1.5
Cas9 PLUS reagent	-	-	0.6
P3000 reagent	1	-	-
Opti-MEM	21.0	22.0	21.4
Total	25	25	25

For Cas9-nickase experiments, two RNP complexes were prepared containing either one or the other gRNA duplex. The reaction was incubated at room temperature for 5 minutes. For lipofection of HEK293T cells, either forward or reverse transfection was conducted. For forward transfection, 1.25 x 10^5 cells were seeded into one well of a 24-well plate one day prior to lipofection. For lipofection, 50 µl of transfection complex was added to the cells. For reverse transfection, the cells were harvested during incubation of the transfection solution and diluted to 4 x 10^5 cells/ml. First, 50 µl of the transfection solution was added to one well of a 24-well plate, followed by 500 µl of the cell suspension. The cells were incubated with the RNP complex for 24-48 hours at 37 °C. The transfection solution was prepared as follows and incubated at room temperature for 20 minutes:

Table 40: Components and volumes for transfection of HEK293T in a 24-well plate. Lipofectamine 3000, RNAiMAX or CRISPRMAX were used to transfect the cells.

Component	**Volume/well**
RNP complex with gRNA1	12.5 µl
RNP complex with gRNA2	12.5 µl
Lipofectamine reagent	1.2 µl
Opti-MEM	23.8 µl
Total	50 µl

3.5.2 Cultivation and transfection of induced pluripotent stem cells (iPSCs)

The following protocols refer to cultivation of feeder-free iPSCs.

3.5.2.1 Coating of tissue culture plates

For feeder-free cultivation of iPSCs, tissue culture plates were coated with Vitronectin (VTN-N) recombinant human protein. Vitronectin aliquots were stored at -80 °C and thawed at room temperature. The thawed Vitronectin was diluted 1:100 in DPBS. The Vitronectin solution was added to the respective well (used volumes are shown in table 41) and incubated for 1 hour at 37 °C. The culture plate was wrapped with Parafilm and stored at 4 °C for up to 7 days if not used immediately. Prior to using, the coated plates were warmed at 37 °C and the Vitronectin solution was removed from the wells immediately before seeding the cells.

Table 41: Required volume of Vitronectin solution.

Culture plate	Volume/well
6-well plate	1 ml
12-well plate	0.5 ml
24-well plate	0.25 ml
10-cm dish	6 ml
8-well chamber culture slide	0.25 ml

3.5.2.2 Thawing of iPSCs

E8 Flex + medium was supplemented with RevitaCell (1 x) (Thermo Fisher Scientific, Waltham, MA, USA), which increases the cell survival after thawing. One well of a 6-well plate per cryovial was coated with Vitronectin. Cryopreserved iPSCs were partially thawed at 37 °C using a water bath. When only a small ice crystal was left, 1 ml of E8 Flex + with RevitaCell was added drop-wise to the cryovial. The cell suspension was gently collected, transferred to a 50 ml tube and topped up with 8 ml of E8 Flex + with RevitaCell. To remove the freezing medium, the cells were centrifuged at 120 x g for 3 minutes and the cell pellet was gently resuspended in 1 ml E8 Flex + with RevitaCell. The cell suspension was then seeded into the coated well of a 6-well plate and cultivated in a CO_2 incubator at 37 °C. If the cells attached well, the medium was changed to 2 ml E8 Flex + after 24 hours. If just a few cells attached, the medium was topped up with 1 ml fresh E8 Flex +. The medium was changed daily until passaging.

3.5.2.3 Passaging of iPSC colonies

Induced pluripotent stem cells grow in colonies and should be passaged when they are well compacted and approximately 70% confluent. The culture also requires passaging if a high number of differentiated cells is observed.

Feeder-free iPSC colonies were cultured in 6-well plates coated with Vitronectin and usually one well was passaged every 3 to 4 days to maintain the culture. The cells were washed with 2 ml of DPBS per well and detached with 1 ml Cell Dissociation Buffer or ReLeSR (STEMCELL Technologies Germany GmbH, Köln, Germany). Both reagents are enzyme-free and enable a gentle dissociation of the iPSC colonies without breaking them into single cells. The dissociation solutions were incubated for approximately 3-5 minutes at room temperature and removed prior to adding 2 ml of pre-warmed E8 Flex + medium. A 5 ml or 10 ml pipette was used to gently collect the cell suspension. The procedure was repeated a second time and the cell suspension was transferred to a 50 ml tube. The cell suspension was diluted with E8 Flex + medium to the desired split ratio. Established cultures were splitted between 1:4 and 1:10. If the wells showed a high confluence, split ratios were adapted to 1:10 between 1:20. Prior to seeding of the cells, the wells were prepared by removing the Vitronectin solution and adding E8 Flex medium. The cells were seeded and incubated at 37 °C. The medium was changed the next day and every second day thereafter until passaging of the cells.

3.5.2.4 Cryopreservation of iPSCs

Cells were frozen when the culture was 70-80% confluent. One well of a 6-well plate was used to prepare 3 to 5 cryovials. For freezing medium, 10% DMSO was prepared in Knockout Serum Replacement (KSR) (Thermo Fisher Scientific, Waltham, MA, USA) and 1 ml of the medium was used per cryovial. The cells were detached using the protocol for passaging of iPSC colonies and the resulting cell suspension was centrifuged at 120 x g for 1 minute. After discarding the supernatant, the cell pellet was resuspended in the required volume of freezing medium. One milliliter of the cell suspension was transferred into each cryovial and after adapting the cells to -80 °C overnight, the cryovials were transferred to liquid nitrogen tanks for long-term storage.

3.5.2.5 Single cell passaging of iPSCs

Single cell passaging was performed prior to transfection, FACS sorting or subcloning of iPSCs. To increase the survival of single cells, the culture medium was supplemented with RevitaCell (1 x) (Thermo Fisher Scientific, Waltham, MA, USA) or CloneR (1 x) (STEMCELL Technologies Germany GmbH, Köln, Germany). The latter was used for CRISPR editing experiments including electroporation followed by FACS sorting and subcloning. These procedures represent a high stress level for the cells over a long period. CloneR can be used in the cell culture for up to 4 days without altering the cell morphology or physiology, whereas

RevitaCell should be removed from the culture after approximately 24 hours. The cells to be passaged were washed with 2 ml DPBS per well of a 6-well plate and dissociated with 1 ml Accutase. After 3-5 minutes incubation at 37 °C, 1-2 ml of E8 Flex + medium were added without removing the Accutase solution. A P1000 pipette was used to gently triturate the cells. The suspension was collected in a 50 ml tube and centrifuged at 300 x g for 5 minutes. The resulting cell pellet was resuspended in the respective amount of E8 Flex + medium with RevitaCell or CloneR. Prior to electroporation the cells were resuspended in E8 Flex – with RevitaCell or CloneR. After seeding the cells onto the cell culture plates, they were incubated at 37 °C.

3.5.2.6 Electroporation of iPSCs

The iPS cells were transfected by electroporation using the Neon Transfection System (Thermo Fisher Scientific, Waltham, MA, USA). Electroporation was performed when cells were 70-90% confluent. The cells were harvested using Accutase and the cell pellet was resuspended in 2 ml DPBS. After counting the cells using the Tecan plate reader (Tecan Deutschland GmbH, Crailsheim, Germany), the cells were again centrifuged for 5 minutes at 300 x g and resuspended in 1 x DPBS containing calcium and magnesium to a final concentration of 5 x 10^5 cells/100 µl. The 100 µl of cell suspension was mixed with 30 µg endotoxin-free plasmid DNA and collected with the Neon pipette provided with a 100 µl Neon pipette tip. The pipette was inserted into the pipette station already containing 3 ml of DPBS supplemented with calcium and magnesium. The electroporation was conducted with 1400 volt, 5 milliseconds and 3 pulses. The electroporated cells were seeded in a pre-coated well of a 12-well plate containing 1 ml of E8 Flex – supplemented with RevitaCell or CloneR (1 x) and incubated at 37 °C for 48-72 hours with medium change every 24 hours.

3.5.2.7 Fluorescence-activated cell sorting (FACS) of iPSCs

Fluorescence-activated cell sorting (FACS) is used to separate a cell population based on light scattering and fluorescence labels enabling the isolation of particular cells of interest.

To perform gene editing experiments, the iPSCs were transfected with CRISPR constructs containing a GFP expression cassette. The GFP expression was used to isolate transfected from untransfected cells by means of FACS (Figure 19).

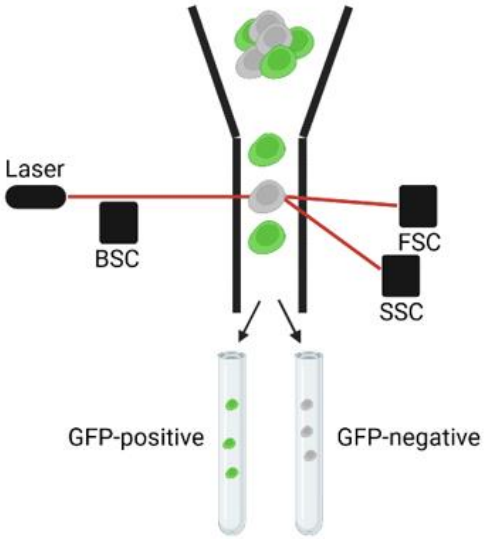

Figure 19: Scheme of fluorescence-activated cell sorting (FACS). The cell mixture is analysed and sorted in a liquid flow. Through vibration, single droplets are formed which usually have the right size to hold a single cell. The single cell passages a laser beam and the resulting light scatter is measured by different detectors. One detector measures forward scatter and a second detector measures side scatter. These parameters correlate with the cell size and structure and are used for characterization of the cells. After detection, the cells are deposited in different tubes depending on their fluorescence signal. Created with BioRender.com.

The iPS cells were prepared for sorting as follows: a 24-well plate was coated with Vitronectin and sorting medium consisting of E8 Flex + supplemented with CloneR and Knockout Serum Replacement (KSR) was warmed-up in a 37 °C water bath. The cells were harvested 48 hours post transfection using Accutase. After transferring the cells to a 50 ml tube, they were mixed with E8 Flex + medium to a final volume of 10 ml. The cell suspension was filtered through a 40 µm nylon mesh into a fresh 50 ml tube and counted using the Tecan plate reader before centrifugation at 300 x g for 5 minutes. The cell pellet was resuspended in sorting medium to a final concentration of 1 x 10^6 cells in 250 µl. The cell suspension was transferred to a 15 ml tube and kept on ice. Sorting of the cells was done by Dr. Kristin Bieber at the FACS Core Facility Berg, University of Tuebingen. The cells were sorted as a bulk under sterile conditions at 4 °C based on GFP expression with a target ratio about 10%. An unstained negative control was also included. The sorted cells were dispensed into a 15 ml tube containing 1 ml sorting medium. Before seeding, the cells were centrifuged and resuspended in fresh sorting medium. The bulk of sorted cells was seeded in pre-coated 24-well plates and kept at room temperature for 15 minutes to adapt the cells to the changing temperatures before incubation at 37 °C in the CO_2 incubator. The sorting medium was changed to E8 Flex+ 1-2 days after sorting and the cells were further expanded when reaching 70-90% confluence.

3.5.2.8 Subcloning of iPSCs

To evaluate the CRISPR genome editing on the level of iPSC clones, the cells were transfected with the respective CRISPR constructs, followed by FACS sorting and subcloning. The edited cells were expanded to approximately 70% confluence in 6-well plates after electroporation and sorting. The medium was removed and the cells were washed with 2 ml DPBS. Dissociation of the cells was achieved by adding 1 ml Accutase and incubation at 37 °C for 3-5 minutes. The reaction was stopped using 1-2 ml E8 Flex + medium. After transferring the cell suspension to a 50 ml tube, centrifugation at 300 x g for 5 minutes was carried out to obtain a cell pellet. The pellet was resuspended in 10 ml E8 Flex + medium supplemented with CloneR (1 x). After trituration of the cells to dissociate them into single cells, they were counted using the Tecan plate reader. The cell suspension was serially diluted in order to generate a single cell suspension at 1 x 10^3 cells/ml. One to two milliliters of the final cell dilution was seeded onto a pre-coated 10 cm-dish already containing 9 ml E8 Flex + medium supplemented with CloneR (1 x). The cells were incubated for 48 hours at 37 °C in a CO_2 incubator. After 48 hours the medium was changed daily to 10 ml E8 Flex + for 8 days. After 8 days, the single cell-derived colonies were manually picked and transferred to pre-coated 24-well plates. The medium was aspirated from the 10 cm-dish and the cells were washed with 10 ml DPBS. The iPSC colonies were gently detached with 5 ml of cell dissociation buffer. To keep the cells in place, the buffer was just incubated for a few seconds at 37 °C without detaching the colonies completely from the dish. The cell dissociation buffer was aspirated and 10 ml of E8 Flex + medium was added to the dish. Using a P100 pipette, the individual colonies were picked and transferred to a 24-well plate containing 500 µl E8 Flex+ medium supplemented with CloneR. The medium was changed daily until the wells were 70-90% confluent. The confluence was reached after 5 days, where the cells were washed and detached with ReLeSR. After aspiration of ReLeSR, 1 ml E8 Flex + medium was added to collect the cells. A freshly coated 24-well plate was loaded with 500 µl of the cell suspension for further expansion and the remaining 500 µl were used for DNA extraction with the Lucigen QuickExtract DNA extraction solution (see 3.3.2 DNA isolation from cell cultures).

3.5.2.9 Lipofection of iPS cells with ribonucleoproteins (RNPs)

Preparation of crRNAs, tracrRNA and Cas9 nickase enzyme was performed according to the protocol 3.5.1.5 Lipofection of HEK293T with ribonucleoproteins (RNPs). Induced pluripotent stem cells were additionally transfected using Lipofectamine Stem. Formation of the RNP complex was conducted in a 24-well plate using the following protocol:

Table 42: Components and volumes for RNP complex formation based on transfection with different lipofection reagents.

Component	3000 (µl per well)	RNAiMAX (µl per well)	CRISPRMAX (µl per well)	Stem (µl per well)
gRNA duplex (1 µM)	1.5	1.5	1.5	1.5
Nickase enzyme (1 µM)	1.5	1.5	1.5	1.5
Cas9 PLUS reagent	-	-	0.6	-
P3000 reagent	1	-	-	-
Opti-MEM	21.0	22.0	21.4	22.0
Total	25	25	25	25

For Cas9-nickase experiments, two RNP complexes were prepared containing either one or the other gRNA duplex. The reaction was incubated at room temperature for 5 minutes. For transfection of iPS cells, 5 x 10^4 single cells/well were seeded onto a 24-well plate one day prior to lipofection. On the day of transfection, the old medium was removed and 300 µl fresh medium without antibiotics was added to the cells. Likewise, 300 µl medium was mixed with transfection solution and added to the wells. The cells were incubated with the RNP complex for 24-48 hours at 37 °C. The transfection solution was prepared as follows and incubated at room temperature for 20 minutes:

Table 43: Components and volumes for transfection of iPS cells in a 24-well plate. Lipofectamine 3000, RNAiMAX, CRISPRMAX or Stem were used to transfect the cells.

Component	Volume/well
RNP complex with gRNA1	12.5 µl
RNP complex with gRNA2	12.5 µl
Lipofectamine reagent	1.2 µl
Opti-MEM	23.8 µl
Total	50 µl

3.5.2.10 Fixation, DAPI staining, embedding and fluorescence microscopy of iPS cells

iPS cells were seeded in Falcon® 8-well culture slides (Corning, Inc., Corning, NY, USA) coated with vitronectin. Prior to fixation, the culture medium was removed and the cells were washed twice with 500 µl 1 x DPBS. To fixate the cells, 500 µl of 4% paraformaldehyde was added to each well and incubated for 15 minutes. The cells were washed three times with 500 µl 1 x DPBS for 10 minutes to remove the paraformaldehyde.

The fluorescent dye DAPI (4',6-Diamidino-2-phenylindol) was used to stain the nuclei of the cells. DAPI (1 µg/µl in DPBS) was added to each well (200 µl/well) and incubated for 1 minute. After incubation, the cells were washed twice with 500 µl 1 x DPBS for 5 minutes.

All steps were performed at room temperature.

For embedding, the polystyrene chamber was carefully removed and small drops of DAKO Fluorescent Mounting Medium (Agilent Technologies Deutschland GmbH, Waldbronn, Germany) were distributed on the glass slide. Coverslips were mounted on top of the medium.

Imaging was performed with the fluorescence microscope (Axio Imager Z1) equipped with an apotome and a camera (AxioCam MRm, Carl Zeiss AG, Oberkochen, Germany). Image capture was performed using the imaging software ZEN2.3 (Carl Zeiss AG, Oberkochen, Germany). Z-stacks were taken with 1x1 binning, 63x magnification and 10 phases.

3.6 Variant nomenclature

Variant nomenclature in this study is in accordance with Human Genome Variation Society recommendations (den Dunnen et al., 2016) and based on GenBank accession numbers NM_130837.3 and NM_032317.3.

3.7 *In silico* analysis

The web-based tools NNSplice (Reese et al., 1997) and MaxEntScan (Yeo & Burge, 2004) were used to predict splice sites. The minimum score for splice sites was set to 0.4 using NNSplice and the Maximum Entropy Model was selected to score splice sites with MaxEntScan. *In silico* prediction of missense variants was performed using MutationTaster (Schwarz et al., 2014) and Polyphen-2 (Adzhubei et al., 2010). Allele frequencies were retrieved from the Genome Aggregation Database gnomAD V.2.1.1 (Karczewski et al., 2020).

4 Results

4.1 "2n" CRISPR/Cas9 nickase genome editing targeting the deep intronic mutation c.610+364G>A in *OPA1*

4.1.1 Genotyping of CRISPR/Cas9 nickase-treated patient-derived iPSCs

The Cas9 variant D10A nickase introduces single-strand nicks in the target genomic sequence. The need of a gRNA pair to perform double-strand breaks increases the specificity of genome editing and thereby reduces the number of unwanted off-target effects. Patient-derived iPSCs were treated with a CRISPR/Cas9 nickase approach including a pair of gRNAs ("2n") to target the deep intronic mutation (DIM) c.610+364G>A in *OPA1*. The transfected cells were selected with puromycin followed by DNA extraction and genotyping of the treated iPSC bulk. Transfection of the patient-derived iPSCs was performed by Jasmin Haderspeck during her PhD studies in the Institute for Neuroanatomy and Developmental Biology, University Hospital Tuebingen. Genotyping of the CRISPR-treated cells was done in our laboratory and was part of my PhD work. The genomic region between exon 4 and exon 5 of the *OPA1* gene was amplified from DNA extracted from treated iPSCs. The resulting PCR product was subcloned to obtain individual bacterial clones. The bacterial clones were Sanger sequenced to detect various CRISPR/Cas9 nickase-induced indels (Figure 20).

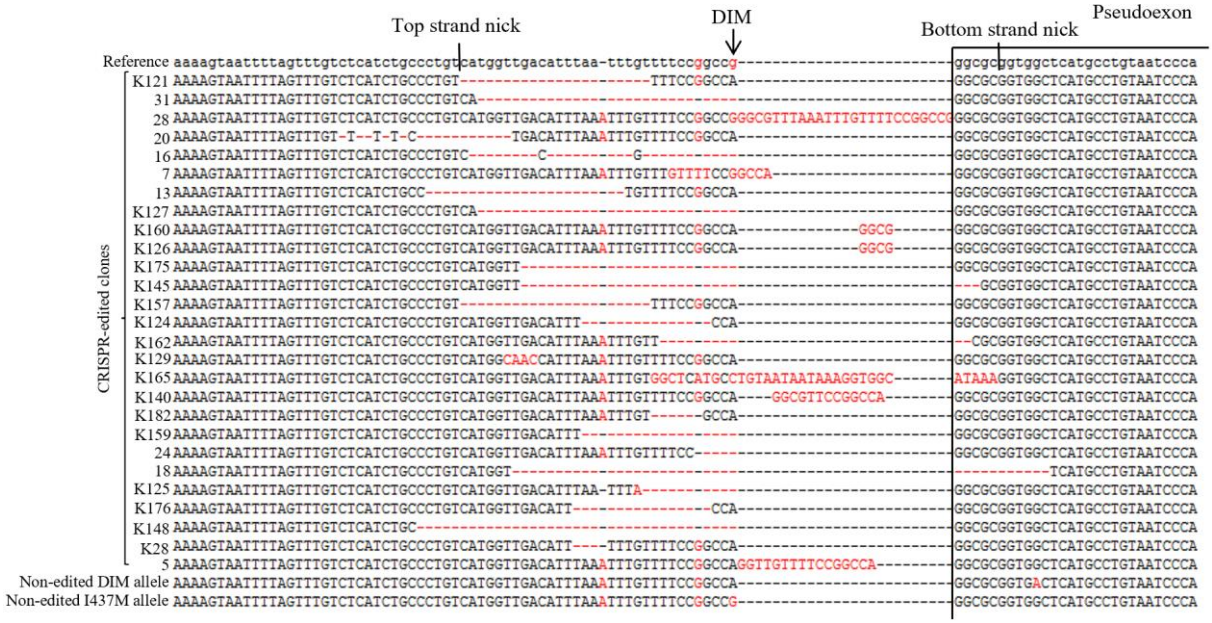

Figure 20: CRISPR/Cas9 nickase-induced editings in patient-derived iPSCs. Sanger sequencing of individual bacterial clones obtained by cloning of PCR products from genomic DNA of CRISPR/Cas9 nickase-treated *OPA1*-mutant iPS cells.

The single nucleotide polymorphism (SNP) rs7624750 in exon 4 of *OPA1* was sequenced to investigate the allele-specificity of the CRISPR/Cas9 nickase-editing (Table 44). The paternal allele harboring the missense variant c.1311A>G; p.(I437M) is hereafter referred to as the I437M allele and the maternal allele carrying the DIM c.610+364G>A is designated as DIM allele (Pedigree see figure 8). The I437M allele carries a guanine (G) at the SNP site and the mutant DIM allele carries an adenine (A). In total, 51 individual bacterial clones, corresponding to 51 alleles were sequenced. Out of those, 20 alleles were identified as I437M and 31 as DIM alleles. Four out of twenty I437M alleles and 23/31 DIM alleles were edited by the CRISPR machinery.

Table 44: Allele-specificity of CRISPR/Cas9 nickase-induced editings. Number of edited and non-edited I437M or DIM alleles. Discrimination of alleles is based on the genotype of SNP rs7624750.

	I437M allele	**DIM allele**	**In total**
Edited	4	23	27
Non-edited	16	8	24
In total	20	31	51

Splice site prediction using *in silico* tools NNSPLICE (Reese et al., 1997) and MaxEntScan (Yeo & Burge, 2004) was done to evaluate if the detected CRISPR/Cas9 nickase editings result in the elimination of the DIM-induced cryptic acceptor (3´) splice site (Table 45). The 3´splice site score of the unedited wild-type (clone 1) and mutant (clone 3) sequence is shown as a reference. Deletion of the DIM predicted in 7/10 cases also eliminated the acceptor splice site. Editings of clones 7 and 28 restored the wild-type guanine (G) at the DIM position, resulting in a predicted loss of the acceptor splice site in clone 28 but not in clone 7. NNSPLICE also predicted an additional 3´splice site in clone 5 with a score of 0.44 and a donor splice site introduced by editing seen in clone K93 with a score of 0.54.

Table 45: Splice site prediction of CRISPR/Cas9 nickase-edited target region. Acceptor splice site (3´ss) score was determined using NNSPLICE and MaxEntScan.

Clone number	**SNP rs7624750**	**c.610+364**	**NNSPLICE 3´ss score**	**MaxEntScan 3´ss score**
1	G	G	-	-1.81
3	A	A	0.82	6.15
K4(28)	A	A	0.89	7.42
K49(121)/K85(157)	A	A	0.82	8.78
K52(124)	A	A	0.49	4.91
K53(125)	A	deleted	0.43	4.75
K54(126)/K88(160)	A	A	0.86	-5.91

K57(129)	A	A	0.82	6.15
K68(140)	A	A	0.72	2.21
K73(145)	A	deleted	-	-3.08
K76(148)	A	deleted	-	-7.11
K87(159)	A	deleted	-	-4.59
K88(160)	A	A	0.86	-16.30
K90(162)	A	deleted	-	-11.81
K93(165)	A	C	0.54 (5´ss)	-37.79/-14.49 (5´ss)
K103(175)	A	deleted	-	-1.89
K104(176)	G	A	-	4.46
K110(182)	A	A	-	5.09
5	A	A	0.82/0.44	4.57
7	A	G	0.90	7.61
13	A	A	0.84	8.88
16	G	deleted	-	-0.48
18	G	deleted	-	-22.05
20	A	A	0.82	6.15
24	G	deleted	-	-5.66
28	A	G	-	-1.81
31/K55(127)	A	deleted	0.84	6.91

4.1.2 Splicing analysis of CRISPR/Cas9 nickase-induced editings using minigene constructs

Minigene assays were used to evaluate the splicing pattern induced by the different Cas9-nickase editings. An *OPA1* minigene construct was generated by Tobias Bonifert, Institute for Ophthalmic Research, University Hospital Tuebingen. The minigene construct consists of a pSPL3 backbone (Buckler et al., 1991; Burn et al., 1995) and a gene insert comprising the wild-type sequence from exon 4b to exon 5 of *OPA1*. In addition to the wild-type construct, a construct including the DIM was prepared. Furthermore, *OPA1* minigene constructs were generated with inclusion of 10 different Cas9 nickase editings using *in vitro* mutagenesis (IVM) of the original WT construct (editings seen in clone K76, 31, K103, K73, K87, K53, K93, K90, 7 and 28). The editings were selected based on the elimination of the DIM. Clone 31, K53 and 7 editings were also included despite prediction of the DIM acceptor splice site. After the IVM PCR, the template vector construct was digested using *Dpn*I. The *Dpn*I-digested product was purified prior to phosphorylation and ligation. Competent *E.coli* cells were transformed with the ligation and were used to propagate the plasmid constructs. To verify the correct inclusion of the indels, the extracted plasmids were Sanger sequenced. The resulting minigene constructs were used to transfect HEK293T cells. Genomic RNA was isolated from the HEK293T cells 24 hours post transfection and used to synthesize cDNA. The splicing pattern induced by the Cas9-nickase

editings was visualized by RT-PCR using a vector-specific primer together with an *OPA1* minigene-specific primer and further characterized by subcloning of the PCR products and Sanger sequencing (Figure 21).

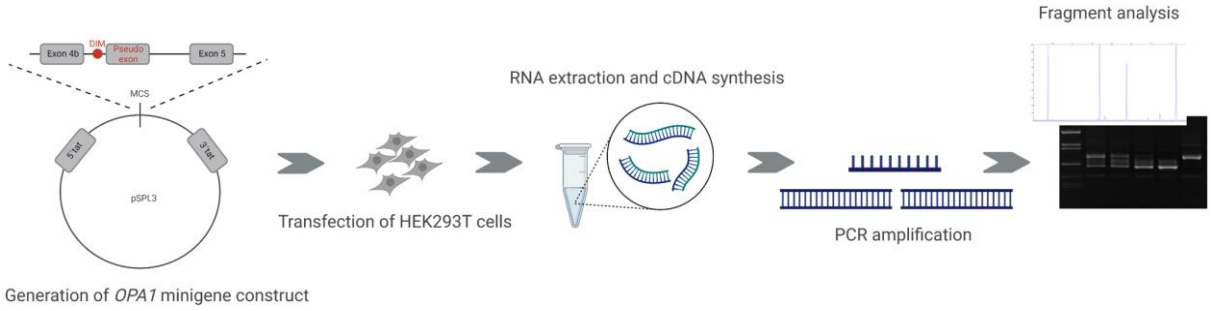

Figure 21: Minigene assay workflow to analyse Cas9 nickase editings. *OPA1* minigene constructs including the different CRISPR editings were generated by inverse PCR of the wild-type construct. The wild-type *OPA1* minigene construct and a minigene construct harboring the DIM c.610+364G>A served as control. Created with BioRender.com.

No mutant transcript containing the pseudoexon (284 bp) was detected in 8/10 editing events, corresponding to complete rescue of missplicing (Figure 22). An alternative wild-type transcript lacking exon 5 was identified in clone 28 (123 bp). Clone 31 partially restored normal splicing, showing a slight decrease of the DIM transcript and an increase of the wild-type transcript (191 bp), while clone 7 showed no rescue at all. These results are in line with the splice site predictions of NNSPLICE and MaxEntScan.

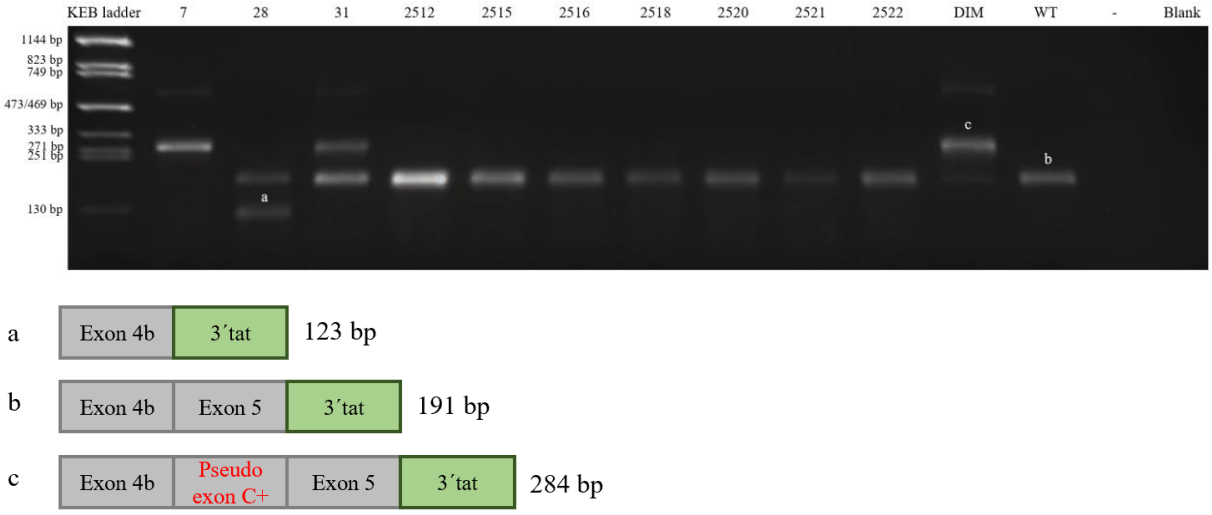

Figure 22: Minigene assay to analyse splicing rescue of CRISPR/Cas9 nickase-edited alleles. The agarose gel shows the RT-PCR products derived from HEK293T cells transfected with pSPL3 vectors harboring either the wild-type sequence (lane 13), the DIM sequence (lane 12) or constructs harboring Cas9 nickase editings (lanes 2-11). 2512 = clone K53(125), 2515 = clone K73(145), 2516 = clone K76(148), 2518 = clone K87(159), 2520 = clone K90(162), 2521 = clone K93(165), 2522 = K103(175). Blank control without DNA sample. Primers binding to

OPA1 exon 4b (HsOPA1-Ex4bint_F) and the 3´ tat exon (pSPL3seqcDNA_R) were used for RT-PCR. Schemes of the amplified products are presented below the agarose gel image. Grey boxes represent *OPA1* exons. The green exon represents the 3´ vector-resident exon.

4.2 "4n" CRISPR/Cas9 nickase genome editing targeting the deep intronic mutation c.610+364G>A in *OPA1*

4.2.1 Design of gRNA pairs

The "4n" approach was designed to further improve the CRISPR/Cas9 nickase genome editing. This strategy uses two pairs of gRNAs instead of one pair, further increasing the target specificity and thereby minimizing the risk of off-target effects. Placing one gRNA pair upstream and one gRNA pair downstream of the pseudoexon allows to eliminate the entire pseudoexon, thereby increasing the rescue of missplicing. In total, 9 gRNAs forming 6 different gRNA pairs were designed using the web-based platform Benchling (Figure 23 and Table 46).

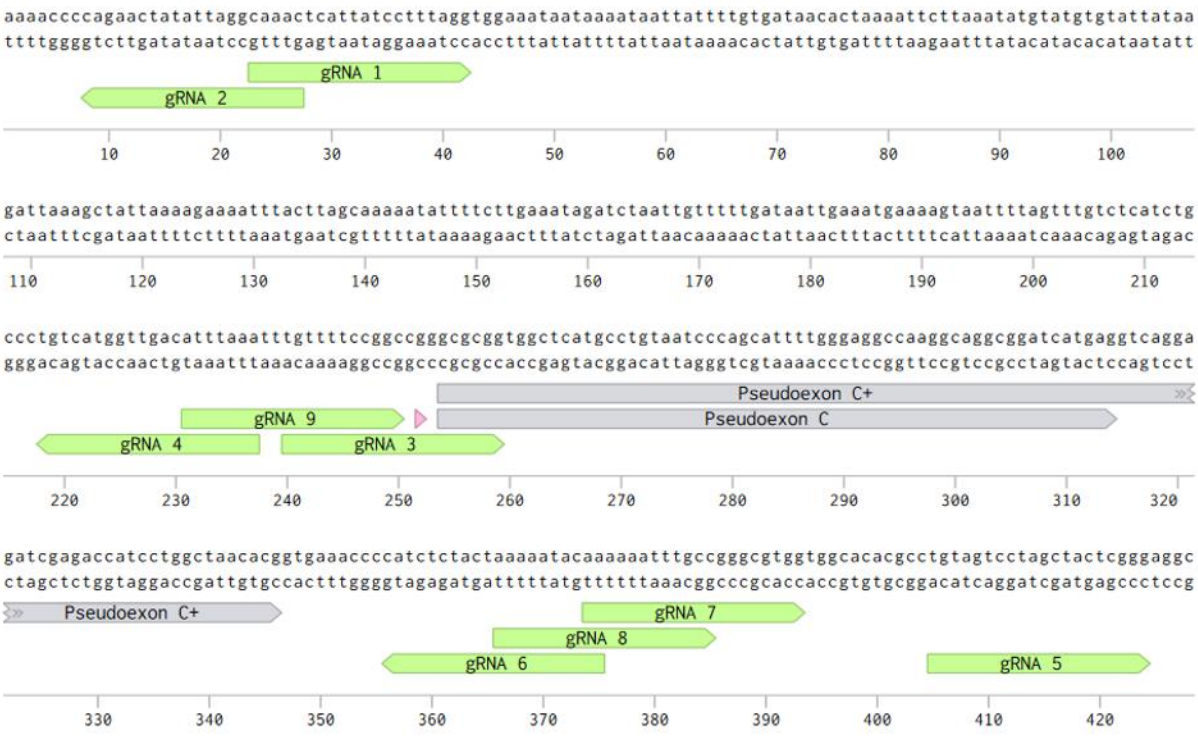

Figure 23: gRNA design for CRISPR/Cas9 nickase genome editing. Guide RNAs (shown as green arrows) were designed using the web-based platform Benchling. The upper DNA strand is depicted in 5´- 3´direction (+ strand), the complementary strand is depicted in 3´- 5´direction (- strand). The two pseudoexons are shown as grey arrows. The red triangle indicates the position of the DIM. The illustration was made using Benchling.com.

Table 46: Summary of gRNA pairs designed for CRISPR/Cas9 nickase genome editing. Guides were designed using the web-based platform Benchling regarding their location and on-target score. The on-target score is based on Doench, Fusi et al., 2016 and ranges between 0-100. A high score predicts a high cleavage efficacy of the gRNA pair.

gRNA pair	gRNA	Strand	Sequence	PAM	On-target score
1	1	+	caaactcattatcctttagg	tgg	54.4
	2	-	gtttgcctaatatagttctg	ggg	64.5
2	3	+	tgttttccggccgggcgcgg	tgg	54.2
	4	-	tttaaatgtcaaccatgaca	ggg	71.1
3	9	+	atttaaatttgttttccggc	cgg	47.2
	4	-	tttaaatgtcaaccatgca	ggg	71.1
4	5	+	tgtagtcctagctactcggg	agg	71.5
	6	-	ttgtatttttagtagagatg	ggg	53.8
5	7	+	aaaaaatttgccgggcgtgg	tgg	55.9
	6	-	ttgtatttttagtagagatg	ggg	53.8
6	8	+	aaaaatacaaaaaatttgcc	ggg	57.9
	6	-	ttgtatttttagtagagatg	ggg	53.8

4.2.2 Cleavage efficacy analysis of gRNA pairs

The cleavage efficacy of the individual gRNA pairs was determined to select the most efficient one for the "4n" CRISPR/Cas9 nickase approach. The designed gRNA pairs were cloned into the backbone vector pX461 expressing SpCas9n (D10A nickase mutant) and EGFP. HEK293T cells were transfected with the Cas9 nickase constructs and genomic DNA was extracted 72 hours post transfection. To analyse the cleavage efficacy of the gRNA pairs, the region of interest was amplified from the extracted genomic DNA using primers gRNApair1_F and gRNA-pair1_R_FAM for gRNA pair 1, JH_Fwd2_FAM and JH_CRISPR_Intr4_large_R1 for gRNA pair 2 and 3, OPA1intr4b_g4-6_FAM and OPA1intr4b_g4-6_R for gRNA pair 4, 5 and 6, respectively. The FAM-label on one of the primers allows the analysis of fragments on a capillary sequencer. The PCR product from gRNA pair 1 and gRNA pair 2/3 was too large for fragment analysis and required a prior restriction digest. The PCR product of gRNA pair 1 (403 bp) was cut with *Spe*I into two fragments of 126 bp and 277 bp, the latter of which carried the FAM label. Accordingly, the 126 bp fragment was not visible in the fragment analysis. The PCR product from gRNA pair 2 and 3 (590 bp) was digested with *Bsa*I resulting in two fragments of 290 and 300 bp, the latter of which carried the FAM-label. The fluorescently-labelled PCR fragments were analysed on a capillary sequencer using the GeneScan mode and further evaluated using the GeneMapper software 5 (Applied Biosystems, Waltham, MA, USA) (Figure 24A-B, supplemental figure S1). Figure 24A and B show representative GeneMapper

electropherograms. The fluorescence intensity (y-axis) of the peak is relative to the amount of the fragment, the x-axis indicates the size (in bp) of the fragment. Figure 24A represents the positive control and shows a peak corresponding to the non-edited fragment and additional peaks compatible with indels generated by the CRISPR/Cas9 nickase machinery. In contrast, the negative control shows no additional peaks (Figure 24B). The cleavage efficacy was determined by calculating the ratio of the edited fragments to the total amount of fragments based on the area under the curve provided by GeneMapper. The calculated cleavage efficacy for gRNA pair 1 was 10% and 14% for gRNA pair 2 (Figure 24C, supplemental figure S1A-B). None of the other gRNA pairs showed peaks compatible with edited fragments (supplemental figure S1C-F), resulting in a cleavage efficacy of 0%.

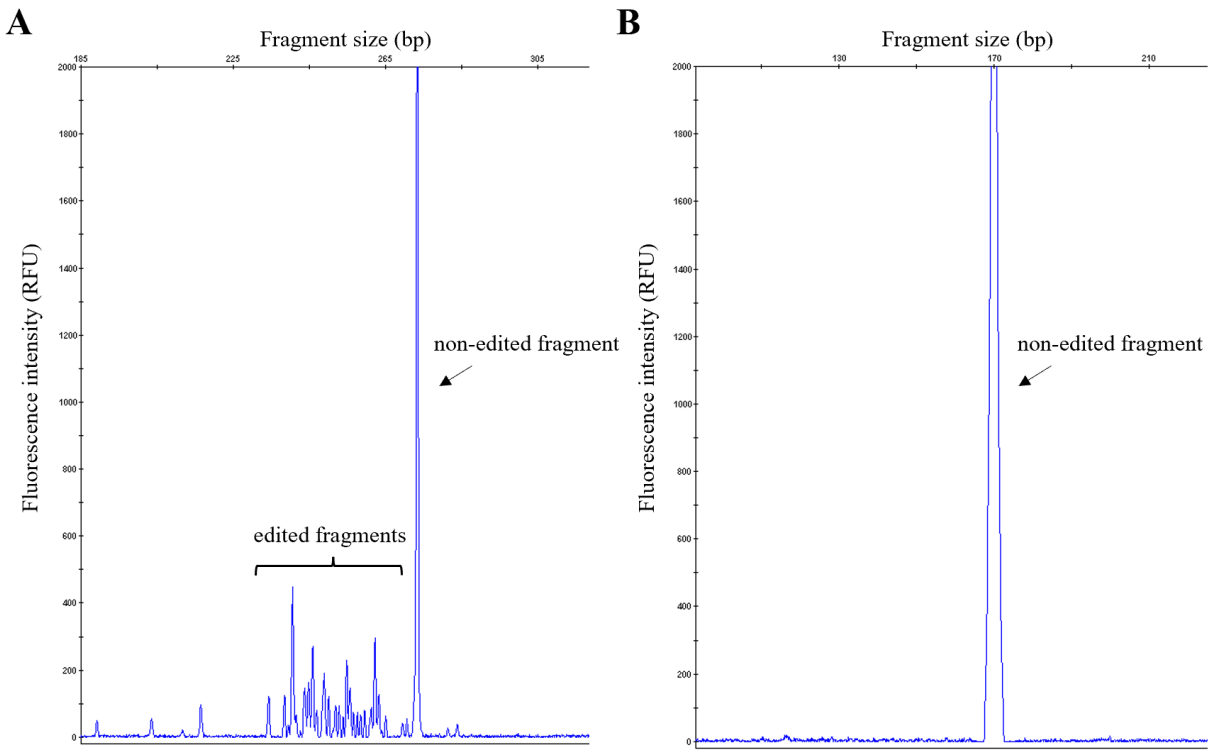

C

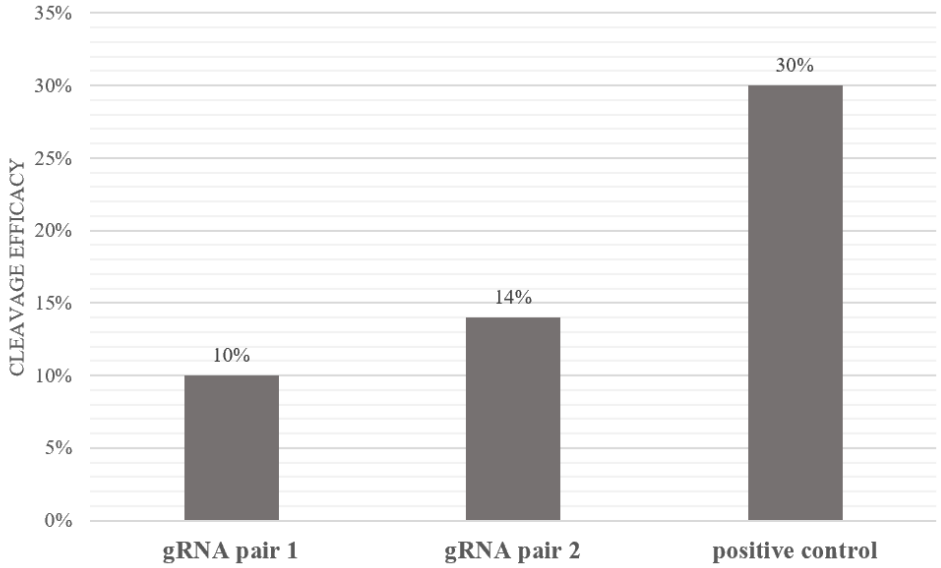

Figure 24: Cleavage efficacy analysis of CRISPR/Cas9 nickase gRNA pairs after transfection of HEK293T cells with plasmid constructs. GeneScan analysis of fluorescently-labelled PCR fragments amplified from genomic DNA of CRISPR/Cas9 nickase-treated HEK293T cells. **(A)** Representative electropherogram of edited cells (positive control: Cas9 nickase construct with a gRNA pair targeting the *ABCA4* gene) **(B)** Representative electropherogram of non-edited cells (Negative control: Amplification of genomic DNA from untransfected HEK293T cells with primer pair OPA1intr4b_g4-6_FAM and OPA1intr4b_g4-6_R) **(C)** Cleavage efficacy of gRNA pair 1, gRNA pair 2 and positive control.

4.2.3 CRISPR/Cas9 nickase genome editing by RNP delivery

As described in the previous chapter, Cas9 nickase genome editing with plasmids resulted in only low cleavage efficacy (0-14%), likely because the gRNAs used contained T-strands that are known to impair expression (Gao et al., 2018). To circumvent this issue, the CRISPR machinery was delivered using ribonucleoproteins (RNPs) instead of plasmids in the following experiment. In this method, cells are transfected with Cas9 nickase and gRNAs without the need of expression from a plasmid construct. HEK293T cells were transfected using Lipofectamine RNAiMAX with Cas9 nickase and gRNA pair 2, which had shown the highest efficacy (14%) in the plasmid transfection experiments. The cleavage efficacy was again analysed using fragment analysis. The CRISPR-treated cells showed no additional fragment peaks in comparison to the negative control (Supplemental figure S2). Similar results were obtained from transfection with other Lipofection reagents such as Lipofectamine 3000 or CRISPRMAX (results not shown). In addition to HEK293T cells, patient-derived iPSCs were transfected with RNPs delivered by Lipofectamine 3000, RNAiMAX, CRISPRMAX or Stem. The rate of cell survival

and transfection efficacy in iPSCs was already low, so that the further evaluation of the cleavage efficacy was not possible.

4.2.4 CRISPR/Cas9 nickase genome editing in patient-derived iPSCs

As described in Chapter 4.2.2, a cleavage efficacy of 14% by gRNA pair 2 was the maximum cleavage efficacy that could be established in HEK293T cells (Figure 24C). Based on these results, patient-derived iPSCs were transfected with the Cas9 nickase construct pX461 containing gRNA pair 2. Instead of using lipofection, transfection of iPSCs was performed using electroporation. Forty-eight hours after electroporation, GFP expression indicated a transfection efficacy of approximately 30-50% (Figure 25). Fragment analysis revealed a cleavage efficacy of 5% (Figure 26, supplemental figure S3).

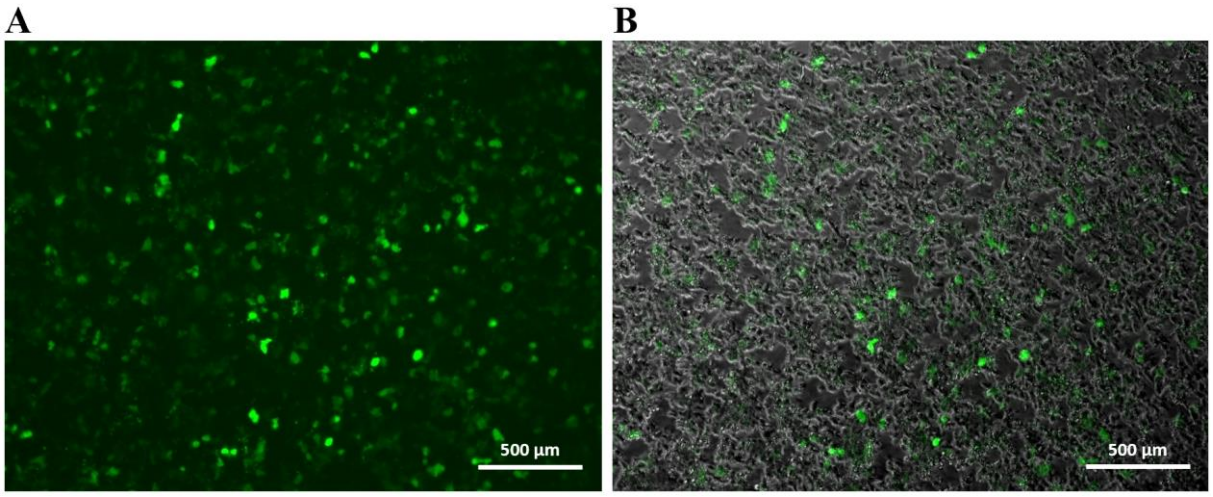

Figure 25: Transfection efficacy assessed by GFP expression after electroporation of patient-derived iPSCs with CRISPR/Cas9 nickase gRNA pair 2 plasmid construct. Fluorescence microscopy images were taken 48 hours post electroporation **(A)** GFP signal in electroporated iPS single cells **(B)** Overlay of transmission light and GFP images of electroporated iPS single cells.

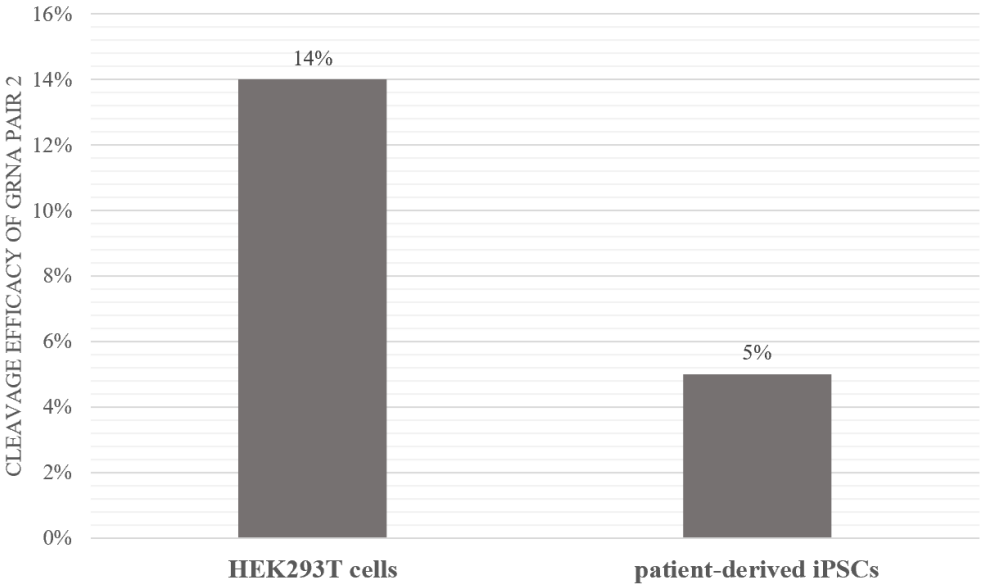

Figure 26: Cleavage efficacy of CRISPR/Cas9 nickase gRNA pair 2 in patient-derived iPSCs versus HEK293T cells. GeneScan analysis of fluorescently-labelled PCR fragments amplified from genomic DNA of CRISPR/Cas9 nickase-treated iPS single cells or HEK293T cells (plasmid transfection).

4.3 CRISPR/Cpf1 genome editing targeting the deep intronic mutation c.610+364G>A in *OPA1*

4.3.1 Design of gRNA pairs

As described in the previous chapters, targeting the DIM based on the Cas9 nickase strategy resulted in low cleavage efficacy for both plasmid and RNP delivery of CRISPR components. Because of the low efficacy of Cas9 nickase in general (Banakar et al., 2020), and the restricted design of gRNA pairs due to the T-rich sequence of the target region, the CRISPR/Cas9 nickase approach was no longer pursued. In search of an appropriate CRISPR strategy to target the DIM in *OPA1*, the nuclease Cpf1 (Cas12a) appeared as a suitable candidate. The advantage of Cpf1 over Cas9 nickase, with respect to the *OPA1* target region, is the recognition site of the nucleases. Cas9 nickase uses a G-rich recognition site, whereas Cpf1 depends on a T-rich PAM matching with the T-rich target region. For editing with Cpf1, four guide RNAs were designed using Benchling: two gRNAs upstream of the pseudoexon, one covering the DIM, and one downstream of the pseudoexon, which could be paired with a gRNA upstream to increase the editing efficacy (Figure 27 and Table 47).

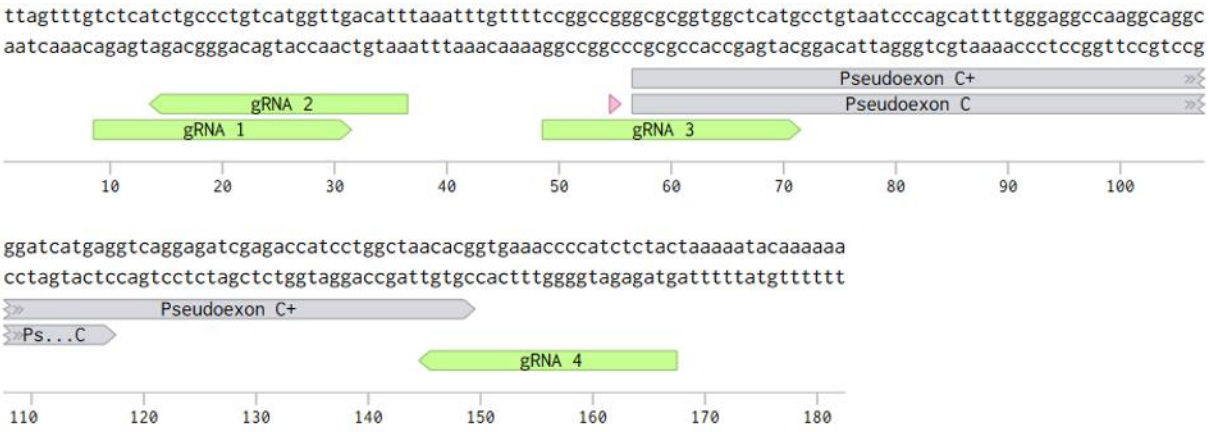

Figure 27: gRNA design for CRISPR/Cpf1 genome editing. Guide RNAs (shown as green arrows) were designed using the web-based platform Benchling. The upper DNA strand is depicted in 5′- 3′ direction (+ strand), the complementary strand is depicted in 3′- 5′ direction (- strand). The two pseudoexons are shown as grey arrows. The red triangle indicates the position of the DIM. The illustration was made using Benchling.com.

Table 47: Summary of gRNA pairs designed for CRISPR/Cpf1 genome editing. Guides were designed using the web-based platform Benchling.

gRNA	Strand	Sequence	PAM
1	+	tctcatctgccctgtcatggttg	tttg
2	-	aatgtcaaccatgacagggcaga	ttta
3	+	ccggccgggcgcggtggctcatg	tttt
4	-	gtagagatggggtttcaccgtgt	ttta

4.3.2 Cleavage efficacy analysis of gRNAs

To determine the cleavage efficacy of the individual gRNAs, patient-derived iPSCs were electroporated with the AsCpf1 plasmid construct pY094 including the respective gRNAs and an EGFP expression cassette. The transfection efficacy was determined 48 hours post electroporation and genomic DNA was harvested from the cells. The transfection efficacy was assessed based by GFP expression of the cells and was approximately 50 – 60% (Figure 28). Electroporation of iPSCs with the CRISPR/Cpf1 construct including gRNA 4 resulted in approximately 90% cell death and no GFP signal in five independent electroporation experiments and also after using an endotoxin-free plasmid preparation. Therefore, gRNA 4 was excluded from subsequent analysis.

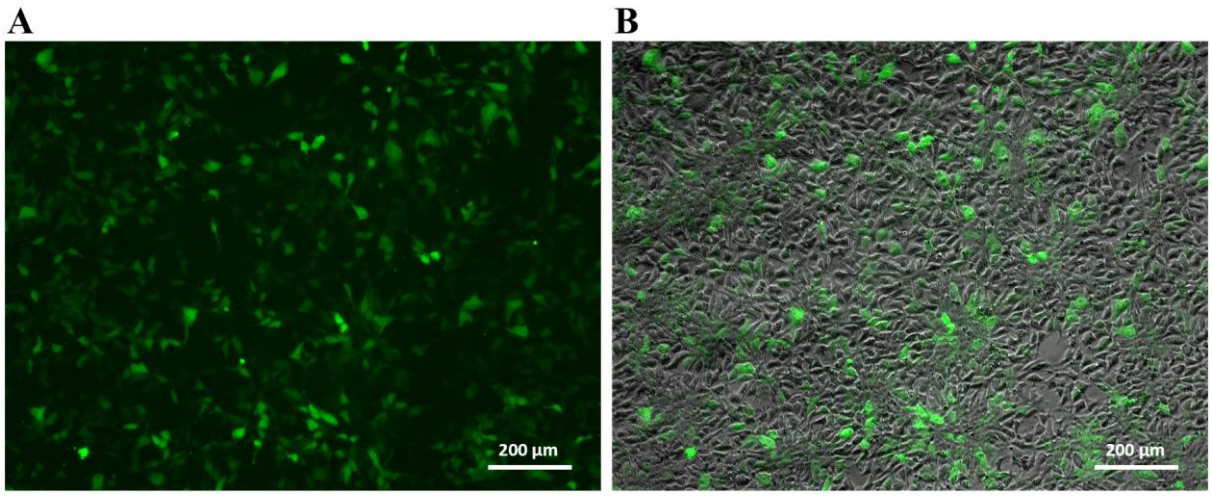

Figure 28: Transfection efficacy assessed by GFP expression after electroporation of patient-derived iPSCs with CRISPR/Cpf1 gRNA 1 plasmid construct. Representative image for CRISPR/Cpf1 constructs with gRNA 1, 2 and 3. Fluorescence microscopy images were taken 48 hours post electroporation **(A)** GFP signal in electroporated iPS single cells **(B)** Overlay of transmission light and GFP images of electroporated iPS single cells.

To evaluate the cleavage efficacy of the remaining gRNAs, the sequence region around the cleavage sites was amplified by PCR from the extracted genomic DNA with the following primer pair: Fluorescently-labelled forward primer JH_Fwd2_FAM and reverse primer JH_CRISPR_Intr4_large_R1. The amplification was followed by a restriction digest using *Bsa*I to generate smaller PCR fragments (300 bp + 290 bp). The fluorescently-labelled 300 bp fragment was detected by the capillary sequencer using GeneScan mode. The fragment analysis of gRNA 1 and gRNA 2 revealed additional small peaks, in comparison to the negative control, corresponding to fragments including indels generated from Cpf-editing (Supplemental figure S4A-B)). In contrast, treatment with gRNA 3 did not result in edited fragments (Supplemental figure S4C). The calculated cleavage efficacy was 6% for gRNA 1 and 3% for gRNA 2 (Figure 29). A positive control construct targeting the *CLEC16A* gene based on Ma et al., 2018 was also included in the experiment and showed a cleavage efficacy of 10% (Figure 29, supplemental figure S4D). Ma et al. described a 20-30% indel rate for *CLEC16A* in hiPSCs determined by a T7 endonuclease I assay (Ma et al., 2018).

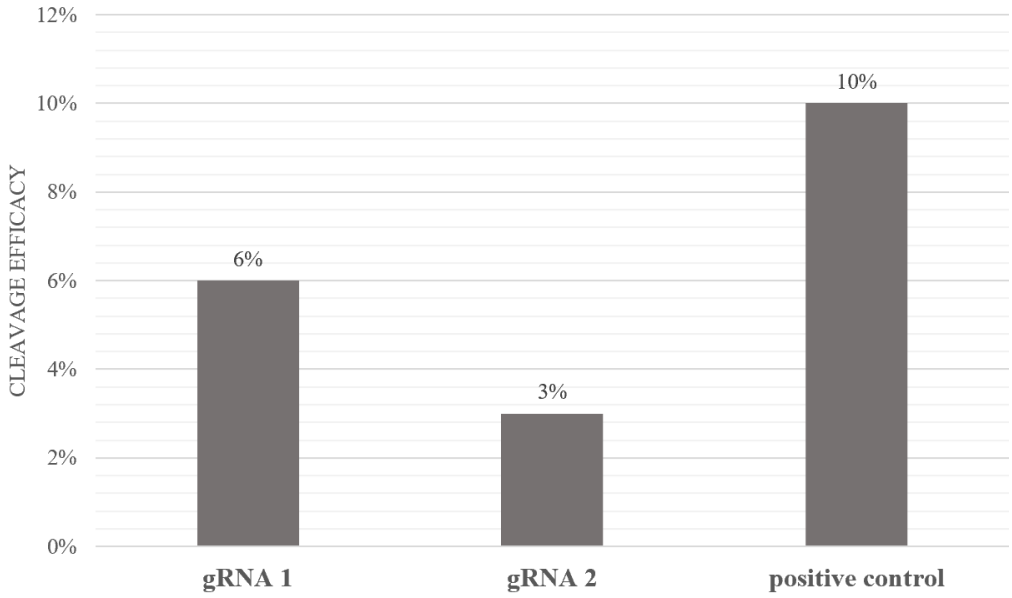

Figure 29: Cleavage efficacy analysis of CRISPR/Cpf1 gRNAs after electroporation of patient-derived iPSCs with plasmid constructs. GeneScan analysis of fluorescently-labelled PCR fragments amplified from genomic DNA of CRISPR/Cpf1-treated iPS single cells. A Cpf1 construct with a gRNA targeting the *CLEC16A* gene served as positive control.

4.3.3 Fluorescence-activated cell sorting (FACS) of CRISPR/Cpf1-treated iPSCs

To obtain a better estimate of the cutting efficacy of the gRNAs, the amount of untransfected cells was reduced by FACS sorting of iPSCs based on the GFP expression mediated by the CRISPR/Cpf1 plasmid. iPS single cells were sorted 48 hours post electroporation with the Cpf1-gRNA 1 and gRNA 2 construct. Sorting was performed at the FACS Core Facility Berg, University of Tuebingen. To identify and exclude remaining cell aggregates (douplets) in the single cell suspension, forward scatter (FSC) plots were performed followed by side scatter (SSC) plots allowing a more precise definition of the single cells (singlets). The FACS analysis of gRNA 1 revealed 71.52% viable cells, of which 93.01% were FSC singlets. Further douplet discrimination using back scatter (BSC) parameters resulted in 99.84% single cells (SSC singlets) (Figure 30A-C). Approximately 17% of the SSC singlets showed a moderate to high GFP expression (Figure 30D-E). The target ratio for sorting was set to 10.12% including exclusively cells with a high GFP expression. In total, 278.377 cells were counted, of which 25.275 cells were sorted. For gRNA 2, 73.30% viable cells were identified, of which 93.24% accounted for FSC singlets and 99.83% for SSC singlets (Figure 30F-H). Approximately 16% of SSC singlets revealed a moderate to high GFP expression (Figure 30I-J). Using a target ratio of 10.14%, 36.528 cells were sorted from a total number of 386.237.

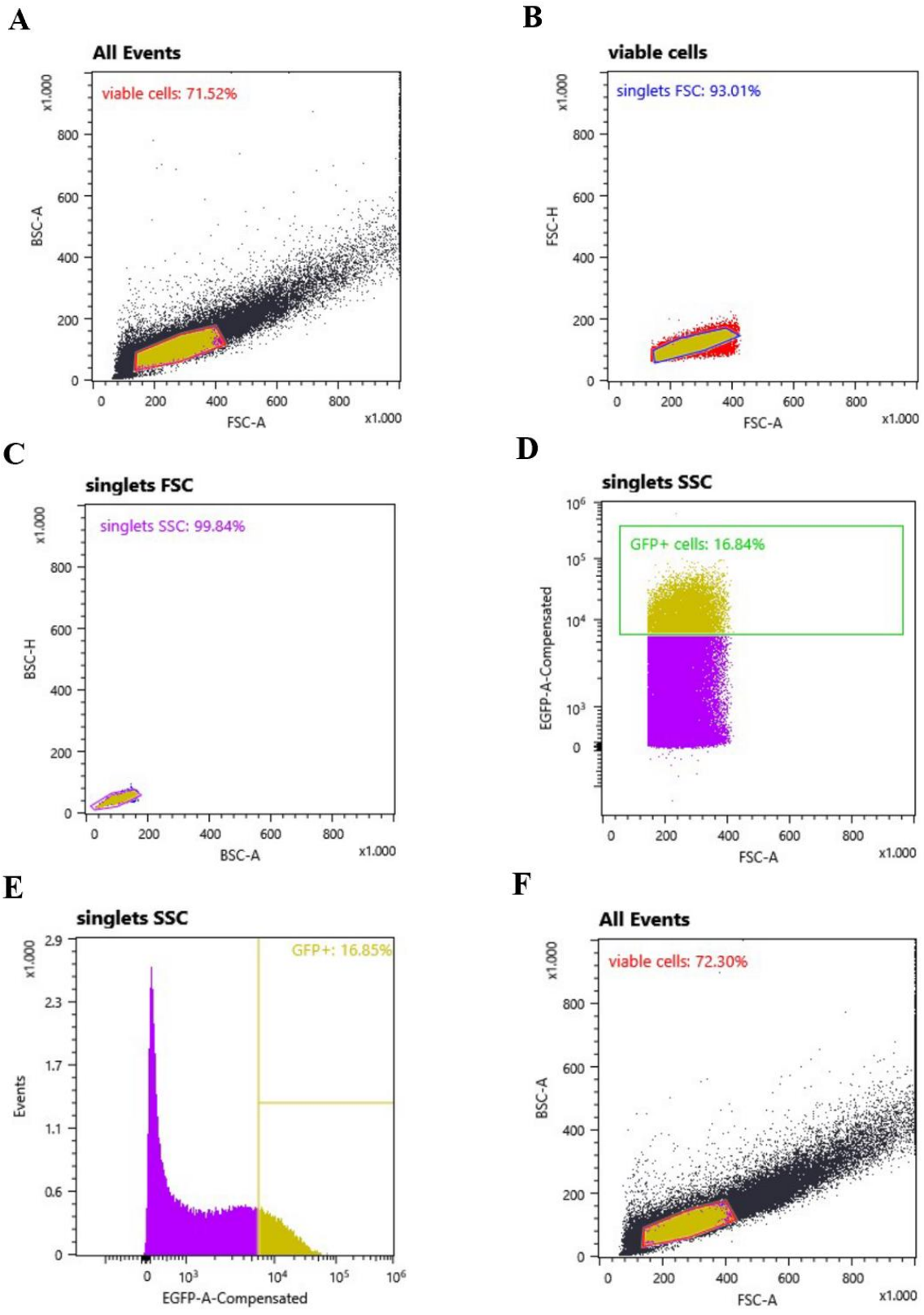
A
All Events
viable cells: 71.52%
BSC-A
FSC-A
x1.000
B
viable cells
singlets FSC: 93.01%
FSC-H
FSC-A
x1.000
C
singlets FSC
singlets SSC: 99.84%
BSC-H
BSC-A
x1.000
D
singlets SSC
GFP+ cells: 16.84%
EGFP-A-Compensated
FSC-A
x1.000
E
singlets SSC
GFP+: 16.85%
Events
EGFP-A-Compensated
F
All Events
viable cells: 72.30%
BSC-A
FSC-A
x1.000

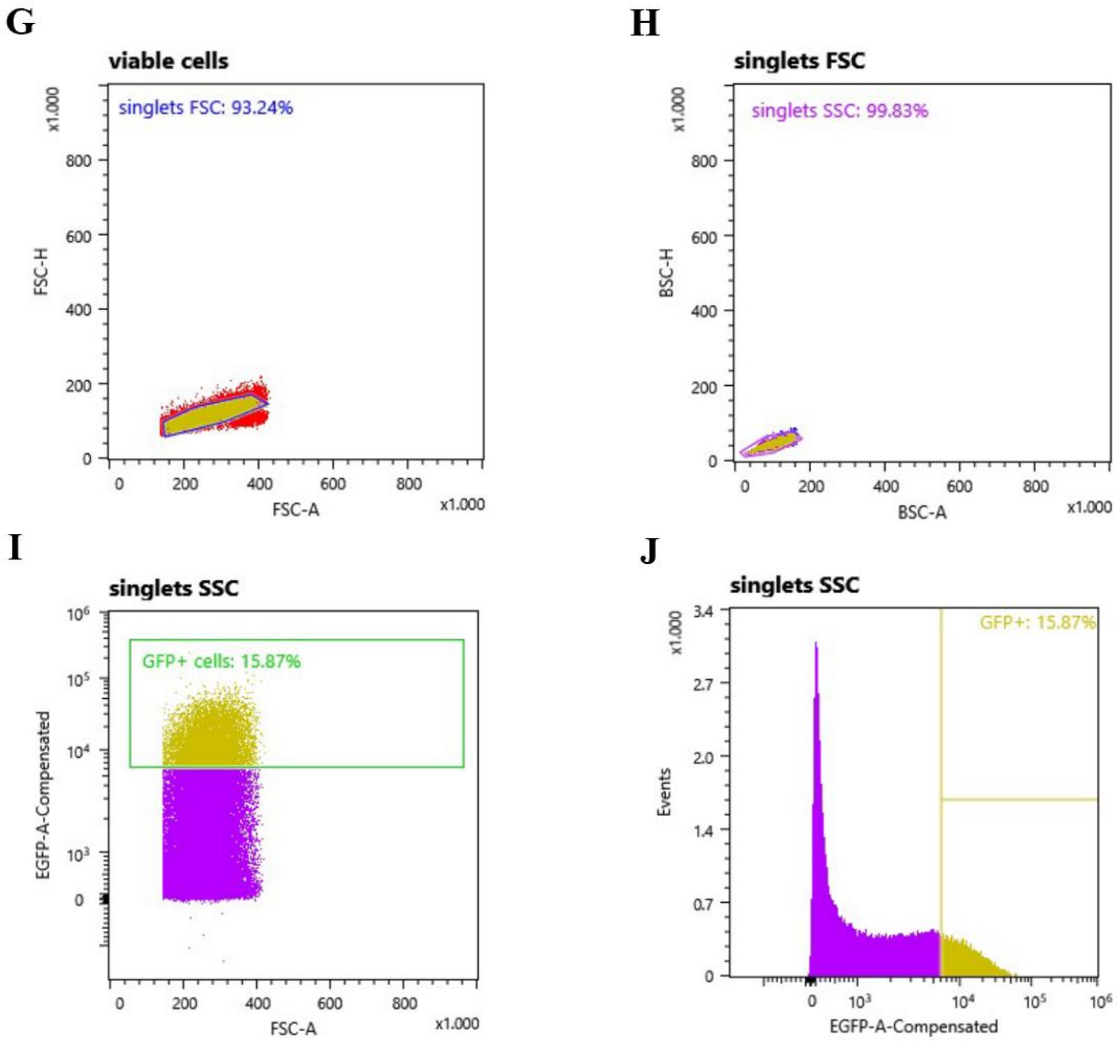

Figure 30: Sorting of CRISPR/Cpf1-treated iPSCs based on FACS. Patient-derived iPS single cells were GFP-sorted 48 hours post electroporation with CRISPR/Cpf1 plasmid. FSC: forward scatter, BSC: back scatter, SSC: side scatter **(A-E)** Sorting data of cells transfected with Cpf1-gRNA1. **(F-J)** Sorting data of cells transfected with Cpf1-gRNA2. **(A)/(F)** Scatter plot of FSC-A versus BSC-A of all cells to identify viable cells. **(B)/(G)** Scatter plot of FSC-A versus FSC-H of all viable cells to identify single cells (FSC singlets). **(C)/(H)** Scatter plot of BSC-A versus BSC-H of FSC singlets to further identify single cells (SSC singlets). **(D)/(I)** Scatter plot of FSC-A versus EGFP-A-compensated of SSC singlets to identify GFP-positive cells. **(E)/(J)** Histogram (number of events versus EGFP-A-compensated) showing GFP-positive SSC singlets.

After cell propagation, genomic DNA was extracted to analyse cleavage efficacy, which was found to be 16% for gRNA 1 and 15% for gRNA 2 (Figure 31, supplemental figure S5).

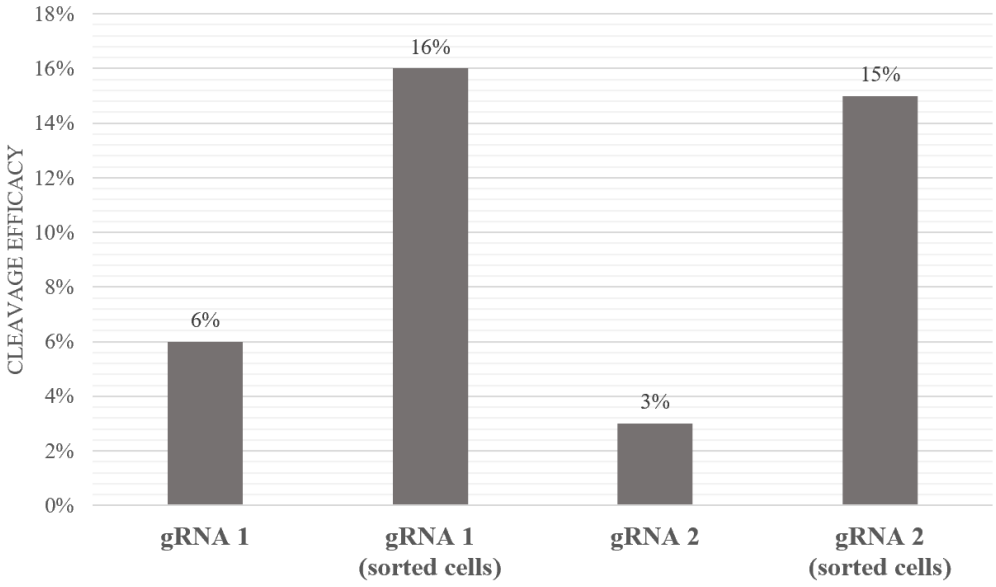

Figure 31: Cleavage efficacy of CRISPR/Cpf1 gRNAs prior versus post sorting. GeneScan analysis of fluorescently-labelled PCR fragments amplified from genomic DNA of CRISPR/Cpf1-treated and sorted iPS single cells.

4.3.4 Subcloning and genotyping of GFP-sorted iPSCs

One of the gRNAs was selected for further investigation at the clonal cell level. For this purpose, the sorted iPS cell bulk transfected with the Cpf1-gRNA1 construct was serially diluted to obtain single cell clones. The Cpf1-gRNA1 construct was selected because the cleavage efficacy was slightly higher compared with gRNA2 and the cleavage site was closer to the DIM. After propagation of the single cell clones into colonies, 48 colonies were picked and cultured separately. Five of the 48 colonies did not grow after picking and were discarded. A portion of the remaining 43 colonies was used for isolation of genomic DNA with QuickExtract extraction solution, and the remaining cells were further cultured. To screen the clones for Cpf1-induced editings, the region of interest was amplified from the extracted genomic DNA using forward primer JH_CRISPR_Intr4b_F2 and reverse primer JH_CRISPR_Intr4_large_R1. No PCR product was obtained from one of the clones, so a total of 42 clones were analysed for editing events by Sanger sequencing. Sixteen out of forty-two clones showed an overlay of sequence traces in the electropherogram, possibly due to indels. Accordingly, the cutting efficacy was 38% at the clonal cell level, compared to 16% in the iPSC bulk.

4.3.5 Transcript analysis of edited iPSC clones by Pyrosequencing

Transcript analysis was performed to assess a potential rescue of missplicing in the edited iPSC clones. The ratio of corrected DIM transcripts was determined by pyrosequencing. Genomic

RNA was isolated from the clones and cDNA was synthesized using reverse transcription. Alleles without a pseudoexon were amplified based on the location of the used primer pair (forward primer: Hs_OPA1_N158S_F and reverse primer: Hs_OPA1_N158S_Rbi). The forward primer is situated in exon 3 of *OPA1* and the reverse primer is located at the junction between exon 4b and 5, exclusively amplifying the I437M allele or the corrected DIM allele (Figure 32A). To discriminate the I437M allele and corrected DIM allele after amplification, primer Hs_OPA1_N158S_seq was used to sequence SNP rs7624750 in exon 4. The allele ratio of the SNP was obtained from the software tool Allele Quantification (AQ) (PyroMark Q96 ID Software, Qiagen N.V., Hilden, Germany) and used to quantify the relative abundance of corrected DIM transcripts by calculating the ratio of A allele (DIM allele) to G allele (I437M allele) (e.g. clone 19: (7 (A) / 93 (G)) x 100 = 8%) (Figure 32B-C). Pyrosequencing was performed on 13 of 16 edited clones, since two clones were discarded due to cultivation issues and one clone could not be amplified. No splicing rescue was observed in 8/13 clones, but 5/13 showed splicing rescue, ranging from 8% to 79% (Figure 32C).

A

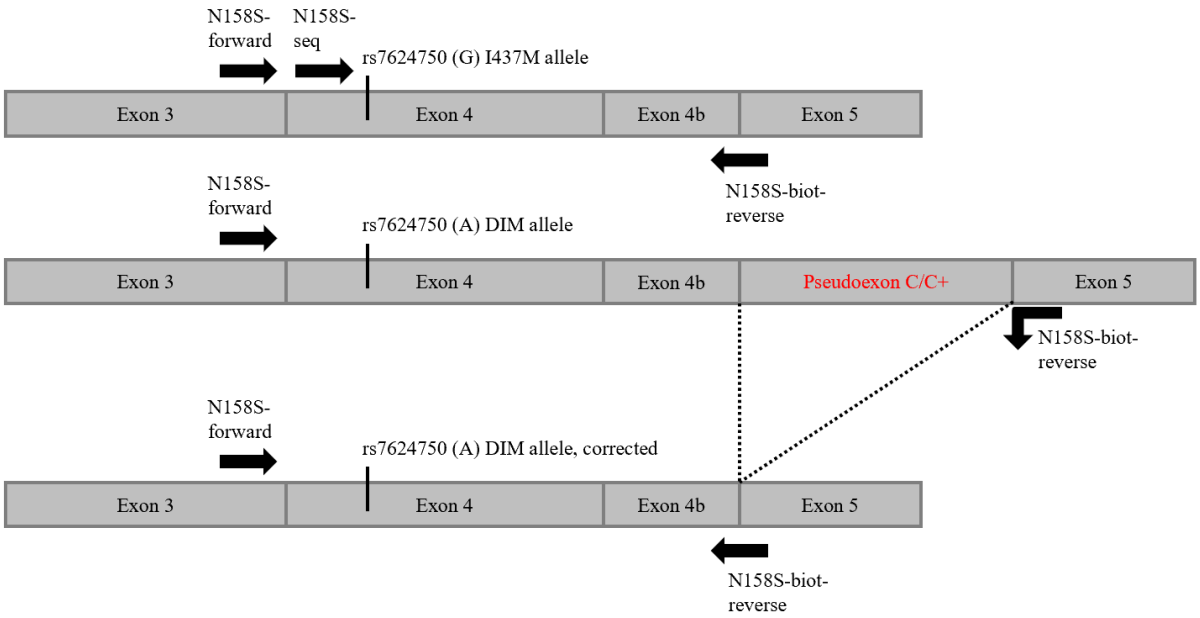

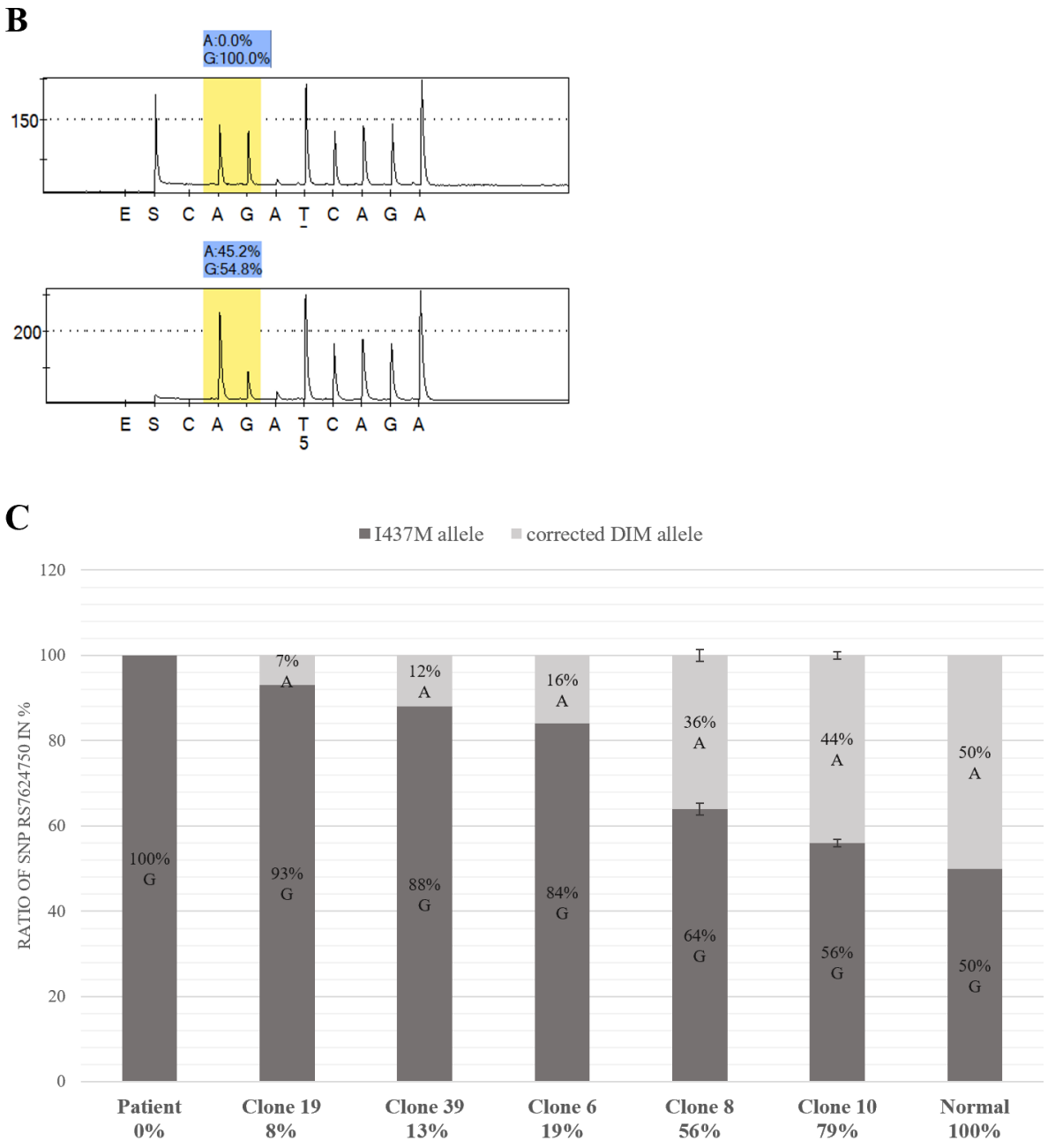

Figure 32: Pyrosequencing assay to analyse splicing rescue in CRISPR/Cpf1-edited iPSC clones. (A) N158S-forward and N158S-biot-reverse primer were used to amplify the I437M allele or corrected DIM allele from cDNA of Cpf1-edited iPSC clones. SNP rs7624750 in exon 4 was sequenced using N158S-seq primer to discriminate both alleles. Modified illustration from Bonifert et al., 2016. **(B)** Representative pyrograms of the pyrosequencing assay. The position of SNP rs7624750 is highlighted in yellow boxes. Peak height is shown on the y-axis. E and S indicate enzyme and substrate, respectively. The upper pyrogram is representative for a RT-PCR product from an unedited clone (only the I437M-allele is detected). The lower pyrogram is representative for a RT-PCR product from an edited clone (both alleles are detected). **(C)** Splicing rescue of edited iPSC clones 6, 8, 10, 19 and 39. The y-axis represents the percentages of G (I437M allele) and A (corrected DIM allele). The percentage of corrected DIM transcript (shown below the individual bars) was determined based on the ratio of A allele to G allele. Measurements for clones 8 and 10 were performed using three biological replicates. Error bars represent SD.

4.3.6 Quantification of transcripts by RT-PCR and fragment analysis

The transcript pattern of iPSC clones 8 and 10 was further analysed using RT-PCR followed by fragment analysis to quantify the transcripts. The DIM c.610+364G>A leads to the inclusion of two different pseudoexons (445 bp (C) and 477 bp (C+)) in the transcript, which both result in a frameshift and the formation of a premature termination codon (PTC). Since most transcripts harboring a PTC are subject to nonsense mediated mRNA decay (NMD) (Frischmeyer & Dietz, 1999), cells were treated with cycloheximide 7 hours prior RNA isolation to inhibit the degradation of mutant transcripts. In parallel, cells were not treated with cycloheximide. Following cDNA synthesis, the sequence region between exon 3 and exon 6 of *OPA1* was amplified. Figure 33A shows the resulting RT-PCR products of untreated versus cycloheximide treated iPSC clones 8 and 10. Since exons 4 and 4b are alternatively spliced, various transcripts are generated. Accordingly, the RT-PCR resulted in four products: (a) corresponds to a transcript without exons 4 and 4b, (b) corresponds to a transcript without exon 4b, (c) corresponds to a transcript including exons 4 and 4b, and (d) corresponds to a transcript that includes exons 4 and 4b and either the smaller pseudoexon (445 bp) or the larger pseudoexon (477 bp). The appearance of two bands at (c) is due to heteroduplex formation. The transcript derived from the DIM allele was only weakly expressed in untreated cells but considerably increased in the cycloheximide-treated samples, indicating NMD degradation of the mutant transcript. Clones 8 and 10 showed a decreased amount of the DIM transcript in comparison to the negative control (unedited iPSCs). The effect was even more noticeable in clone 10 compared to clone 8, which was consistent with the splicing rescue observed in the pyrosequencing experiments (50% rescue for clone 8 and 80% rescue for clone 10). The PCR products were diluted and further analysed on the capillary sequencer using GeneScan mode to quantify the ratio of DIM versus I437M transcripts. The unedited patient cells revealed 29% of DIM transcript, which was considerably reduced in edited cells (9% in clone 8 and to 4% in clone 10) (Figure 33B).

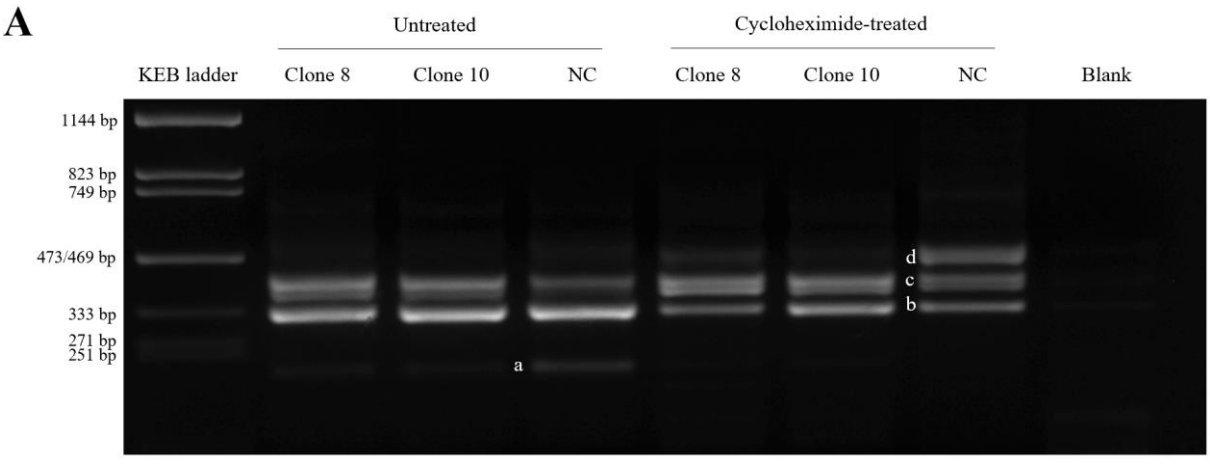

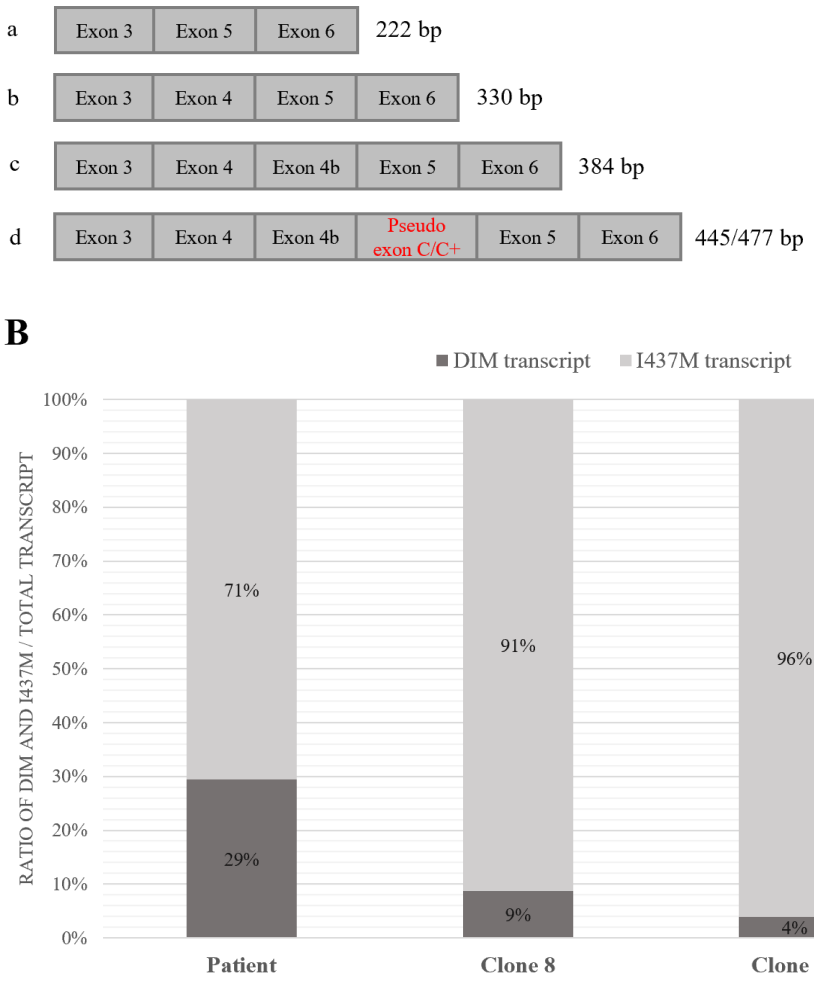

Figure 33: Transcript analysis of CRISPR/Cpf1-edited iPSC clones 8 and 10. (A) Agarose gel electrophoresis showing RT-PCR products from untreated and treated cells (100 µg/ml cycloheximide). The negative control (NC) corresponds to patient-derived iPS cells electroporated without CRISPR/Cpf1 plasmid constructs. Blank control without DNA sample. Primers binding to exon 3 (OPA1_cDNA_Ex3-6_F_FAM) and exon 6 (OPA1_cDNA_Ex3-6_R) were used for amplification from cDNA. A scheme of the amplified products is shown below the agarose gel image. Exons 4 and 4b are alternatively spliced. **(B)** Fragment analysis to quantify the ratio of DIM and I437M transcripts in edited cell clones 8 and 10. Fluorescently-labelled PCR fragments from cells treated with cycloheximide were analysed on a capillary sequencer using GeneScan mode. For comparison, unedited patient cells are shown and a representation of the expected normal state in wild-type cells.

4.3.7 Genotyping of CRISPR/Cpf1-edited iPSC clones

To further characterize the Cpf1-induced editing events in the iPSC clones, genomic DNA from the 14 edited clones was used to amplify the region of interest by PCR. The resulting PCR products were subcloned using the CloneJET PCR Cloning Kit to obtain plasmids harboring either the I437M or the DIM allele. The plasmids were propagated in bacteria colonies, isolated and Sanger sequenced. In this manner, indels could be properly determined and also assessed

if the I437M or the DIM allele was edited. The majority of observed editings were small deletions up to 7 bp and located approximately 20 bp upstream of the DIM. In two clones, a deletion of 13 bp and 27 bp was found. The DIM was not eliminated by any of the observed editings. In 6/14 clones, the I437M allele was edited and no editing was observed on the DIM allele, therefore no splicing rescue was observed in these clones. One clone showed neither an edit of the I437M allele nor of the DIM allele. This clone was misidentified as edited in the first genotyping due to sequence background. Two clones harbored the 13 bp and 27 bp deletions on the DIM allele but did not result in rescue of the missplicing. The remaining 5 clones (clone 6, 8, 10, 19 and 39), illustrated in Figure 34, presented similar editings of rather small size occurring on the DIM and have shown rescue of DIM-induced missplicing in the transcript analysis.

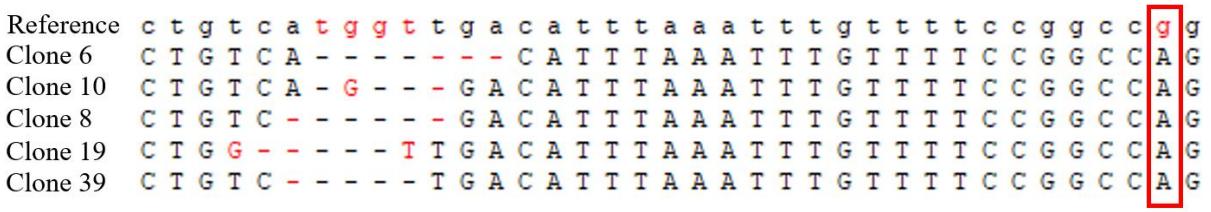

Figure 34: CRISPR/Cpf1-induced editings in iPSC clones presenting splicing rescue. Sanger sequencing of individual bacterial clones obtained by cloning of PCR products from genomic DNA of edited iPSC clones. The red box indicates the position of DIM c.610+364G>A.

4.3.8 Splicing rescue analysis of CRISPR/Cpf1-induced editings in HEK293T cells

To confirm the splicing rescue effects observed in the pyrosequencing experiment in an iPSC-independent system, minigene assays were performed in HEK293T cells. *OPA1* minigene constructs (exon 4b to exon 5) including editings seen in clones 6, 8 and 10 were generated according to the principle described in chapter 4.1.2 (in the following case, the original *OPA1* minigene construct including the DIM was used for generation of the editing constructs). After transfection of HEK293T cells, genomic RNA was extracted and used for RT-PCR (Figure 35). The following primer pair with binding sites in the *tat* exons of the pSPL3 vector was used for amplification: pSPL3seqcDNA_F_FAM and pSPL3seqcDNA_R.

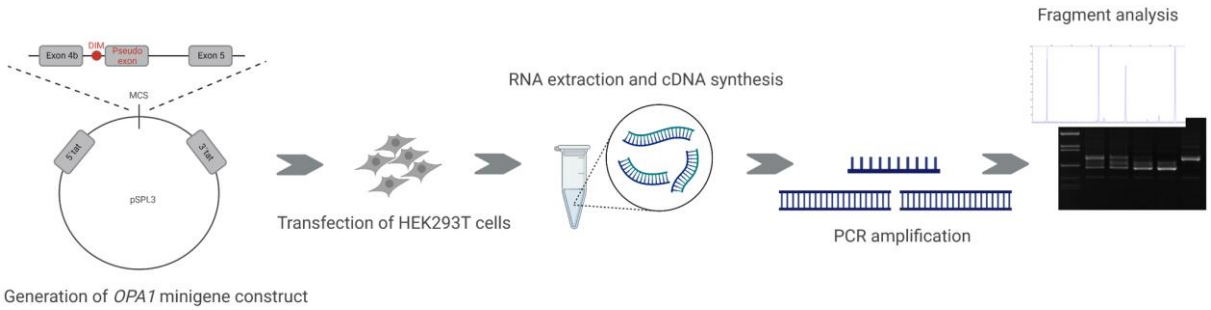

Figure 35: Minigene assay workflow to analyse Cpf1 editings. *OPA1* minigene constructs including the different CRISPR editings were generated by inverse PCR of the mutant (DIM) construct. The wild-type *OPA1* minigene construct and the mutant minigene construct served as control. Created with BioRender.com.

The resulting RT-PCR revealed three different bands corresponding to (a) the wild-type transcript including only exon 5, (b) the full-length wild-type transcript with exons 4b and 5, or (c) the mutant transcript including exon 4b, the smaller or larger pseudoexon and exon 5 (Figure 36A). In all cases, part of the *tat* exons were also included in the transcripts due to the location of the primer pair in the pSPL3 vector. The mutant (DIM) construct expressed all three transcripts. The wild-type construct and the mutant construct including the editings solely generated the wild-type transcripts, revealing a full rescue of missplicing without significant differences between the editings. This observation was confirmed in a GeneScan fragment analysis using the capillary sequencer after quantification of the mutant and wild-type transcripts (Figure 36B).

A

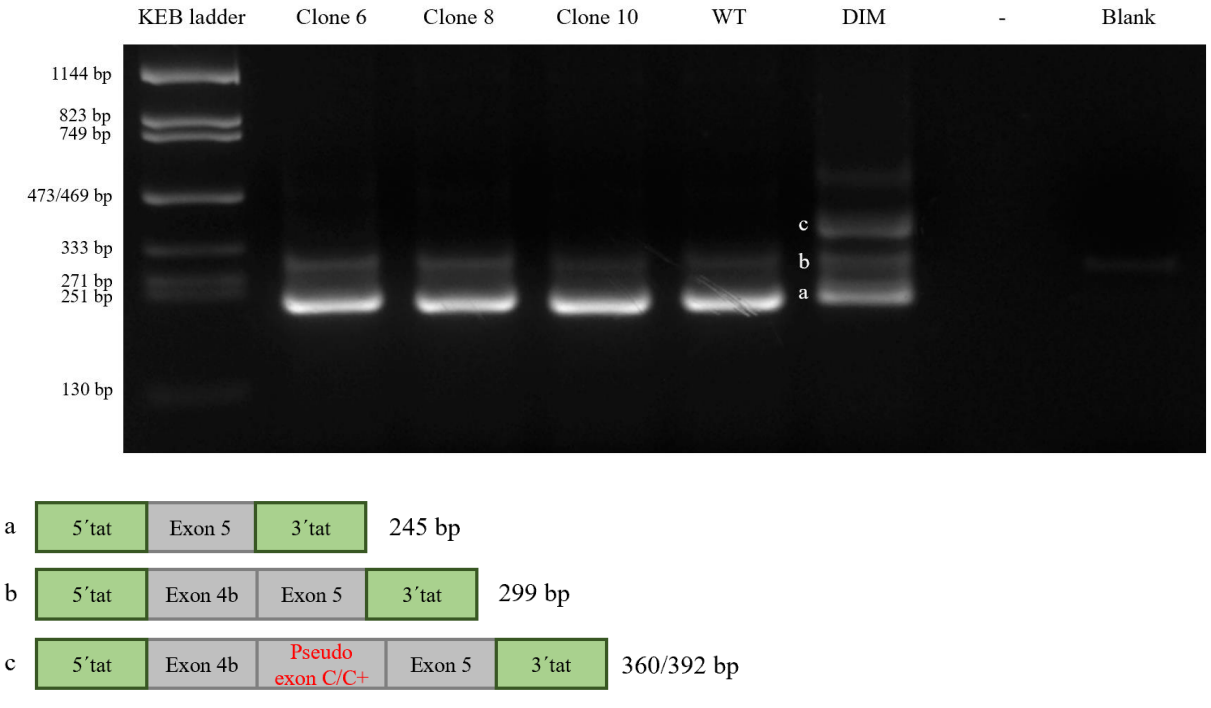

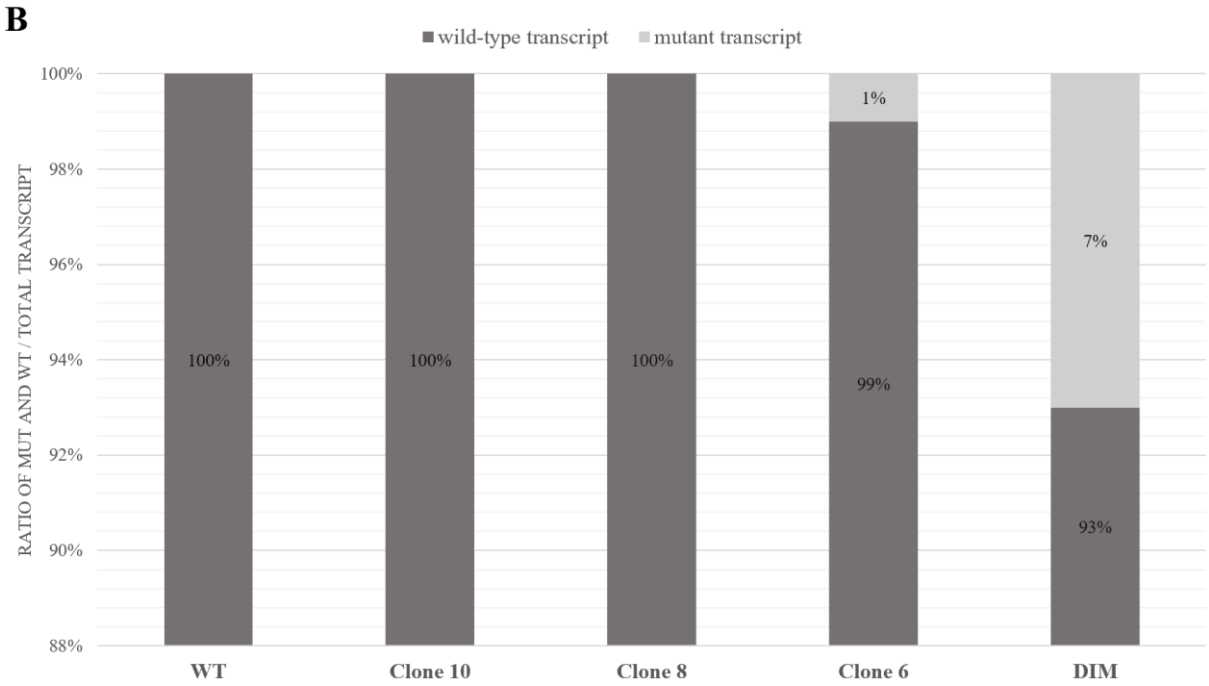

Figure 36: Minigene assay to analyse splicing rescue of CRISPR/Cpf1-editings. Minigene constructs comprised exon 4b to exon 5 of the *OPA1* gene. HEK293T cells were transfected with wild-type (WT), mutant (DIM) minigene constructs or minigene constructs including Cpf1 editings seen in clones 6, 8 and 10. **(A)** Agarose gel electrophoresis showing RT-PCR products obtained from genomic RNA isolated from transfected HEK293T cells. Blank control without DNA sample. Primers binding to the two vector-derived exons were used for amplification (pSPL3seqcDNA_F_FAM and pSPL3seqcDNA_R). A scheme of the amplified products is shown below the agarose gel image. Grey boxes represent *OPA1* exons. Green boxes represent vector-resident exons. **(B)** Fragment analysis to quantify ratio of mutant and wild-type transcripts. Fluorescently-labelled PCR fragments were analysed on a capillary sequencer using GeneScan mode.

The splicing assay was repeated with an extended minigene construct including a larger region of the *OPA1* gene, hereafter referred to as midigene construct. The *OPA1* midigene construct comprised the genomic region between exon 3 and exon 5 (Figure 37).

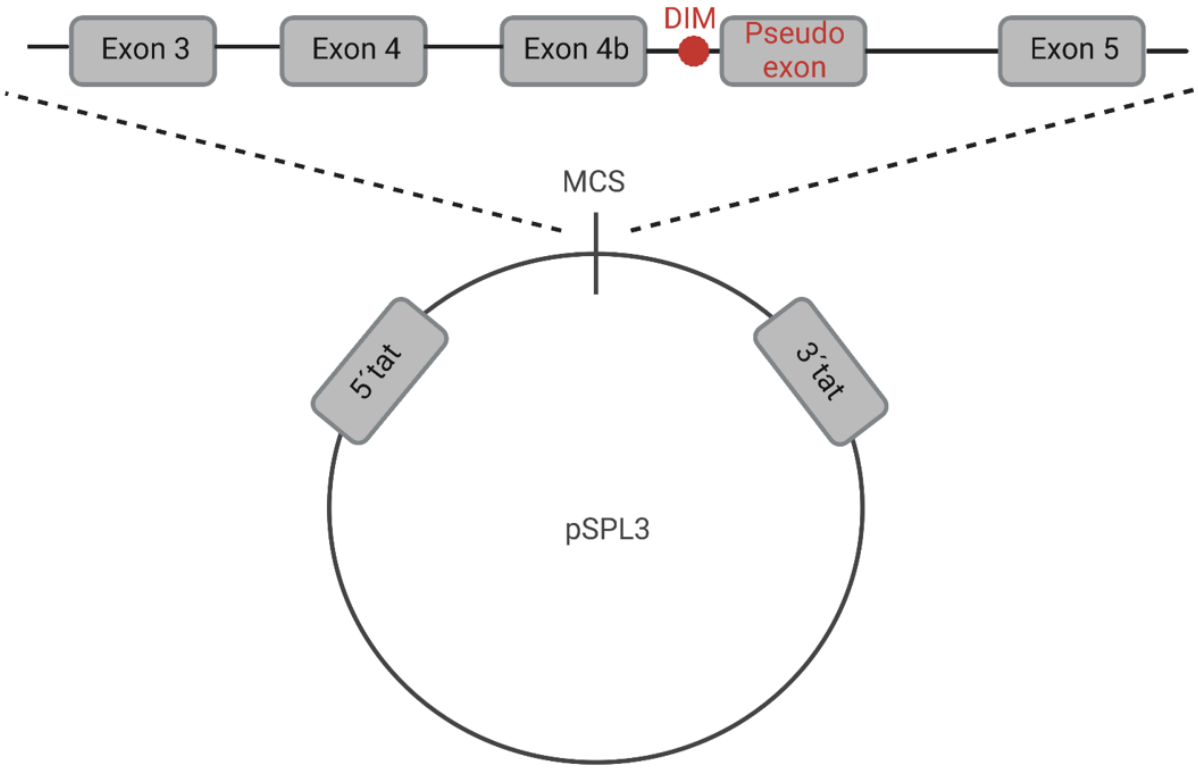

Figure 37: *OPA1* midigene construct. *OPA1* midigene constructs including the different CRISPR editings were generated by inverse PCR of the mutant (DIM) construct. The wild-type *OPA1* midigene construct and the mutant midigene construct served as control. Created with BioRender.com.

The RT-PCR showed four different bands: the wild-type transcript including (a) exon 3 and exon 5, (b) exon 3, exon 4 and exon 5, or (c) the full-length wild-type transcript with exon 3, exon 4, exon 4b and exon 5 (Figure 38A). The remaining band (d) corresponds to the mutant transcript containing the different pseudoexons. More variability between the editing constructs could be observed in the midigene assay. All three constructs showed reduced amounts of mutant transcript in comparison to the DIM construct. The effect was most apparent in the construct with clone 10 editing which showed transcript levels similar to those obtained with the wild-type construct. The amount of mutant transcript increased with the editing of clone 8 and even more with the editing seen in clone 6. Quantification of mutant and wild-type transcripts revealed 81% mutant transcripts with the DIM construct, which decreased to 35% with the clone 6 construct, 18% with the clone 8 construct, and as low as 6% with the clone 10 construct (Figure 38B). These results were in line with the pyrosequencing experiments, where clone 6 showed a splicing rescue of 20%, clone 8 of 50%, and clone 10 the highest rescue of 80%.

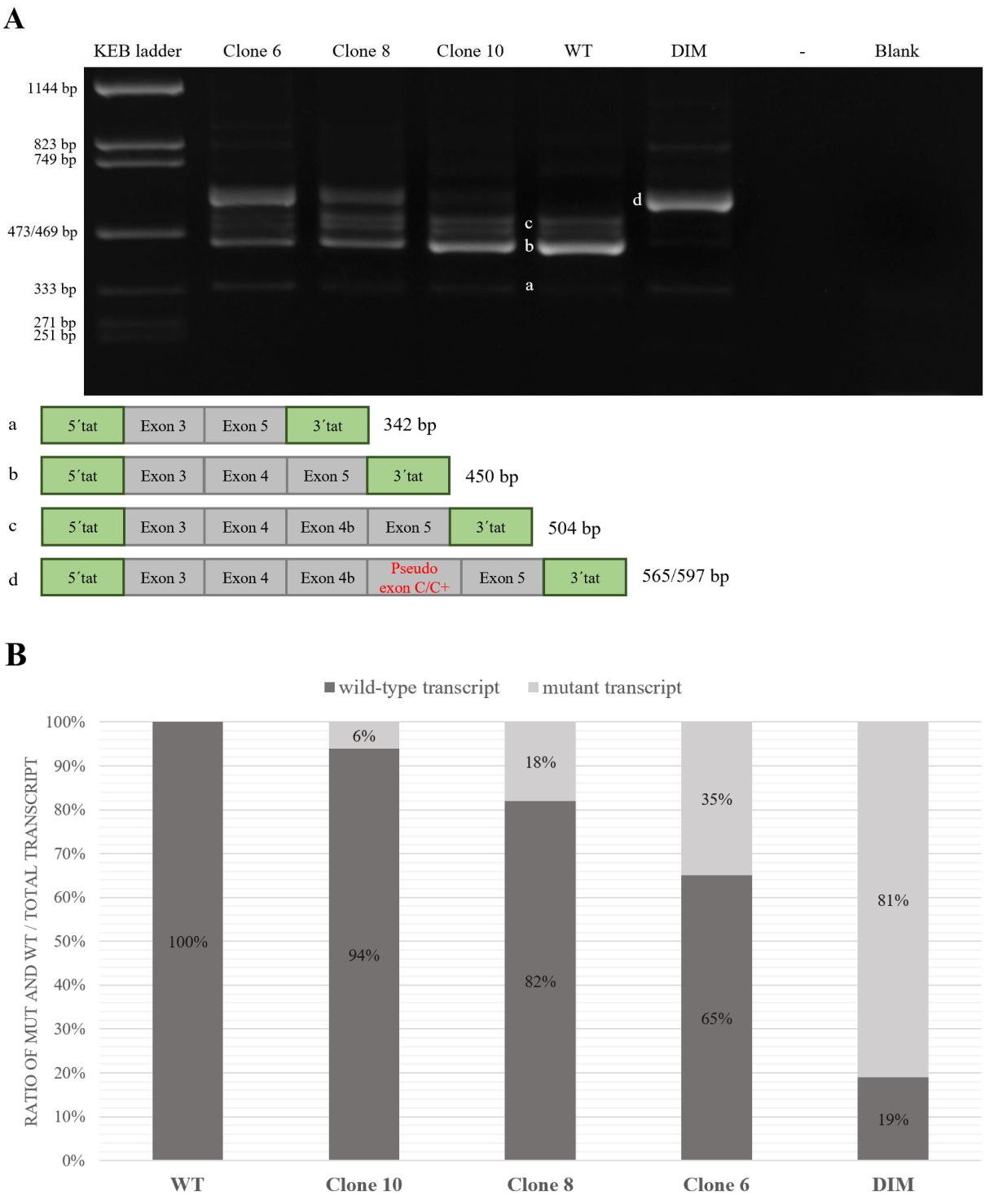

Figure 38: Midigene assay to analyse splicing rescue of CRISPR/Cpf1-editings. Midigene constructs comprised exon 3 to exon 5 of the *OPA1* gene. HEK293T cells were transfected with wild-type (WT), mutant (DIM) midigene constructs or midigene constructs including Cpf1 editings seen in clones 6, 8 and 10. **(A)** Agarose gel electrophoresis showing RT-PCR products obtained from genomic RNA isolated from transfected HEK293T cells. Blank control without DNA sample. Primers binding to the vector-derived tat exons were used for amplification (pSPL3seqcDNA_F_FAM and pSPL3seqcDNA_R). Schemes of the amplified products are shown below the gel image. Grey boxes represent *OPA1* exons. Green boxes represent vector-resident exons. **(B)** Fragment analysis to quantify ratio of mutant and wild-type transcripts.

Fluorescently-labelled PCR fragments were analysed on a capillary sequencer using GeneScan mode.

4.3.9 Analysis of OPA1 protein expression in CRISPR/Cpf1-edited iPSC clones

CRISPR/Cpf1-editing of patient-derived iPS cells revealed a rescue of the DIM-induced mis-splicing up to 80%. Since the DIM leads to a frameshift and PTC, a reduced protein expression of OPA1 can be expected in patient-derived cells. To analyse the OPA1 protein level in the Cpf1-edited clones, Western blotting was performed. Protein lysates from iPSC clones 8 and 10 showing the highest splicing rescue were included in the experiment. Protein samples from unedited patient-derived iPSCs and a wild-type iPSC line generated from a healthy proband served as controls. Immunostaining was performed for OPA1 and ß-actin. The latter was included as control to verify loading of equal protein amounts. In Western blots, OPA1 is represented by two bands of approximately 80 kDa and 100 kDa, corresponding to the respective OPA1 isoforms (Figure 39A). Western blotting revealed a reduction of OPA1 protein expression in the patient line to approximately 50% of the control line (Figure 39B). Clone 8 and clone 10 showed a statistically significant increase of OPA1 protein compared with the patient line, but not to the same level of the control line. Clone 10 exhibited a slightly higher protein increase compared to clone 8, consistent with the observed splicing rescue of 50% for clone 8 and 80% for clone 10.

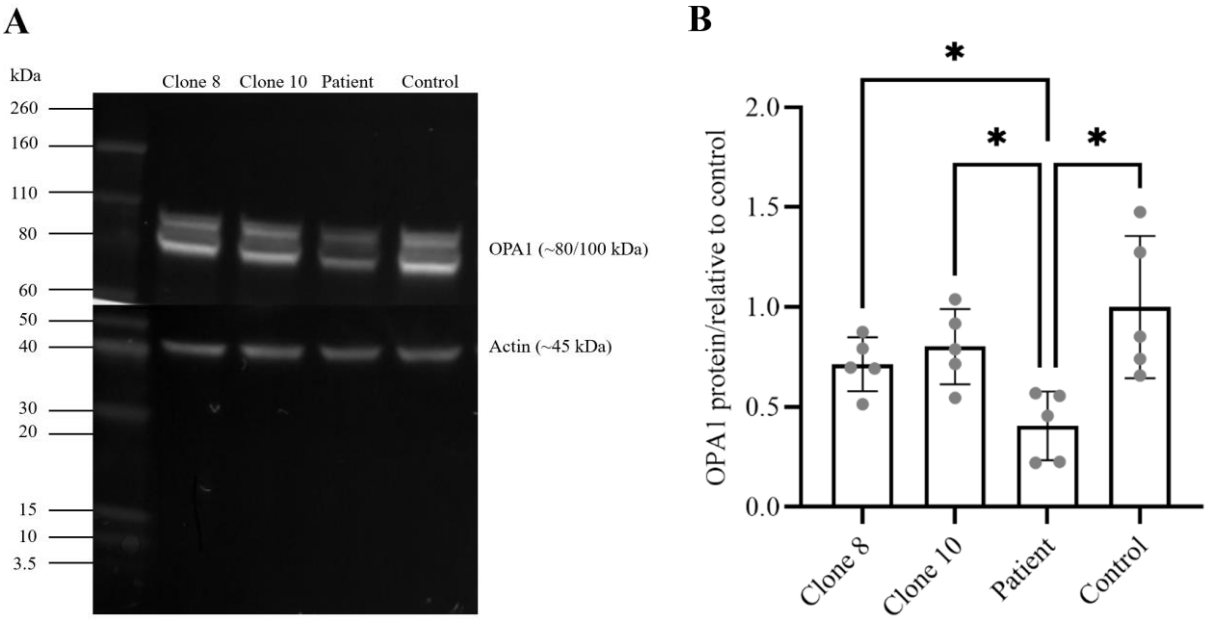

Figure 39: Western blot to analyse OPA1 protein expression. Protein lysates were harvested from CRISPR/Cpf1-edited iPSC clones 8 and 10, unedited patient-derived iPSCs and control iPSCs **(A)** Representative blot with stained proteins for OPA1 isoforms (~80 and 100 kDa) and loading control ß-actin (~45 kDa). **(B)** Statistical evaluation of OPA1 protein expression in

clone 8, clone 10 and patient cell line relative to control line (ANOVA test, *$P < 0.05$). Mean of biological replicates n=5. Error bars represent SD.

4.3.10 Analysis of mitochondria in CRISPR/Cpf1-edited iPSC clones

OPA1 plays a crucial role in mitochondrial function, particularly in the fusion of mitochondria and maintenance of cristae structure. Therefore, a further aim of this work was to investigate mitochondria morphology in the edited clones in comparison to wild-type cells from a healthy proband and unedited patient-derived cells. For this purpose, the cells were electroporated with a plasmid construct expressing GFP (mito-meGFP) with a human COX8 presequence targeting the mitochondrial matrix. The transfected cells were fixed 48 hours post electroporation with 4% paraformaldehyde, stained with DAPI and embedded. The mitochondria were imaged with an Apotome and z-stacks were generated. Figure 40 shows maximum intensity projections (MIP) transforming the 3D data from the z-stacks into a 2D image. The control cells from a healthy proband showed mitochondria with a homogeneous morphology and round shape (Figure 40A). The unedited patient-derived iPSCs appeared to form rather elongated mitochondria and defining single mitochondria was more challenging in these cells compared to wild-type cells (Figure 40B). Mitochondria of cells from clones 8 and 10 cells were more heterogeneous (Figure 40C and D).

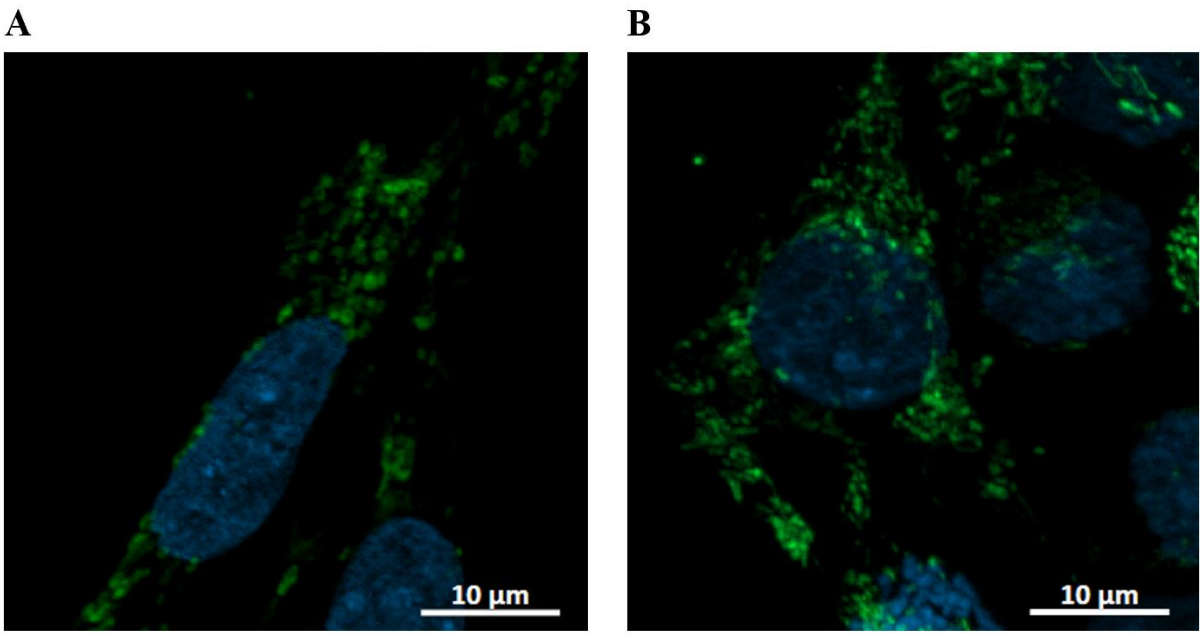

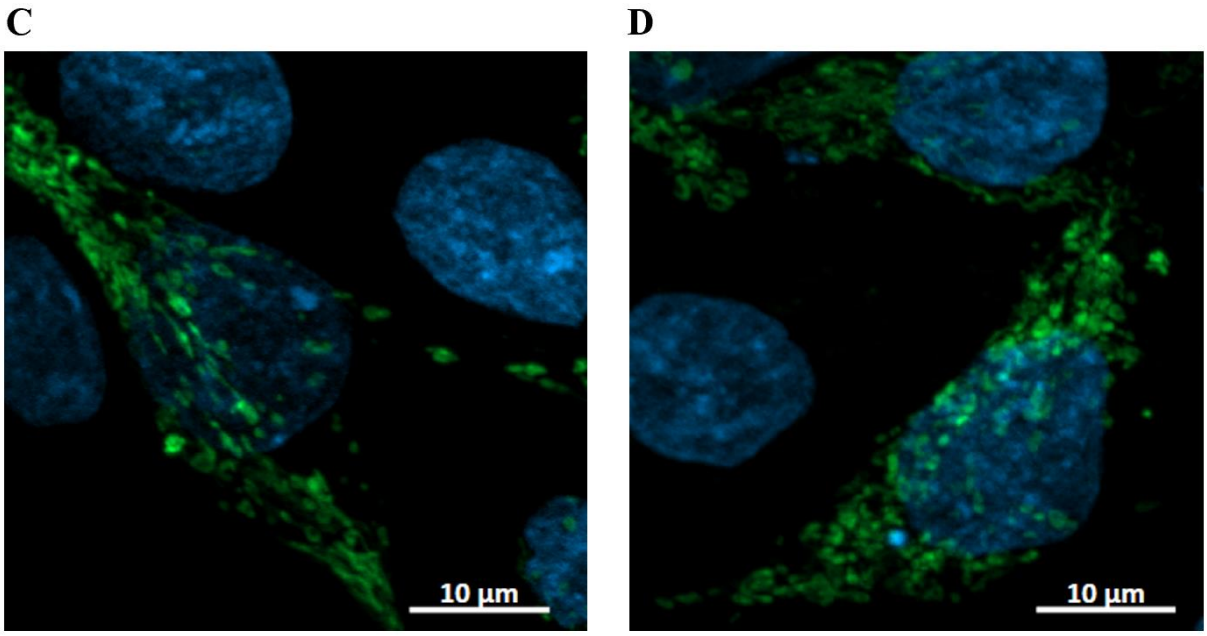

Figure 40: Analysis of mitochondria morphology in CRISPR/Cpf1 edited iPSC clones and controls. iPS single cells were transfected with mito-meGFP plasmid and fixed 48 hours post transfection. Presented are maximum intensity projections (MIPs) of the z-stacks. Mito-meGFP labeling is depicted in green, DAPI-labeling in blue. **(A)** Representative image of wild-type iPS cells from a healthy proband **(B)** Representative image of patient-derived iPS cells harboring the DIM **(C)** Representative image of Cpf1-edited iPSC clone 10 **(D)** Representative image of Cpf1-edited iPSC clone 8.

To further evaluate the mitochondrial morphology, the CellProfiler software was used. Two morphological features were evaluated, namely size and eccentricity. The generated MIP images were further processed by enhancing foci speckles and applying a threshold to define the borders of the mitochondria (Figure 41A). Box plots were created for the area (in μm^2) and the eccentricity of the mitochondria provided by the CellProfiler analysis (Figure 41B and C). Neither the area nor the shape of the mitochondria showed a difference between the edited clones, the patient line and the control cells.

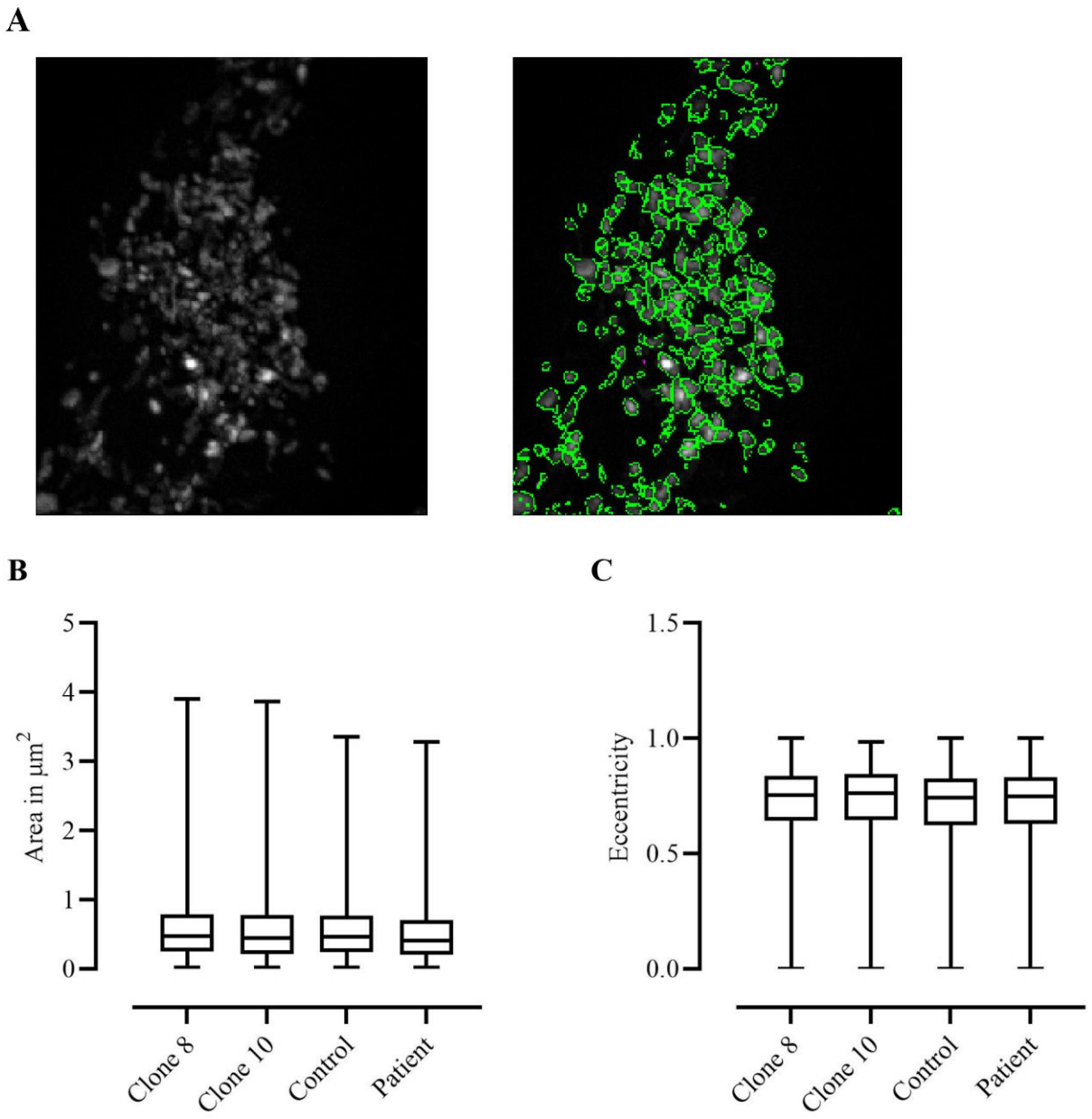

Figure 41: Analysis of mitochondria using CellProfiler. (A) Representative example of object (mitochondria) identification by the software. Mito-meGFP staining used as input is shown on the left side. Mitochondria borders identified by the CellProfiler software are shown by a green outline (image on the right side). **(B)** Box plot representing the area (in µm^2) of mitochondria from Cpf1-edited clones and control or patient cells. **(C)** Eccentricity box plot representing the shape of the mitochondria from Cpf1-edited clones and control or patient cells. The value 0 corresponds to a round shape and 1 refers to an elongated shape.

4.3.11 Investigations on the mechanism of splicing rescue

The CRISPR/Cpf1-induced editings comprised rather small deletions that are distant from the DIM and thus do not eliminate the mutation. Nevertheless, rescue of the DIM-induced missplicing up to 80% was achieved with the observed editing events, rising questions about the possible mechanism behind the splicing rescue. A probable explanation would be the

integration or more likely the disruption of binding elements for splicing regulators. Splicing regulators include intronic splicing silencers repressing splice-site activation and intronic splicing enhancers promoting splice-site activation. To determine if splicing regulator elements were up- or downregulated in the edited sequences, an *in silico* prediction of regulator elements was performed using HEXplorer scores in cooperation with Heiner Schaal, Institute for Virology, University Hospital Duesseldorf (Erkelenz et al., 2014). *In silico* prediction of clone 8 editing revealed some additional binding elements for SR proteins (Figure 42A). Clone 10 provided similar results with the additional prediction of a second acceptor splice site generated by the Cpf1-induced editing (Figure 42B). The prediction score of 8.04 is even higher compared to the score predicted for the acceptor splice site activated by the DIM (6.2). This observation raised the hypothesis that the new acceptor splice site might compete with the DIM splice site, thereby skipping the pseudoexon and restoring normal splicing.

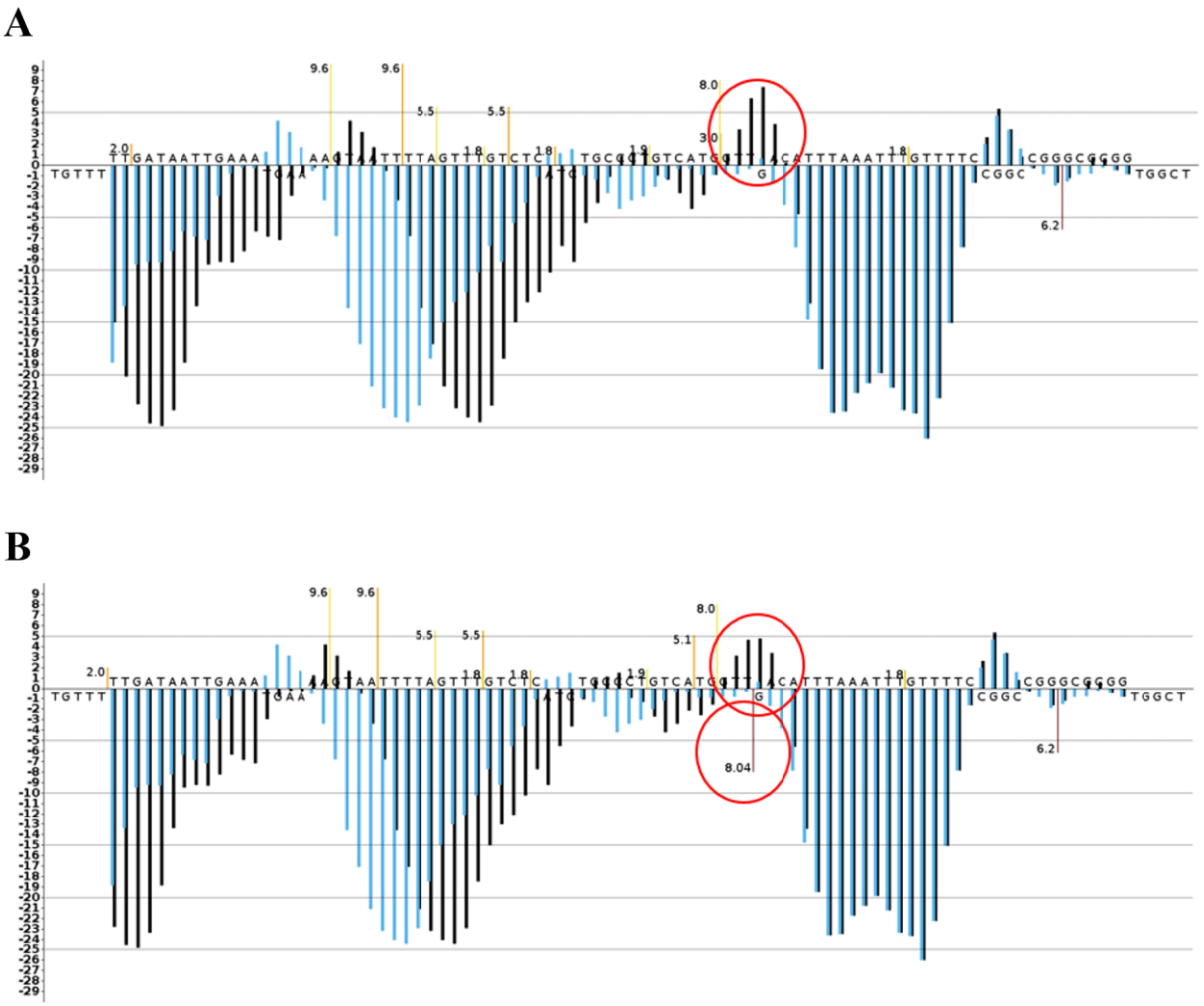

Figure 42: Prediction of splicing regulatory elements using HEXplorer score. Blue lines represent splicing profile of reference sequence, black lines represent profile of edited sequence. Yellow lines and brown lines indicate splice sites with MaxEnt prediction score. The red circles

mark additional binding motifs for SR proteins and additional splice sites. **(A)** Splicing profile of clone 8 editing **(B)** Splicing profile of clone 10 editing.

To investigate this hypothesis, the *OPA1* midigene construct including clone 10 editing was used to mutate the acceptor splice site induced by the editing. Substitution of AG to GG using *in vitro* mutagenesis (IVM) should eliminate the additional splice site and reverse the splicing rescue effect of clone 10. Repetition of the midigene assay revealed no significant difference between the original clone 10 construct and the construct harboring the mutated acceptor splice site (Figure 43). The amount of mutant transcript did not increase upon the *in vitro* mutagenesis, contradicting the hypothesis that the generated acceptor splice site promotes the rescue of mis-splicing.

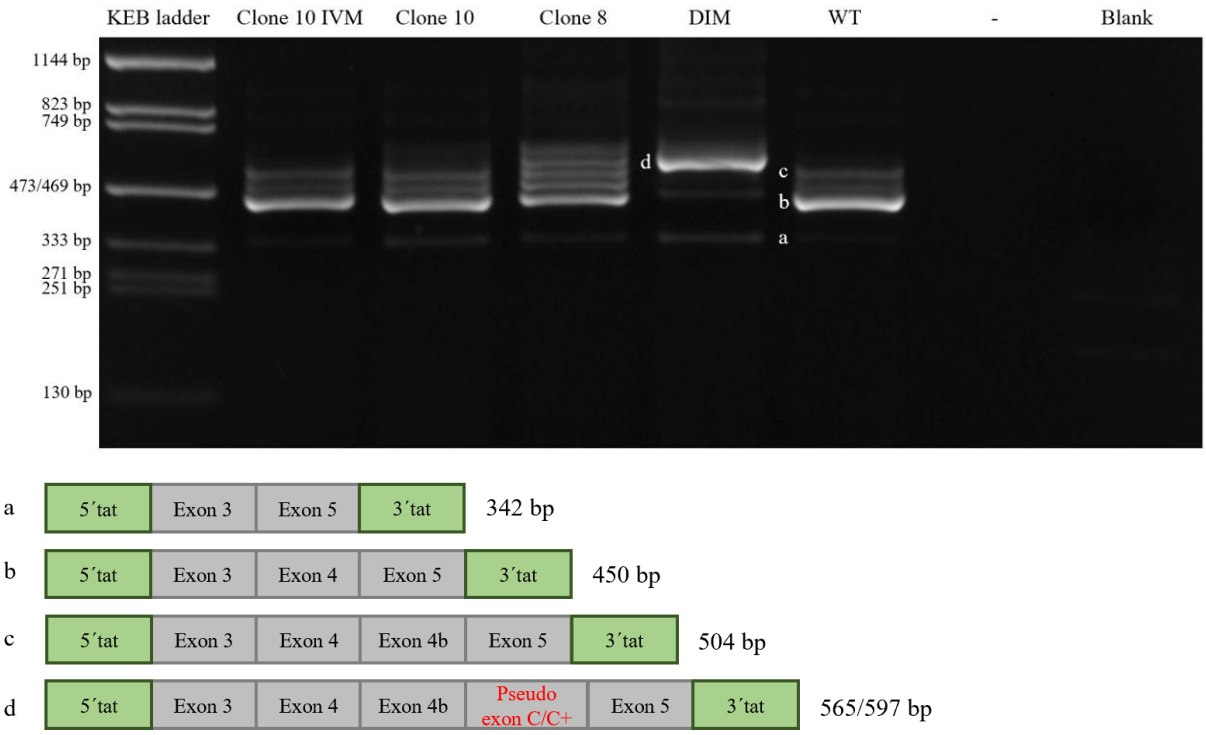

Figure 43: *In vitro* mutagenesis (IVM) of the 3´ splice site generated by iPSC clone 10 CRISPR/Cpf1 editing. The agarose gel image shows RT-PCR products obtained from genomic RNA isolated from HEK293T cells that were transfected with midigene constructs. Blank control without DNA sample. Primers binding to the vector-derived tat exons were used for amplification (pSPL3seqcDNA_F_FAM and pSPL3seqcDNA_R). Schemes of the amplified products are shown below the gel image. Grey boxes represent *OPA1* exons. Green boxes represent vector-resident exons.

4.4 *DNAJC30* screening in LHON and OA patients

1202 patients of a Central European cohort (1197 index patients and 5 affected family members), including 800 patients diagnosed with Leber´s hereditary optic neuropathy (LHON) and 402 patients with optic atrophy (OA), were screened for putatively pathogenic variants in *DNAJC30*. The screening of patients was performed in collaboration with Ting Xiao, Institute for Ophthalmic Research, University Hospital Tuebingen with equal distribution of work. The entire single exon gene *DNAJC30* was amplified by PCR from genomic DNA followed by Sanger sequencing (Primer pair: DNAJC30_Ex1_F and DNAJC30_Ex1_R). The following criteria were applied to determine likely pathogenic variants: Disease causing prediction in web-based tools MutationTaster (https://www.mutationtaster.org/) and PolyPhen-2 (http://genetics.bwh.harvard.edu/pph2/) for missense variants. Allele frequency of <0.01 in the normal population determined with the Genome Aggregation database, gnomAD V.2.1.1 (https://gnomad.broadinstitute.org/). Variants in homozygous state or in compound heterozygous state with a second likely pathogenic variant. Segregation analysis was conducted if DNA from family members was available. Allelic cloning was performed to confirm biallelism for compound heterozygous variants.

Putatively disease-causing variants were detected in 35/1202 individuals from 32 families (Table 48). In detail, 29/800 LHON cases and 6/402 OA cases harbored pathogenic variants in the *DNAJC30* gene. Thirty patients were male and five female. The majority of cases harbored the missense variant c.152A>G; p.(Y51C), which was already described in Stenton et al. 2021, in homozygous state (Figure 44). In addition, the nonsense variant c.610G>T; p.(E204*) and the 3 bp inframe deletion c.230_232del; p.(H77del) were identified in five patients from four families. The nonsense variant occurred in compound heterozygous state with the missense variant c.152A>G; p.(Y51C). The missense variant as well as the deletion are located in the J domain of the DNAJC30 protein (Figure 45). The nonsense variant was found upstream of the transmembrane domain.

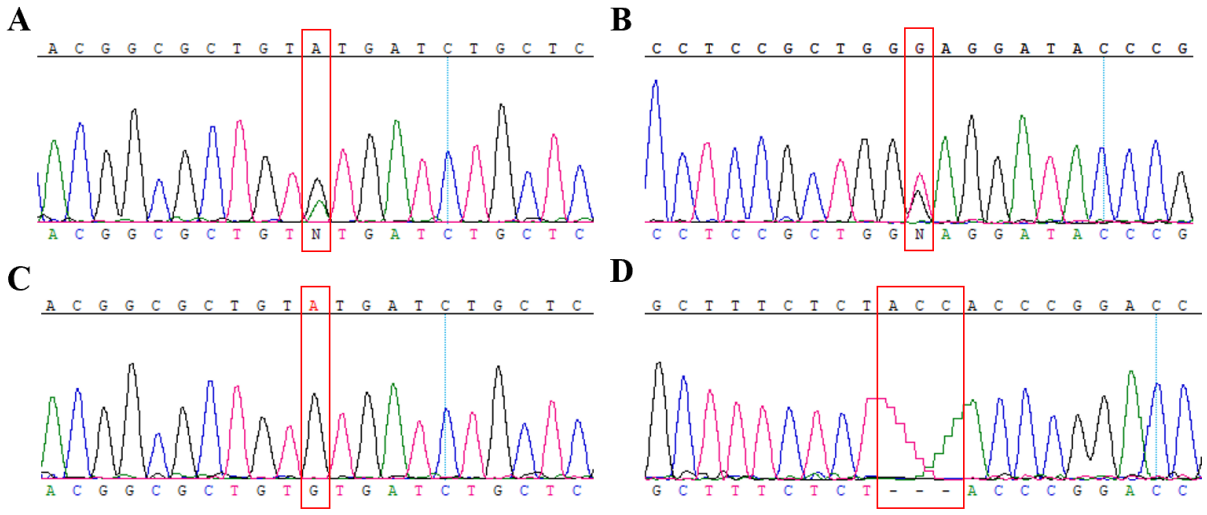

Figure 44: Representative electropherograms of detected pathogenic sequence variants. The red box highlights the position of the variants. **(A)-(B)** Exemplary sequence electropherograms showing missense variant c.152A>G (A) and the nonsense variant c.610G>T (B) identified in compound heterozygous state in patients LHON 96, LHON 573 and LHON 1149. **(C)** Exemplary sequence electropherogram showing the 3-bp deletion c.230_232del that was identified in homozygous state in patient OAK 559 and his brother. **(D)** Exemplary sequence electropherogram showing the missense variant c.152A>G in homozygous state that was identified in 30 patients. Adapted from Kieninger et al., 2022.

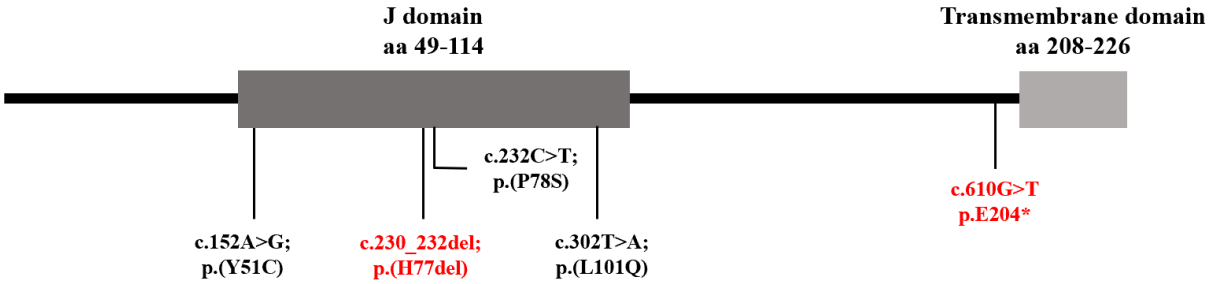

Figure 45: Scheme of the DNAJC30 protein domains and location of identified variants. Variant p.(Y51C), p.(P78S) and p.(L101Q) from Stenton et al., 2021 are located in the J domain (shown as dark grey rectangle). The variant p.(H77del), detected in our cohort, is also located in the J domain. Variant p.(E204*) is located upstream of the transmembrane domain (shown as light grey rectangle). Novel variants detected in our study are indicated in red. Adapted from Kieninger et al., 2022.

Table 48. Summary of LHON and OA patients with variants in *DNAJC30*. Hom: homozygous, Compd het: compound heterozygous, SS: Sanger sequencing, WGS: whole genome sequencing, NA: not available. Adapted from Kieninger et al. 2022.

Patient	Gender	Clinical Diagnosis	Variant	Allele Status	Method	Segregation Analysis	Family Relation
LHON 59 (1316)	Male	LHON	c.152A>G; p.(Y51C)	Hom	SS	Yes	Brother of patient LHON 59 (1824)
LHON 59 (1824)	Male	LHON	c.152A>G; p.(Y51C)	Hom	SS	Yes	Brother of patient LHON 59 (1316)
LHON 84	Male	LHON	c.152A>G; p.(Y51C)	Hom	SS	NA	NA
LHON 96	Male	LHON	c.152A>G; p.(Y51C) c.610G>T; p.(E204*)	Compd het	SS	Allelic cloning	NA
LHON 210	Male	LHON	c.152A>G; p.(Y51C)	Hom	SS	NA	NA
LHON 238	Female	LHON	c.152A>G; p.(Y51C)	Hom	SS	NA	NA
LHON 246	Male	LHON	c.152A>G; p.(Y51C)	Hom	SS	NA	NA
LHON 286	Female	LHON	c.152A>G; p.(Y51C)	Hom	SS	NA	NA
LHON 347	Male	LHON	c.152A>G; p.(Y51C)	Hom	SS	NA	NA
LHON 377	Male	LHON	c.152A>G; p.(Y51C)	Hom	SS	NA	NA
LHON 380	Male	LHON	c.152A>G; p.(Y51C)	Hom	SS	NA	NA
LHON 466	Male	LHON	c.152A>G; p.(Y51C)	Hom	SS	NA	NA
LHON 507	Female	LHON	c.152A>G; p.(Y51C)	Hom	SS	Yes	NA
LHON 526	Male	LHON	c.152A>G; p.(Y51C)	Hom	SS	NA	NA
LHON 573	Male	LHON	c.152A>G; p.(Y51C) c.610G>T; p.(E204*)	Compd het	SS	Allelic cloning	NA
LHON 582	Male	LHON	c.152A>G; p.(Y51C)	Hom	SS	NA	NA
LHON 600	Male	LHON	c.152A>G; p.(Y51C)	Hom	SS	NA	NA
LHON 606	Male	LHON	c.152A>G; p.(Y51C)	Hom	SS	NA	NA
LHON 612	Male	LHON	c.152A>G; p.(Y51C)	Hom	SS	NA	NA
LHON 749 (12040)	Male	LHON	c.152A>G; p.(Y51C)	Hom	SS	Yes	Twin of patient LHON 749 (14508)
LHON 749 (14508)	Male	LHON	c.152A>G; p.(Y51C)	Hom	SS	Yes	Twin of patient LHON 749 (12040)
LHON 760	Male	LHON	c.152A>G; p.(Y51C)	Hom	SS	Yes	NA
LHON 785	Female	LHON	c.152A>G; p.(Y51C)	Hom	SS	NA	NA
LHON 895	Male	LHON	c.152A>G; p.(Y51C)	Hom	SS	NA	NA
LHON 1076	Male	LHON	c.152A>G; p.(Y51C)	Hom	SS	NA	NA
LHON 1088	Male	LHON	c.152A>G; p.(Y51C)	Hom	SS	NA	NA
LHON 1089	Female	LHON	c.152A>G; p.(Y51C)	Hom	SS	NA	NA
LHON 1129	Male	LHON	c.152A>G; p.(Y51C)	Hom	SS	NA	NA
LHON 1149	Male	LHON	c.152A>G; p.(Y51C) c.610G>T; p.(E204*)	Compd het	SS	Allelic cloning	NA
OAK 317	Male	OA	c.152A>G; p.(Y51C)	Hom	SS	NA	NA
OAK 559 (19776)	Male	OA	c.230_232del; p.(H77del)	Hom	SS	Yes	Brother of patient OAK 559 (31530)
OAK 559 (31530)	Male	OA	c.230_232del; p.(H77del)	Hom	WGS	Yes	Brother of patient OAK 559 (19776)
OAK 627	Male	DOA	c.152A>G; p.(Y51C)	Hom	SS	NA	NA
OAK 715	Male	OA	c.152A>G; p.(Y51C)	Hom	SS	NA	NA
OAK 767	Male	DOA	c.152A>G; p.(Y51C)	Hom	WGS	NA	NA

5 Discussion

5.1 CRISPR genome editing to rescue missplicing induced by *OPA1* deep intronic mutation

The development of gene therapy approaches for the treatment of inherited diseases has become increasingly important in recent years. In particular, deep intronic variants represent an attractive target for CRISPR/Cas-based gene therapies since CRISPR-mediated non-homologous end joining (NHEJ) generates indels of unknown sizes which can only be tolerated in non-coding regions.

The deep intronic mutation (DIM) c.2991+1655A>G in the *CEP290* gene is known as the most common mutation associated with Leber congenital amaurosis type 10 (LCA10), which causes inherited blindness in early childhood. Researchers demonstrated that the splicing defect caused by the DIM can be corrected both *in vitro* and *in vivo* by using CRISPR/Cas genome editing as well as antisense oligonucleotides (AONs) (Dulla et al., 2018; Maeder et al., 2019). Drugs based on these studies are currently in ongoing clinical trials (Leroy et al., 2021).

In 2016, Bonifert et al. aimed to rescue aberrant splicing induced by the *OPA1* DIM c.610+364G>A by applying AONs (Bonifert et al., 2016). The experiments were conducted in patient-derived fibroblasts and a rescue effect of approximately 55% was obtained with an AON targeting the cryptic acceptor splice site created by the DIM. The aim of the present work was to develop an alternative strategy based on CRISPR/Cas genome editing to potentially correct the *OPA1* DIM c.610+364G>A-induced missplicing with an even higher efficiency and thereby provide a proof-of-concept study for possible future therapies of patients suffering from a severe syndromic form of optic neuropathy.

5.1.1 "2n" CRISPR/Cas9 nickase genome editing eliminates the DIM c.610+364G>A in *OPA1*

Cas9 nickases generate single-strand nicks in the target DNA instead of the typical double-strand breaks induced by wild-type Cas9 enzymes. To generate a double-strand break with nickases, two appropriately spaced and oriented gRNAs are required. The double-nicking strategy was shown to significantly reduce off-target modifications (Ran et al., 2013). High precision is especially required in context with the development of gene therapies or other clinical applications. Due to the high specificity of the double-nicking strategy and the reduced risk of off-target effects, in this thesis a Cas9-D10A nickase directed by a gRNA pair ("2n") was

chosen as the first approach to eliminate the *OPA1* DIM c.610+364G>A in patient-derived iPSCs. Indeed, with this approach, various Cas9 nickase-induced insertions, deletions and indels could be detected in patient-derived iPSCs. According to literature data, indel sizes between 22 and 138 were achieved using the double-nicking strategy (Shen et al., 2014). The size range of the indels observed in the present thesis was between 3 and 35 bp. Indel sizes can vary depending on the location of the gRNAs and depending on the corresponding target sequence (Owens et al., 2019). In addition, the mentioned study used Cas9-D10A as well as Cas9-H840A nickases expressed by mRNA in cell embryos (Shen et al., 2014). The obtained editings are most likely also depending on the used nickase variants, delivery methods and target cells or organisms.

The majority of the observed editings occurred only once in the bacterial clones studied. In about half of the bacterial clones, the DIM was removed or replaced by another nucleotide. In two clones, the wild-type "G" was restored. Of a total of 51 bacterial clones sequenced, approximately 60% carried the maternal DIM allele and 40% carried the paternal I437M allele, roughly corresponding to the expected 50/50 allele distribution in the diploid patient-derived iPS cells. Cas9 nickase-induced editings were observed in 74% of the DIM alleles and in only 20% of the I437M alleles. These data demonstrate specificity for the DIM allele achieved by using Cas9 nickase with properly selected gRNAs covering the DIM. A high allele specificity reduces the risk of off-target effects and is therefore particularly crucial for clinical applications. High specificity is especially achieved if the variant is creating a PAM sequence or the variant is located in the seed region of the Cas9-gRNA, which comprises approximately up to 12 nucleotides upstream of the PAM (Jiang et al., 2013; Wu et al., 2020). Even single-base mismatches in the seed region can properly inhibit cleavage, which is also demonstrated in the present study (Cong et al., 2013; Smith et al., 2015; Yoshimi et al., 2014). CRISPR/Cas9-based allele specificity was also proved to be useful for targeted disruption of mutant alleles with dominant negative effects or abnormal gain-of-function causing autosomal dominant disorders and the specificity was shown to vary depending on the Cas9 variant used (Diakatou et al., 2021; Giannelli et al., 2018; György et al., 2019; Li et al., 2018).

Insertions, deletions or indels associated with the elimination of the DIM were selected for minigene assays to determine splicing patterns and possible splicing rescue induced by the Cas9 nickase editings. Complete rescue of missplicing was achieved with 8/10 editing events. The 28 bp deletion observed in clone 31 partially restored normal splicing. The indel from clone 7, on the other hand, did not result in any detectable splicing rescue in the minigene assay. Why

was no or only partial rescue observed in clone 7 and 31 despite elimination of the DIM or even restoration of the wild-type nucleotide? The acceptor splice site activated by the DIM was removed, but the Cas9 nickase-induced deletion and indel created a novel acceptor splice site. It is known, that splice sites can be "weak" or "strong" (Roca et al., 2005). "Strong" splice sites have higher similarities to consensus motifs and are more likely to be used by the splicing machinery than "weak" splice sites. The acceptor splice site created by the editing in clone 31 might be "weaker" compared to the one from clone 7, explaining the partial rescue observed in clone 31. The splice site prediction scores reported by MaxEntScan and NNSplice are indeed higher in clone 7 than in clone 31 implying that the acceptor splice site created by clone 7 corresponds to a "stronger" and thus more likely used splice site.

The minigene assays provide a useful tool to determine splicing patterns induced by the CRISPR editings and the obtained results were in line with the *in silico* predictions from NNSPLICE and MaxEntScan, supporting the validity of the predictions programs as well as the performed splicing assays. In 2014, Sharma et al. investigated the functional impact of different cystic fibrosis-associated splice-site variants using minigene assays and compared the results with those of eight different *in silico* tools. They also demonstrated that the majority of experimental evaluations were in line with bioinformatic predictions (Sharma et al., 2014). Minigene assays also have the advantage that they allow the investigation of a variant independently of the counter allele, i.e. the resulting transcripts can only be assigned to the variant. In patient cells, however, the additional transcripts of the other allele make an assignment more difficult. Nonetheless, minigene assays also have some disadvantages: (1) the lack of the entire genomic context, since due to the size of the introns usually only a few consecutive exons can be accommodated in a minigene plasmid and splicing is not always sequential. (2) the absence of tissue-specific splicing factors, (3) plasmids are episomal and have no chromatin structure, thus the artificial system only partially reflects the natural expression of genes in patient-derived cells or tissue.

In summary, the present thesis demonstrated that "2n" CRISPR/Cas9 nickase genome editing can be used to specifically edit the mutant allele and eliminate the *OPA1* DIM c.610+364G>A, thereby restoring normal splicing to full extent.

5.1.2 Studies on the cleavage efficacy of different gRNA pairs to develop "4n" CRISPR/Cas9 nickase approach

The CRISPR/Cas9 nickase-induced editings might create novel acceptor or donor splice sites. Therefore, the aim of the present thesis was to eliminate the entire pseudoexon and thus potentially improve restoration of normal splicing in patient-derived iPSCs. To eliminate such a large gene segment, the "4n" CRISPR/Cas9 nickase approach was chosen. For this purpose, six gRNA pairs were designed *in silico*, which are located upstream and downstream of the pseudoexon sequence. These gRNA pairs should be combined in such way that a double-strand break is generated upstream and downstream of the pseudoexon, which is repaired by NHEJ and thus eliminating the DIM as well as the pseudoexon.

First, the gRNA pairs were tested individually in HEK293T cells for their cleavage efficacy to decide which of the pairs are suitable for the "4n" Cas9 nickase approach. The cleavage efficacy of a gRNA correlates with the associated indel frequency. Indel detection can be done by Sanger sequencing followed by analysis with the web-based tools TIDE (https://tide.nki.nl/) or Synthego (https://ice.synthego.com/#/). TIDE and Synthego analyse two input sequences (unedited reference sequence versus edited sequence) and determine the indel frequency. The advantage of this method is that it only requires Sanger sequencing of the region of interest and is therefore relatively quick and easy. A disadvantage is that sequences with poor quality are often not analysed by the software tools. In addition, TIDE and Synthego are not designed for the analysis of Cas9 nickase genome editing. If there is a restriction site which can be used to distinguish the edited sequence from the reference sequence, a restriction fragment polymorphism (RFLP) analysis can be performed. Other methods to detect indels include next generation sequencing (NGS), T7 endonuclease I (T7E1) assays or amplicon analysis (IDAA). Since NGS is an expensive method that requires access to certain equipment and the T7E1 assay did not provide reliable data (data not shown), the cleavage efficacy of the gRNA pairs in this thesis was determined based on the Indel detection by Amplicon Analysis (IDAA) method consisting of two steps: PCR amplification using a fluorescence-labelled primer and subsequent analysis of the fluorescence-labelled amplicons on a capillary sequencer (Lonowski et al., 2017; Yang et al., 2015). The amplicon analysis method enables indel detection with a resolution and sensitivity comparable to NGS at lower costs and workload (Bennett et al., 2020; Yang et al., 2015).

Indel formation could only be obtained with two of the six gRNA pairs tested. The highest indel frequency of 14% was obtained with gRNA pair 2. In the literature, indel frequencies of up to

approximately 40% have been observed in CRISPR/Cas9 nickase-treated HEK293T cells (Chiang et al., 2016; Gopalappa et al., 2018; Ran et al., 2013). Why did the double-nicking strategy achieve a rather low cleavage efficacy in the present thesis? The low cleavage efficacy might be attributed to the sequence of the selected gRNAs. The majority of gRNAs contain stretches of up to five thymine (T) bases. T-stretches are known to function as transcription termination signals for the RNA polymerase III (Pol III) (Arimbasseri et al., 2013). The expression of gRNAs from plasmid constructs in eukaryotes is commonly driven by Pol III promoters such as U6, which also holds true for the present study. Gao et al. investigated to what extent different T-stretches are related to the termination efficiency of different Pol III promoters. They showed that already a stretch of four T bases can act as a minimal terminator and full termination is reached with a stretch of six or more T bases (Gao et al., 2018). In the present work, no indel formation was observed with gRNA pairs containing four to five T bases in their sequence. In contrast, the gRNA pairs associated with a low indel frequency contain a stretch of three to four T bases. Apparently, the different T-stretches lead to reduced expression of the gRNAs resulting in a low cleavage efficacy. In order to exclude this issue, gRNAs without a T-stretch or at least less than three to four T bases need to be designed for the double-nicking strategy or the gRNAs need to be expressed from e.g. RNA polymerase II promoters (Pol II). Pol II promoters such as CMV are usually used to express the Cas9 enzyme. Pol II-driven expression of gRNAs results in the addition of nucleotides to the ends of the gRNAs, which restricts their function and reduces the genome editing efficiency (Yoshioka et al., 2015). Consequently, the transcript needs to be further processed by ribozymes, tRNAs or the endoribonuclease Csy4 to produce efficient gRNAs (Gao & Zhao, 2014; Nissim et al., 2014; Yoshioka et al., 2015). Since the sequence region around the *OPA1* DIM contains many T-stretches and the selection of gRNAs for the double-nicking strategy was limited, no suitable gRNA pairs containing less T bases could be designed. To avoid a time-consuming generation of a Poly II-based expression system, I opted for a plasmid-independent delivery of the CRISPR system using ribonucleoproteins (RNPs). Direct delivery of recombinant Cas9 enzyme and gRNAs was shown to result in efficient genome editing of human cell lines with indel frequencies up to 79% (Kim et al., 2014). In the present work, no indels were detected after transfection of HEK293T cells with Cas9 nickase enzyme and gRNA pair 2. Compared to this, gRNA pair 2 resulted in an indel frequency of 14% after plasmid transfection. Monitoring of the transfection efficiency using fluorescence microscopy revealed lower efficiencies after transfection with RNPs in comparison to plasmid transfection. Most likely, the poor transfection efficiency

coupled with the overall low efficiency of the Cas9 nickase-gRNA pair 2 led to the poor cleavage efficiency results associated with the RNP approach.

Since the elimination of the DIM in patient-derived iPSCs was the main goal of the work, further focus was placed on editing of the patient-derived cells. Due to the poor results from the transfection with RNPs, the CRISPR components for editing of the iPSCs were again expressed from plasmid constructs. Different methods can be used to transfect iPSCs, including lipofection and electroporation. According to literature, electroporation is more suitable for efficient transfection of CRISPR components into human iPSCs than lipofection (Li et al., 2016). In the present work, transfection of patient-derived iPSCs with plasmids using Lipofectamine 3000 and Lipofectamine Stem indeed resulted in poor transfection efficacy (data not shown). Hence, delivery of plasmids was performed by electroporation. Electroporation of the cells with the plasmid construct expressing Cas9-D10A nickase and gRNA pair 2 reached a transfection efficacy of 30-50%, however the resulting cleavage efficacy was only 5% and thus even lower than in the treated HEK293T cells (14%).

In summary, genome editing based on the double-nicking strategy revealed comparatively low editing efficiencies in HEK293T cells and patient-derived iPSCs, regardless of whether RNPs or plasmids encoding CRISPR components were used. The poor editing efficiency is most likely due to the selected gRNA pairs or target sequence. It has been demonstrated previously that various factors affect the cleavage efficacy of CRISPR/Cas9 genome editing. For instance, certain sequence motifs such as TT- and GCC-motifs can decrease editing efficiency (Corsi et al., 2022; Graf et al., 2019). Furthermore, reduced editing efficiency associated with Cas9 nickase compared to wild-type Cas9 has also been shown in other studies (De Angeli et al., 2022). The selection of gRNAs in the present thesis was, as already mentioned, limited due to the T-rich target sequence surrounding the DIM and the requirements for the double-nicking strategy with Cas9 nickase. Due to low efficiency and gRNA design limitations, the "4n" CRISPR/Cas9 nickase approach was not pursued. Instead, the focus was shifted to another strategy that appeared to be more suitable for the target sequence: the elimination of the *OPA1* DIM using CRISPR genome editing based on the Cpf1 nuclease.

5.1.3 CRISPR/Cpf1-induced editings in patient-derived iPSCs

Cpf1, also known as Cas12a, can be used as an alternative to Cas9. Unlike Cas9, Cpf1 cuts the target sequence approximately 20 bp downstream of the PAM and generates staggered double-strand break ends (Zetsche et al., 2015). In addition, the single RNA-guided endonuclease

functions without the involvement of a tracrRNA. Why is Cpf1 a suitable candidate for the elimination of the *OPA1* DIM in patient-derived iPSCs? The PAM sequence TTTN of AsCpf1 and LbCpf1 is well suited for the T-rich target region and allows for a wider range of gRNAs. Moreover, AsCpf1 and LbCpf1 were shown to induce highly specific indels in human cells with efficiencies comparable to that of SpCas9 (Kleinstiver et al., 2016).

Electroporation of the patient-derived iPSCs with either AsCpf1-gRNA1, AsCpf1-gRNA2 or AsCpf1-gRNA3 plasmids resulted in comparable transfection efficiencies of 50% to 60%. In contrast, repeated expression of gRNA4 resulted in high cell death and no detectable GFP signal in the remaining cells, indicating that these cells were not transfected. Apoptosis of the transfected cells is most likely due to the fact that gRNA4 is located within a repetitive sequence of the target DNA. The repetitive sequence is an Alu element that starts four nucleotides upstream of the DIM and has a length of 315 bp (Bonifert et al., 2016). Presumably, transfection with AsCpf1-gRNA4 resulted in repetitive cuts throughout the entire genome, affecting cell survival.

Indels were again detected by analysis of fluorescently-labelled amplicons, which showed low cleavage efficacies of up to 6%. Using an U6 promoter-driven crRNA expression cassette, Mao and colleagues achieved an indel rate of 20-30% when targeting the *CLEC16A* gene (Ma et al., 2018). Based on these results, gRNAs targeting the *CLEC16A* gene served a positive control in the present study. However, the editing efficiency that could be achieved for the positive control was only 10%. In both studies, human iPSCs were electroporated with plasmids expressing the CRISPR/Cpf1 components and editing efficiencies were analysed 2-3 days post electroporation. However, in contrast to the present study, in the study by Ma and colleagues, Cpf1 and crRNA were co-expressed from different plasmids and Indel detection was performed by a T7E1 assay, possibly explaining the different efficiencies. In addition, different Cpf1 orthologs were used in both studies (AsCpf1 in the present work and LbCpf1 in Ma et al.), which might also have an effect on the cleavage efficacy. Experiments in yeast and plants showed that AsCpf1 is indeed associated with lower editing efficiencies compared to LbCpf1 (Kim et al., 2021; Verwaal et al., 2018). In mammalian cells, LbCpf1 and AsCpf1 generally exhibit comparable efficiencies, with LbCpf1 performing slightly better in some cases (Tóth et al., 2018; Tu et al., 2017).

The enrichment of transfected cells using e.g. fluorescence-activated cell sorting (FACS) or selection based on antibiotic resistance can provide a better estimate of the cleavage efficacy of gRNAs. The calculated indel frequency was approximately 3- to 5-fold higher after sorting of CRISPR/Cpf1-treated iPSCs, indicating that removal of untransfected cells from the pool

actually increases the percentage of edited cells, which also affects the overall cleavage efficacy (Elkhadragy et al., 2021; Petersen et al., 2019).

After demonstrating efficient indel formation with CRISPR/Cpf1 genome editing using gRNA1 and gRNA2 in the patient-derived iPSC bulk, the editing efficiency was evaluated at the level of clonal cell lines and the spectrum of editing events and the effect of the editings on the splicing process were determined. Various methods can be used to generate single cell clones, including serial dilution and FACS. Isolation of single cells by FACS is less time and labour intensive than serial dilution, which requires manual collection of colonies. However, the generation of single cell clones by FACS had a major impact on cell survival in the present work and resulted in the loss of most iPS cell clones. In contrast, subcloning by serial dilution of FACS-sorted bulk cells followed by colony picking proved to be an efficient method for obtaining iPSC clones: the majority of single cell clones grew into proper colonies and the cell density was low enough to avoid contact between different colonies. Furthermore, Sanger sequencing data of the generated iPSC clones revealed no more than two overlapping traces, indicating well preserved clonality after serial dilution and colony picking.

The cultivation of single cells is often challenging, as the very process of cell isolation causes high stress leading to cell death. In addition, single cell cultures lack cell-cell interactions that play a critical role in cell survival . The serial dilution is likely to be less stressful to the cells than FACS. In addition, culturing the single cell clones on a common tissue culture plate after serial dilution may also have had a positive effect on the cells, as cell communication occurs not only through direct cell interactions but also through the release of cell secretions such as growth factors, which can promote the viability and proliferation of surrounding cells.

The gRNA1-transfected and sorted cell bulk was used for subcloning because gRNA1 showed a slightly higher editing efficiency than gRNA2 in the bulk analysis and its cleavage site is closer to the DIM. Surprisingly, the determined editing efficiency in the iPSC clones was almost twice as high as in the bulk analysis. The editing events observed in the iPSC clones included deletions between 4 bp and 27 bp, but the majority harboured rather small deletions of up to 7 bp. The observed indels are consistent with reports from Ma et al., who described Cpf1-induced deletions with sizes of around 10 bp obtained from editing with single gRNAs in iPSCs. None of the deletions eliminated the DIM, because of the distance (20-30 bp) between the cleavage site of the gRNA and the DIM. As expected, the Cpf1 approach did not show specificity for the DIM allele, as the most efficient gRNA is not specific for the DIM sequence. In

conclusion, the CRISPR/Cpf1 approach using gRNA1 resulted in Indel formation in patient-derived iPSCs but without eliminating the DIM.

5.1.4 CRISPR/Cpf1-based rescue of *OPA1* DIM-induced missplicing

Do CRISPR/Cpf1-generated deletions reduce defective splicing despite preservation of the DIM? To address this question, the relative amount of correctly spliced transcripts in the edited iPSC clones was determined by pyrosequencing. Correctly spliced DIM alleles were discriminated from I437M alleles by a common SNP. This approach has been previously described as an efficient method to quantify AON-mediated splice correction in patient-derived fibroblasts carrying the DIM (Bonifert et al., 2016).

Surprisingly, 38% of the sequenced iPSC clones revealed restoration of correct splicing with efficiencies ranging from 8% up to 79%. This shows that deletions that differ in only a few nucleotides may be associated with different levels of splicing rescue. No splicing rescue was detected in 8/13 clones: Six of these clones harboured Cpf1-induced editings on the I437M allele but not on the DIM allele. The remaining two clones carried deletions of 13 bp and 27 bp on the DIM allele. Interestingly, the rather small deletions correlated with splicing rescue whereas the two larger deletions did not result in splicing rescue. One possible reason for this could be that the smaller deletions interrupt or even integrate a regulatory element crucial for splicing and thus restore correct splicing, whereas the larger deletions could change the context by introducing or eliminating additional regulatory elements and thus reverse the rescue effect.

According to Bonifert and colleagues, treatment of patient-derived fibroblasts with AONs targeting the cryptic acceptor splice site or predicted branch point resulted in splicing rescue efficiencies of up to 55% (Bonifert et al., 2016). Consequently, more correctly spliced transcripts were detected with CRISPR/Cpf1 genome editing than with AON transfection.

Furthermore, I437M and DIM transcripts were identified and quantified in iPSC clones with the highest splicing rescue efficiency by RT-PCR and subsequent fragment analysis. Compared with non-edited patient-derived iPSCs, the aberrant DIM transcript was reduced more than 3-fold in clone 8 and even 7-fold in clone 10, whereas the proportion of correctly spliced transcripts was increased, corroborating the pyrosequencing results. Identification of the RT-PCR fragments based on their sizes revealed alternative transcripts with or without exon 4 and 4b (Delettre et al., 2001). The proportion of the transcript missing exon 4b was similar to that of the full-length transcript, while the transcript missing exon 4b and 4 hardly occurred and the

transcript missing only exon 4 was not detected at all. The relative abundance of alternative *OPA1* transcripts was shown to vary depending on the respective tissue (Akepati et al., 2008; Delettre et al., 2001). Interestingly, no alternative transcripts were observed in association with the aberrant transcript. Two misspliced transcripts were observed, either including the shorter pseudoexon (61 bp) or the larger pseudoexon (93 bp), with the latter accounting for the majority of DIM transcripts. Incorporation of the larger pseudoexon introduces a stop codon after 87 bp into the open reading frame, and that of the smaller version results in a frameshift leading to a premature termination codon (PTC) 84 bp downstream in exon 5 (Bonifert et al., 2014).

RT-PCR combined with fragment analysis proved that CRISPR/Cpf1-mediated splicing correction in patient-derived iPSCs was particularly efficient in clone 10. In addition, it could be demonstrated that cycloheximide treatment increased the amount of misspliced transcripts in control cells, reinforcing the assumption that the aberrant *OPA1* transcripts are degraded by nonsense-mediated mRNA decay (NMD) (Bonifert et al., 2014).

Further characterization of CRISPR/Cpf1-induced editings was performed using minigene splicing assays. Interestingly, using this approach, the level of splicing rescue was consistent for clone 6, clone 8 and clone 10, with no significant differences. Complete rescue of missplicing was achieved by all three editings, as shown by RT-PCR results consistent with those of the wild-type construct. Expansion of the minigene construct to include additional *OPA1* exons resulted in a broader range of RT-PCR fragments, the proportion of which varied depending on the construct. All editings were associated with reduced misspliced transcripts compared to the mutant construct, but none of them showed complete splicing rescue. The clone 10 editing performed best, followed by clone 8 and clone 6, which is consistent with the observations of the pyrosequencing assay. The transcript including the larger pseudoexon was again the most abundant mutant transcript. However, the proportion of the respective wild-type transcripts differed from those obtained in the patient-derived iPSCs: The transcript lacking exon 4b was more abundant than the full length transcript in the minigene assays.

In summary, minigene assays confirmed Cpf1-mediated splicing correction in an iPSC-independent system, with clone 10 editing showing the highest similarity to the wild-type control. It was also shown that results can vary depending on the exons involved in the assay. The inclusion of a larger genomic region of *OPA1* in the minigene constructs better reflects the natural splicing process and thus provides more reliable results. It has also been shown previously that flanking exons and their adjacent intronic segments can influence the recognition of alternative exons (Cooper, 2005).

5.1.5 CRISPR/Cpf1-induced increase of OPA1 protein expression in patient-derived iPSCs

Reduced levels of OPA1 protein were associated with the DIM in patient-derived fibroblasts (Bonifert et al., 2014). Protein analysis in the present work revealed a reduction of OPA1 expression in patient-derived iPSCs by approximately 50% compared to control cells, confirming the results of Bonifert and colleagues. Moreover, the OPA1 protein level was significantly increased in CRISPR/Cpf1-edited iPSC clones 8 and 10 compared with non-edited patient cells. Clone 10 showed a slightly higher expression of OPA1 than clone 8, consistent with the different levels of splicing rescue observed in the clones.

Thus, the present work has shown that a 60-80% rescue of correctly spliced transcripts by CRISPR/Cpf1 editing results in a substantial increase of OPA1 protein .

5.1.6 Mitochondrial morphology in patient-derived iPSCs after CRISPR/Cpf1 genome editing

The OPA1 protein plays a crucial role in mitochondrial function and dynamics. Mutations in the *OPA1* gene were associated with increased apoptosis, fragmentation of the mitochondrial network, reduced mtDNA content and impaired ATP synthesis (Amati-Bonneau et al., 2008; Del Dotto et al., 2018; Harvey et al., 2022; Olichon et al., 2007; Zanna et al., 2008). Increased mitochondrial fragmentation was also observed in patient-derived fibroblasts harbouring the DIM c.610+364G>A (Bonifert et al., 2014). Consequently, the aim of this thesis was to investigate the mitochondrial morphology in patient-derived iPSC and CRISPR-edited clones in comparison with a wild-type control. Interestingly, the wild-type control revealed well-defined and round-shaped mitochondria, whereas the patient-derived control appeared to have rather diffuse and elongated mitochondria. Indeed, it has already been described that iPSCs typically exhibit short and round-shaped mitochondria and also reduced numbers of mitochondria compared to somatic cells (Bukowiecki et al., 2014; Prigione et al., 2010). However, the mitochondria of the edited clones could not be unambiguously assigned to those of either the wild-type control or the non-edited patient cells.

Considering the general lack of branched mitochondrial networks in iPSCs, fragmentation cannot be used as an indicator for aberrant mitochondria. Instead, the area and shape of mitochondria were measured to determine differences or similarities between the processed clones and controls. However, no significant differences between unedited patient cells and the wild-type control were detected. Due to time constraints, further analysis of the mitochondria could not

be performed. In order to characterize the edited clones more precisely, a functional evaluation of the mitochondria would be required, e.g. by measuring the oxygen consumption rate (OCR), to determine mitochondrial respiration, or by analysing the mitochondrial membrane potential, e.g. by cell staining using tetramethylrhodamine ethyl ester (TMRE). However, it must be taken into account that iPSCs differ significantly from somatic cells not only in terms of mitochondrial morphology but also in regard to bioenergetics. In general, the mitochondria of iPSCs were shown to resemble those of embryonic stem cells (ESCs) revealing perinuclear distribution and immature cristae as well as reduced mtDNA copy numbers (Prigione et al., 2010). iPSCs also mainly contain of less active mitochondria and the production of ATP is predominantly attributed to glycolysis rather than oxidative phosphorylation (Bukowiecki et al., 2014; Prigione et al., 2010; Varum et al., 2011). Because pluripotency of iPSCs affects the mitochondrial morphology and physiology, it would be advisable to perform further analyses on differentiated cells.

5.1.7 What is the mechanism associated with CRISPR/Cpf1-induced splicing rescue?

CRISPR/Cpf1 treatment of patient-derived iPSCs revealed efficient restoration of correct splicing, although the DIM was not eliminated by the generated editings. In fact, the cryptic acceptor splice site was still present in the edited sequences according to NNSplice prediction (data not shown). Most likely, the observed rescue of missplicing was impacted by the introduction or deletion of splicing regulatory elements and associated splicing factors (SFs) such as SR proteins or hnRNPs (Krecic & Swanson, 1999; Lee & Rio, 2015; Zahler et al., 1992). The Cpf1 editings may have eliminated a conserved binding motif of a splicing enhancer or even introduced a binding site for a splicing silencer, thereby restoring correct splicing. This assumption could also explain why larger deletions did not result in splicing rescue. Those editings might affect additional regulatory elements, further altering the splicing context. Bonifert and colleagues identified a binding motif for the splice enhancer Sc35 in the relevant sequence region (Bonifert et al., 2016), which may be eliminated by the obtained editings. However, the Sc35 binding element is still present in clone 19, which also showed some degree of rescue.

In silico prediction of SF binding motifs proved to be challenging since most of them are poorly conserved (Liu et al., 2000; Siala et al., 2014). HEXplorer profiles (Erkelenz et al., 2014) revealed additional binding elements for SR proteins in clone 8 and 10. SR proteins were described to enhance the usage of downstream donor splice sites and upstream acceptor splice sites, whereas upstream donors and downstream acceptors are inhibited (Erkelenz et al., 2013;

Ptok et al., 2021). Furthermore, HEXplorer predicted an additional acceptor splice site with a considerable score in clone 10 generated by the Cpf1 editing, which might compete with the adjacent acceptor splice site created by the DIM thereby restoring correct splicing. However, elimination of the novel splice site did not result in an increased number of aberrant transcripts, refuting the hypothesis that this additional splice site could prevent missplicing. Thus, the underlying mechanism of the splicing rescue remains undetermined.

5.1.8 Final conclusions

In the present work, induced missplicing of the *OPA1* deep intronic variant c.610+364G>A was successfully corrected in patient-derived iPSCs using CRISPR/Cpf1 genome editing. Up to 80% of mutant transcripts were corrected with CRISPR/Cpf1, which is a surprising result since the generated editings did not eliminate the DIM. Most likely, restoration of proper splicing is due to an editing-induced deletion or even insertion of a splicing regulatory element (SRE). If the splice correction is associated with the deletion of a regulatory element, the use of AONs could be a potential strategy for targeted therapy of patients carrying the DIM. However, identification of such elements proved to be challenging, as *in silico* predictions were only informative to a limited extent. Fluorescence-based splicing reporter could provide a useful method to identify the crucial SREs in future experiments (Wang & Wang, 2014).

Further characterization of the edited iPSC clones also demonstrated a significant increase of OPA1 protein expression compared to non-edited patient cells. Additionally, fluorescence-imaging revealed differences in the mitochondrial morphology in non-edited patient cells versus healthy control cells. To properly characterize the mitochondria of the edited clones, further studies would be necessary, especially also with regard to the mitochondrial physiology.

5.2 *DNAJC30* screening in Leber´s hereditary optic neuropathy and optic atrophy patients

Somewhat surprisingly, in 2021, Stenton and colleagues identified biallelic variants in the nuclear gene *DNAJC30* as a cause of autosomal recessive Leber hereditary optic neuropathy (arLHON) (Stenton et al, 2021). Until this discovery, the underlying genetic etiology of LHON was attributed to pathogenic variants in the mitochondrial genome. In a first independent replication study, we were able to confirm that arLHON is associated with pathogenic biallelic variants in *DNAJC30*. In detail, we identified putatively pathogenic variants in the *DNAJC30* gene in 35/1202 individuals from 32 families, which corresponds to a detection rate of 2.9%. More

specifically, 29/800 LHON cases (3.6%) and 6/402 OA cases (1.5%) were associated with pathogenic variants in *DNAJC30*. Thus, we demonstrated for the first time that *DNAJC30* variants not only cause LHON but may also provide an explanation for genetically unsolved OA cases. The majority of the individuals with *DNAJC30* variants were male (90%), whereas only 10% were female. Stenton et al. reported a male to female ratio of 10:1 in their arLHON cohort, similar to our ratio of 6:1 (male to female ratio in the entire cohort was 1.8:1) (Stenton et al., 2021). Male predominance is a hallmark in classical LHON caused by mtDNA mutations (mtLHON) and our results confirm that this also holds true for arLHON. In order to explain the unequal penetrance of arLHON in male and female individuals, Stenton et al. determined the mRNA expression and protein level of *DNAJC30* in male and female control fibroblast cell lines. However, no sex-dependent differences in *DNAJC30* expression could be detected (Stenton et al., 2021). The male predominance in arLHON could not be explained by genetic causes so far. Possibly, more complex processes play a role here, such as the sex-specific hormone balance or anatomical differences. In addition to male predominance, clinical investigations of arLHON patients revealed other similarities to mtLHON, including initial peripapillary microangiopathy and cecocentral visual field defects (Kieninger et al., 2022; Stenton et al., 2021). Furthermore, it was shown that therapy with the antioxidant Idebenone, which is usually used in context with mtLHON, also induces a clinically relevant recovery (CRR) in arLHON patients appearing to be even higher compared to Idebenone-induced CRR in mtLHON patients (Stenton et al., 2021; Stenton et al., 2022). Differences between mtLHON and arLHON are evident with regard to onset of the disease and recovery: arLHON patients have an earlier and more frequent bilateral onset of the disease and a more frequent occurrence of CRR (Kieninger et al., 2022; Stenton et al., 2021; Stenton et al., 2022).

The majority of arLHON patients described by Stenton et al. carries the *DNAJC30* variant c.152A>G; p.(Y51C) (Stenton et al., 2021). This missense variant was also identified as the most common variant in our patient cohort, 30/35 individuals harbor the putatively pathogenic variant in homozygous state. In some cases, this missense variant was found in single heterozygous state, which may be due to the relatively high allele frequency of this variant in the general population (MAF = 0.001097). Furthermore, it is possible that a second likely pathogenic variant is located outside the analysed regions, such as in distant regulatory regions. The relatively high allele frequency of the c.152A>G variant is mostly due to a founder effect (Kieninger et al., 2022; Stenton et al., 2021).

Stenton et al. also described two other *DNAJC30* variants associated with arLHON: c.232C>T; p.(P78S) and c.302T>A; (L101Q) (Stenton et al., 2021). These variants were not detected in our cohort, however, we were able to identify two novel likely disease causing variants: the nonsense variant c.610G>T; p.(E204*), which occurred in compound heterozygous state with the common c.152A>G variant in three patients with suspected LHON, and the in-frame deletion c.230_232del; p.(H77del) which was found in two siblings in homozygous state.

What pathological mechanism may be related to the *DNAJC30* variants? The missense variant c.152A>G and the novel deletion c.230_232del are located in the conserved J domain of the DNAJC30 protein. Proteins with a J domain are known to act as co-chaperones for heat-shock proteins, which play a key role in protein homeostasis (Kampinga et al., 2019). Variants in the J domain were shown to induce degradation of the DNAJC30 protein (Stenton et al., 2021). The nonsense variant c.610G>T; p.(E204*) is located upstream of the transmembrane domain and generates PTC-containing transcripts, which are usually degraded by the NMD pathway. However, researchers demonstrated that intronless genes are mostly insensitive to NMD, suggesting that the nonsense variant c.610G>T; p.(E204*) in the single-exon gene *DNAJC30* produces a truncated protein (Brocke et al., 2002; Maquat & Li, 2001). Reduced levels of functional DNAJC30 protein were linked to decreased ATP synthesis, mitochondrial dysfunction, and neuronal aberrations in mice (Tebbenkamp et al., 2018). Furthermore, Stenton and colleagues found reduced turnover of mitochondrial respiratory complex I proteins in fibroblasts from arLHON patients resulting in malfunction of the complex I subunit, suggesting that DNAJC30 is crucial for the exchange of respiratory chain subunits (Stenton et al., 2021).

In conclusion, our study represents the first large-scale screening of *DNAJC30* in patients with suspected LHON and OA since the publication of Stenton et al. in 2021. We confirmed the important role of *DNAJC30* variants in the context of arLHON, but also in other hereditary optic neuropathies. Stenton and colleagues studied patients with an Eastern European background. In contrast, patients in our cohort were from Central Europe, particularly Germany. Thus, we were able to show that *DNAJC30* variants occur not only in Eastern European patients, but also in Central European patients. The missense variant c.152A>G accounts for approximately 90% of the total disease alleles in both Eastern European and Central European patients. We also identified two novel *DNAJC30* variants that are most likely causative for arLHON and OA. Together with the study by Stenton et al., we demonstrated the importance of *DNAJC30* in the genetic diagnosis of LHON patients and patients with other hereditary optic neuropathies.

6 Summary

Hereditary optic neuropathies are characterized by painless, progressive and bilateral loss of vision due to the degeneration of retinal ganglion cells whose axons form the optic nerve. The conditions are caused by mutations in nuclear- or mitochondrial-encoded genes associated with mitochondrial functions. Mutation-induced disruption of the mitochondria results, among other things, in deficient ATP levels promoting cell death of retinal ganglion cells which have a high ATP demand. The most common inherited optic neuropathies are Leber´s hereditary optic neuropathy (LHON) and dominant optic atrophy (DOA). LHON usually occurs in the first or second decade of life and affects predominantly men. The condition is mainly caused by three point mutations in the mitochondrial DNA and was therefore exclusively associated with maternal inheritance. In 2021, an autosomal-recessive form of LHON caused by biallelic variants in the nuclear-encoded gene *DNAJC30* was described for the first time (Stenton et al., 2021).

The onset of DOA usually occurs in the first or second decade of life. The disease is characterized by high inter- and intrafamilial variation with incomplete penetrance. The majority of DOA patients experience isolated DOA restricted to the eye, but 20% of patients suffer from syndromic forms mainly including neurological dysfunctions. This condition is also known as DOA plus or Behr syndrome. More than 60% of DOA cases are caused by mutations in the *OPA1* gene. *OPA1* encodes a GTPase which locates to the inner mitochondrial membrane and is especially crucial for mitochondrial fusion and the maintenance of cristae structure.

CRISPR genome editing of patient-specific iPSCs to rescue missplicing induced by *OPA1* deep intronic mutation

A severe form of Behr syndrome has been observed in patients carrying the *OPA1* deep intronic mutation c.610+364G>A in *trans* with a missense variant that acts as an intralocus modifier (Bonifert et al., 2014). The deep intronic mutation (DIM) creates a cryptic acceptor splice site producing aberrant *OPA1* transcripts harbouring a premature termination codon. The mutant transcripts are degraded by the cellular control mechanism "nonsense-mediated mRNA decay", resulting in decreased expression of the OPA1 protein. The disease phenotype is eventually caused by haploinsufficiency. The aim of the present thesis was to rescue the DIM-induced missplicing in patient-derived induced pluripotent stem cells (iPSCs) using CRISPR genome editing. Two Cas nucleases were tested in the process: Cas9 nickase and Cas12a, also known as Cpf1. The Cas9 variant only induces single-strand nicks into the target DNA, thus a pair of

gRNAs is required for a double-strand break allowing a higher target specificity in comparison to wild-type Cas9. However, editing of patient-derived cells with Cas9 nickase only resulted in low cleavage efficacies. Genome editing using Cpf1, on the other hand, reached splicing correction up to 80%. Rescue of missplicing was additionally confirmed in iPSC-independent minigene assays. Interestingly, splice correction occurred despite retention of the DIM and the cryptic acceptor splice site assuming that the splice correction is associated with elimination or even introduction of a splicing regulatory element caused by the Cpf1-editings. Further characterization of Cpf1-edited iPSC clones also revealed a statistically significant increase of OPA1 protein expression compared to non-edited patient cells. In conclusion, the present thesis demonstrates successful CRISPR/Cpf1-based rescue of missplicing caused by the DIM c.610+364G>A in patient-derived iPSCs.

DNAJC30 screening of patients with suspected Leber´s hereditary optic neuropathy and optic atrophy

In a further project, we investigated the genetic cause of a previously unexplained Central European cohort of suspected LHON and optic atrophy patients by screening the entire *DNAJC30* gene (Kieninger et al., 2022). Retrospective screening of 1202 patients revealed putatively pathogenic *DNAJC30* variants in 35 individuals from 32 families, corresponding to a detection rate of 2.9%. The majority of patients carries the already described missense variant c.152A>G; p.(Y51C). We also identified two novel likely pathogenic variants, thereby expanding the mutation spectrum of *DNAJC30.* Our results confirm the importance of *DNAJC30* variants in context with hereditary optic neuropathies.

7 Zusammenfassung

Hereditäre Optikusneuropathien sind durch einen schmerzlosen, fortschreitenden und beidseitigen Verlust des Sehvermögens gekennzeichnet, der auf die Degeneration der retinalen Ganglienzellen zurückzuführen ist, deren Axone den Sehnerv bilden. Die Erkrankungen werden durch Mutationen in nukleär oder mitochondrial kodierten Genen verursacht, die mit mitochondrialen Funktionen in Verbindung stehen. Die mutationsbedingte Beeinträchtigung der Mitochondrien führt unter anderem zu ATP-Mangel, der den Zelltod der retinalen Ganglienzellen fördert, die einen hohen ATP-Bedarf haben. Die häufigsten vererbten Optikusneuropathien sind die Lebersche hereditäre Optikusneuropathie (LHON) und die dominante Optikusatrophie (DOA). LHON tritt in der Regel im ersten oder zweiten Lebensjahrzehnt auf und betrifft vorwiegend Männer. Die Erkrankung wird hauptsächlich durch drei Punktmutationen in der mitochondrialen DNA verursacht und wurde daher ausschließlich mit mütterlicher Vererbung in Verbindung gebracht. Im Jahr 2021 wurde zum ersten Mal eine autosomal-rezessive Form der LHON beschrieben, die durch bi-allelische Varianten im kernkodierten Gen *DNAJC30* verursacht wird (Stenton et al., 2021).

Der Ausbruch der DOA erfolgt in der Regel im ersten oder zweiten Lebensjahrzehnt. Die Krankheit ist durch eine hohe inter- und intrafamiliäre Variation mit unvollständiger Penetranz gekennzeichnet. Bei der Mehrheit der DOA-Patienten tritt eine isolierte, auf das Auge beschränkte DOA auf, aber 20% der Patienten leiden an syndromalen Formen, die hauptsächlich neurologische Störungen umfassen. Dieser Zustand wird auch als DOA plus oder Behr-Syndrom bezeichnet. Mehr als 60% der DOA-Fälle werden durch Mutationen im *OPA1*-Gen verursacht. *OPA1* kodiert für eine GTPase, die an der inneren Mitochondrienmembran lokalisiert ist und insbesondere für die mitochondriale Fusion und die Aufrechterhaltung der Cristae-Struktur entscheidend ist.

CRISPR-Genom-Editierung in Patienten-spezifischen iPSCs zur Behebung von fehlerhaftem Spleißen, verursacht durch eine tief-intronische *OPA1*-Mutation

Eine schwere Form des Behr-Syndroms wurde bei Patienten festgestellt, die die tief-intronische *OPA1*-Mutation c.610+364G>A in *trans* mit einer Missense-Variante tragen, welche als Intralocus-Modifikator wirkt (Bonifert et al., 2014). Die tief-intronische Mutation (DIM) erzeugt eine kryptische Akzeptor-Spleißstelle, die zu aberranten *OPA1*-Transkripten führt, die ein vorzeitiges Terminationscodon enthalten. Die mutierten Transkripte werden durch den zelleigenen

Kontrollmechanismus „Nonsense-mediated mRNA Decay“ abgebaut, was zu einer verminderten Expression des OPA1-Proteins führt. Der Krankheitsphänotyp wird schließlich durch Haploinsuffizienz verursacht. Ziel der vorliegenden Arbeit war es, das DIM-induzierte fehlerhafte Spleißen in von Patienten stammenden induzierten pluripotenten Stammzellen (iPSCs) durch CRISPR-Genom-Editierung zu beheben. Dabei wurden zwei Cas-Nukleasen getestet: Cas9-Nickase und Cas12a, auch bekannt als Cpf1. Die Cas9-Variante verursacht nur Einzelstrangbrüche in der Ziel-DNA, so dass für einen Doppelstrangbruch ein Paar an gRNAs erforderlich ist, was eine höhere Zielspezifität im Vergleich zum Wildtyp-Cas9 ermöglicht. Die Editierung von Patientenzellen mit Cas9-Nickase führte jedoch nur zu einer geringen Spaltungseffizienz. Die Genom-Editierung mit Cpf1 erreichte dagegen eine Spleiß-Korrektur von bis zu 80%. Die Rettung des fehlerhaften Spleißens wurde zusätzlich in iPSC-unabhängigen Minigen-Assays bestätigt. Interessanterweise trat die Spleiß-Korrektur trotz der Beibehaltung der DIM und der kryptischen Akzeptor-Spleißstelle auf, was vermuten lässt, dass die Spleiß-Korrektur mit der Eliminierung oder sogar Einführung eines regulatorischen Spleiß-Elements, verursacht durch die Cpf1-Editierungen, verbunden ist. Die weitere Charakterisierung der Cpf1-editierten iPSC-Klone ergab auch einen statistisch signifikanten Anstieg der OPA1-Proteinexpression im Vergleich zu nicht-editierten Patientenzellen. Zusammenfassend lässt sich sagen, dass die vorliegende Arbeit eine erfolgreiche CRISPR/Cpf1-basierte Korrektur des durch die DIM c.610+364G>A verursachten „Fehl-Spleißen“ in Patienten-spezifischen iPSCs zeigt.

DNAJC30-Screening von Patienten mit Verdacht auf hereditäre Lebersche Optikusneuropathie und Optikusatrophie

In einem weiteren Projekt untersuchten wir die genetische Ursache einer bisher ungeklärten mitteleuropäischen Kohorte von Patienten mit Verdacht auf LHON und Optikusatrophie durch Screening des gesamten *DNAJC30*-Gens (Kieninger et al., 2022). Beim retrospektiven Screening von 1202 Patienten wurden bei 35 Individuen aus 32 Familien mutmaßlich pathogene *DNAJC30*-Varianten entdeckt, was einer Detektionsrate von 2,9% entspricht. Die Mehrheit der Patienten trägt die bereits beschriebene Missense-Variante c.152A>G; p.(Y51C). Zusätzlich identifizierten wir zwei neuartige, wahrscheinlich pathogene Varianten und erweitern damit das Mutationsspektrum von *DNAJC30*. Unsere Ergebnisse bestätigen die Bedeutung von *DNAJC30*-Varianten im Zusammenhang mit hereditären Optikusneuropathien.

8 Bibliography

Adebayo, M., Singh, S., Singh, A. P., & Dasgupta, S. (2021). Mitochondrial fusion and fission: The fine-tune balance for cellular homeostasis. *Faseb j*, *35*(6), e21620.

Adzhubei, I. A., Schmidt, S., Peshkin, L., Ramensky, V. E., Gerasimova, A., Bork, P., Kondrashov, A. S., & Sunyaev, S. R. (2010). A method and server for predicting damaging missense mutations. *Nat Methods*, *7*(4), 248-249.

Akepati, V. R., Müller, E. C., Otto, A., Strauss, H. M., Portwich, M., & Alexander, C. (2008). Characterization of OPA1 isoforms isolated from mouse tissues. *J Neurochem*, *106*(1), 372-383.

Al-Harbi, T. M., Abdulmana, S. O., Bashir, S., & Dridi, W. (2019). Novel MFN2 Missense Mutation Induces Hereditary Axonal Motor and Sensory Neuropathy in a Saudi Arabian Family. *J Clin Neuromuscul Dis*, *21*(1), 25-29.

Almind, G. J., Ek, J., Rosenberg, T., Eiberg, H., Larsen, M., Lucamp, L., Brøndum-Nielsen, K., & Grønskov, K. (2012). Dominant optic atrophy in Denmark - report of 15 novel mutations in OPA1, using a strategy with a detection rate of 90%. *BMC Med Genet*, *13*, 65.

Alok, A., Sandhya, D., Jogam, P., Rodrigues, V., Bhati, K. K., Sharma, H., & Kumar, J. (2020). The Rise of the CRISPR/Cpf1 System for Efficient Genome Editing in Plants. *Front Plant Sci*, *11*, 264.

Amati-Bonneau, P., Valentino, M. L., Reynier, P., Gallardo, M. E., Bornstein, B., Boissière, A., Campos, Y., Rivera, H., de la Aleja, J. G., Carroccia, R., Iommarini, L., Labauge, P., Figarella-Branger, D., Marcorelles, P., Furby, A., Beauvais, K., Letournel, F., Liguori, R., La Morgia, C., Carelli, V. (2008). OPA1 mutations induce mitochondrial DNA instability and optic atrophy 'plus' phenotypes. *Brain*, *131*(Pt 2), 338-351.

Arimbasseri, A. G., Rijal, K., & Maraia, R. J. (2013). Transcription termination by the eukaryotic RNA polymerase III. *Biochim Biophys Acta*, *1829*(3-4), 318-330.

Banakar, R., Schubert, M., Collingwood, M., Vakulskas, C., Eggenberger, A. L., & Wang, K. (2020). Comparison of CRISPR-Cas9/Cas12a Ribonucleoprotein Complexes for Genome Editing Efficiency in the Rice Phytoene Desaturase (OsPDS) Gene. *Rice (N Y)*, *13*(1), 4.

Barrangou, R., Fremaux, C., Deveau, H., Richards, M., Boyaval, P., Moineau, S., Romero, D. A., & Horvath, P. (2007). CRISPR provides acquired resistance against viruses in prokaryotes. *Science*, *315*(5819), 1709-1712.

Bennett, E. P., Petersen, B. L., Johansen, I. E., Niu, Y., Yang, Z., Chamberlain, C. A., Met, Ö., Wandall, H. H., & Frödin, M. (2020). INDEL detection, the 'Achilles heel' of precise genome editing: a survey of methods for accurate profiling of gene editing induced indels. *Nucleic Acids Res*, *48*(21), 11958-11981.

Bennett, J. L. (2019). Optic Neuritis. *Continuum (Minneap Minn), 25*(5), 1236-1264.

Bentley, D. L. (2014). Coupling mRNA processing with transcription in time and space. *Nat Rev Genet, 15*(3), 163-175.

Bonifert, T., Gonzalez Menendez, I., Battke, F., Theurer, Y., Synofzik, M., Schöls, L., & Wissinger, B. (2016). Antisense Oligonucleotide Mediated Splice Correction of a Deep Intronic Mutation in OPA1. *Mol Ther Nucleic Acids, 5*(11), e390.

Bonifert, T., Karle, K. N., Tonagel, F., Batra, M., Wilhelm, C., Theurer, Y., Schoenfeld, C., Kluba, T., Kamenisch, Y., Carelli, V., Wolf, J., Gonzalez, M. A., Speziani, F., Schüle, R., Züchner, S., Schöls, L., Wissinger, B., & Synofzik, M. (2014). Pure and syndromic optic atrophy explained by deep intronic OPA1 mutations and an intralocus modifier. *Brain, 137*(Pt 8), 2164-2177.

Bosch, D. G., Boonstra, F. N., Gonzaga-Jauregui, C., Xu, M., de Ligt, J., Jhangiani, S., Wiszniewski, W., Muzny, D. M., Yntema, H. G., Pfundt, R., Vissers, L. E., Spruijt, L., Blokland, E. A., Chen, C. A., Lewis, R. A., Tsai, S. Y., Gibbs, R. A., Tsai, M. J., Lupski, J. R., Schaaf, C. P. (2014). NR2F1 mutations cause optic atrophy with intellectual disability. *Am J Hum Genet, 94*(2), 303-309.

Brocke, K. S., Neu-Yilik, G., Gehring, N. H., Hentze, M. W., & Kulozik, A. E. (2002). The human intronless melanocortin 4-receptor gene is NMD insensitive. *Hum Mol Genet, 11*(3), 331-335.

Brouns, S. J., Jore, M. M., Lundgren, M., Westra, E. R., Slijkhuis, R. J., Snijders, A. P., Dickman, M. J., Makarova, K. S., Koonin, E. V., & van der Oost, J. (2008). Small CRISPR RNAs guide antiviral defense in prokaryotes. *Science, 321*(5891), 960-964.

Buckler, A. J., Chang, D. D., Graw, S. L., Brook, J. D., Haber, D. A., Sharp, P. A., & Housman, D. E. (1991). Exon amplification: a strategy to isolate mammalian genes based on RNA splicing. *Proc Natl Acad Sci U S A, 88*(9), 4005-4009.

Bukowiecki, R., Adjaye, J., & Prigione, A. (2014). Mitochondrial function in pluripotent stem cells and cellular reprogramming. *Gerontology, 60*(2), 174-182.

Burn, T. C., Connors, T. D., Klinger, K. W., & Landes, G. M. (1995). Increased exon-trapping efficiency through modifications to the pSPL3 splicing vector. *Gene, 161*(2), 183-187.

Camara, J., Neto, A., Pires, I. M., Villasana, M. V., Zdravevski, E., & Cunha, A. (2022). A Comprehensive Review of Methods and Equipment for Aiding Automatic Glaucoma Tracking. *Diagnostics (Basel), 12*(4).

Carelli, V., Ghelli, A., Zanna, C., Baracca, A., Sgarbi, G., & Martinuzzi, A. (2004). Severe Defect of Complex I–Dependent ATP Synthesis Shapes the Mitochondria–Driven Path of Apoptotic Cell Death in Leber's Hereditary Optic Neuropathy (LHON). *Investigative Ophthalmology & Visual Science, 45*(13), 1624-1624.

Carelli, V., Ross-Cisneros, F. N., & Sadun, A. A. (2004). Mitochondrial dysfunction as a cause of optic neuropathies. *Prog Retin Eye Res, 23*(1), 53-89.

Chang, H. H. Y., Pannunzio, N. R., Adachi, N., & Lieber, M. R. (2017). Non-homologous DNA end joining and alternative pathways to double-strand break repair. *Nat Rev Mol Cell Biol*, *18*(8), 495-506.

Chen, K., Wang, Y., Zhang, R., Zhang, H., & Gao, C. (2019). CRISPR/Cas Genome Editing and Precision Plant Breeding in Agriculture. *Annu Rev Plant Biol*, *70*, 667-697.

Chiang, T. W., le Sage, C., Larrieu, D., Demir, M., & Jackson, S. P. (2016). CRISPR-Cas9(D10A) nickase-based genotypic and phenotypic screening to enhance genome editing. *Sci Rep*, *6*, 24356.

Cipolat, S., Martins de Brito, O., Dal Zilio, B., & Scorrano, L. (2004). OPA1 requires mitofusin 1 to promote mitochondrial fusion. *Proc Natl Acad Sci U S A*, *101*(45), 15927-15932.

Cohn, A. C., Toomes, C., Potter, C., Towns, K. V., Hewitt, A. W., Inglehearn, C. F., Craig, J. E., & Mackey, D. A. (2007). Autosomal dominant optic atrophy: penetrance and expressivity in patients with OPA1 mutations. *Am J Ophthalmol*, *143*(4), 656-662.

Cong, L., Ran, F. A., Cox, D., Lin, S., Barretto, R., Habib, N., Hsu, P. D., Wu, X., Jiang, W., Marraffini, L. A., & Zhang, F. (2013). Multiplex genome engineering using CRISPR/Cas systems. *Science*, *339*(6121), 819-823.

Cooper, T. A. (2005). Use of minigene systems to dissect alternative splicing elements. *Methods*, *37*(4), 331-340.

Corsi, G. I., Qu, K., Alkan, F., Pan, X., Luo, Y., & Gorodkin, J. (2022). CRISPR/Cas9 gRNA activity depends on free energy changes and on the target PAM context. *Nat Commun*, *13*(1), 3006.

Crick, F. H. (1958). On protein synthesis. *Symp Soc Exp Biol*, *12*, 138-163.

Currie, J. N., Lessell, S., Lessell, I. M., Weiss, J. S., Albert, D. M., & Benson, E. M. (1988). Optic neuropathy in chronic lymphocytic leukemia. *Arch Ophthalmol*, *106*(5), 654-660.

Davies, V. J., Hollins, A. J., Piechota, M. J., Yip, W., Davies, J. R., White, K. E., Nicols, P. P., Boulton, M. E., & Votruba, M. (2007). Opa1 deficiency in a mouse model of autosomal dominant optic atrophy impairs mitochondrial morphology, optic nerve structure and visual function. *Hum Mol Genet*, *16*(11), 1307-1318.

De Angeli, P., Reuter, P., Hauser, S., Schöls, L., Stingl, K., Wissinger, B., & Kohl, S. (2022). Effective splicing restoration of a deep-intronic ABCA4 variant in cone photoreceptor precursor cells by CRISPR/SpCas9 approaches. *Mol Ther Nucleic Acids*, *29*, 511-524.

Del Dotto, V., Fogazza, M., Musiani, F., Maresca, A., Aleo, S. J., Caporali, L., La Morgia, C., Nolli, C., Lodi, T., Goffrini, P., Chan, D., Carelli, V., Rugolo, M., Baruffini, E., & Zanna, C. (2018). Deciphering OPA1 mutations pathogenicity by combined analysis of human, mouse and yeast cell models. *Biochim Biophys Acta Mol Basis Dis*, *1864*(10), 3496-3514.

Del Dotto, V., Ullah, F., Di Meo, I., Magini, P., Gusic, M., Maresca, A., Caporali, L., Palombo, F., Tagliavini, F., Baugh, E. H., Macao, B., Szilagyi, Z., Peron, C., Gustafson, M. A., Khan, K., La Morgia, C., Barboni, P., Carbonelli, M., Valentino, M. L., Carelli, V. (2020). SSBP1 mutations cause mtDNA depletion underlying a complex optic atrophy disorder. *J Clin Invest*, *130*(1), 108-125.

Delettre, C., Griffoin, J. M., Kaplan, J., Dollfus, H., Lorenz, B., Faivre, L., Lenaers, G., Belenguer, P., & Hamel, C. P. (2001). Mutation spectrum and splicing variants in the OPA1 gene. *Hum Genet*, *109*(6), 584-591.

Deltcheva, E., Chylinski, K., Sharma, C. M., Gonzales, K., Chao, Y., Pirzada, Z. A., Eckert, M. R., Vogel, J., & Charpentier, E. (2011). CRISPR RNA maturation by trans-encoded small RNA and host factor RNase III. *Nature*, *471*(7340), 602-607.

den Dunnen, J. T., Dalgleish, R., Maglott, D. R., Hart, R. K., Greenblatt, M. S., McGowan-Jordan, J., Roux, A. F., Smith, T., Antonarakis, S. E., & Taschner, P. E. (2016). HGVS Recommendations for the Description of Sequence Variants: 2016 Update. *Hum Mutat*, *37*(6), 564-569.

den Hollander, A. I., Koenekoop, R. K., Yzer, S., Lopez, I., Arends, M. L., Voesenek, K. E., Zonneveld, M. N., Strom, T. M., Meitinger, T., Brunner, H. G., Hoyng, C. B., van den Born, L. I., Rohrschneider, K., & Cremers, F. P. (2006). Mutations in the CEP290 (NPHP6) gene are a frequent cause of Leber congenital amaurosis. *Am J Hum Genet*, *79*(3), 556-561.

Diakatou, M., Dubois, G., Erkilic, N., Sanjurjo-Soriano, C., Meunier, I., & Kalatzis, V. (2021). Allele-Specific Knockout by CRISPR/Cas to Treat Autosomal Dominant Retinitis Pigmentosa Caused by the G56R Mutation in NR2E3. *Int J Mol Sci*, *22*(5).

Diecke, S., Jung, S. M., Lee, J., & Ju, J. H. (2014). Recent technological updates and clinical applications of induced pluripotent stem cells. *Korean J Intern Med*, *29*(5), 547-557.

Dimos, J. T., Rodolfa, K. T., Niakan, K. K., Weisenthal, L. M., Mitsumoto, H., Chung, W., Croft, G. F., Saphier, G., Leibel, R., Goland, R., Wichterle, H., Henderson, C. E., & Eggan, K. (2008). Induced pluripotent stem cells generated from patients with ALS can be differentiated into motor neurons. *Science*, *321*(5893), 1218-1221.

Ding, R., Chao, C. C., & Gao, Q. (2022). High-efficiency of genetic modification using CRISPR/Cpf1 system for engineered CAR-T cell therapy. *Methods Cell Biol*, *167*, 1-14.

Doench, J. G., Fusi, N., Sullender, M., Hegde, M., Vaimberg, E. W., Donovan, K. F., Smith, I., Tothova, Z., Wilen, C., Orchard, R., Virgin, H. W., Listgarten, J., & Root, D. E. (2016). Optimized sgRNA design to maximize activity and minimize off-target effects of CRISPR-Cas9. *Nat Biotechnol*, *34*(2), 184-191.

Dulla, K., Aguila, M., Lane, A., Jovanovic, K., Parfitt, D. A., Schulkens, I., Chan, H. L., Schmidt, I., Beumer, W., Vorthoren, L., Collin, R. W. J., Garanto, A., Duijkers, L., Brugulat-Panes, A., Semo, M., Vugler, A. A., Biasutto, P., Adamson, P., & Cheetham, M. E. (2018). Splice-Modulating Oligonucleotide QR-110 Restores CEP290 mRNA

and Function in Human c.2991+1655A>G LCA10 Models. *Mol Ther Nucleic Acids*, *12*, 730-740.

Ehses, S., Raschke, I., Mancuso, G., Bernacchia, A., Geimer, S., Tondera, D., Martinou, J. C., Westermann, B., Rugarli, E. I., & Langer, T. (2009). Regulation of OPA1 processing and mitochondrial fusion by m-AAA protease isoenzymes and OMA1. *J Cell Biol*, *187*(7), 1023-1036.

Eiberg, H., Hansen, L., Kjer, B., Hansen, T., Pedersen, O., Bille, M., Rosenberg, T., & Tranebjaerg, L. (2006). Autosomal dominant optic atrophy associated with hearing impairment and impaired glucose regulation caused by a missense mutation in the WFS1 gene. *J Med Genet*, *43*(5), 435-440.

Eiberg, H., Kjer, B., Kjer, P., & Rosenberg, T. (1994). Dominant optic atrophy (OPA1) mapped to chromosome 3q region. I. Linkage analysis. *Hum Mol Genet*, *3*(6), 977-980.

Elkhadragy, L., Regan, M. R., W, M. T., Goli, K. D., Patel, S., Garcia, K., Stewart, M., Schook, L. B., Gaba, R. C., & Schachtschneider, K. M. (2021). Generation of genetically tailored porcine liver cancer cells by CRISPR/Cas9 editing. *Biotechniques*, *70*(1), 37-48.

Engler, C., Kandzia, R., & Marillonnet, S. (2008). A one pot, one step, precision cloning method with high throughput capability. *PLoS One*, *3*(11), e3647.

Erkelenz, S., Mueller, W. F., Evans, M. S., Busch, A., Schöneweis, K., Hertel, K. J., & Schaal, H. (2013). Position-dependent splicing activation and repression by SR and hnRNP proteins rely on common mechanisms. *Rna*, *19*(1), 96-102.

Erkelenz, S., Theiss, S., Otte, M., Widera, M., Peter, J. O., & Schaal, H. (2014). Genomic HEXploring allows landscaping of novel potential splicing regulatory elements. *Nucleic Acids Res*, *42*(16), 10681-10697.

Felicio, A. C., Godeiro-Junior, C., Alberto, L. G., Pinto, A. P., Sallum, J. M., Teive, H. G., & Barsottini, O. G. (2008). Familial Behr syndrome-like phenotype with autosomal dominant inheritance. *Parkinsonism Relat Disord*, *14*(4), 370-372.

First CRISPR therapy dosed. (2020). *Nat Biotechnol*, *38*(4), 382.

Frezza, C., Cipolat, S., Martins de Brito, O., Micaroni, M., Beznoussenko, G. V., Rudka, T., Bartoli, D., Polishuck, R. S., Danial, N. N., De Strooper, B., & Scorrano, L. (2006). OPA1 controls apoptotic cristae remodeling independently from mitochondrial fusion. *Cell*, *126*(1), 177-189.

Frischmeyer, P. A., & Dietz, H. C. (1999). Nonsense-mediated mRNA decay in health and disease. *Hum Mol Genet*, *8*(10), 1893-1900.

Gao, Y., & Zhao, Y. (2014). Self-processing of ribozyme-flanked RNAs into guide RNAs in vitro and in vivo for CRISPR-mediated genome editing. *J Integr Plant Biol*, *56*(4), 343-349.

Gao, Z., Herrera-Carrillo, E., & Berkhout, B. (2018). Delineation of the Exact Transcription Termination Signal for Type 3 Polymerase III. *Mol Ther Nucleic Acids*, *10*, 36-44.

Garneau, J. E., Dupuis, M., Villion, M., Romero, D. A., Barrangou, R., Boyaval, P., Fremaux, C., Horvath, P., Magadán, A. H., & Moineau, S. (2010). The CRISPR/Cas bacterial immune system cleaves bacteriophage and plasmid DNA. *Nature*, *468*(7320), 67-71.

Gasiunas, G., Barrangou, R., Horvath, P., & Siksnys, V. (2012). Cas9-crRNA ribonucleoprotein complex mediates specific DNA cleavage for adaptive immunity in bacteria. *Proc Natl Acad Sci U S A*, *109*(39), E2579-2586.

Ge, Y., Shi, X., Boopathy, S., McDonald, J., Smith, A. W., & Chao, L. H. (2020). Two forms of Opa1 cooperate to complete fusion of the mitochondrial inner-membrane. *Elife*, *9*.

Giannelli, S. G., Luoni, M., Castoldi, V., Massimino, L., Cabassi, T., Angeloni, D., Demontis, G. C., Leocani, L., Andreazzoli, M., & Broccoli, V. (2018). Cas9/sgRNA selective targeting of the P23H Rhodopsin mutant allele for treating retinitis pigmentosa by intravitreal AAV9.PHP.B-based delivery. *Hum Mol Genet*, *27*(5), 761-779.

González, F., Boué, S., & Izpisúa Belmonte, J. C. (2011). Methods for making induced pluripotent stem cells: reprogramming à la carte. *Nat Rev Genet*, *12*(4), 231-242.

Gopalappa, R., Suresh, B., Ramakrishna, S., & Kim, H. H. (2018). Paired D10A Cas9 nickases are sometimes more efficient than individual nucleases for gene disruption. *Nucleic Acids Res*, *46*(12), e71.

Graf, R., Li, X., Chu, V. T., & Rajewsky, K. (2019). sgRNA Sequence Motifs Blocking Efficient CRISPR/Cas9-Mediated Gene Editing. *Cell Rep*, *26*(5), 1098-1103.e1093.

Grieger, J. C., & Samulski, R. J. (2005). Packaging capacity of adeno-associated virus serotypes: impact of larger genomes on infectivity and postentry steps. *J Virol*, *79*(15), 9933-9944.

György, B., Nist-Lund, C., Pan, B., Asai, Y., Karavitaki, K. D., Kleinstiver, B. P., Garcia, S. P., Zaborowski, M. P., Solanes, P., Spataro, S., Schneider, B. L., Joung, J. K., Géléoc, G. S. G., Holt, J. R., & Corey, D. P. (2019). Allele-specific gene editing prevents deafness in a model of dominant progressive hearing loss. *Nat Med*, *25*(7), 1123-1130.

Haft, D. H., Selengut, J., Mongodin, E. F., & Nelson, K. E. (2005). A guild of 45 CRISPR-associated (Cas) protein families and multiple CRISPR/Cas subtypes exist in prokaryotic genomes. *PLoS Comput Biol*, *1*(6), e60.

Hamedani, A. G., Wilson, J. A., Avery, R. A., & Scherer, S. S. (2021). Optic Neuropathy in Charcot-Marie-Tooth Disease. *J Neuroophthalmol*, *41*(2), 233-238.

Harvey, J. P., Yu-Wai-Man, P., & Cheetham, M. E. (2022). Characterisation of a novel OPA1 splice variant resulting in cryptic splice site activation and mitochondrial dysfunction. *Eur J Hum Genet*, *30*(7), 848-855.

Hauser, S., Schuster, S., Theurer, Y., Synofzik, M., & Schöls, L. (2016). Generation of optic atrophy 1 patient-derived induced pluripotent stem cells (iPS-OPA1-BEHR) for disease modeling of complex optic atrophy syndromes (Behr syndrome). *Stem Cell Res*, *17*(2), 426-429.

Head, B., Griparic, L., Amiri, M., Gandre-Babbe, S., & van der Bliek, A. M. (2009). Inducible proteolytic inactivation of OPA1 mediated by the OMA1 protease in mammalian cells. *J Cell Biol*, *187*(7), 959-966.

Hockemeyer, D., & Jaenisch, R. (2016). Induced Pluripotent Stem Cells Meet Genome Editing. *Cell Stem Cell*, *18*(5), 573-586.

Hryhorowicz, M., Lipiński, D., Zeyland, J., & Słomski, R. (2017). CRISPR/Cas9 Immune System as a Tool for Genome Engineering. *Arch Immunol Ther Exp (Warsz)*, *65*(3), 233-240.

Huang, T., Santarelli, R., & Starr, A. (2009). Mutation of OPA1 gene causes deafness by affecting function of auditory nerve terminals. *Brain Res*, *1300*, 97-104.

Hudson, G., Amati-Bonneau, P., Blakely, E. L., Stewart, J. D., He, L., Schaefer, A. M., Griffiths, P. G., Ahlqvist, K., Suomalainen, A., Reynier, P., McFarland, R., Turnbull, D. M., Chinnery, P. F., & Taylor, R. W. (2008). Mutation of OPA1 causes dominant optic atrophy with external ophthalmoplegia, ataxia, deafness and multiple mitochondrial DNA deletions: a novel disorder of mtDNA maintenance. *Brain*, *131*(Pt 2), 329-337.

Huoponen, K. (2001). Leber hereditary optic neuropathy: clinical and molecular genetic findings. *Neurogenetics*, *3*(3), 119-125.

Ishino, Y., Shinagawa, H., Makino, K., Amemura, M., & Nakata, A. (1987). Nucleotide sequence of the iap gene, responsible for alkaline phosphatase isozyme conversion in Escherichia coli, and identification of the gene product. *J Bacteriol*, *169*(12), 5429-5433.

Jansen, R., Embden, J. D., Gaastra, W., & Schouls, L. M. (2002). Identification of genes that are associated with DNA repeats in prokaryotes. *Mol Microbiol*, *43*(6), 1565-1575.

Janssen, B. D., Chen, Y. P., Molgora, B. M., Wang, S. E., Simoes-Barbosa, A., & Johnson, P. J. (2018). CRISPR/Cas9-mediated gene modification and gene knock out in the human-infective parasite Trichomonas vaginalis. *Sci Rep*, *8*(1), 270.

Jiang, W., Bikard, D., Cox, D., Zhang, F., & Marraffini, L. A. (2013). RNA-guided editing of bacterial genomes using CRISPR-Cas systems. *Nat Biotechnol*, *31*(3), 233-239.

Jinek, M., Chylinski, K., Fonfara, I., Hauer, M., Doudna, J. A., & Charpentier, E. (2012). A programmable dual-RNA-guided DNA endonuclease in adaptive bacterial immunity. *Science*, *337*(6096), 816-821.

Jonasdottir, A., Eiberg, H., Kjer, B., Kjer, P., & Rosenberg, T. (1997). Refinement of the dominant optic atrophy locus (OPA1) to a 1.4-cM interval on chromosome 3q28-3q29, within a 3-Mb YAC contig. *Hum Genet*, *99*(1), 115-120.

Jüschke, C., Klopstock, T., Catarino, C. B., Owczarek-Lipska, M., Wissinger, B., & Neidhardt, J. (2021). Autosomal dominant optic atrophy: A novel treatment for OPA1 splice defects using U1 snRNA adaption. *Mol Ther Nucleic Acids*, *26*, 1186-1197.

Kampinga, H. H., Andreasson, C., Barducci, A., Cheetham, M. E., Cyr, D., Emanuelsson, C., Genevaux, P., Gestwicki, J. E., Goloubinoff, P., Huerta-Cepas, J., Kirstein, J., Liberek, K., Mayer, M. P., Nagata, K., Nillegoda, N. B., Pulido, P., Ramos, C., De Los Rios, P., Rospert, S., Marszalek, J. (2019). Function, evolution, and structure of J-domain proteins. *Cell Stress Chaperones*, *24*(1), 7-15.

Karczewski, K. J., Francioli, L. C., Tiao, G., Cummings, B. B., Alföldi, J., Wang, Q., Collins, R. L., Laricchia, K. M., Ganna, A., Birnbaum, D. P., Gauthier, L. D., Brand, H., Solomonson, M., Watts, N. A., Rhodes, D., Singer-Berk, M., England, E. M., Seaby, E. G., Kosmicki, J. A., Genome Aggregation Database, C. (2020). The mutational constraint spectrum quantified from variation in 141,456 humans. *Nature*, *581*(7809), 434-443.

Kieninger, S., Xiao, T., Weisschuh, N., Kohl, S., Rüther, K., Kroisel, P. M., Brockmann, T., Knappe, S., Kellner, U., Lagrèze, W., Mazzola, P., Haack, T. B., Wissinger, B., & Tonagel, F. (2022). DNAJC30 disease-causing gene variants in a large Central European cohort of patients with suspected Leber's hereditary optic neuropathy and optic atrophy. *J Med Genet*.

Kim, D., Hager, M., Brant, E., & Budak, H. (2021). Efficient genome editing in wheat using Cas9 and Cpf1 (AsCpf1 and LbCpf1) nucleases. *Funct Integr Genomics*, *21*(3-4), 355-366.

Kim, D., Kim, J., Hur, J. K., Been, K. W., Yoon, S. H., & Kim, J. S. (2016). Genome-wide analysis reveals specificities of Cpf1 endonucleases in human cells. *Nat Biotechnol*, *34*(8), 863-868.

Kim, E., Koo, T., Park, S. W., Kim, D., Kim, K., Cho, H. Y., Song, D. W., Lee, K. J., Jung, M. H., Kim, S., Kim, J. H., Kim, J. H., & Kim, J. S. (2017). In vivo genome editing with a small Cas9 orthologue derived from Campylobacter jejuni. *Nat Commun*, *8*, 14500.

Kim, J. Y., Nam, Y., Rim, Y. A., & Ju, J. H. (2022). Review of the Current Trends in Clinical Trials Involving Induced Pluripotent Stem Cells. *Stem Cell Rev Rep*, *18*(1), 142-154.

Kim, S., Kim, D., Cho, S. W., Kim, J., & Kim, J. S. (2014). Highly efficient RNA-guided genome editing in human cells via delivery of purified Cas9 ribonucleoproteins. *Genome Res*, *24*(6), 1012-1019.

Kjer, P. (1957). Hereditary infantile optic atrophy with dominant transmission. *Acta Genet Stat Med*, *7*(2), 290-291.

Klebe, S., Depienne, C., Gerber, S., Challe, G., Anheim, M., Charles, P., Fedirko, E., Lejeune, E., Cottineau, J., Brusco, A., Dollfus, H., Chinnery, P. F., Mancini, C., Ferrer, X., Sole, G., Destée, A., Mayer, J. M., Fontaine, B., de Seze, J., Durr, A. (2012). Spastic paraplegia gene 7 in patients with spasticity and/or optic neuropathy. *Brain*, *135*(Pt 10), 2980-2993.

Kleinstiver, B. P., Tsai, S. Q., Prew, M. S., Nguyen, N. T., Welch, M. M., Lopez, J. M., McCaw, Z. R., Aryee, M. J., & Joung, J. K. (2016). Genome-wide specificities of CRISPR-Cas Cpf1 nucleases in human cells. *Nat Biotechnol*, *34*(8), 869-874.

Krecic, A. M., & Swanson, M. S. (1999). hnRNP complexes: composition, structure, and function. *Curr Opin Cell Biol*, *11*(3), 363-371.

Kreivi, J. P., & Lamond, A. I. (1996). RNA splicing: unexpected spliceosome diversity. *Curr Biol*, *6*(7), 802-805.

La Morgia, C., Carbonelli, M., Barboni, P., Sadun, A. A., & Carelli, V. (2014). Medical management of hereditary optic neuropathies. *Front Neurol*, *5*, 141.

Leal, A. F., & Alméciga-Díaz, C. J. (2022). Efficient CRISPR/Cas9 nickase-mediated genome editing in an in vitro model of mucopolysaccharidosis IVA. *Gene Ther*.

Leber, T. (1871). Ueber hereditäre und congenital-angelegte Sehnervenleiden. *Albrecht von Graefes Archiv für Ophthalmologie*, *17*(2), 249-291.

Lee, Y., & Rio, D. C. (2015). Mechanisms and Regulation of Alternative Pre-mRNA Splicing. *Annu Rev Biochem*, *84*, 291-323.

Lee, Y. J., Jeong, S. Y., Karbowski, M., Smith, C. L., & Youle, R. J. (2004). Roles of the mammalian mitochondrial fission and fusion mediators Fis1, Drp1, and Opa1 in apoptosis. *Mol Biol Cell*, *15*(11), 5001-5011.

Lenaers, G., Hamel, C., Delettre, C., Amati-Bonneau, P., Procaccio, V., Bonneau, D., Reynier, P., & Milea, D. (2012). Dominant optic atrophy. *Orphanet J Rare Dis*, *7*, 46.

Lenaers, G., Neutzner, A., Le Dantec, Y., Jüschke, C., Xiao, T., Decembrini, S., Swirski, S., Kieninger, S., Agca, C., Kim, U. S., Reynier, P., Yu-Wai-Man, P., Neidhardt, J., & Wissinger, B. (2021). Dominant optic atrophy: Culprit mitochondria in the optic nerve. *Prog Retin Eye Res*, *83*, 100935.

Leroy, B. P., Birch, D. G., Duncan, J. L., Lam, B. L., Koenekoop, R. K., Porto, F. B. O., Russell, S. R., & Girach, A. (2021). LEBER CONGENITAL AMAUROSIS DUE TO CEP290 MUTATIONS-SEVERE VISION IMPAIRMENT WITH A HIGH UNMET MEDICAL NEED: A Review. *Retina*, *41*(5), 898-907.

Li, D., Wang, J., Jin, Z., & Zhang, Z. (2019). Structural and evolutionary characteristics of dynamin-related GTPase OPA1. *PeerJ*, *7*, e7285.

Li, H. L., Fujimoto, N., Sasakawa, N., Shirai, S., Ohkame, T., Sakuma, T., Tanaka, M., Amano, N., Watanabe, A., Sakurai, H., Yamamoto, T., Yamanaka, S., & Hotta, A. (2015).

Precise correction of the dystrophin gene in duchenne muscular dystrophy patient induced pluripotent stem cells by TALEN and CRISPR-Cas9. *Stem Cell Reports*, *4*(1), 143-154.

Li, H. L., Gee, P., Ishida, K., & Hotta, A. (2016). Efficient genomic correction methods in human iPS cells using CRISPR-Cas9 system. *Methods*, *101*, 27-35.

Li, P., Kleinstiver, B. P., Leon, M. Y., Prew, M. S., Navarro-Gomez, D., Greenwald, S. H., Pierce, E. A., Joung, J. K., & Liu, Q. (2018). Allele-Specific CRISPR-Cas9 Genome Editing of the Single-Base P23H Mutation for Rhodopsin-Associated Dominant Retinitis Pigmentosa. *Crispr j*, *1*(1), 55-64.

Liu, H. X., Chew, S. L., Cartegni, L., Zhang, M. Q., & Krainer, A. R. (2000). Exonic splicing enhancer motif recognized by human SC35 under splicing conditions. *Mol Cell Biol*, *20*(3), 1063-1071.

Liu, Y., Conlon, D. M., Bi, X., Slovik, K. J., Shi, J., Edelstein, H. I., Millar, J. S., Javaheri, A., Cuchel, M., Pashos, E. E., Iqbal, J., Hussain, M. M., Hegele, R. A., Yang, W., Duncan, S. A., Rader, D. J., & Morrisey, E. E. (2017). Lack of MTTP Activity in Pluripotent Stem Cell-Derived Hepatocytes and Cardiomyocytes Abolishes apoB Secretion and Increases Cell Stress. *Cell Rep*, *19*(7), 1456-1466.

Lonowski, L. A., Narimatsu, Y., Riaz, A., Delay, C. E., Yang, Z., Niola, F., Duda, K., Ober, E. A., Clausen, H., Wandall, H. H., Hansen, S. H., Bennett, E. P., & Frödin, M. (2017). Genome editing using FACS enrichment of nuclease-expressing cells and indel detection by amplicon analysis. *Nat Protoc*, *12*(3), 581-603.

Lunkes, A., Hartung, U., Magariño, C., Rodríguez, M., Palmero, A., Rodríguez, L., Heredero, L., Weissenbach, J., Weber, J., & Auburger, G. (1995). Refinement of the OPA1 gene locus on chromosome 3q28-q29 to a region of 2-8 cM, in one Cuban pedigree with autosomal dominant optic atrophy type Kjer. *Am J Hum Genet*, *57*(4), 968-970.

Ma, X., Chen, X., Jin, Y., Ge, W., Wang, W., Kong, L., Ji, J., Guo, X., Huang, J., Feng, X. H., Fu, J., & Zhu, S. (2018). Small molecules promote CRISPR-Cpf1-mediated genome editing in human pluripotent stem cells. *Nat Commun*, *9*(1), 1303.

Maeder, M. L., Stefanidakis, M., Wilson, C. J., Baral, R., Barrera, L. A., Bounoutas, G. S., Bumcrot, D., Chao, H., Ciulla, D. M., DaSilva, J. A., Dass, A., Dhanapal, V., Fennell, T. J., Friedland, A. E., Giannoukos, G., Gloskowski, S. W., Glucksmann, A., Gotta, G. M., Jayaram, H., . . . Jiang, H. (2019). Development of a gene-editing approach to restore vision loss in Leber congenital amaurosis type 10. *Nat Med*, *25*(2), 229-233.

Makarova, K. S., Grishin, N. V., Shabalina, S. A., Wolf, Y. I., & Koonin, E. V. (2006). A putative RNA-interference-based immune system in prokaryotes: computational analysis of the predicted enzymatic machinery, functional analogies with eukaryotic RNAi, and hypothetical mechanisms of action. *Biol Direct*, *1*, 7.

Malik, N., & Rao, M. S. (2013). A review of the methods for human iPSC derivation. *Methods Mol Biol*, *997*, 23-33.

Maquat, L. E., & Li, X. (2001). Mammalian heat shock p70 and histone H4 transcripts, which derive from naturally intronless genes, are immune to nonsense-mediated decay. *Rna*, *7*(3), 445-456.

Margolin, E., & Shemesh, A. (2022). Toxic and Nutritional Optic Neuropathy. In *StatPearls*. StatPearls Publishing Copyright © 2022, StatPearls Publishing LLC.

Mashima, Y., Kigasawa, K., Shinoda, K., Wakakura, M., & Oguchi, Y. (2017). Visual prognosis better in eyes with less severe reduction of visual acuity one year after onset of Leber hereditary optic neuropathy caused by the 11,778 mutation. *BMC Ophthalmol*, *17*(1), 192.

Mendelsohn, D. H., Schnabel, K., Mamilos, A., Sossalla, S., Pabel, S., Duerr, G. D., Keller, K., Schmitt, V. H., Barsch, F., Walter, N., Wong, R. M. Y., El Khassawna, T., Niedermair, T., Alt, V., Rupp, M., & Brochhausen, C. (2022). Structural Analysis of Mitochondrial Dynamics—From Cardiomyocytes to Osteoblasts: A Critical Review. *International Journal of Molecular Sciences*, *23*(9), 4571.

Mojica, F. J., Díez-Villaseñor, C., García-Martínez, J., & Soria, E. (2005). Intervening sequences of regularly spaced prokaryotic repeats derive from foreign genetic elements. *J Mol Evol*, *60*(2), 174-182.

Mojica, F. J. M., Díez-Villaseñor, C., García-Martínez, J., & Almendros, C. (2009). Short motif sequences determine the targets of the prokaryotic CRISPR defence system. *Microbiology (Reading)*, *155*(Pt 3), 733-740.

Montes, M., Sanford, B. L., Comiskey, D. F., & Chandler, D. S. (2019). RNA Splicing and Disease: Animal Models to Therapies. *Trends Genet*, *35*(1), 68-87.

Mullis, K. B., & Faloona, F. A. (1987). Specific synthesis of DNA in vitro via a polymerase-catalyzed chain reaction. *Methods Enzymol*, *155*, 335-350.

Nishimasu, H., & Nureki, O. (2017). Structures and mechanisms of CRISPR RNA-guided effector nucleases. *Curr Opin Struct Biol*, *43*, 68-78.

Nissim, L., Perli, S. D., Fridkin, A., Perez-Pinera, P., & Lu, T. K. (2014). Multiplexed and programmable regulation of gene networks with an integrated RNA and CRISPR/Cas toolkit in human cells. *Mol Cell*, *54*(4), 698-710.

Nunnari, J., & Suomalainen, A. (2012). Mitochondria: in sickness and in health. *Cell*, *148*(6), 1145-1159.

Olichon, A., Emorine, L. J., Descoins, E., Pelloquin, L., Brichese, L., Gas, N., Guillou, E., Delettre, C., Valette, A., Hamel, C. P., Ducommun, B., Lenaers, G., & Belenguer, P. (2002). The human dynamin-related protein OPA1 is anchored to the mitochondrial inner membrane facing the inter-membrane space. *FEBS Lett*, *523*(1-3), 171-176.

Olichon, A., Landes, T., Arnauné-Pelloquin, L., Emorine, L. J., Mils, V., Guichet, A., Delettre, C., Hamel, C., Amati-Bonneau, P., Bonneau, D., Reynier, P., Lenaers, G., & Belenguer,

P. (2007). Effects of OPA1 mutations on mitochondrial morphology and apoptosis: relevance to ADOA pathogenesis. *J Cell Physiol*, *211*(2), 423-430.

Owens, D. D. G., Caulder, A., Frontera, V., Harman, J. R., Allan, A. J., Bucakci, A., Greder, L., Codner, G. F., Hublitz, P., McHugh, P. J., Teboul, L., & de Bruijn, M. (2019). Microhomologies are prevalent at Cas9-induced larger deletions. *Nucleic Acids Res*, *47*(14), 7402-7417.

Pan, Q., Shai, O., Lee, L. J., Frey, B. J., & Blencowe, B. J. (2008). Deep surveying of alternative splicing complexity in the human transcriptome by high-throughput sequencing. *Nat Genet*, *40*(12), 1413-1415.

Park, I. H., Arora, N., Huo, H., Maherali, N., Ahfeldt, T., Shimamura, A., Lensch, M. W., Cowan, C., Hochedlinger, K., & Daley, G. Q. (2008). Disease-specific induced pluripotent stem cells. *Cell*, *134*(5), 877-886.

Patel, A. A., & Steitz, J. A. (2003). Splicing double: insights from the second spliceosome. *Nat Rev Mol Cell Biol*, *4*(12), 960-970.

Patel, H. R., & Margo, C. E. (2017). Pathology of Ischemic Optic Neuropathy. *Arch Pathol Lab Med*, *141*(1), 162-166.

Pernas, L., & Scorrano, L. (2016). Mito-Morphosis: Mitochondrial Fusion, Fission, and Cristae Remodeling as Key Mediators of Cellular Function. *Annu Rev Physiol*, *78*, 505-531.

Pesch, U. E., Leo-Kottler, B., Mayer, S., Jurklies, B., Kellner, U., Apfelstedt-Sylla, E., Zrenner, E., Alexander, C., & Wissinger, B. (2001). OPA1 mutations in patients with autosomal dominant optic atrophy and evidence for semi-dominant inheritance. *Hum Mol Genet*, *10*(13), 1359-1368.

Petersen, B. L., Möller, S. R., Mravec, J., Jørgensen, B., Christensen, M., Liu, Y., Wandall, H. H., Bennett, E. P., & Yang, Z. (2019). Improved CRISPR/Cas9 gene editing by fluorescence activated cell sorting of green fluorescence protein tagged protoplasts. *BMC Biotechnol*, *19*(1), 36.

Praefcke, G. J., & McMahon, H. T. (2004). The dynamin superfamily: universal membrane tubulation and fission molecules? *Nat Rev Mol Cell Biol*, *5*(2), 133-147.

Pretegiani, E., Rufa, A., Gallus, G. N., Cardaioli, E., Malandrini, A., & Federico, A. (2011). Spastic paraplegia in 'dominant optic atrophy plus' phenotype due to OPA1 mutation. *Brain*, *134*(Pt 11), e195.

Prigione, A., Fauler, B., Lurz, R., Lehrach, H., & Adjaye, J. (2010). The senescence-related mitochondrial/oxidative stress pathway is repressed in human induced pluripotent stem cells. *Stem Cells*, *28*(4), 721-733.

Ptok, J., Müller, L., Ostermann, P. N., Ritchie, A., Dilthey, A. T., Theiss, S., & Schaal, H. (2021). Modifying splice site usage with ModCon: Maintaining the genetic code while changing the underlying mRNP code. *Comput Struct Biotechnol J*, *19*, 3069-3076.

Ran, F. A., Cong, L., Yan, W. X., Scott, D. A., Gootenberg, J. S., Kriz, A. J., Zetsche, B., Shalem, O., Wu, X., Makarova, K. S., Koonin, E. V., Sharp, P. A., & Zhang, F. (2015). In vivo genome editing using Staphylococcus aureus Cas9. *Nature*, *520*(7546), 186-191.

Ran, F. A., Hsu, P. D., Lin, C. Y., Gootenberg, J. S., Konermann, S., Trevino, A. E., Scott, D. A., Inoue, A., Matoba, S., Zhang, Y., & Zhang, F. (2013). Double nicking by RNA-guided CRISPR Cas9 for enhanced genome editing specificity. *Cell*, *154*(6), 1380-1389.

Reese, M. G., Eeckman, F. H., Kulp, D., & Haussler, D. (1997). Improved splice site detection in Genie. *J Comput Biol*, *4*(3), 311-323.

Reynier, P., Amati-Bonneau, P., Verny, C., Olichon, A., Simard, G., Guichet, A., Bonnemains, C., Malecaze, F., Malinge, M. C., Pelletier, J. B., Calvas, P., Dollfus, H., Belenguer, P., Malthièry, Y., Lenaers, G., & Bonneau, D. (2004). OPA3 gene mutations responsible for autosomal dominant optic atrophy and cataract. *J Med Genet*, *41*(9), e110.

Roca, X., Sachidanandam, R., & Krainer, A. R. (2005). Determinants of the inherent strength of human 5' splice sites. *Rna*, *11*(5), 683-698.

Rosenberg, T., Nørby, S., Schwartz, M., Saillard, J., Magalhães, P. J., Leroy, D., Kann, E. C., & Duno, M. (2016). Prevalence and Genetics of Leber Hereditary Optic Neuropathy in the Danish Population. *Invest Ophthalmol Vis Sci*, *57*(3), 1370-1375.

Saiki, R. K., Scharf, S., Faloona, F., Mullis, K. B., Horn, G. T., Erlich, H. A., & Arnheim, N. (1985). Enzymatic amplification of beta-globin genomic sequences and restriction site analysis for diagnosis of sickle cell anemia. *Science*, *230*(4732), 1350-1354.

Sarzi, E., Seveno, M., Piro-Mégy, C., Elzière, L., Quilès, M., Péquignot, M., Müller, A., Hamel, C. P., Lenaers, G., & Delettre, C. (2018). OPA1 gene therapy prevents retinal ganglion cell loss in a Dominant Optic Atrophy mouse model. *Sci Rep*, *8*(1), 2468.

Schlaeger, T. M., Daheron, L., Brickler, T. R., Entwisle, S., Chan, K., Cianci, A., DeVine, A., Ettenger, A., Fitzgerald, K., Godfrey, M., Gupta, D., McPherson, J., Malwadkar, P., Gupta, M., Bell, B., Doi, A., Jung, N., Li, X., Lynes, M. S., Daley, G. Q. (2015). A comparison of non-integrating reprogramming methods. *Nat Biotechnol*, *33*(1), 58-63.

Schubert, M. S., Thommandru, B., Woodley, J., Turk, R., Yan, S., Kurgan, G., McNeill, M. S., & Rettig, G. R. (2021). Optimized design parameters for CRISPR Cas9 and Cas12a homology-directed repair. *Sci Rep*, *11*(1), 19482.

Schunder, E., Rydzewski, K., Grunow, R., & Heuner, K. (2013). First indication for a functional CRISPR/Cas system in Francisella tularensis. *Int J Med Microbiol*, *303*(2), 51-60.

Schwarz, J. M., Cooper, D. N., Schuelke, M., & Seelow, D. (2014). MutationTaster2: mutation prediction for the deep-sequencing age. *Nat Methods*, *11*(4), 361-362.

Sharma, N., Sosnay, P. R., Ramalho, A. S., Douville, C., Franca, A., Gottschalk, L. B., Park, J., Lee, M., Vecchio-Pagan, B., Raraigh, K. S., Amaral, M. D., Karchin, R., & Cutting,

G. R. (2014). Experimental assessment of splicing variants using expression minigenes and comparison with in silico predictions. *Hum Mutat*, *35*(10), 1249-1259.

Sheck, L., Davies, W. I. L., Moradi, P., Robson, A. G., Kumaran, N., Liasis, A. C., Webster, A. R., Moore, A. T., & Michaelides, M. (2018). Leber Congenital Amaurosis Associated with Mutations in CEP290, Clinical Phenotype, and Natural History in Preparation for Trials of Novel Therapies. *Ophthalmology*, *125*(6), 894-903.

Shen, B., Zhang, W., Zhang, J., Zhou, J., Wang, J., Chen, L., Wang, L., Hodgkins, A., Iyer, V., Huang, X., & Skarnes, W. C. (2014). Efficient genome modification by CRISPR-Cas9 nickase with minimal off-target effects. *Nat Methods*, *11*(4), 399-402.

Siala, O., Rebai, A., & Fakhfakh, F. (2014). Slight variations in the SC35 ESE sequence motif among human chromosomes: a computational approach. *Gene*, *545*(1), 102-110.

Smets, K., Deconinck, T., Baets, J., Sieben, A., Martin, J. J., Smouts, I., Wang, S., Taroni, F., Di Bella, D., Van Hecke, W., Parizel, P. M., Jadoul, C., De Potter, R., Couvreur, F., Rugarli, E., & De Jonghe, P. (2014). Partial deletion of AFG3L2 causing spinocerebellar ataxia type 28. *Neurology*, *82*(23), 2092-2100.

Smith, C., Abalde-Atristain, L., He, C., Brodsky, B. R., Braunstein, E. M., Chaudhari, P., Jang, Y. Y., Cheng, L., & Ye, Z. (2015). Efficient and allele-specific genome editing of disease loci in human iPSCs. *Mol Ther*, *23*(3), 570-577.

Steinsapir, K. D., & Goldberg, R. A. (1994). Traumatic optic neuropathy. *Surv Ophthalmol*, *38*(6), 487-518.

Stenton, S. L., Sheremet, N. L., Catarino, C. B., Andreeva, N. A., Assouline, Z., Barboni, P., Barel, O., Berutti, R., Bychkov, I., Caporali, L., Capristo, M., Carbonelli, M., Cascavilla, M. L., Charbel Issa, P., Freisinger, P., Gerber, S., Ghezzi, D., Graf, E., Heidler, J., Prokisch, H. (2021). Impaired complex I repair causes recessive Leber's hereditary optic neuropathy. *J Clin Invest*, *131*(6).

Stenton, S. L., Tesarova, M., Sheremet, N. L., Catarino, C. B., Carelli, V., Ciara, E., Curry, K., Engvall, M., Fleming, L. R., Freisinger, P., Iwanicka-Pronicka, K., Jurkiewicz, E., Klopstock, T., Koenig, M. K., Kolářová, H., Kousal, B., Krylova, T., La Morgia, C., Nosková, L., Prokisch, H. (2022). DNAJC30 defect: a frequent cause of recessive Leber hereditary optic neuropathy and Leigh syndrome. *Brain*, *145*(5), 1624-1631.

Takahashi, K., Tanabe, K., Ohnuki, M., Narita, M., Ichisaka, T., Tomoda, K., & Yamanaka, S. (2007). Induction of pluripotent stem cells from adult human fibroblasts by defined factors. *Cell*, *131*(5), 861-872.

Takahashi, K., & Yamanaka, S. (2006). Induction of pluripotent stem cells from mouse embryonic and adult fibroblast cultures by defined factors. *Cell*, *126*(4), 663-676.

Takahashi, M. (2013). [Retinal cell therapy using iPS cells]. *Rinsho Shinkeigaku*, *53*(11), 1016.

Tazi, J., Bakkour, N., & Stamm, S. (2009). Alternative splicing and disease. *Biochim Biophys Acta*, *1792*(1), 14-26.

Tebbenkamp, A. T. N., Varela, L., Choi, J., Paredes, M. I., Giani, A. M., Song, J. E., Sestan-Pesa, M., Franjic, D., Sousa, A. M. M., Liu, Z. W., Li, M., Bichsel, C., Koch, M., Szigeti-Buck, K., Liu, F., Li, Z., Kawasawa, Y. I., Paspalas, C. D., Mineur, Y. S., Sestan, N. (2018). The 7q11.23 Protein DNAJC30 Interacts with ATP Synthase and Links Mitochondria to Brain Development. *Cell*, *175*(4), 1088-1104.e1023.

Tóth, E., Czene, B. C., Kulcsár, P. I., Krausz, S. L., Tálas, A., Nyeste, A., Varga, É., Huszár, K., Weinhardt, N., Ligeti, Z., Borsy, A., Fodor, E., & Welker, E. (2018). Mb- and FnCpf1 nucleases are active in mammalian cells: activities and PAM preferences of four wild-type Cpf1 nucleases and of their altered PAM specificity variants. *Nucleic Acids Res*, *46*(19), 10272-10285.

Tu, M., Lin, L., Cheng, Y., He, X., Sun, H., Xie, H., Fu, J., Liu, C., Li, J., Chen, D., Xi, H., Xue, D., Liu, Q., Zhao, J., Gao, C., Song, Z., Qu, J., & Gu, F. (2017). A 'new lease of life': FnCpf1 possesses DNA cleavage activity for genome editing in human cells. *Nucleic Acids Res*, *45*(19), 11295-11304.

Ule, J., & Blencowe, B. J. (2019). Alternative Splicing Regulatory Networks: Functions, Mechanisms, and Evolution. *Mol Cell*, *76*(2), 329-345.

Van Craenenbroeck, K., Vanhoenacker, P., & Haegeman, G. (2000). Episomal vectors for gene expression in mammalian cells. *Eur J Biochem*, *267*(18), 5665-5678.

van der Torre, M. H., Novak-Frazer, L., & Rautemaa-Richardson, R. (2020). Detecting Azole-Antifungal Resistance in Aspergillus fumigatus by Pyrosequencing. *J Fungi (Basel)*, *6*(1).

Vanegas, K. G., Jarczynska, Z. D., Strucko, T., & Mortensen, U. H. (2019). Cpf1 enables fast and efficient genome editing in Aspergilli. *Fungal Biol Biotechnol*, *6*, 6.

Varum, S., Rodrigues, A. S., Moura, M. B., Momcilovic, O., Easley, C. A. t., Ramalho-Santos, J., Van Houten, B., & Schatten, G. (2011). Energy metabolism in human pluripotent stem cells and their differentiated counterparts. *PLoS One*, *6*(6), e20914.

Vaz-Drago, R., Custódio, N., & Carmo-Fonseca, M. (2017). Deep intronic mutations and human disease. *Hum Genet*, *136*(9), 1093-1111.

Verwaal, R., Buiting-Wiessenhaan, N., Dalhuijsen, S., & Roubos, J. A. (2018). CRISPR/Cpf1 enables fast and simple genome editing of Saccharomyces cerevisiae. *Yeast*, *35*(2), 201-211.

Vignal, C., Uretsky, S., Fitoussi, S., Galy, A., Blouin, L., Girmens, J. F., Bidot, S., Thomasson, N., Bouquet, C., Valero, S., Meunier, S., Combal, J. P., Gilly, B., Katz, B., & Sahel, J. A. (2018). Safety of rAAV2/2-ND4 Gene Therapy for Leber Hereditary Optic Neuropathy. *Ophthalmology*, *125*(6), 945-947.

Votruba, M., Moore, A. T., & Bhattacharya, S. S. (1997). Genetic refinement of dominant optic atrophy (OPA1) locus to within a 2 cM interval of chromosome 3q. *J Med Genet*, *34*(2), 117-121.

Wang, Y., & Wang, Z. (2014). Systematical identification of splicing regulatory cis-elements and cognate trans-factors. *Methods*, *65*(3), 350-358.

Waterham, H. R., Koster, J., van Roermund, C. W., Mooyer, P. A., Wanders, R. J., & Leonard, J. V. (2007). A lethal defect of mitochondrial and peroxisomal fission. *N Engl J Med*, *356*(17), 1736-1741.

Weisschuh, N., Schimpf-Linzenbold, S., Mazzola, P., Kieninger, S., Xiao, T., Kellner, U., Neuhann, T., Kelbsch, C., Tonagel, F., Wilhelm, H., Kohl, S., & Wissinger, B. (2021). Mutation spectrum of the OPA1 gene in a large cohort of patients with suspected dominant optic atrophy: Identification and classification of 48 novel variants. *PLoS One*, *16*(7), e0253987.

Will, C. L., & Lührmann, R. (2011). Spliceosome structure and function. *Cold Spring Harb Perspect Biol*, *3*(7).

Wu, J., Tang, B., & Tang, Y. (2020). Allele-specific genome targeting in the development of precision medicine. *Theranostics*, *10*(7), 3118-3137.

Xu, X., Wang, P., Jia, X., Sun, W., Li, S., Xiao, X., Hejtmancik, J. F., & Zhang, Q. (2021). Pathogenicity evaluation and the genotype-phenotype analysis of OPA1 variants. *Mol Genet Genomics*, *296*(4), 845-862.

Xue, Y., Hu, X., Wang, D., Li, D., Li, Y., Wang, F., Huang, M., Gu, X., Xu, Z., Zhou, J., Wang, J., Chai, R., Shen, J., Chen, Z. Y., Li, G. L., Yang, H., Li, H., Zuo, E., & Shu, Y. (2022). Gene editing in a Myo6 semi-dominant mouse model rescues auditory function. *Mol Ther*, *30*(1), 105-118.

Yang, Z., Steentoft, C., Hauge, C., Hansen, L., Thomsen, A. L., Niola, F., Vester-Christensen, M. B., Frödin, M., Clausen, H., Wandall, H. H., & Bennett, E. P. (2015). Fast and sensitive detection of indels induced by precise gene targeting. *Nucleic Acids Res*, *43*(9), e59.

Yee, J. K. (2016). Off-target effects of engineered nucleases. *Febs j*, *283*(17), 3239-3248.

Yeo, G., & Burge, C. B. (2004). Maximum entropy modeling of short sequence motifs with applications to RNA splicing signals. *J Comput Biol*, *11*(2-3), 377-394.

Yoshimi, K., Kaneko, T., Voigt, B., & Mashimo, T. (2014). Allele-specific genome editing and correction of disease-associated phenotypes in rats using the CRISPR-Cas platform. *Nat Commun*, *5*, 4240.

Yoshioka, S., Fujii, W., Ogawa, T., Sugiura, K., & Naito, K. (2015). Development of a mono-promoter-driven CRISPR/Cas9 system in mammalian cells. *Sci Rep*, *5*, 18341.

Yu-Wai-Man, P., Griffiths, P. G., & Chinnery, P. F. (2011). Mitochondrial optic neuropathies - disease mechanisms and therapeutic strategies. *Prog Retin Eye Res*, *30*(2), 81-114.

Yu-Wai-Man, P., Griffiths, P. G., Gorman, G. S., Lourenco, C. M., Wright, A. F., Auer-Grumbach, M., Toscano, A., Musumeci, O., Valentino, M. L., Caporali, L., Lamperti, C., Tallaksen, C. M., Duffey, P., Miller, J., Whittaker, R. G., Baker, M. R., Jackson, M. J., Clarke, M. P., Dhillon, B., Chinnery, P. F. (2010). Multi-system neurological disease is common in patients with OPA1 mutations. *Brain*, *133*(Pt 3), 771-786.

Yu, D. Y., Cringle, S. J., Balaratnasingam, C., Morgan, W. H., Yu, P. K., & Su, E. N. (2013). Retinal ganglion cells: Energetics, compartmentation, axonal transport, cytoskeletons and vulnerability. *Prog Retin Eye Res*, *36*, 217-246.

Yu, J., Vodyanik, M. A., Smuga-Otto, K., Antosiewicz-Bourget, J., Frane, J. L., Tian, S., Nie, J., Jonsdottir, G. A., Ruotti, V., Stewart, R., Slukvin, II, & Thomson, J. A. (2007). Induced pluripotent stem cell lines derived from human somatic cells. *Science*, *318*(5858), 1917-1920.

Zahler, A. M., Lane, W. S., Stolk, J. A., & Roth, M. B. (1992). SR proteins: a conserved family of pre-mRNA splicing factors. *Genes Dev*, *6*(5), 837-847.

Zanna, C., Ghelli, A., Porcelli, A. M., Karbowski, M., Youle, R. J., Schimpf, S., Wissinger, B., Pinti, M., Cossarizza, A., Vidoni, S., Valentino, M. L., Rugolo, M., & Carelli, V. (2008). OPA1 mutations associated with dominant optic atrophy impair oxidative phosphorylation and mitochondrial fusion. *Brain*, *131*(Pt 2), 352-367.

Zetsche, B., Gootenberg, J. S., Abudayyeh, O. O., Slaymaker, I. M., Makarova, K. S., Essletzbichler, P., Volz, S. E., Joung, J., van der Oost, J., Regev, A., Koonin, E. V., & Zhang, F. (2015). Cpf1 is a single RNA-guided endonuclease of a class 2 CRISPR-Cas system. *Cell*, *163*(3), 759-771.

Zhang, X. H., Tee, L. Y., Wang, X. G., Huang, Q. S., & Yang, S. H. (2015). Off-target Effects in CRISPR/Cas9-mediated Genome Engineering. *Mol Ther Nucleic Acids*, *4*(11), e264.

Zhang, Y., Long, C., Li, H., McAnally, J. R., Baskin, K. K., Shelton, J. M., Bassel-Duby, R., & Olson, E. N. (2017). CRISPR-Cpf1 correction of muscular dystrophy mutations in human cardiomyocytes and mice. *Sci Adv*, *3*(4), e1602814.

Zhao, X., Zhang, Y., Lu, L., & Yang, H. (2020). Therapeutic Effects of Idebenone on Leber Hereditary Optic Neuropathy. *Curr Eye Res*, *45*(10), 1315-1323.

Zuccarelli, M., Vella-Szijj, J., Serracino-Inglott, A., & Borg, J. J. (2020). Treatment of Leber's hereditary optic neuropathy: An overview of recent developments. *Eur J Ophthalmol*, *30*(6), 1220-1227.

9 Statement of contribution to collaborative work

Retrospective *DNAJC30* screening of 1202 patients with Leber hereditary optic neuropathy or optic atrophy was performed in collaboration with **Ting Xiao**, Institute of Ophthalmology, University Hospital Tübingen, Germany. The data for this project were collected and analysed in equal parts by **Sinja Kieninger** and **Ting Xiao**.

10 Acknowledgement / Danksagung

An dieser Stelle möchte ich mich bei allen bedanken, die diese Arbeit ermöglicht haben.

Als erstes geht ein großes Dankeschön an Prof. Dr. Bernd Wissinger, der mir die Möglichkeit gegeben hat meine Doktorarbeit in seiner Arbeitsgruppe zu absolvieren und dabei auch die Betreuung meiner Arbeit übernommen hat. Ich möchte mich bei dir bedanken Bernd, dass du immer ein offenes Ohr für uns Doktoranden hattest und dich bei unserer Betreuung stets bemüht hast und uns zur Seite gestanden bist.

Ich möchte mich auch bei Prof. Dr. Stefan Liebau bedanken für die Übernahme der Zweitbetreuung und Zweitbegutachtung meiner Arbeit. Auch möchte ich mich für alle hilfreichen Ratschläge bedanken, die Sie mir in unseren Betreuungsgesprächen gegeben haben.

Als nächstes möchte ich mich bei meinen Kolleginnen Dr. Susanne Kohl, Dr. Nicole Weisschuh und Dr. Peggy Reuter für die große Unterstützung an meinem Projekt bedanken, ohne euer Wissen und eure Hilfe wäre das alles gar nicht möglich gewesen. Nicole, vielen Dank für deine Hilfe beim Schreiben meiner Thesis und all deinen Bemühungen und Verbesserungsvorschlägen. Außerdem möchte ich mich bedanken für deine Unterstützung in allen Splicing Fragen und auch im *DNAJC30* Projekt. Peggy, bei dir möchte ich mich nochmal bedanken vor allem auch zuletzt für deine Hilfe bezüglich der Mitochondrien Analysen.

Außerdem möchte ich mich bei meinem Doktoranden Kollegen Pietro De Angeli und meinen Doktoranden Kolleginnen Ting Xiao und Maria Solaki bedanken, die in der ganzen Zeit auch zu guten Freunden für mich geworden sind. Pietro, a special thanks goes to you for helping me with all kinds of CRISPR questions and setting up the iPSC work in our lab with me. Ting and Maria, thank you very much for helping me with the Western Blots and also for helping taking care of the iPS cells.

Vielen Dank auch an Britta Baumann, Jennifer Schröder und Eva Weber für eure Hilfe in allen Labor-technischen Fragen und viele nette Gespräche.

Auch möchte ich mich bei Dr. Stefan Hauser und seinem gesamten Team für die Bereitstellung der iPSCs bedanken, die das Projekt überhaupt erst ermöglicht haben.

Ein weiterer Dank gilt Prof. Dr. Heiner Schaal für die *in silico* Prädiktionen und die damit verbundenen Bemühungen.

I would also like to thank Virginia Cora and Dr. Natalia Pashkovskaia for all the advice around culturing and working with the iPS cells.

Als letztes aber ganz besonders möchte ich mich bei meinen Eltern und meinen Freunden bedanken. Danke, dass Ihr immer an meiner Seite gestanden seid, vor allem auch in den schwierigen Phasen und zu jeder Zeit an mich geglaubt habt und immer die richtigen Worte für mich gefunden habt. Ohne euch hätte ich das alles nicht geschafft.

11 Supplementary material

11.1 Cleavage efficacy analysis of gRNAs and gRNA pairs

Analysis of fluorescently-labelled PCR products from genomic DNA of CRISPR-treated HEK293T and iPS cells using GeneScan and GeneMapper software 5 (Applied Biosystems, Waltham, MA, USA) to determine the cleavage efficacy of gRNAs or gRNA pairs.

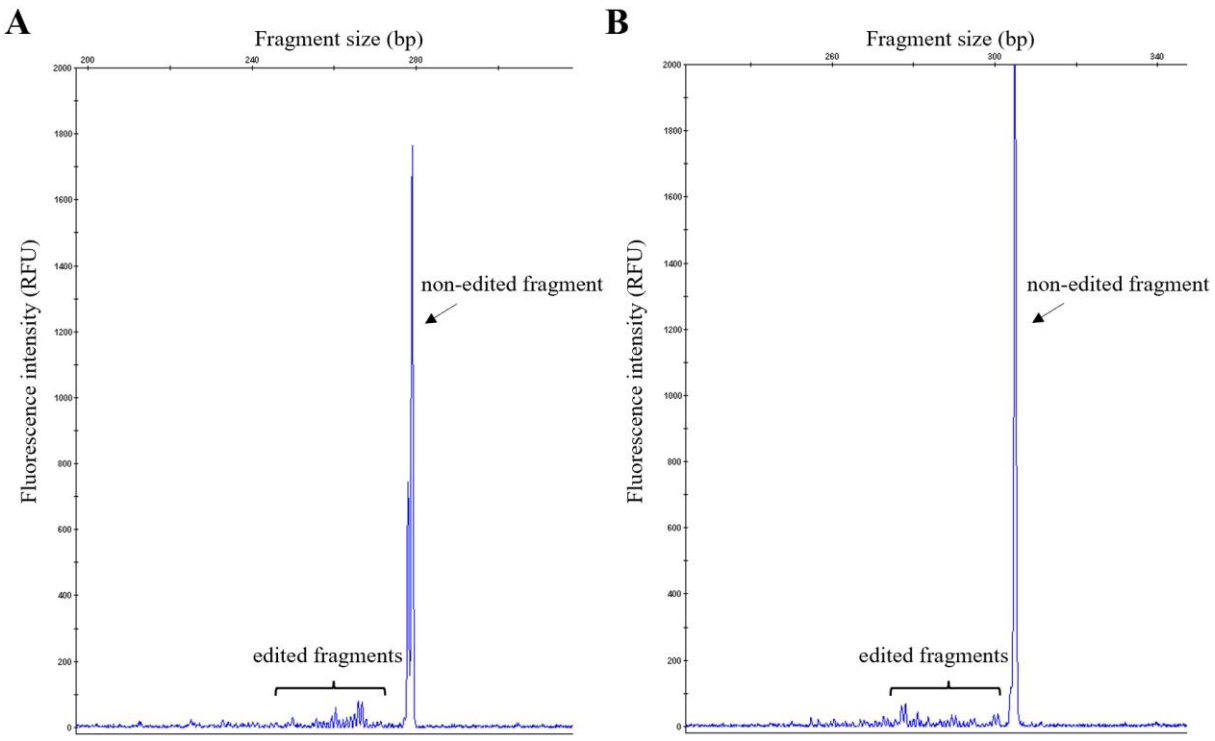

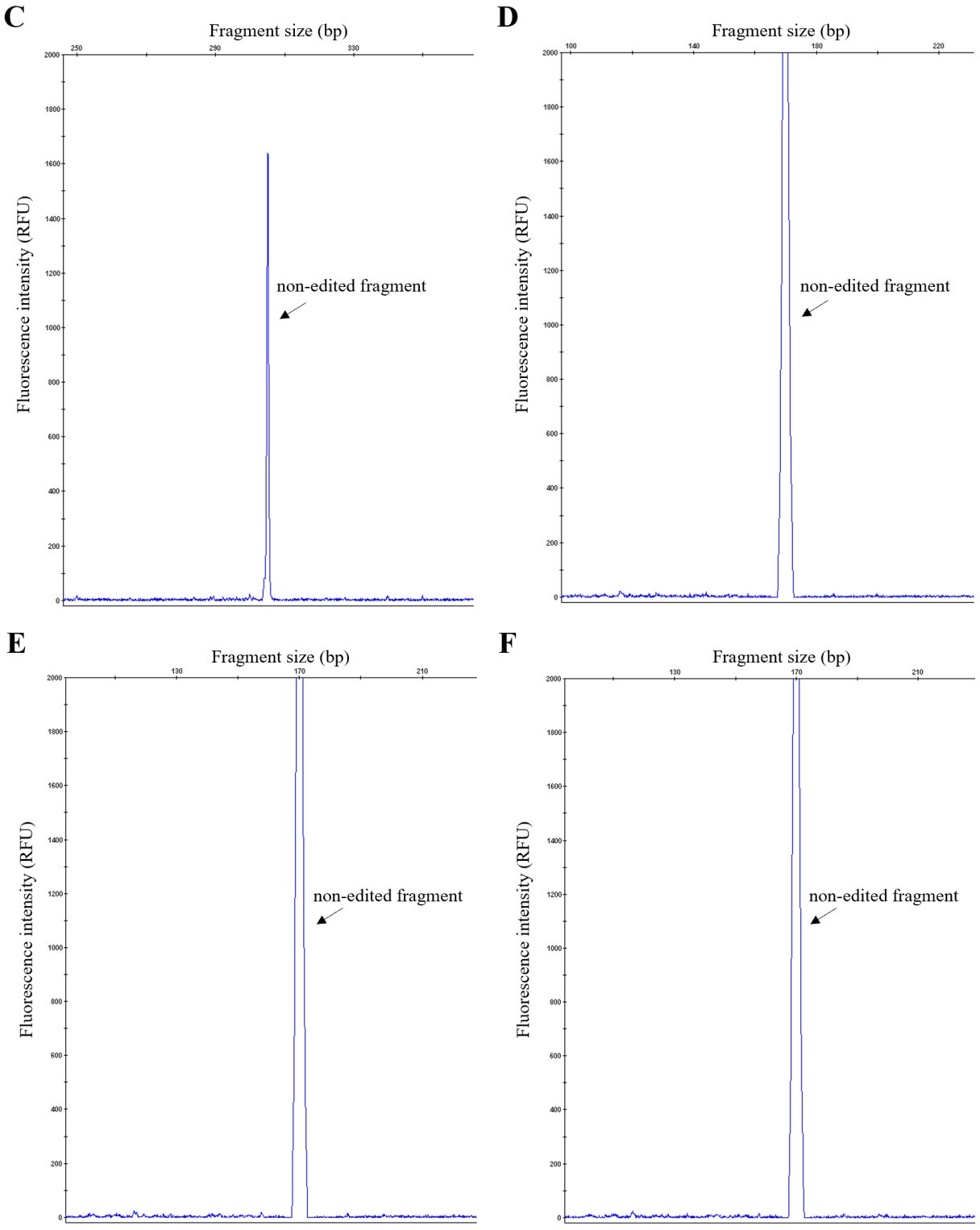
C
Fragment size (bp)
Fluorescence intensity (RFU)
non-edited fragment
D
Fragment size (bp)
Fluorescence intensity (RFU)
non-edited fragment
E
Fragment size (bp)
Fluorescence intensity (RFU)
non-edited fragment
F
Fragment size (bp)
Fluorescence intensity (RFU)
non-edited fragment

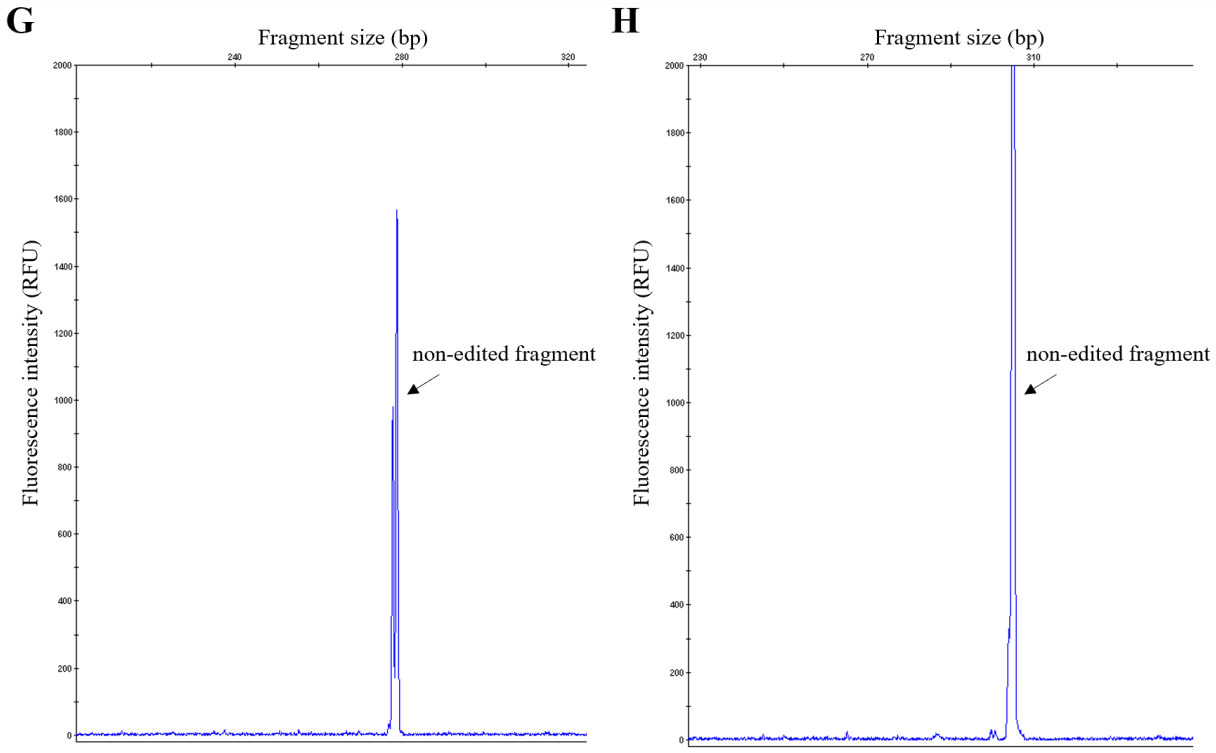

Figure S1: Cleavage efficacy analysis of CRISPR/Cas9 nickase gRNA pairs after transfection of HEK293T cells with plasmid constructs. GeneScan analysis of fluorescently-labelled PCR fragments amplified from genomic DNA of CRISPR/Cas9 nickase-treated HEK293T cells. **(A)-(F)** Transfection with construct containing gRNA pair 1 **(A)**, gRNA pair 2 **(B)**, gRNA pair 3 **(C)**, gRNA pair 4 **(D)**, gRNA pair 5 **(E)** or gRNA pair 6 **(F)**. **(G)-(H)** Negative controls: Amplification of genomic DNA from untransfected HEK293T cells with primer pair gRNApair1_F and gRNApair1_R_FAM **(G)** or JH_Fwd2_FAM and JH_CRISPR_Intr4_large_ R1 **(H)**.

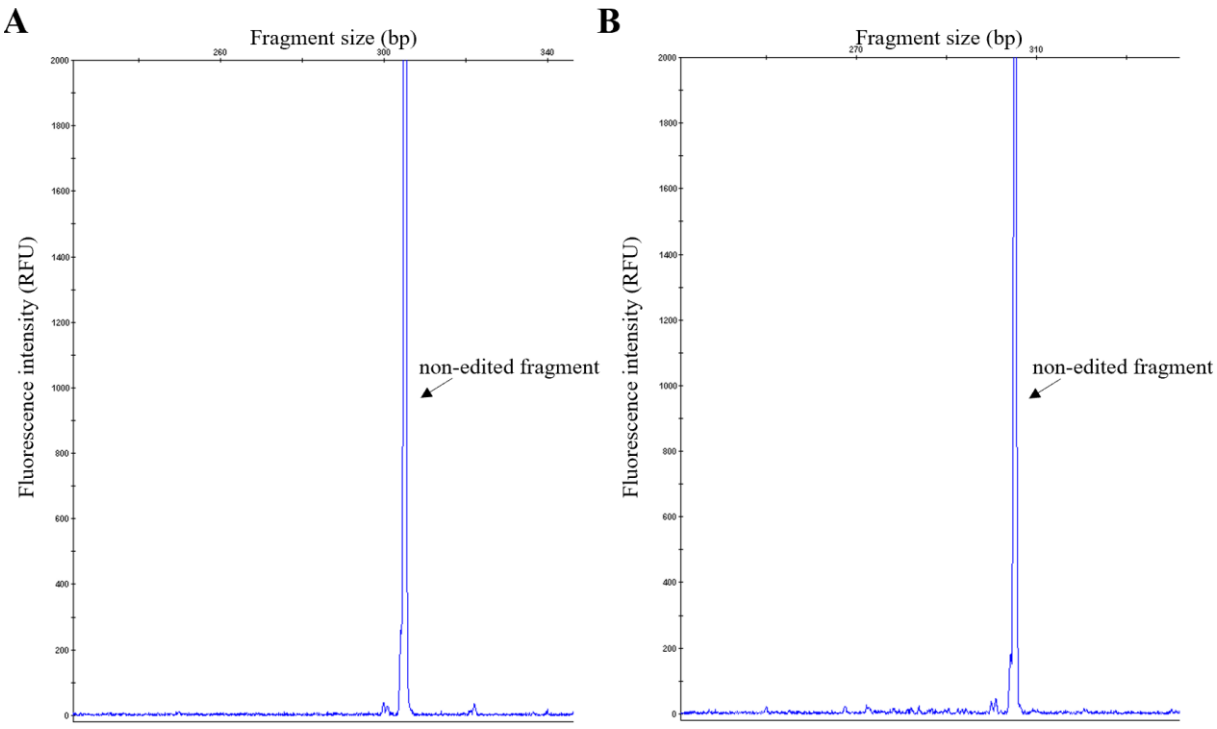

Figure S2: Cleavage efficacy analysis of CRISPR/Cas9 nickase gRNA pair 2 after transfection of HEK293T cells using RNP delivery. GeneScan analysis of fluorescently-labelled PCR fragments amplified from genomic DNA of CRISPR/Cas9 nickase-treated HEK293T cells showed no peaks compatible with edited fragments**. (A)** Transfection of Cas9 nickase and gRNA pair 2 using Lipofectamine RNAiMAX **(B)** Transfection of Cas9 nickase without gRNA using Lipofectamine RNAiMAX (negative control).

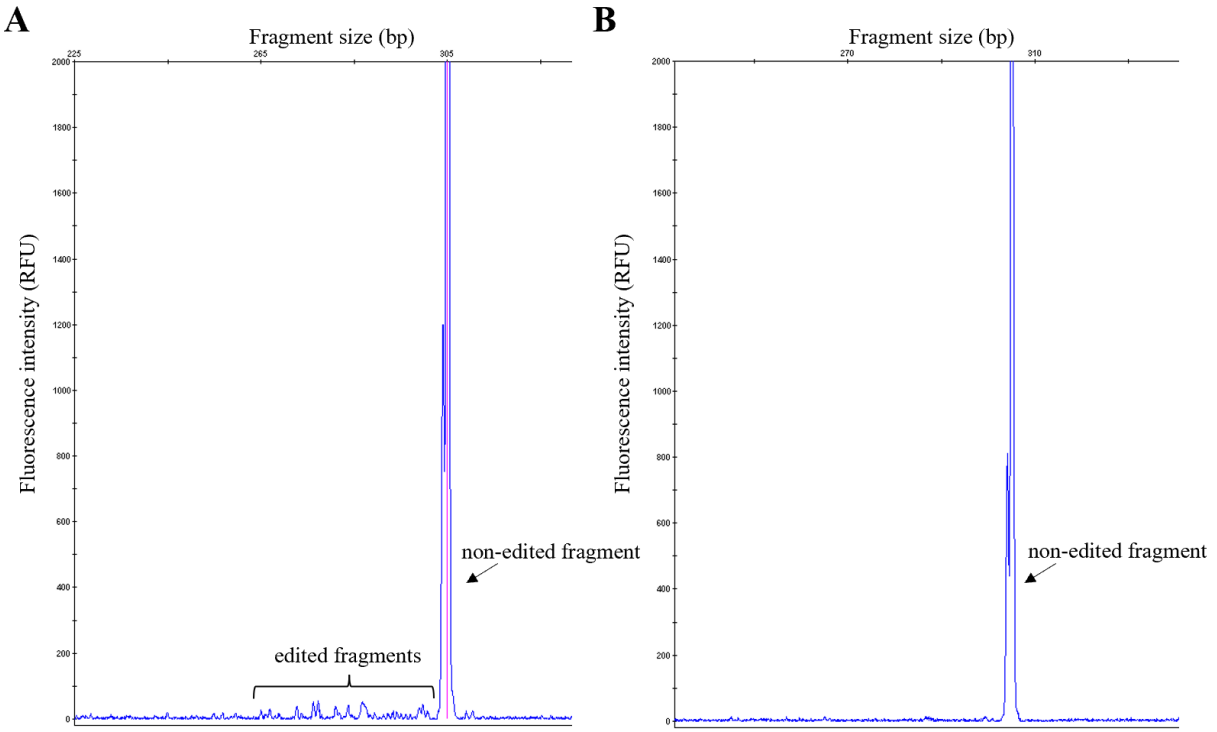

Figure S3: Cleavage efficacy analysis of CRISPR/Cas9 nickase gRNA pair 2 after electroporation of patient-derived iPSCs with plasmid constructs. GeneScan analysis of fluorescently-labelled PCR fragments amplified from genomic DNA of CRISPR/Cas9 nickase-treated iPS single cells. **(A)** Electroporation with Cas9 nickase gRNA pair 2 construct **(B)** Negative control (mock-electroporated cells).

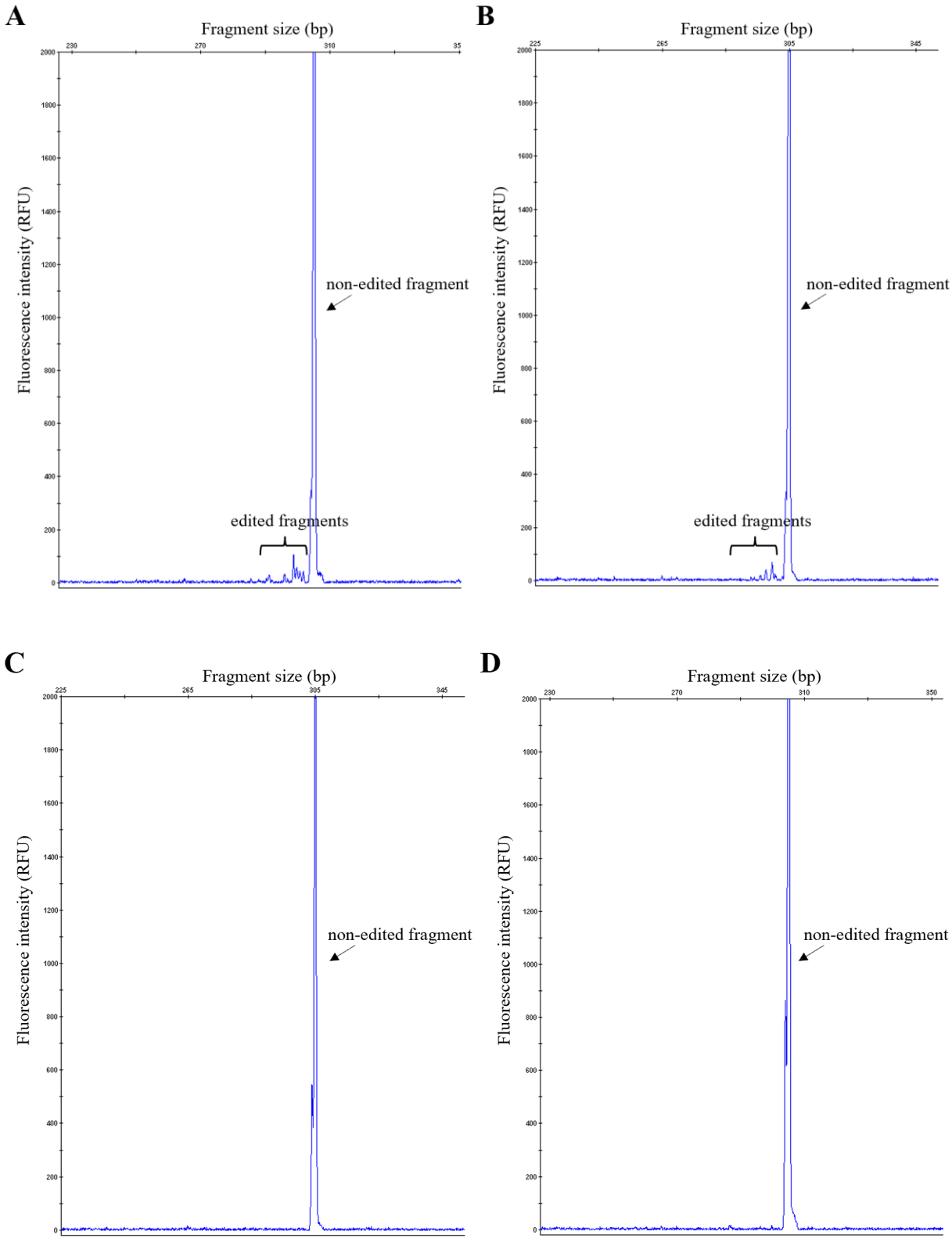

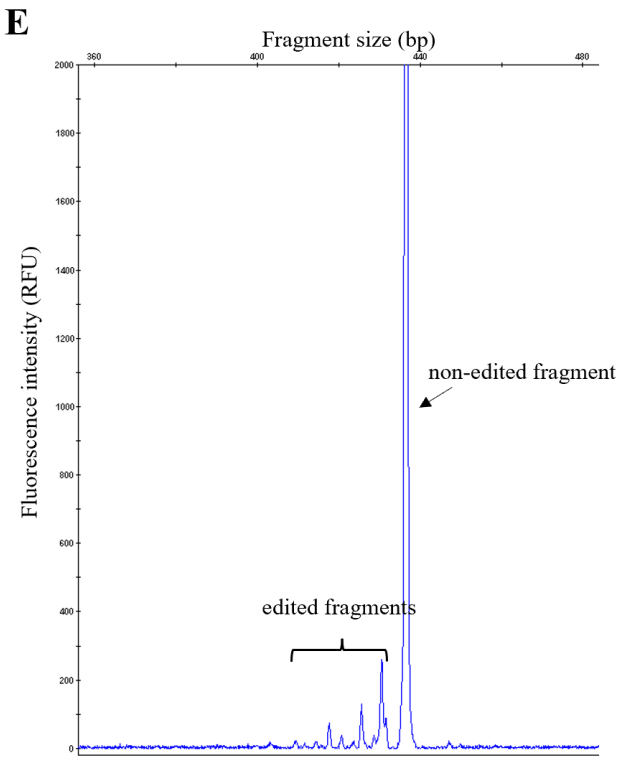

Figure S4: Cleavage efficacy analysis of CRISPR/Cpf1 gRNAs after electroporation of patient-derived iPSCs with plasmid constructs. GeneScan analysis of fluorescently-labelled PCR fragments amplified from genomic DNA of CRISPR/Cpf1-treated iPS single cells **(A)** Electroporation with gRNA 1 construct **(B)** Electroporation with gRNA 2 construct **(C)** Electroporation with gRNA 3 construct **(D)** Negative control (mock-electroporated cells) **(E)** Positive control (Cpf1 construct with a gRNA targeting the *CLEC16A* gene).

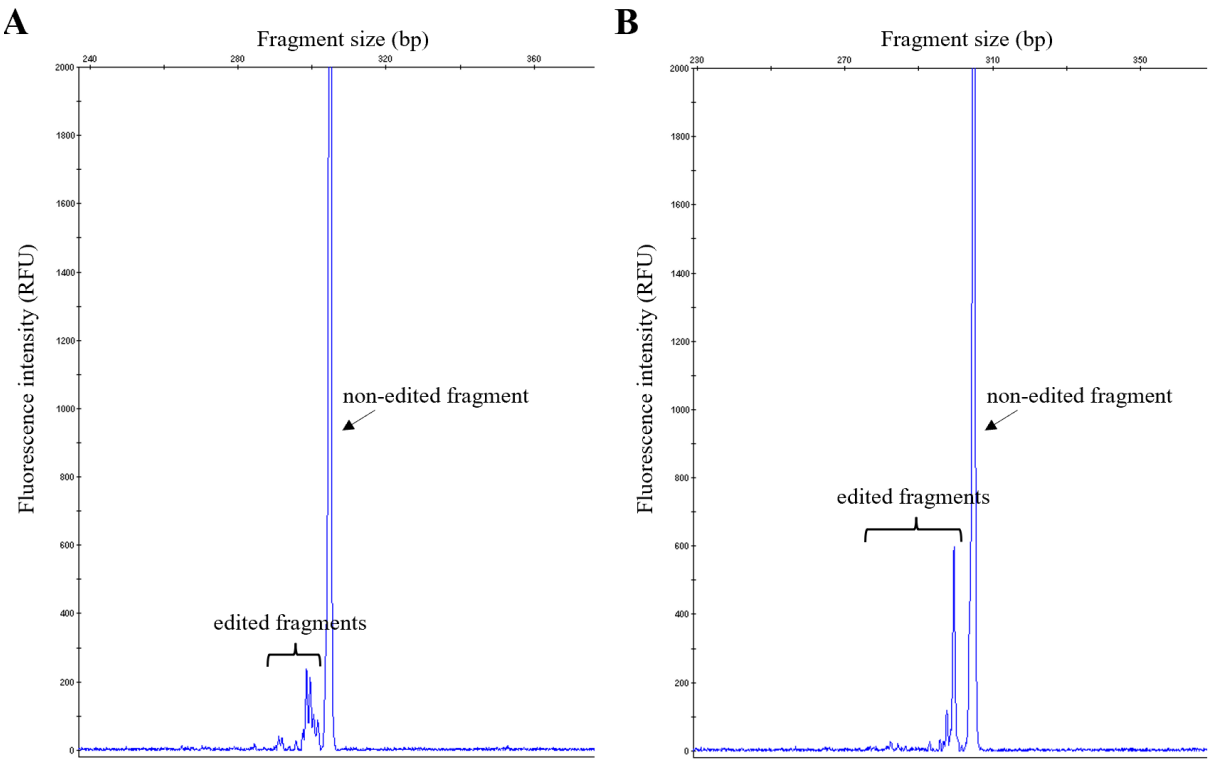

Figure S5: Cleavage efficacy analysis of CRISPR/Cpf1 gRNAs after electroporation of patient-derived iPSCs with plasmid constructs and FACS sorting. GeneScan analysis of fluorescently-labelled PCR fragments amplified from genomic DNA of CRISPR/Cpf1-treated and sorted iPS single cells**. (A)** Electroporation with gRNA 1 construct **(B)** Electroporation with gRNA 2 construct.

12 List of abbreviations

°C	degree celcius
µg	microgram
µl	microlitres
µm	micrometre
µM	micromolar
3´ss	acceptor splice site
5´ss	donor splice site
aa	amino acids
AAV	adeno-associated virus
Alu	*Arthrobacter luteus*
AMD	age-related macular degeneration
AON	antisense oligonucleotide
APS	adenosine 5´-phosphosulfate
AQ	Allele Quantification
arLHON	autosomal recessive LHON
As	*Acidaminococcus sp.*
ATP	adenosine triphosphate
bp	base pair
BSA	bovine serum albumin
BSC	back scatter
BTN	biotinylated
C/C+	cryptic exon
Cas	CRISPR-associated protein
Cas9n	Cas9 nickase
cDNA	complementary DNA
cm	centimetre
CMV	cytomegalovirus
CO	control

Compd het	compound heterozygous
Cpf1	CRISPR-associated endonuclease in *Prevotella* and *Francisella* 1
CRISPR	clustered regularly interspaced short palindromic repeats
CRR	clinically relevant recovery
crRNA	CRISPR RNA
DAPI	4´,6-diamidino-2-phenylinodile
ddH_2O	double distilled water
ddNTPs	dideoxynucleotide triphosphates
DIM	deep intronic mutation
DMD	Duchenne muscular dystrophy
DMEM	Dulbecco´s Modified Eagle Medium
DMSO	dimethyl sulfoxide
DNA	deoxyribonucleic acid
DNAJC30	DNAJ/HSP40 homolog subfamily c member 30
dNTPs	deoxynucleotide triphosphates
DOA	dominant optic atrophy
DSB	double-strand break
DTT	dithiothreitol
DZNE	Deutsches Zentrum für Neurodegenerative Erkrankungen
E.coli	*Escherichia coli*
EDTA	ethylenediaminetetraacetic acid
EGFP	enhanced GFP
ESC	embryonic stem cell
ESE	exonic splicing enhancer
ESS	exonic splicing silencer
F	forward
FACS	fluorescence-activated cell sorting
FAM	carboxyfluorescein
FBS	fetal bovine serum
FSC	forward scatter

g	gram
GDP	guanosine diphosphate
GFP	green fluorescent protein
gRNA	guide RNA
GTP	guanosine triphosphate
HDR	homology-directed repair
HEK293T	human embryonic kidney cells
HF	High-Fidelity
hnRNP	heterogeneous nuclear ribonucleoprotein
Hom	homozygous
HRP	horseradish peroxidase
IDAA	Indel detection by amplicon analysis
i.e.	id est, „that is“
Indels	insertions/deletions
iPSC	induced pluripotent stem cell
ISE	intronic splicing enhancer
ISS	intronic splicing silencer
IVM	in vitro mutagenesis
kb	kilobase
kDa	kilodalton
KSR	Knockout Serum Replacement
L	litres
Lb	*Lachnospiraceae bacterium*
LCA	Leber congenital amaurosis
LHON	Leber´s hereditary optic neuropathy
M	molar
mA	milliampere
MAF	minor allele frequency
MCS	multiple cloning site
mg	milligram

min	minutes
MIP	maximum intensity projection
ml	millilitres
mM	millimolar
MPS-IVA	mucopolysaccharidosis IV type A
mRNA	messenger RNA
mtDNA	mitochondrial DNA
mtLHON	LHON associated with mutations in mitochondrial DNA
mut	mutant
NA	not available
NC	negative control
ng	nanogram
NGS	next-generation sequencing
NHEJ	non-homologous end joining
nm	nanomolar
NMD	nonsense-mediated mRNA decay
nt	nucleotides
OA	optic atrophy
OAK	optic atrophy, Kjer´s type
OCR	oxygen consumption rate
OPA1	OPA1 mitochondrial dynamin like GTPase
PAM	protospacer adjacent motif
PBS	phosphate-buffered saline
PCR	polymerase chain reaction
pmol	picomol
PNK	polynucleotide kinase
Pol	polymerase
PTC	premature termination codon
R	reverse
RFLP	restriction fragment length polymorphism

RFU	relative fluorescence unit
RNA	ribonucleic acid
RNP	ribonucleoprotein
ROS	reactive oxygen species
RPE	retinal pigment epithelium
rpm	revolutions per minute
RT-PCR	reverse transcription PCR
Sa	*Staphylococcus aureus*
SD	standard deviation
SDS	sodium dodecyl sulfate
sec	seconds
SF	splicing factor
SNP	single nucleotide polymorphism
snRNP	small nuclear ribonucleoprotein
Sp	*Streptococcus pyogenes*
SR proteins	serine and arginine-rich proteins
SRE	serum response element
SS	Sanger sequencing
SSC	side scatter
T7EI	T7 endonuclease I
Taq	*Thermus aquaticus*
TBE	Tris-borate-EDTA
TBS	Tris-buffered saline
TE	Tris-EDTA
TMRE	tetramethylrhodamine ethyl ester
tracrRNA	trans-activating crRNA
tRNA	transfer-RNA
U	units
UV	ultraviolet
VTN-N	Vitronectin

WGS	whole-genome sequencing
WT	wild-type

13 List of figures

14 List of tables